



Manole-Stelian ȘERBULEA Adrian PRICEPUTU Adrian ANDRONIC

Constantin UNGUREANU Daniel-Marcel MANOLI

**GEOTECHNICAL ENGINEERING**  
2<sup>nd</sup> Edition

M. S. Șerbulea A. Priceputu A. Andronic  
C. Ungureanu D. M. Manoli

**GEOTECHNICAL ENGINEERING**

2<sup>nd</sup> Edition

Editura PRINTECH

## **TABLE OF CONTENTS**

Table of figures .....	5
1 The object and a brief history of Geotechnical Engineering.....	13
2 Origin of soils.....	21
2.1 The rock cycle .....	22
2.2 Igneous rocks .....	22
2.3 Weathering .....	24
2.3.1 Physical weathering .....	24
2.3.2 Chemical weathering.....	25
2.3.3 Biological weathering .....	27
2.4 Transport of weathering products .....	27
2.5 Sedimentary rocks .....	30
2.6 Metamorphic rocks.....	31
2.7 Test your understanding .....	32
3 Soil grading .....	33
3.1 Screening method.....	34
3.2 Hydrometer method .....	38
3.3 Graphical representation of grain size analysis.....	44
3.4 Test your understanding .....	49
4 Simple indices of soil .....	53
4.1 Porosity and voids ratio.....	54
4.2 Moisture content.....	56
4.3 Unit weight and density .....	60
4.3.1 Particle density .....	60
4.3.2 Dry density .....	65
4.3.3 Saturated density .....	67
4.3.4 Bulk density .....	68
4.3.5 Submerged density .....	71
4.3.6 Saturation ratio .....	73
4.4 Density index .....	74
4.5 Test your understanding .....	76
5 Clay minerals .....	79
5.1 Generalities .....	79

---

5.2	Electro-chemical bonds .....	79
5.3	Solid phase .....	81
5.4	The clay-water electrolyte system.....	89
5.5	Attraction and rejection forces equilibrium .....	89
5.6	Test your understanding .....	91
6	Bonded water .....	93
6.1	Consistency limits of cohesive soils .....	96
6.2	Shrinkage limit .....	102
6.3	Laboratory methods of determining the Atterberg limits .....	102
6.3.1	Plastic limit .....	102
6.3.2	Liquid limit .....	103
6.4	Test your understanding .....	108
7	Unbonded water .....	111
7.1	Unbounded groundwater .....	111
7.2	Capillary water .....	113
7.3	Gravitational water .....	116
7.3.1	The constant head permeameter .....	118
7.3.2	The variable head permeameter .....	120
7.4	In-situ pumping tests .....	122
7.5	Dynamic effect of water upon cohesionless soils .....	125
7.6	Filters .....	128
7.7	Test your understanding .....	129
8	Short review of strength of materials, theory of elasticity and plasticity applied to Soil Mechanics .....	133
8.1	State of stress .....	133
8.2	Pole of Mohr's circle.....	150
8.3	State of strain.....	153
8.4	Law of effective stresses .....	160
8.5	Plane problems .....	162
8.6	Stress coordinates.....	164
8.7	Test your understanding.....	168
9	Soil compressibility and consolidation .....	171
9.1	Compressibility .....	171
9.2	Linear one-dimensional consolidation theory .....	177
9.3	Laboratory tests .....	181
9.3.1	The procedure of the compressibility test .....	182
9.3.2	The procedure of the consolidation test .....	185
9.4	Test your understanding .....	187
10	Soil shearing strenght .....	191

---

10.1	Mohr-Coulomb failure criterion.....	191
10.1.1	Generalities .....	191
10.1.2	The effect of overconsolidation over the shear resistance parameters .....	193
10.1.3	Shear stress paths in s – t total coordinates .....	199
10.1.4	Stress paths in total vs effective coordinates.....	211
10.1.5	Mohr-Coulomb failure criterion in principal stresses .....	211
10.2	Tests for assessing the shearing strength parameters .....	214
10.2.1	Direct shearing test.....	220
10.2.2	Triaxial compression test .....	225
10.3	Test your understanding .....	230
11	The effects of soil upon structures .....	237
11.1	General notions .....	237
11.2	Vertical stresses.....	241
11.3	State of rest.....	243
11.4	Coulomb’s model for active thrust.....	245
11.5	Culmann’s graphical method .....	246
11.6	Rankine model in active and passive case .....	248
11.1	Test your understanding .....	252
12	Site investigation.....	255
12.1	Planning the site investigation .....	256
12.2	Manual drilling.....	258
12.3	Direct circulation drilling .....	259
12.4	Reverse circulation drilling .....	261
12.5	Sampling methods.....	262
12.5.1	Moulds .....	262
12.5.2	Boxes.....	263
12.5.3	Shelby (Osterberg) tubes.....	264
12.6	Standard penetration test (SPT) .....	265
12.6.1	Density index .....	269
12.6.2	Consistency index .....	271
12.6.3	Unit weight.....	272
12.6.4	Internal friction angle .....	273
12.6.5	Undrained cohesion.....	274
12.6.6	Linear deformation modulus .....	275
12.7	Cone penetration test (CPT).....	275
12.7.1	Tip (cone) resistance .....	276
12.7.2	Sleeve friction .....	277
12.7.3	Friction ratio.....	277

---

12.7.4	Soil Behaviour Type (SBT) index .....	278
12.7.5	Equivalent SPT value .....	280
12.7.6	Density index .....	281
12.7.7	Unit weight.....	282
12.7.8	Internal friction angle.....	282
12.7.9	Undrained cohesion.....	283
12.7.10	Linear deformation modulus .....	283
12.8	Dynamic probing (DP).....	283
12.8.1	Dynamic point resistance .....	285
12.8.2	Density index .....	285
12.8.3	Static cone resistance .....	287
12.8.4	Oedometric modulus .....	287
12.9	Plate load test .....	288
12.10	Menard pressuremeter .....	295
12.11	Marchetti dilatometer test (DMT).....	296
12.12	Vane test.....	298
12.13	Test your understanding.....	299
	Bibliography.....	305

## TABLE OF FIGURES

Fig. 1.1: Robert Hooke.....	14
Fig. 1.2: Leonhard Euler .....	14
Fig. 1.3: Giordano Ricatti .....	15
Fig. 1.4: Thomas Young .....	15
Fig. 1.5: Siméon Denis Poisson .....	15
Fig. 1.6: Gabriel L. J. B. Lamé .....	15
Fig. 1.7: Augustin-Louis Cauchy .....	16
Fig. 1.8: George Green.....	16
Fig. 1.9: Joseph-Louis Lagrange.....	17
Fig. 1.10: Charles Augustin de Coulomb.....	17
Fig. 1.11: Carl Culmann.....	17
Fig. 1.12: Christian Otto Mohr.....	17
Fig. 1.13: Henri Édouard Tresca .....	18
Fig. 1.14: Richard Edler von Mises .....	18
Fig. 1.15: Daniel Charles Drucker .....	19
Fig. 1.16: William Prager.....	19
Fig. 1.17: Henry Darcy.....	19
Fig. 1.18: Karl von Terzaghi .....	19
Fig. 1.19: Maurice Anthony Biot .....	19
Fig. 2.1: Bowen’s Reaction Series .....	23
Fig. 2.2: Types of soil deposits .....	28
Fig. 2.3: Colluvial and proluvial deposits .....	29
Fig. 3.1: Sieving test assembly.....	35
Fig. 3.2: Soil particles remained on the sieves after the test .....	37
Fig. 3.3: Hydrometer measurements .....	41
Fig. 3.4: Depth of buoyancy.....	41
Fig. 3.5: Meniscus correction.....	43
Fig. 3.6: Example of histogram and grading curve.....	45
Fig. 3.7: Important diameters on the grading curve .....	46
Fig. 3.8: Uniformity coefficient .....	46
Fig. 3.9: Assessing the percentages for a fraction.....	47
Fig. 3.10: Ternary diagram .....	48

---

Fig. 3.11: Assessing the fines for the ternary diagram.....	48
Fig. 4.1: The phases of the soil .....	53
Fig. 4.2: Simplified phase diagram .....	54
Fig. 4.3: The steps for finding the moisture content by oven drying [13] ...	56
Fig. 4.4: Desiccator [15].....	59
Fig. 4.5: Examples of pyknometers .....	62
Fig. 4.6: Steps in performing the pyknometer test.....	63
Fig. 4.7: Pyknometer test principles.....	65
Fig. 4.8: Phase diagram for dry soil .....	66
Fig. 4.9: Phase diagram for saturated soil .....	67
Fig. 4.10: General phase diagram .....	68
Fig. 4.11: Measuring the interior dimensions of the mould.....	69
Fig. 4.12: Steps in finding the bulk density .....	70
Fig. 4.13: Optional additional steps after finding the bulk density .....	71
Fig. 4.14: Phase diagram for soil in submerged conditions .....	72
Fig. 6.1: The adoption complex of clay minerals.....	94
Fig. 6.2: Soil-water characteristic curve .....	95
Fig. 6.3: Water movement across the adsorption complex .....	96
Fig. 6.4: Soil's volume and consistency index variation as functions of the moisture content .....	98
Fig. 6.5: Plasticity limit variation as functions of the clay percentage .....	100
Fig. 6.6: Plasticity chart (Unified Soil Classification System) .....	100
Fig. 6.7: Rolling the soil cylinders against the sandblasted glass .....	103
Fig. 6.8: The Nagaraj model of the soil's structure near the liquid limit [19] .....	104
Fig. 6.9: The Casagrande cup.....	105
Fig. 6.10: Flow curve for determining the liquid limit by Casagrande cup method.....	106
Fig. 6.11: The penetrometer apparatus.....	107
Fig. 6.12: Flow curve for determining the liquid limit by free fall cone method .....	108
Fig. 7.1 Unconfined aquifer .....	112
Fig. 7.2 Confined aquifer .....	112
Fig. 7.3: Free water distribution in the ground .....	112
Fig. 7.4: Formation of the capillary meniscus.....	113
Fig. 7.5: Capillary rise depending on the relative distance between walls	114
Fig. 7.6: Equilibrium of forces in a capillary tube .....	115
Fig. 7.7: Hydrostatic state .....	116
Fig. 7.8: Steady state seepage .....	116

Fig. 7.9: Water flow through soils .....	118
Fig. 7.10 The constant head permeameter .....	119
Fig. 7.11 The variable head permeameter .....	121
Fig. 7.12: Pumping test .....	123
Fig. 7.13: Foundation liquefaction by vertical seepage .....	126
Fig. 7.14 Inverse filter .....	128
Fig. 7.15: Filter material rule .....	128
Fig. 8.1: Solid body in equilibrium under the action of a set of external forces .....	134
Fig. 8.2: Material point bounded by planes parallel with the local coordinate system of axes .....	134
Fig. 8.3: Denomination of the stresses acting on the faces of the material point .....	136
Fig. 8.4: Stresses on a plane inclined with angle $\theta$ with respect to the direction $Oy$ .....	138
Fig. 8.5: Stresses on a principal plane having the direction $Ox'$ .....	140
Fig. 8.6: Mohr's circle defined for two pairs of values acting on two perpendicular planes .....	143
Fig. 8.7: Mohr's circle representation using two pairs of values acting on two random planes .....	144
Fig. 8.8: Mohr's circle representation using two pairs of values that act on two perpendicular planes .....	146
Fig. 8.9: Mohr's circle representation using principal stresses .....	146
Fig. 8.10: Stresses on a random plane in a three-dimensional state of stress .....	148
Fig. 8.11: Mohr's circles in a three-dimensional state of stress .....	148
Fig. 8.12: Pole position determination and the determination of a pair of values acting on a plane inclined with angle $\theta$ with respect to the vertical .....	152
Fig. 8.13: One-dimensional and two-dimensional states of strains .....	154
Fig. 8.14: Representation of the state of strain around a point .....	157
Fig. 8.15: Defining the linear deformation moduli function of the chosen material behaviour model .....	158
Fig. 8.16: Strain softening type relation .....	159
Fig. 8.17: Karl Terzaghi's one-dimensional consolidation mechanical model .....	161
Fig. 8.18: Stress state representation in the $\sigma_1 - \sigma_2 - \sigma_3$ coordinate system .....	165
Fig. 8.19: Stress path representation example for the monoaxial compression test .....	168



Fig. 9.1: Oedometric modulus representation in decimal and semi-logarithmic scales ..... 173

Fig. 9.2: Compressibility modulus representation using  $\sigma - e$  variation in decimal scale ..... 174

Fig. 9.3: Specific volume and voids ratio variations with the applied load 175

Fig. 9.4: Pre-consolidation stress – origin and determination method..... 177

Fig. 9.5: Stress and drainage conditions for an infinitesimal element subjected to one-dimensional consolidation ..... 179

Fig. 9.6: The oedometer apparatus ..... 182

Fig. 9.7: Compressibility tests conducted on collapsible soils..... 184

Fig. 9.8: Compressibility test conducted on expansive soils ..... 185

Fig. 9.9: The logarithm of time method for determining the coefficient of consolidation ..... 186

Fig. 10.1: Shear resistance models ..... 192

Fig. 10.2: Approximation of Mohr's envelope through the intrinsic line .... 193

Fig. 10.3: Stresses, strains and displacements necessary to determine the dilatancy/contraction parameters for the direct shear test..... 195

Fig. 10.4: Stresses, strains and displacements necessary to determine the dilatancy/contraction parameters for the triaxial shear test..... 195

Fig. 10.5: Shear stress variation against axial strain ..... 196

Fig. 10.6: The convergence of the mobilization curves for an overconsolidated soil and normally consolidated soil for the same value of the deviatoric stress to the same value of the deviator for large mobilizations, considering a constant spherical stress..... 197

Fig. 10.7: Peak failure criterion vs. residual failure criterion ..... 198

Fig. 10.8: Peak and residual values obtained for different overconsolidation ratios..... 198

Fig. 10.9: Intrinsic line for an isotropic consolidated sample - sheared by axial loading..... 201

Fig. 10.10: The  $k_f$  line for an isotropic consolidated sample - sheared by axial loading..... 201

Fig. 10.11: Critical stress state line for an isotropic consolidated sample - sheared by axial loading..... 202

Fig. 10.12: Stress state tangent to the intrinsic line ..... 202

Fig. 10.13: The intrinsic line of a sample anisotropically  $k_0$  consolidated and sheared along an unloading stress path, appropriate to the active thrust case ..... 205

Fig. 10.14: The  $k_f$  line of a sample anisotropically  $k_0$  consolidated and sheared along an unloading stress path, appropriate to the active thrust case..... 205

Fig. 10.15: Stress paths that do not lead to failure due to the compression limit .....	206
Fig. 10.16: Obtaining the shear resistance parameters from three values of the consolidation stress and one type of stress path.....	207
Fig. 10.17: Obtaining the shear strength parameters using one value of the consolidation stress and three types of stress paths .....	207
Fig. 10.18: Intrinsic line for a $k_0$ anisotropically consolidated sample that is sheared on an unloading stress path, specific for the passive resistance ...	208
Fig. 10.19: $K_f$ line for a $k_0$ anisotropically consolidated sample, sheared on an unloading stress path, which is specific for the passive resistance .....	209
Fig. 10.20: Intrinsic line for a $k_0$ anisotropically consolidated sample, sheared on a vertical stress path .....	210
Fig. 10.21: $K_f$ line for a $k_0$ anisotropically consolidated sample, sheared on a vertical stress path.....	210
Fig. 10.22: Total and effective stress representation for the results of a CU type triaxial test.....	211
Fig. 10.23: Mohr-Coulomb representation in $\sigma_2 = 0$ plane .....	213
Fig. 10.24: Elastic-perfect plastic strain model with equal tension and compression resistances .....	214
Fig. 10.25: The necessary number of tests for the direct shearing test .....	215
Fig. 10.26: The necessary number of tests for the triaxial test .....	216
Fig. 10.27: Direct shear device major components [26] [27] .....	220
Fig. 10.28: The direct shearing apparatus conceptual components .....	222
Fig. 10.29: Shaping the specimens for the direct shear test.....	224
Fig. 10.30: Placing the test specimen inside the shear box .....	224
Fig. 10.31: The triaxial compression test apparatus.....	227
Fig. 10.32: Possible stress paths starting from isotropic consolidation (CU, CD).....	229
Fig. 10.33: Possible stress paths starting from anisotropic consolidation ( $CK_0U$ , $CK_0D$ ) .....	230
Fig. 11.1 Active thrust (retaining wall).....	237
Fig. 11.2: Passive resistance (arch bridge).....	238
Fig. 11.3 State of rest .....	238
Fig. 11.4 Mobilization curve .....	239
Fig. 11.5 Retaining wall .....	239
Fig. 11.6 Horizontally loaded pile .....	240
Fig. 11.7 Active thrust.....	240
Fig. 11.8 Passive resistance.....	240
Fig. 11.9 Stress paths for active thrust and passive resistance.....	240

Fig. 11.10: Total and effective vertical stresses and the pore water pressure in a soil mass .....	241
Fig. 11.11: Total and effective horizontal stresses and the pore water pressure in a soil mass .....	243
Fig. 11.12 Coulomb's model for active thrust .....	245
Fig. 11.13 Culmann's graphical method .....	247
Fig. 11.14 Rankine Model.....	248
Fig. 11.15 Reaching the failure criterion by attaining the active pressure (unloading stress path) .....	249
Fig. 11.16: Example of active stress distribution.....	250
Fig. 11.17: Example for computing the active pressure point of application .....	251
Fig. 11.18 .....	252
Fig. 11.19 .....	252
Fig. 12.1 Manually dug trench. ....	258
Fig. 12.2 Mechanically excavated trench.....	258
Fig. 12.3 Principle of manual drilling. ....	259
Fig. 12.4 Manual drilling. ....	259
Fig. 12.5: Mechanical drilling principle.....	260
Fig. 12.6: Mechanical drilling (wire line) .....	260
Fig. 12.7: Drilling bit .....	261
Fig. 12.8: Core catcher .....	261
Fig. 12.9: Retrieving the soil sample in Shelby tube .....	261
Fig. 12.10: Core boxes .....	261
Fig. 12.11: Reverse circulation drilling.....	262
Fig. 12.12: Sampling moulds at the soil's surface.....	263
Fig. 12.13: Shaping a block sample .....	264
Fig. 12.14: Waxing the Shelby tubes .....	265
Fig. 12.15: Sealed Shelby tube.....	265
Fig. 12.16 The Standard Penetration Test.....	266
Fig. 12.17 Modern split spoon sampler.....	267
Fig. 12.18: The Cone Penetration Test .....	276
Fig. 12.19: Non-normalized SBT chart [57] .....	279
Fig. 12.20: Normalized SBT <sub>n</sub> chart [58] .....	280
Fig. 12.21: Dynamic probing heavy (DPH) equipment .....	284
Fig. 12.22: Plate load test equipment .....	289
Fig. 12.23: Preparation steps prior to the plate load test.....	291
Fig. 12.24: Load-settlement chart for the plate load test.....	295
Fig. 12.25: Menard pressuremeter sketch .....	296

Fig. 12.26 DMT blade.....	297
Fig. 12.27: The DMT equipment .....	297
Fig. 12.28: Test steps .....	298
Fig. 12.29: The Vane Test.....	299



## **1 THE OBJECT AND A BRIEF HISTORY OF GEOTECHNICAL ENGINEERING**

Geotechnical engineering is the branch of technical sciences which deals with soils from a technical point of view. When used as a foundation ground, the soil is computed in terms of strength and stability just as any other structure, it may be used as a construction material and be reinforced like a composite element or it could act as a load upon other embedded structures. A special interest of geotechnical engineering is the stability analysis of soil masses, namely of the so-called landslides affecting large areas of land, especially in the hill or mountain regions.

Soils are detrital sedimentary rocks which consist in three phases: a mixture of mineral particles, water with dissolved salts and gas consisting mainly of air and water vapours. As it will be developed later on, the solid mineral part of the soil forms the “skeleton” of the material while the fluids fill the “voids”. It must be clearly understood that the soil is not a solid with wholes such as Swiss cheese, but rather an empty space filled with solid beads, so that the voids or the pores are in contact.

In this lecture notes book, by “Soil Physics” we are going to understand the set of laws and properties describing the constituents of the material, while by “Soil Mechanics”, the behaviour of the material under the action of various loads.

Further on, we are going to use two types of parameters: nature and state ones. The parameters of nature show describe those properties that do not alter when the material changes its environmental conditions (for example when it dries or when it is loaded), while the state parameters describe precisely the soli characteristic variation when the environmental conditions change. Even if at the first glance the border between nature and state parameters should be clear, there are exceptions, especially when non-linear parameters are simplified as linear or when various features are disregarded for the sake of simplification. A good example is the set of shearing strength parameters that

even if it is fixed in some conditions, such as in drained conditions, over 100-300kPa normal stress loading, it may be a completely set of values in undrained conditions over 700-1000kPa range.

Historically, most of the physical properties of soil (such as the grain size distribution or the moisture content) are known and studied for as long as people used materials for constructing structures, but the study of mechanical properties started only as late as the XVII-th century with the contributions of Robert Hooke (Fig. 1.1) who published in 1660 the famous anagram “ceiinossttuv” whose key, “ut tensio sic vis” he published only in 1678 due to the direct scientific competition with Isaac Newton. In the shape it was published it may be translated as “the elongation is proportional with the force” and it was the result of studying the behaviour of springs in the elastic range. This equation was obviously dependent on the physical configuration and geometry of the loaded system (such as its diameter or length). It is Thomas Young’s (Fig. 1.4) merit to normalize Hooke’s law dividing the force by the area and thus yielding the stress and the elongation by the initial length, resulting the strain and transforming the equation in a material law. Young’s paper was published in 1807, but the idea per se was not his own, it was taken from a paper of Giordano Ricatti (Fig. 1.3) published in 1782, who, at his turn, reformulated it from a Leonhard Euler’s work (Fig. 1.2) issued in 1727.



Fig. 1.1: Robert Hooke  
(1635 - 1703)

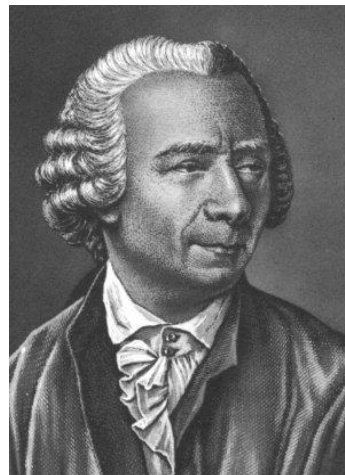


Fig. 1.2: Leonhard Euler  
(1707 – 1783)

Important contributions to the study of stress-strain behaviour belong to Siméon Denis Poisson (Fig. 1.5) who showed, by the effect bearing his name, the distribution of strain on other directions that the one of the loading and also the input of Gabriel Léon Jean Baptiste Lamé (Fig. 1.6) who studied the elastic behaviour under deviatoric stress, the shearing modulus being also known as “second Lamé parameter”.



Fig. 1.3: Giordano Riccati  
(1709 - 1790)



Fig. 1.4: Thomas Young  
(1773 – 1829)



Fig. 1.5: Siméon Denis Poisson  
(1781 - 1842)

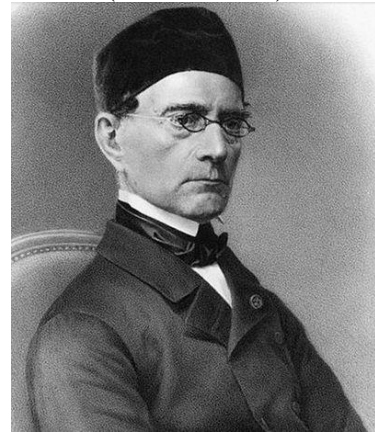


Fig. 1.6: Gabriel L. J. B. Lamé  
(1795 - 1870)

Tensor representation of stresses belongs to Augustin-Louis Cauchy (Fig. 1.7) who also proved the fact that the value of the stresses in a point depend on the normal direction to the studied direction in the point of interest. The



tensor representation through which in the same mathematical object were embedded both scalars (0 order tensor) as well as operations (both scalar and vectorial) allowed the identification of stress invariants as eigenvalues of the tensor, independent on the direction its elements are acting. George Green (Fig. 1.8) had another breakthrough due to the tensor formulation is the energy formulation, by adding to the tensor supplementary operations thus increasing the tensor order and fundamentally contributing to solving the problems of Lagrange (Fig. 1.9) mechanics.



Fig. 1.7: Augustin-Louis Cauchy  
(1789 – 1857)



Fig. 1.8: George Green  
(1793 – 1841)

The notion of shearing strength was first studied by Charles Augustin de Coulomb (Fig. 1.10) who published in 1773 a paper regarding his research on shearing failure of structures, noticing that the material strength is a linear equation between the maximum sharing stress and the normal one.

Lamé described the stress state around one point as an ellipsoid which joins the vertexes of all resultant vectors perpendicular on any plane which passes through that point, and starting from this ellipsoid, Carl Culmann (Fig. 1.11), studying the failure of beams, decomposed the resultants in normal and tangential stresses, obtaining in this way the representation of the stress state as a circle. Wrongly, this representation is recognised as being developed by Christian Otto Mohr (Fig. 1.12), who observed by carrying out a series of shearing tests that there is a common envelope of all stress states for which the capacity has been reached. By approximating this envelope through the

linear criterion proposed by Coulomb, the widely spread model in use nowadays has been obtained.

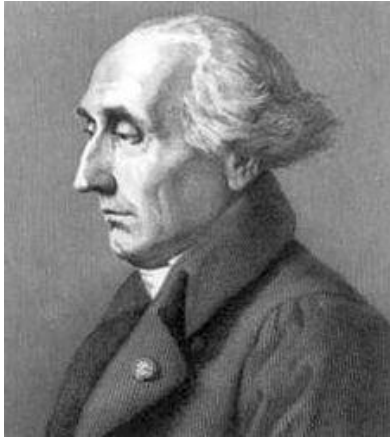


Fig. 1.9: Joseph-Louis  
Lagrange  
(1736 - 1813)

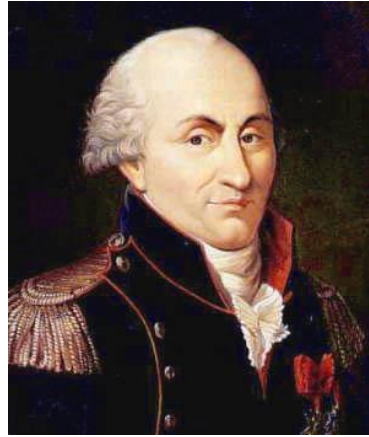


Fig. 1.10: Charles Augustin de Coulomb  
(1736 – 1806)

Expressing the Mohr-Coulomb criterion in three-dimensional coordinates, having as axes the principal stresses, the limit surface of the failure criterion has the shape of a hexagonal pyramid. In order to approach the perfect-elastic material, Henri Édouard Tresca (Fig. 1.13) developed the failure surface of hexagonal prism shape.



Fig. 1.11: Carl Culmann  
(1821 - 1881)



Fig. 1.12: Christian Otto Mohr  
(1795 - 1870)

The main disadvantage of the Mohr-Coulomb criterion and of the associated Tresca criterion is the discontinuity of the failure surface, fact that leads to numerical uncertainty concerning the direction of the normal in the corner points.



Fig. 1.13: Henri Édouard Tresca  
(1814 – 1885)



Fig. 1.14: Richard Edler von Mises  
(1883 - 1953)

This problem was solved by Richard Edler von Mises (Fig. 1.14), who transformed the Tresca criterion in a cylindrical surface having elliptical base, using a statement of the failure law according to the second invariant of the deviatoric tensor. In 1952, Daniel Charles Drucker (Fig. 1.15) and William Prager (Fig. 1.16) proposed a linear failure criterion similar to that of Mohr-Coulomb, which is continuous and has the shape of a conical surface, in which it is generalized the notion of shearing strength through a linear relationship between the first spherical invariant and the second deviatoric invariant.

The father of Geotechnical Engineering, Karl von Terzaghi (Fig. 1.18), observed that the deformation of the soil under compression loads is actually the rearrangement of the solid particles in a denser state, and if the material is saturated, the drainage of water is necessary in order to have settlements. Expressing the stress equilibrium between the solid skeleton and the pore water, he states the law of effective stresses starting from a model involving drainage and deformation on a single direction, generalizing the flow law of Henry Darcy (Fig. 1.17) in unsteady state, considering the behaviour of the solid skeleton as being linear elastic. He calls this process “consolidation”. In 1941, Maurice Anthony Biot generalizes the equation of consolidation in three dimensions.



Fig. 1.15: Daniel Charles Drucker  
(1918 - 2001)



Fig. 1.16: William Prager  
(1903 – 1980)



Fig. 1.17: Henry Darcy  
(1803 – 1858)



Fig. 1.18: Karl von  
Terzaghi  
(1883 - 1953)



Fig. 1.19: Maurice  
Anthony Biot  
(1905 - 1985)

Although at the present day the behaviour of the soil under loads is described using various constitutive laws, the determinant contribution of the fathers of the Theory of Elasticity and Plasticity and of Soil Mechanics leads to ensuring the compatibility of any progress with the simple and efficient physical and mathematical models created by them.



## **2 ORIGIN OF SOILS**

By definition, the term soil stands for a material mainly made of solid particles resulted from weathering of different rock types. The physical properties of soils vary widely function of the parent rock type as well as the intensity and type of the weathering.

In pedology and geology soil is defined as a mixture of mineral grains, organic matter, liquids, gases and organisms that supports plant life. The thickness of the soil layer is generally of tens of centimetres, up to a conventional maximum of 2 meters.

In geotechnical engineering a **soil** is a three phase material composed of: mineral grains (solid particles), water and air that supports foundation systems or can be used as an infrastructure construction material. The thickness of the soils ranges from meters to tens of meters and sometimes to hundreds of meters.

For the foundation and earthworks the material with high organic content is removed due to its inferior mechanical properties, the “geotechnical engineering soil” starting from where the “pedology soil” ends, the latter being usually called “topsoil”.

## 2.1 The rock cycle

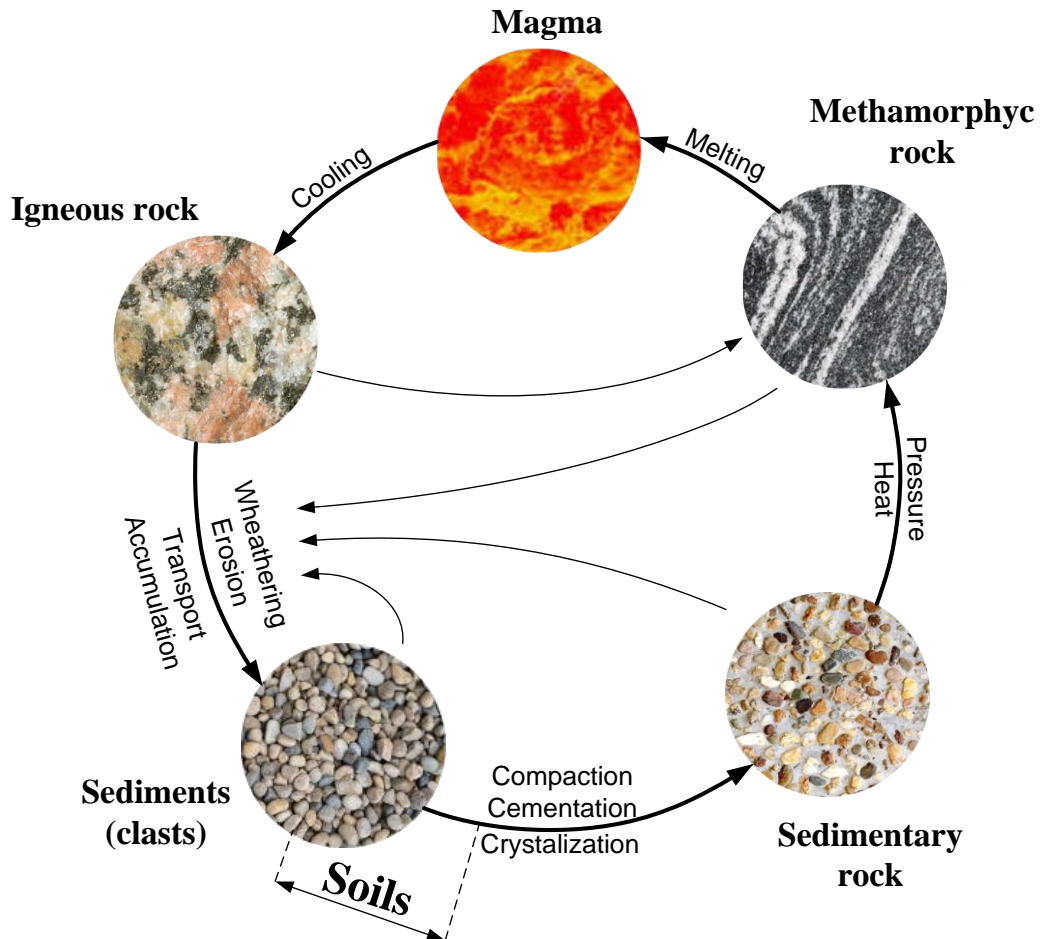


Figure 2.1 The Rock Cycle

Based on the way they are formed there are three major rock types: igneous rocks, sedimentary rocks and metamorphic rocks. The formation cycle and the processes associated with each rock type are represented in Figure 2.1 and will be briefly discussed in the following.

## 2.2 Igneous rocks

The **igneous rocks** are formed by cooling of magma. Magma is a mixture of molten or semi-molten rock, along with gases and other volatile elements,

which originates from the Earth's mantle. The type of igneous rocks formed depends on the initial chemical composition of the magma as well as the rate of cooling.

The minerals formed by the cooling of magma are called primary minerals. Silicon (Si) and Oxygen (O) are the main constituents of the magmas, thus resulting that all the rock forming minerals (the common minerals that make up approximately 90 percent of the Earth's crust) are silicate minerals.

The rate of cooling influences the crystal size. A slow rate of cooling will lead to the formation of coarse crystals, a fast rate of cooling to small crystals, while a very fast rate of cooling to an amorphous structure (no crystals formed).

Each mineral type has a different crystallization temperature (equal to the melting temperature, but reached by decreasing temperature – cooling of magma) resulting in a solidification (crystallization) of some mineral types (Mg and Fe silicate) before other mineral types (Na and K silicate), process described by the Bowen's Reaction Series. The chemical composition of reference minerals shown in Bowen's Reaction Series are given in Fig. 2.1.

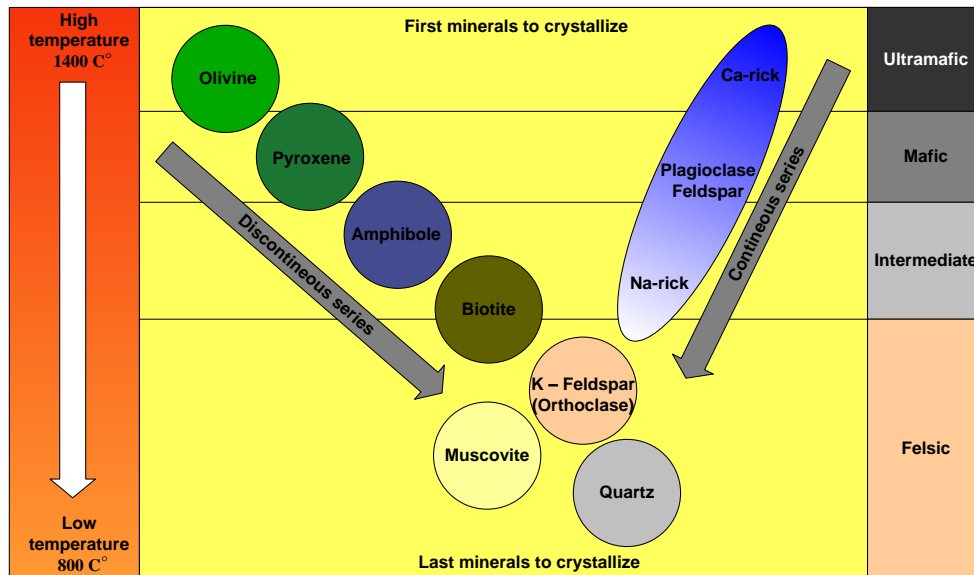


Fig. 2.1: Bowen's Reaction Series



Tab. 2.1: Chemical composition of reference minerals

Mineral	Chemical composition
Olivine	$(\text{Mg,Fe})_2\text{SiO}_4$
Augite (Pyroxene group)	$(\text{Ca,Na})(\text{Mg,Fe,Al,Ti})(\text{Si,Al})_2\text{O}_6$
Hornblende (Amphibole group)	$\text{Ca}_2(\text{Mg, Fe, Al})_5 (\text{Al, Si})_8\text{O}_{22}(\text{OH})_2$
Biotite (Black Mica)	$\text{K}(\text{Mg,Fe})_3(\text{AlSi}_3\text{O}_{10})(\text{F,OH})_2$
Calcium Feldspar	$\text{Ca}(\text{Al}_2\text{Si}_2\text{O}_8)$
Sodium Feldspar	$\text{Na}(\text{Al}_2\text{Si}_2\text{O}_8)$
Potassium Feldspar	$\text{K}(\text{Al}_2\text{Si}_2\text{O}_8)$
Muscovite (White Mica)	$\text{KAl}_2(\text{AlSi}_3\text{O}_{10})(\text{F,OH})_2$
Quartz	$\text{SiO}_2$

### 2.3 Weathering

Weathering is the breaking down of natural and artificial materials through contact with the Earth's atmosphere, water and organisms. It involves chemical, physical and biological processes and "constitutes the first step in the chain of processes that produce sedimentary rocks" [1].

#### 2.3.1 Physical weathering

Physical weathering, also called mechanical weathering, is the process by which rocks are broken into smaller fragments, without changing the chemical or mineralogical composition. By fragmenting the parent rock there is an increase of granular material specific surface which will directly influence the intensity of the chemical and biologic processes.

The main physical weathering factors are: insolation, frost cycles, abrasion, and salt weathering.

**Insolation** is the set of phenomena taking place in the crystalline mass due to the sun exposure variation. During the daytime the rock mass surface heats up and dilates. Due to temperature variation, the exterior part of the soil mass dilates more than the deeper one leading, due mainly to fatigue, to rock exfoliation of the superficial region. The insolation is more severe as the temperature variation from day to night is larger and the rock has a darker colour.

The **frost cycles** play an important role in rock disaggregation in the climate areas with temperature variation around the 0°C point. So, during the thawing periods, the water infiltrates in the rock voids and cracks after which, in cold times, water freezes, expands and exerts high pressures on the void walls pulling them apart.

**Abrasion** is polishing the rocks under the effect of moving fluids (air or water) containing solid particles in suspension. Due to abrasion, the particles become rounded or, in the rock masses, the layers with weaker material are removed uncovering the harder rocks.

Some dissolved salts precipitate and recrystallize filling some voids in the rock. The resulting crystals may increase their volume and push against the rock walls in a fashion similar to the one described for freezing, developing pressures reaching even 1.3 – 1.5MPa which crush neighbouring minerals.

### **2.3.2 Chemical weathering**

Chemical weathering involves changes that can alter both the chemical and the mineralogical composition of rocks. Minerals in the rocks are attacked by water and dissolved atmospheric gases (oxygen, carbon dioxide), causing some components of the minerals to dissolve and be removed in solution [1]. Some minerals constituents can interact in situ and crystallize, thus forming new mineral phases. These chemical changes, combined with the physical weathering break apart the fabric of the parent rock, eventually leading to sound rock blocks and a loose residue of weather resistant grains and secondary minerals.

Each mineral type has a different resistance to chemical weathering. The mineral formed at higher temperatures and pressures in the Bowen's reaction series are less resistant to chemical weathering than those formed at lower temperatures. Moreover, the weathering processes proceed at different rates depending on the climate and the grain size of the rock undergoing weathering.

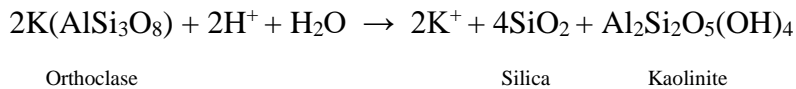
The major chemical weathering processes are: simple solution, hydrolysis, oxidation and reduction.

**Simple solution**, also called *congruent dissolution*, when a mineral goes into solution completely (no precipitate is formed). In the presence of meteoric water simple solution of highly soluble minerals (calcite, dolomite, gypsum, and halite) occurs, forming the well-known lapies surface that are very usual in outcropping limestones. This process is sometimes called carbonation.

Carbonation is one of the main actions upon limestone rock masses, being the origin of the karst phenomena. Although the CO<sub>2</sub> concentration in air is relatively low (0.03%), due to the ease of dissolution, concentrations into water of up to 9% may be reached, rendering it very aggressive not only to rocks but also against buried concrete structures.

**Hydrolysis** is a chemical reaction between acids and silicate minerals that breaks down the minerals and releases metal cations and silica (SiO<sub>2</sub>), but does not lead to the complete dissolution of the silicate minerals. This incomplete dissolution is called *incongruent dissolution*. If minerals containing aluminum (Al) undergo incongruent dissolution during weathering, then clay minerals such as smectite, illite and kaolinite may form as by-products of hydrolysis.

The chemical weathering of orthoclase feldspar to form clay minerals, silica and potassium cations is shown below:



The released potassium cations are carried away in solution as potassium carbonate is consumed by plants.

The clay minerals are secondary minerals and they are of key importance in geotechnical engineering and will be further discussed in this book.

**Oxidation** has the most important influence upon organic substances as well as on some magmatic and metamorphic ones originated in oxygen-free environments. Oxidation is readily noticeable in colour change of minerals. Thus, oxidizing iron (Fe) minerals, the colour changes into yellowish-red or brown, while the minerals with manganese (Mn) turn into greyish-black. Organic matter, originally black or brown, become whitish.

### **2.3.3 Biological weathering**

Biological activity acts upon rocks with a wide set of epigenous factors decaying rocks. Bacteria, aerobic or anaerobic, attack virtually all types of minerals, either directly, synthesizing their component chemical elements, or indirectly, by the action of the aggressive waste resulted from biological activity.

The plants are the most aggressive upon rocks since they extract minerals from the ground water and release, when rotting, substances accelerating dissolution process.

The mechanical effect of plants is mostly carried out by the pressure exerted by roots expanding rock cracks and voids. The largest pressures are induced by taproots plants that may reach as much as 1.5MPa.

At their turn, plants and animals accumulation generate, at their turn, new rocks such as limestone, coal and so on.

### **2.4 Transport of weathering products**

The weathering process generates three types of weathering products that are important to the formation of sedimentary rocks [1]:

- source-rock residues consisting of chemically resistant minerals and rock fragments derived particularly from siliceous rocks such as granite, rhyolite, gneiss, etc.;
- secondary minerals, especially clay minerals, formed in situ by chemical recombination and crystallization, mainly as a result of hydrolysis and oxidation;
- soluble constituents released from parent rocks mainly by hydrolysis and solution.

These weathering products represent soils from the engineering point of view.

These products may remain in place in which case they are called residual and they are usually enriched with organic content from plant or may be transported to other places by gravity, water, wind, and ice.

Depending on their transport agent and deposition environment the transported soils may be classified into several groups:

- Alluvial soils—transported by running water and deposited along streams;
- Lacustrine soils—formed by deposition in quiet lakes;
- Marine soils—formed by deposition in the seas;
- Glacial soils—formed by transportation and deposition of glaciers;
- Aeolian soils—transported and deposited by wind;
- Colluvial soils—formed by mass movement of soil from its original place by gravity, during landslides;
- Proluvial soils –transported by torrent water and settle to the slope toe under the shape of a fan (Fig. 2.3);
- Diluvial soils—formed at the bottom (toe) of the slope by the action of gravity, but not by mass transport.

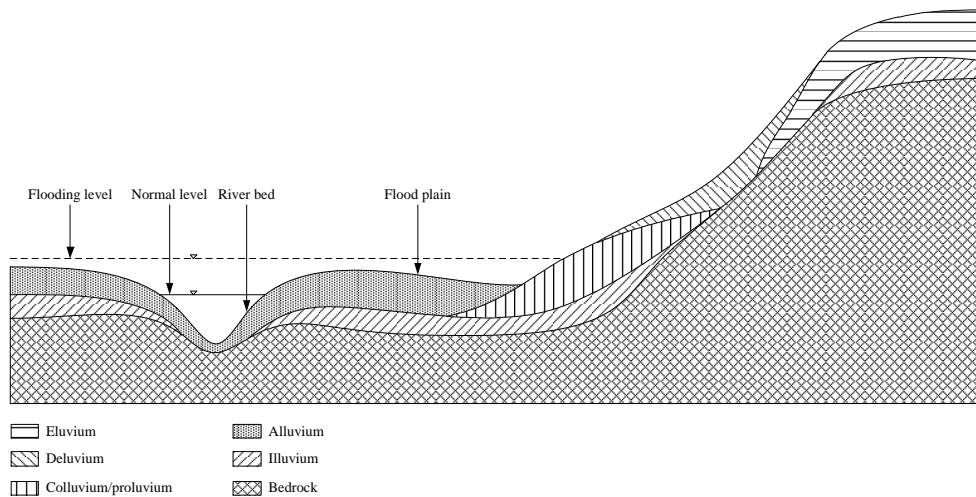


Fig. 2.2: Types of soil deposits

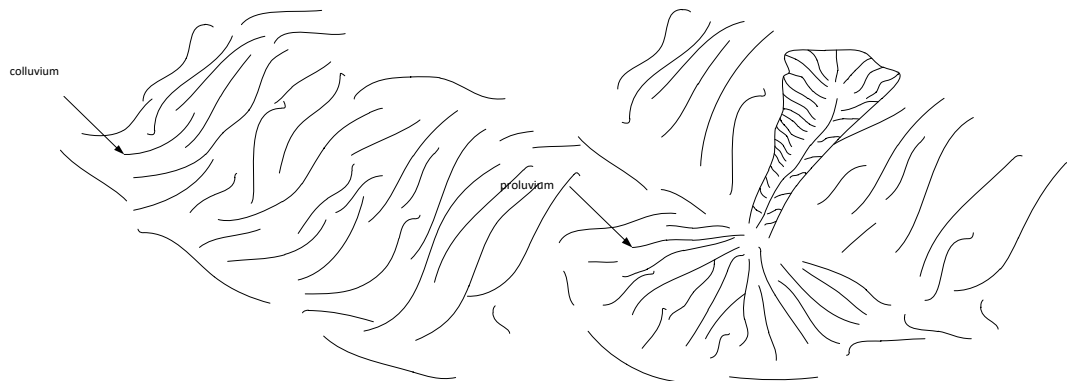


Fig. 2.3: Colluvial and proluvial deposits

Colluvial and proluvial deposits are both formed to the hill or mountain base due to the water flow action with the main difference that the former is the result of a homogenous erosion of the whole surface and the layer shape stretch along the slope toe, while in the case of the latter the material comes from torrential erosion and the final shape of the layer is concentrated under the shape of a cone or a fan generating localised lithological discontinuities. Both types of layers are very heterogeneous in nature and grain size.

Alluvial deposits are formed by running surface waters to the convex bend of the river meanders and over the flood plain. In some cases, alluvium sedimentation may occur to in the riverbed area. Due to the water flow, the shape of the soil grains is generally smooth and rounded.

Lacustrine and marine deposits are made to the bottom of still surface waters, fresh or salt. Generally, the resulting soil layers are homogenous and fine, the colloidal size particles being allowed to settle in the low-disturbance environment. Usually the marine deposits have salt cementation bonds among the grains.

Glacial lithological structures are formed by the slow mountain slope erosion of glaciers resulting in the so-called tills (inhomogeneous and unsorted mix of mineral particles ranging in size from clay to large boulders).

Aeolian soils are transported by the wind and are accumulated in dry environment. Since the wind power cannot pull-out very fine particles with strong cohesive bond or large and heavy particles, this kind of lithological structures range in grain size from silt to sand. The particles have irregular

and scratched surfaces. In few cases, as for loessial soils, cementation occurs before compaction. The structure remains loose and if the normally dry soil with soluble cementation bonds gets moist it collapses into a denser state, fact for which loessial soils are also called collapsible.

Summarizing, depending on the erosion and transportation agent, resultant soils may have sharp (wind) or round particles (water) and may be sorted or unsorted (gravity and water have a strong screening effect). Once the sedimentation process starts, two main processes which strongly impact the mechanical properties occur:

- cementation, being the chemical bond developed among solid particles which provides the soil with additional structural strength;
- compaction, which occurs due to the upper layer's own weight and results in an improvement of the mechanical behaviour of the soil as it densifies and becomes a structure with lesser voids

## **2.5 Sedimentary rocks**

The deposits of gravel, sand, silt, and clay formed by weathering erosion and transport are compacted by overburden pressure as the thickness of the deposits grow and cemented by agents like calcite, quartz, and iron oxide. Cementing agents are carried by groundwater in solution. They fill the spaces between particles and form sedimentary rock. Rocks formed in this way are called detrital sedimentary rocks.

From a geotechnical point of view there is a clear distinction between soils and sedimentary rocks, but geologists include the soils in the sedimentary rock describing them as uncemented detrital sedimentary rocks.

Tab. 2.2: Soils and the corresponding sedimentary rock (after cementation)

<b>Soil type</b>	<b>Sedimentary rock</b>
Gravel	Conglomerate
Sand	Sandstone
Silt	Siltstone
Clay	Mudstone or shale

Sedimentary rocks can also be formed by chemical precipitation and bioaccumulation of organic material (sometimes bioconstruction). This rock

types are classified as chemical sedimentary rock and biochemical sedimentary rocks.

Sedimentary rock may undergo weathering to form sediments (and then soils) or may be subjected to increase of heat and/or pressure and become metamorphic rock.

## **2.6 Metamorphic rocks**

Metamorphism is the process of changing the texture, chemical and mineralogical composition of rocks by heat and pressure without melting (which would result in forming of igneous rocks). During the metamorphism process, some mineral grains are sheared to give a foliated texture to metamorphic rock and new minerals are formed.

By increasing the temperature above 200 C° some clay minerals are transformed (metamorphosed) to chlorite, graphite and mica, forming a rock type named slate. If the temperature increases over 250 – 300 C° the slate is transformed into phyllite. If the temperature and pressure further increase the phyllite turns into schist.

There are many types of metamorphic rocks with distinct mineralogical composition, texture and physical properties. The type of metamorphic rock depends on the parent rock (in case of metamorphic rocks called protolith), and the grade metamorphism (high-grade, low-grade, intermediate-grade function of the intensity of temperature and pressure).

A common property of metamorphic rock is the rock cleavage induced by the schistosity.

When outcropping the metamorphic rock are subjected to weathering and form soil and when they are buried by overlaying rocks or subjected to subduction they melt to form magma and repeat the rock cycle



## **2.7 Test your understanding**

**Problem 2.1**

What are secondary minerals?

**Problem 2.2**

Which is the common grain size for eolian deposits?

**Problem 2.3**

Which is the common grain size for alluvial deposits?

**Problem 2.4**

What is the difference between soil and topsoil?

**Problem 2.5**

Specify 2 weathering agents.

**Problem 2.6**

What are the most common transport agents?

**Problem 2.7**

What is the difference between sedimentary rocks and soils?

### 3 SOIL GRADING

Soil grading (or grain size analysis) represents the description of the soil particle sizes in terms of size ranges, called grading fractions, expressed as a percentage of the total dry weight. Although the concept is the same, grading size ranges differ from one standard to another. In Romania it is implemented the European standard describing the soil grading classification SR EN ISO 14688 – “Geotechnical investigation and testing - Identification and classification of soil” (part 1 [2] and part 2 2005 [3]). The grading fractions specified in the standard are presented below.

Tab. 3.1: Standard grading fractions according to SR EN ISO 14688-1/2004

Soil description	Major fractions	Secondary fractions	Symbol	Particle size [mm]
Very coarse		Large blocks	LBo	> 630
		Blocks	Bo	200 ÷ 630
		Cobbles	Co	63 ÷ 200
Coarse	Gravel (Gr)	Coarse gravel	CGr	20 ÷ 63
		Medium gravel	MGr	6.3 ÷ 20
		Fine gravel	FGr	2 ÷ 6.3
	Sand (Sa)	Coarse sand	CSa	0.63 ÷ 2
		Medium sand	MSa	0.2 ÷ 0.63
		Fine sand	FSa	0.063 ÷ 0.2
Fine	Silt (Si)	Coarse silt	CSi	0.02 ÷ 0.063
		Medium silt	MSi	0.0063 ÷ 0.02
		Fine silt	FSi	0.002 ÷ 0.0063
		Clay	Cl	≤ 0.002

A certain soil sample usually has particles belonging to more than one of the grading sizes shown in Tab. 3.1 and the name of the soil is determined function of the proportions in which the grading fractions are found. In order

to precisely assess a soil description in terms of particle sizes, a grading analysis should be performed. The standard currently in-force that describes the methodology of performing a grading analysis is STAS 1913/5-85 – “Foundation ground. Determination of grain size” [4]. Although this standard states at the beginning that the described procedures are applied to soils classified according to a standard different from SR EN ISO 14688-1/2004 [2], its methods are still applicable.

The standard methods for assessing the soil grading are:

- direct measuring – for grains larger than 125mm;
- sieving (screening) method – for grains larger than 0.063mm;
- hydrometer method – for grains smaller than 0.063mm.

These methods may be used exclusively if more than 90% of the mass of the material is suitable for only one method, in terms of particle sizes, otherwise combined methods will be used, each for the applicable case. The samples used for grain size analysis may be either disturbed or undisturbed, independent on the method, since the material will have to break its structure during the procedure.

### **3.1 Screening method**

The screening method is suitable for grain size analysis in cohesionless soils, and it consists of shaking the soil sample through a set of sieves (the standard sizes are given in SR ISO 3310-1 [5], ISO 3310-2 [6] and SR ISO 3310-3 [7]) that have progressively smaller diameters (Fig. 3.1).

The mass of soil necessary for the sieving method depends on the type of material and is usually a choice based on the experience of the operator. According to STAS 1913/5-85 [4], the following minimum material quantities should be used:

- 5kg for cobbles;
- 2kg for gravel;
- 1kg for gravel with sand;
- 400g for coarse and medium sand;
- 100g for fine sand;
- 70g for sand with much fines.

In preparation, the tested sample is first dried in the oven at 105°C. After drying, the sample is scaled on an electric balance that has a precision of at least 0.1% of the total mass. Let's denote the dry mass of the material as  $m_{dry}$ , which we'll use later on.

Then, to make sure the particles are not stuck to each other, thus forming larger clumps that may yield inaccurate results or losing some of the fine material due to it being adhered to larger grains, the sample is placed in a dispersive agent solution (usually Lithium Carbonate  $Li_2CO_3$ ).

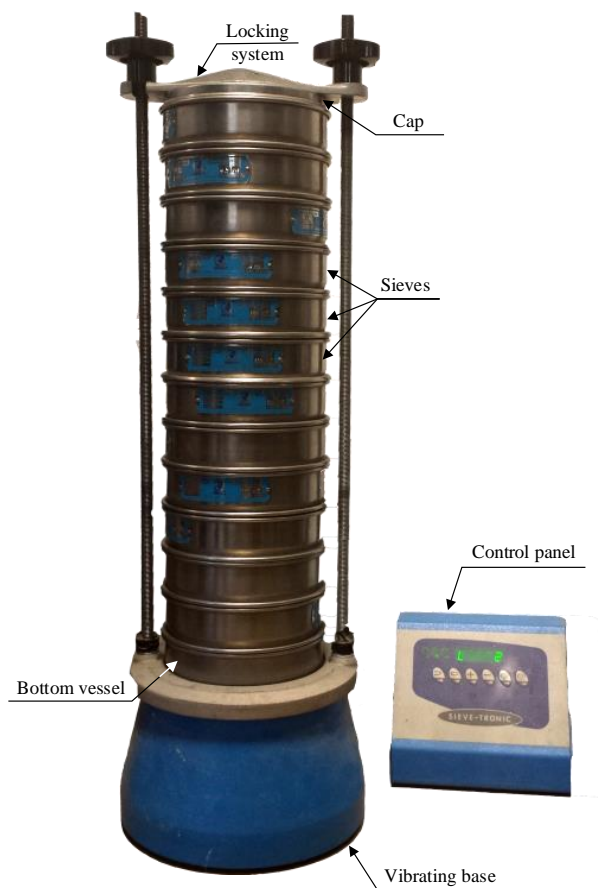


Fig. 3.1: Sieving test assembly

The material is then washed on the 0.063mm sieve to separate the fines (the particles smaller than 0.063mm) from the rest of the sample. Let's denote the

dry mass of the material that passed through the sieve when washed by  $m_{\text{washed}}$ .

The material remained on the 0.063mm sieve will then be dried and scaled. If the dry mass is at least 10% of the total dry mass ( $m_{\text{dry}}$ ), it will undergo sieving test. On the other hand, if the material that passed through the sieve when washed ( $m_{\text{washed}}$ ) will undergo hydrometer test if its mass is at least 10% of the total dry mass ( $m_{\text{dry}}$ ).

Assuming there is enough material for sieving test, the total mass of soil to be sieved will be obtained after drying. Let's denote that mass by  $m_t$ . The sample is then placed on the top of the sieving set and is shaken for 10 minutes if a vibrating table is available or for 15 minutes by hand.

After the sieving, the remained soil mass on each sieve is weighed, including the mass that eventually passed through the last sieve. The sum of the total masses thus measured, should not differ with more than 1% than the initial mass weighed before sieving.

The obtained results are to be used to compute the percentage of mass that remained on the sieves ( $m_{\text{di}}$ ) and the percentage of mass that passed through the sieves ( $m_{\text{pi}}$ ), required for grain size analysis graphical interpretation, discussed in chapter 3.3.

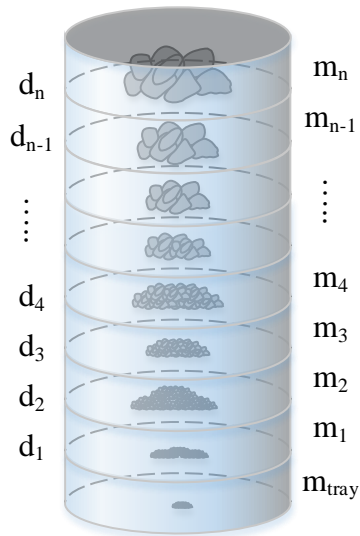


Fig. 3.2: Soil particles remained on the sieves after the test

The mass percentages remained on the sieves, according to Fig. 3.2, are computed as:

$$\begin{aligned}
 m_{d_{\text{tray}}} &= \frac{m_{\text{tray}}}{m_{\text{dry}}} \cdot 100 \\
 m_{d_1} &= \frac{m_1}{m_{\text{dry}}} \cdot 100 \\
 m_{d_2} &= \frac{m_2}{m_{\text{dry}}} \cdot 100 \\
 &\vdots \\
 m_{d_{n-1}} &= \frac{m_{n-1}}{m_{\text{dry}}} \cdot 100 \\
 m_{d_n} &= \frac{m_n}{m_{\text{dry}}} \cdot 100
 \end{aligned} \tag{3.1}$$

where  $m_i$  are the masses that remained on the sieve with diameter  $d_i$ . In other words, the mass  $m_i$  is the mass of particles with diameter smaller than  $d_{i+1}$  and larger than  $d_i$ .

As previously discussed, the test is valid if the error (Err) is less than 1%. The error is computed as the difference between the sum of the masses on the sieves and the mass of the sieved soil, mainly:

$$\text{Err} = \frac{m_t - \sum m_i}{m_t} \cdot 100 < 1\% \quad (3.2)$$

Computing the percentage of masses that passed through the sieves,  $m_p$  can be done as follows:

$$\begin{aligned} m_{p_1} &= \frac{m_{\text{tray}} + m_{\text{washed}}}{m_{\text{dry}}} \cdot 100 \\ m_{p_2} &= m_{p_1} + m_{d_1} \\ m_{p_3} &= m_{p_2} + m_{d_2} \\ &\vdots \\ m_{p_{n-1}} &= m_{p_{n-2}} + m_{d_{n-2}} \\ m_{p_n} &= m_{p_{n-1}} + m_{d_{n-1}} \end{aligned} \quad (3.3)$$

If the errors are acceptable, the percentage of mass on the top sieve ( $m_{dn}$ ) and the percentage of passes through the top sieve ( $m_{pn}$ ) should add up to 100%.

### 3.2 Hydrometer method

The washed material that passed through the 0.063mm sieve will undergo the sedimentation test through the hydrometer method if its dry mass ( $m_{\text{washed}}$ ) is significant with respect to the total dry mass ( $m_{\text{dry}}$ ), i.e. is more than 10% than the total mass.

The hydrometer method is based on Casagrande's idea to measure the size of the fine particles by placing them in a fluid and monitoring the sedimentation of the solids. According to Stoke's law, which describes the falling velocity of a solid sphere through water:

$$v = \frac{\rho_s - \rho_w}{18\eta} \cdot d^2 \quad (3.4)$$

where:

- v – velocity;
- $\rho_s$  – density of solid particles;
- $\rho_w$  – density of water;
- $\eta$  – viscosity of water;
- d – diameter of the solid particles

The hydrometer test is performed using a small amount of fine soil, usually about 50÷100g of dry mass. The sample is mixed with dispersing agent solution, usually sodium hexametaphosphate, but sodium silicate may also be used with good results if the clay content is not very high. The dispersing agent breaks the bonds that may have formed between the particles and prevent them from forming clumps.

The obtained mixture of solids and dispersing agent solution is placed within a sedimentation cylinder (marked for 1000cm<sup>3</sup>) and distilled water is added up to 1000cm<sup>3</sup>. The suspension is then stirred until a homogenous material is formed and the sedimentation process will begin when the stirring ends. The hydrometer is then placed within the suspension at a time t, measured from the start of the sedimentation. The hydrometer will measure the density of the suspension in the vicinity of its bulb, at the depth  $H_r$  (Fig. 3.4). The measured density is a function of the amount of solids present in the suspension at that depth. The diameter of those particles may be expressed based on Stoke's law (3.4):

$$d = \sqrt{\frac{18\eta}{\rho_s - \rho_w} \cdot v} = \sqrt{\frac{18\eta}{\rho_s - \rho_w} \cdot \frac{\text{distance}}{\text{time}}} = \sqrt{\frac{18\eta}{\rho_s - \rho_w} \cdot \frac{H_r}{t}} \quad (3.5)$$

where  $H_r$  is the distance from the surface of the suspension to the centre of buoyancy of the hydrometer and t is the time since the start of the sedimentation.

This implies that the soil particles with diameter smaller than d, from the above equation, are still in suspension above the hydrometer's centre of buoyancy, and the larger particles have already settled below this point.

The depth of the buoyancy point is to be computed function of the hydrometer reading. This is done by obtaining a relation between the depth,  $H_r$ , and the



reading,  $R$ , at certain calibration points. Usually, the calibration points are readings corresponding to 0.995, 1.000, 1.005, 1.010, 1.015, 1.020, 1.025 and 1.030 g/cm<sup>3</sup>. Thus, the following relation will be obtained:

$$H_r = J_1 + J_2 R_h \quad (3.6)$$

where  $H_r$  is the suspension depth,  $R_h$  is the hydrometer reading and  $J_{1,2}$  are the parameters of the equation, obtained through regression.

For a given reading, the depth of the buoyancy point can be obtained using the following relation:

$$H_r = H + \frac{1}{2} \left( h - \frac{V}{S} \right) \quad (3.7)$$

where:

- $H$  – the distance from the top of the bulb to the reading mark;
- $h$  – the height of the bulb;
- $V$  – the volume of the bulb;
- $S$  – interior area of the cylinder.

The hydrometer measures the density  $\rho$  of suspension in water of all the solid particles still afloat by that moment, i.e. having a maximum diameter  $d$ , smaller than the particles that already settled. The hydrometer does not show this density directly, since the density variations are very small, instead it shows a reading  $R$ , representing the most significant figures of density variation (Fig. 3.3). Thus, the density value of the suspension is multiplied by 1000 and the first two figures, “10” are cut off. Therefore, the actual density is computed as:

$$\rho = 1 + \frac{R}{1000} [\text{g/cm}^3] \quad (3.8)$$

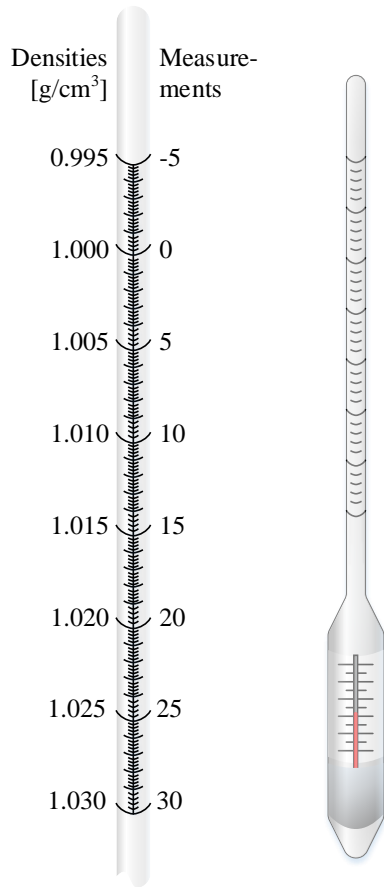


Fig. 3.3: Hydrometer measurements

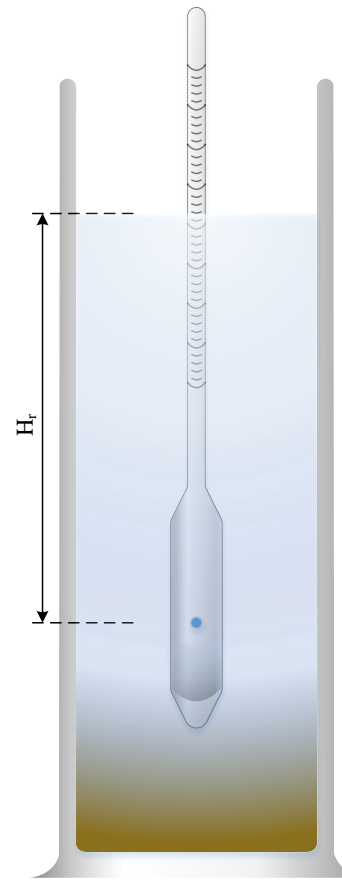


Fig. 3.4: Depth of buoyancy

Assuming that the density measured by the hydrometer is an average density of the fluid and that all the particles larger than  $d$  have already settled, one can express the mass of the suspension depending on the measured density:

$$m_{\text{water+solid}} = \rho \cdot V = \left(1 + \frac{R}{1000} [\text{g/cm}^3]\right) \cdot V \quad (3.9)$$

If the total mass of the suspension is  $1000\text{cm}^3$ , then:

$$m_{\text{water+solid}} = \left(1 + \frac{R}{1000} [\text{g/cm}^3]\right) \cdot 1000 [\text{cm}^3] = 1000 + R [\text{g/cm}^3] \quad (3.10)$$

The total mass may also be expressed as the sum between the solid particles still in suspension and the mass of water:

$$m_{\text{water+solid}} = m_w + m_s \quad (3.11)$$

where  $m_w$  is the mass of water and  $m_s$  is the mass of solids in suspension. The mass of water can further be expressed as:

$$m_w = \rho_w V_w = 1 \cdot V_w \quad (3.12)$$

Where  $\rho_w$  is the density of water (which can be accepted to be equal to  $1\text{g/cm}^3$ ) and  $V_w$  is its volume. But the volume of water is just the difference between the total volume and the volume of the solids,  $V_s$ , which at its turn is the ratio between the mass of the solids,  $m_s$ , and their density,  $\rho_s$ :

$$V_w = V - V_s = 1000 - \frac{m_s}{\rho_s} \quad (3.13)$$

Now, going back to equation (3.11), the total mass may be written as:

$$m_{\text{water+solid}} = 1 \cdot \left( 1000 - \frac{m_s}{\rho_s} \right) + m_s \quad (3.14)$$

But taking into account that the mass may also be expressed as described in (3.10), then these two relations must be equal:

$$\left( 1000 - \frac{m_s}{\rho_s} \right) + m_s = 1000 + R \quad (3.15)$$

$\Leftrightarrow$

$$m_s(\rho_s - 1) = \rho_s \cdot R$$

Therefore, the mass of the solids still in suspension, which are solids with diameters smaller than  $d$ , computed based on the measurement  $R$ , is:

$$m_s = \frac{\rho_s}{\rho_s - 1} R \quad (3.16)$$

So, the mass percentage of solids smaller than  $d$  is:

$$m_p = \frac{m_s}{m_d} 100 = \frac{100 \cdot \rho_s}{m_d (\rho_s - 1)} R \quad (3.17)$$

where  $m_d$  is the dry mass of the soil used for the hydrometer test.

The hydrometer reading is not used as is, since two corrections must be made: a temperature correction,  $C_t$ , compensating against 20°C, at which the hydrometer is calibrated, and a meniscus correction,  $\Delta R$ . The temperature correction is provided in tables in some standards and it may be found in Appendix B of STAS 1913/5-85 [4] or Appendix 1 of STAS 1913/2-76 [8]. In order to obtain a temperature correction, the temperature needs to be read and recording at each hydrometer reading.

The meniscus correction is due to the surface tension of water that creates a rising meniscus on the surface of the cylinder. Moreover, the scale of the instrument may be slightly displaced with respect to the datum, so the meniscus correction must be determined for each hydrometer and is established according to the standard STAS 1913/5-85 [4] and represents the shift of the actual “0” reading in dispersing agent solution with distilled water, at 20°C, with respect to the “0” reading on the scale. Its value may be either positive or negative, depending on the hydrometer and the position of the “0” reading with respect to the top of the meniscus.

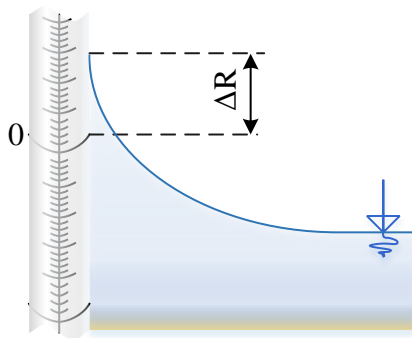


Fig. 3.5: Meniscus correction

Finally, the reading used in computations shall be corrected both with the temperature and the meniscus corrections:

$$R_{\text{corr}} = C_t + \Delta R \quad (3.18)$$

When performing the sedimentation test, a series of readings are made, at different times, after the stirring, over a span of 24h. The usual reading times, for which the diameters,  $d$ , and the percentages,  $m_p$ , are computed are usually: 30", 60", 2', 4', 8', 15', 30', 1h, 2h, 4h, 12h, 16h and 24h.

### **3.3 Graphical representation of grain size analysis**

There are two common ways of graphically expressing the results of the grain size analysis, based on basic statistical analysis: histogram and grading curve. These results may also be displayed on a ternary diagram, which has mainly classification purposes. Both of the graphs use semi-logarithmic scales, in which the percentages, on the vertical axes, are kept in decimal scale, while the diameters, on the horizontal axis, are presented in logarithmic form, to provide better representation over a large variation in diameters.

The histogram is a bar chart representing the percentage of mass between two consecutive diameters ( $m_d$ ). It is basically the same of any histogram interpretation of a large set of data, in which the classes are the diameters of the particles, chosen based on the used sieves (in the case of sieving test) or based on the computed diameters (in the case of hydrometer test). The height of the histogram bar represents the percentage of mass corresponding to that class. When the number of classes increases, the width of the bars decreases and the aspect of the graph tends to a probability density function.

Another, more used, graphical representation is the grading curve, which is the plot of the percentage of mass smaller than a given diameter ( $m_p$ ) against that given diameter ( $d$ ). The grading curve is a cumulative distribution function, which shows the probability of the particles in the sample to have diameters smaller than a certain diameter.

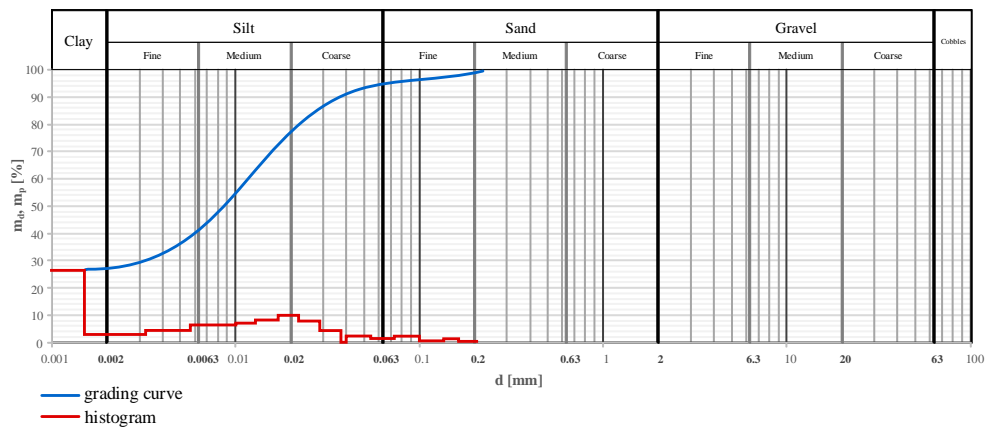


Fig. 3.6: Example of histogram and grading curve

From the grading curve the uniformity coefficient of the soil can be determined:

$$C_U = \frac{d_{60}}{d_{10}} \quad (3.19)$$

where  $d_{60}$  is the diameter corresponding to  $m_p=60\%$  on the grading curve and  $d_{10}$  is the diameter corresponding to  $m_p=10\%$ . In other words,  $d_x$  is the diameter with respect to which  $x\%$  of the mass of the soil has smaller particles.

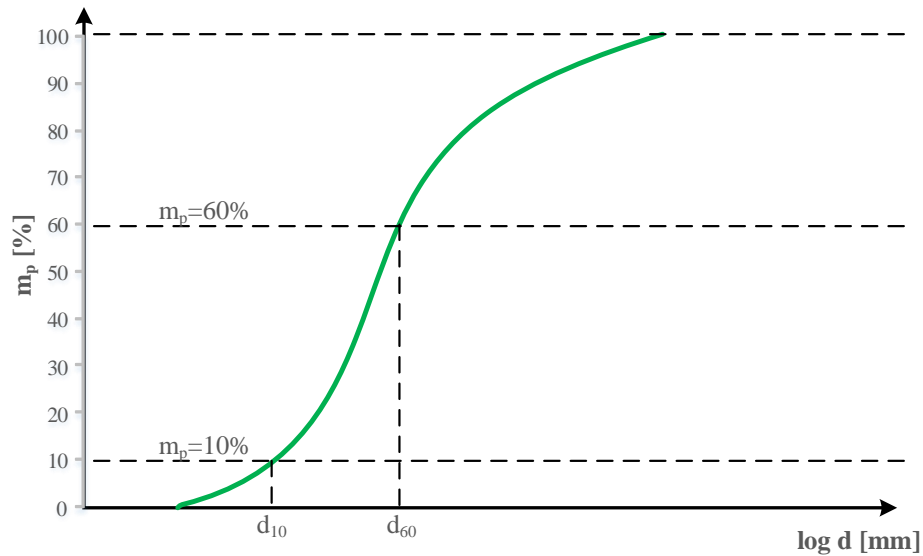


Fig. 3.7: Important diameters on the grading curve

Depending on the values of  $C_U$  the soils may be classified as:

- poorly graded, if  $C_U < 5$ ;
- well graded, if  $5 < C_U < 15$ ;
- very well graded, if  $C_U > 15$ .

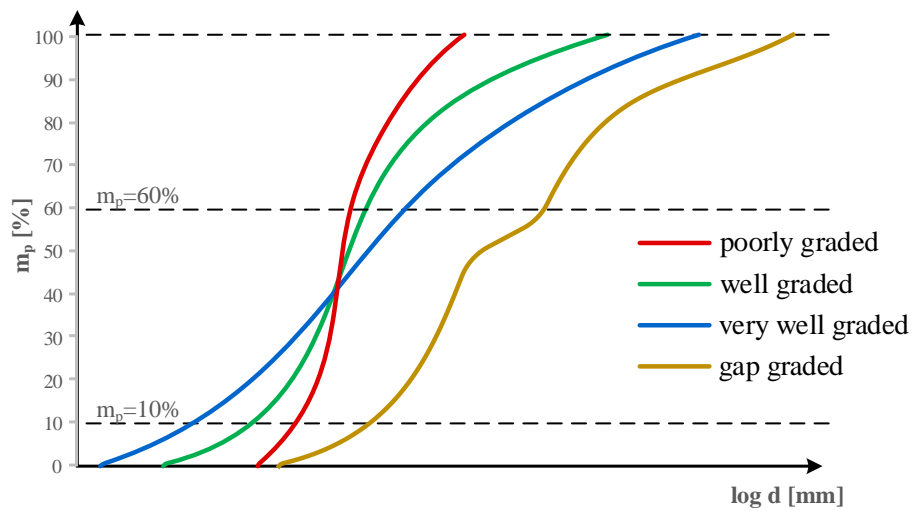


Fig. 3.8: Uniformity coefficient

Also, as it is shown in Fig. 3.8, the grading curve may also be classified as “gap graded”, when some of the sieves had no rested material, which implies that there are no particles in that size range.

The grading curve may also be used to determine the percentages of major grading fractions in the soil (clay, silt, sand, gravel, cobbles and blocks). The most important fractions, further used in soil classification, are clay, silt, sand and gravel. These four fractions are necessary when plotting the soil on the ternary diagram. The percentages for each of the fractions are determined by measuring the vertical distance (in percentage) between the points of intersection of the grading curve with the boundaries of the fractions (Fig. 3.9).

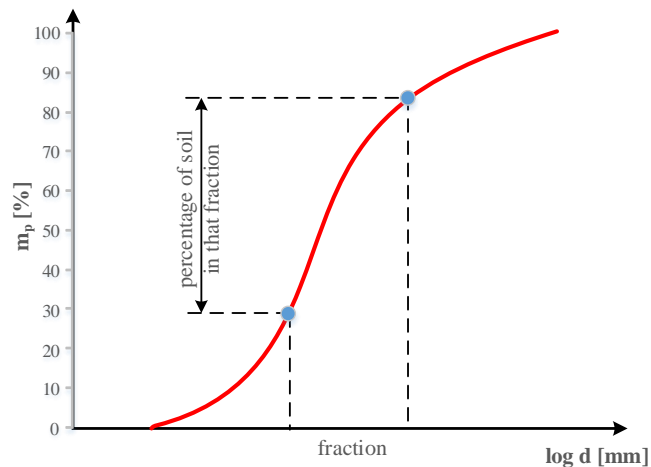


Fig. 3.9: Assessing the percentages for a fraction

Therefore, to find the percentages of clay, for instance, one will have to find the distance between  $m_p=0\%$  and  $m_p$  corresponding to  $d=0.002\text{mm}$ .



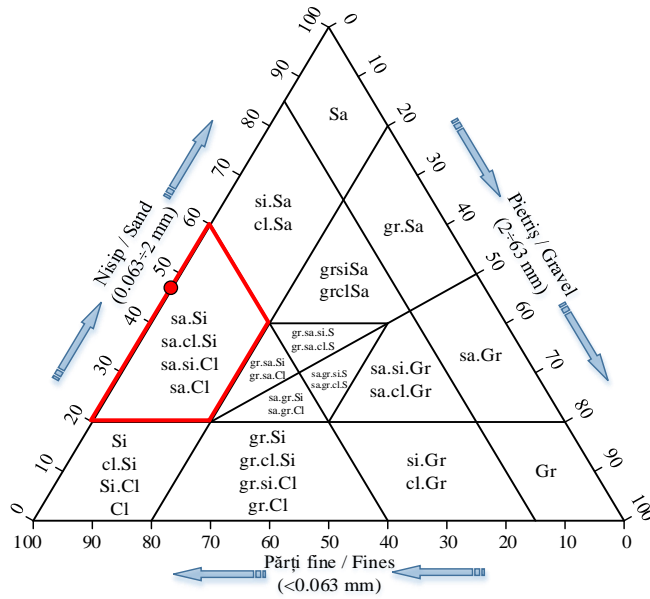


Fig. 3.10: Ternary diagram

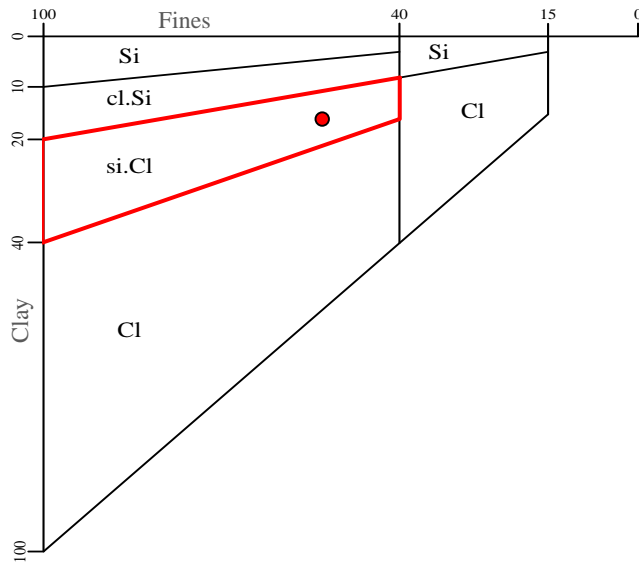


Fig. 3.11: Assessing the fines for the ternary diagram

### **3.4 Test your understanding**

#### **Problem 3.1**

Specify the major grading fractions for fine soils.

#### **Problem 3.2**

Which are the major grading fractions for coarse soils?

#### **Problem 3.3**

What is a grading fraction?

#### **Problem 3.4**

A soil sample with a dry mass of 50 g was analysed for grading classification and the following results were obtained:

d [mm]	m <sub>p</sub> [%]
1.500	100
1.000	92
0.500	88
0.250	72
0.100	51
0.063	40
0.020	31
0.010	25
0.005	20
0.002	10

- Compute the percentages of clay, silt, sand and gravel;
- Classify the soil according to SR EN ISO 14688-1/2004 [2];
- Compute the uniformity coefficient.

#### **Problem 3.5**

A soil sample with a dry mass of 270 g was subjected to a screening test and the following results were obtained:

Sieve size [mm]	Mass on sieve [g]
20.000	65
10.000	38

Sieve size [mm]	Mass on sieve [g]
8.000	25
6.300	36
2.000	34
0.630	28
0.200	19
0.063	25

- a) Compute the percentages of clay, silt, sand and gravel;
- b) Classify the soil according to SR EN ISO 14688-1/2004 [2].

### Problem 3.6

A soil sample with a dry mass of 80g was subjected to a screening test and a hydrometer test. The mass of the screened material is 42.7g. The tables below show the obtained results.

Sieve size [mm]	Mass on sieve [g]
4.000	0.00
2.000	8.47
1.400	1.98
1.000	1.83
0.850	0.77
0.630	1.61
0.500	1.78
0.315	4.97
0.250	2.86
0.180	4.54
0.125	4.67
0.090	2.60
0.063	6.58

d [mm]	m <sub>p</sub> [%]
0.049	42.3
0.036	39.1
0.026	34.7
0.019	29.5
0.014	26.3
0.010	23.9

d [mm]	m <sub>p</sub> [%]
0.007	21.5
0.005	19.9
0.004	18.7
0.003	17.5
0.002	15.5

- a) Compute the percentages of clay, silt, sand and gravel;
- b) Classify the soil according to SR EN ISO 14688-1/2004 [2];
- c) Draw the grading curve.



#### 4 SIMPLE INDICES OF SOIL

Soil can generally be considered a mixture of three components – solid particles, water and air – usually regarded as the three phases of the soil (Fig. 4.1).

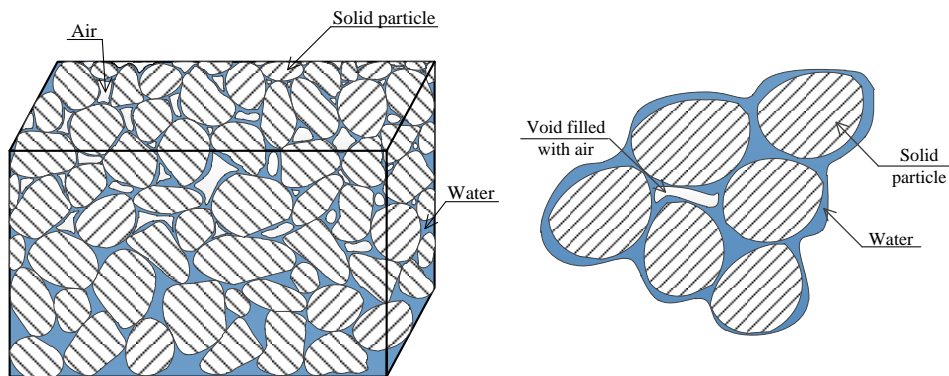


Fig. 4.1: The phases of the soil

Each of these phases has a great influence on the behaviour of soil, therefore it is important to know how much of each is present. Their exact quantity is not relevant, but rather the ratios between them, through means of conventional terms known as the simple indices of soil. To determine them, a simple approach is employed, considering a unit volume of soil conveniently divided into three parts, one for each of the phases (Fig. 4.2). Each of these parts is described by a volume, a density and a mass, as depicted below.

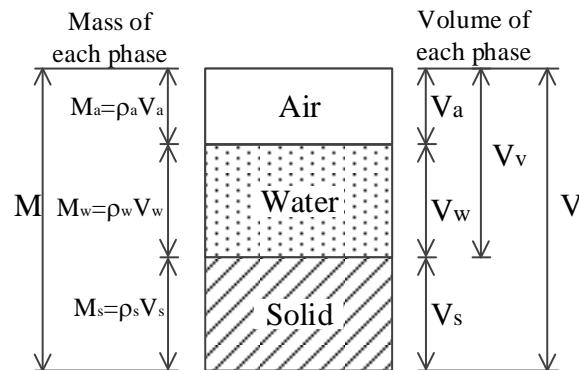


Fig. 4.2: Simplified phase diagram

From Fig. 4.2 the volume of voids is the sum between the volume of water and the volume of air in the sample:

$$V_v = V_w + V_a \tag{4.1}$$

and the total volume is the sum between the volume of voids and the volume of solids:

$$V = V_v + V_s \tag{4.2}$$

#### 4.1 Porosity and voids ratio

Porosity of soils, denoted by “n” and usually expressed in percent, is the ratio between the volume of voids ( $V_v$ ) in the sample and the total volume of the sample ( $V$ ):

$$n = \frac{V_v}{V} \cdot 100 \tag{4.3}$$

Another way of expressing the voids in the soil is through the voids ratio, denoted by “e” (and usually expressed as dimensionless ratio), defined as the ratio between the volume of voids ( $V_v$ ) and the volume of solid particles ( $V_s$ ) in the sample:

$$e = \frac{V_v}{V_s} \tag{4.4}$$

Since they both express the same physical quantity, the voids ratio can be expressed function of the porosity or vice versa, usually only one of them being necessary to describe the same property of the soil. So, replacing (4.2) in (4.3) yields:

$$n = \frac{V_v}{V} \cdot 100 = \frac{V_v}{V_v + V_s} \cdot 100 \quad (4.5)$$

Dividing both the numerator and the denominator of (4.5) by  $V_s$  and taking into account (4.4), we obtain:

$$n = \frac{V_v}{V_v + V_s} \cdot 100 = \frac{\frac{V_v}{V_s}}{\frac{V_v}{V_s} + \frac{V_s}{V_s}} \cdot 100 = \frac{e}{e + 1} \cdot 100 \quad (4.6)$$

The same proof is valid for conversing from porosity into voids ratio. Expressing the porosity into percent, the two equalities are written as:

$$\begin{aligned} n &= \frac{e}{e + 1} \cdot 100 \\ e &= \frac{\frac{n}{100}}{1 - \frac{n}{100}} \end{aligned} \quad (4.7)$$

Although there are some laboratory procedures to assess the voids in a material such as soil (e.g. mercury intrusion porosimetry [9]), they are not used in common engineering practice since they provide unnecessary detailed results, such as the pore size distribution of the sample. In fact, it is considered that there are no direct laboratory methods in geotechnical engineering practice for assessing  $n\%$  and  $e$ , indirect methods usually being employed such as considering the relationships between porosity and other geotechnical indices.



## 4.2 Moisture content

Moisture content, denoted by “w” and usually expressed in percent, is the ratio between the water mass ( $M_w$ ) and the mass of the solid particles ( $M_s$ ) or water weight ( $W_w$ ) and weight of solids ( $W_s$ ) in a sample:

$$w\% = \frac{M_w}{M_s} \cdot 100 = \frac{W_w}{W_s} \cdot 100 \quad (4.8)$$

In order to find the moisture content, according to STAS 1913/1-82 [10], BS 1377-2:1990 [11] and ASTM D 2216-1998 [12], a certain amount of soil at natural moisture content is collected from the sample as shown in Fig. 4.3 a). The sample from which the soil mass is taken may be either in an undisturbed state as shown in the picture or in a disturbed state preserving the in-situ moisture (such as a sealed vessel).

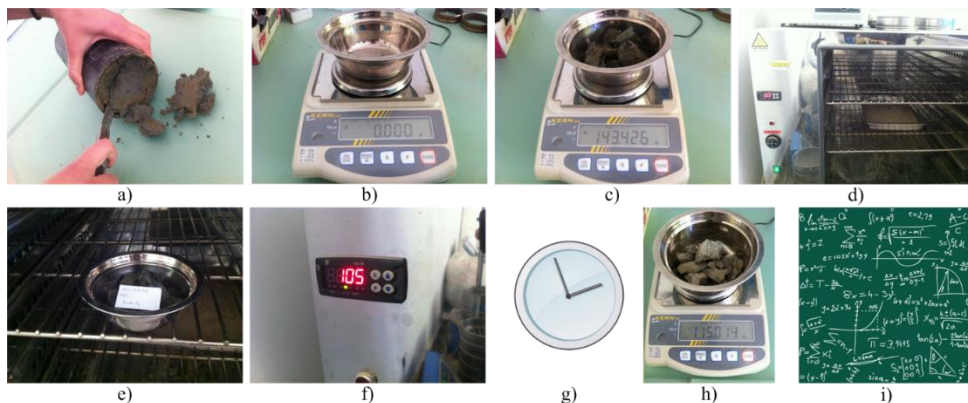


Fig. 4.3: The steps for finding the moisture content by oven drying [13]

The minimum weight of soil necessary to perform the test varies with the soil grading as described by standards, as following:

- a) Romanian Standard STAS 1913/1-82 [14] recommends the minimum total mass of the tested samples to be the following:
  - i) cohesive soils – 75 g;
  - ii) fine sand – 100 g;
  - iii) medium and coarse sand – 200 g;
  - iv) gravel with sand – 1 kg;
  - v) cobbles – 2...6 kg.

- b) British Standard BS 1377-2: recommends the following minimum masses of one sample:
  - i) fine-grained soils – 30 g;
  - ii) medium-grained soils – 300 g;
  - iii) coarse-grained soils – 3 kg.
  
- c) American Standard ASTM D 2216-98 [12] recommends the minimum mass of moist material to be representative of the total sample, depending on the maximum particle size (100% passing) and the required precision of reported moisture content, as following:
  - i) 2 mm or less – 20 g for both 0.1% and 1% precision;
  - ii) 4.75 mm – 100 g for 0.1% and 20 g for 1% precision;
  - iii) 9.5 mm – 500 g for 0.1% and 50 g for 1% precision;
  - iv) 19.0 mm – 2.5 kg for 0.1% and 250 g for 1% precision;
  - v) 37.5 mm – 10 kg for 0.1% and 1 kg for 1% precision;
  - vi) 75.0 mm – 50 kg for 0.1% and 5 kg for 1% precision.

To perform the procedure, a vessel, a balance (Fig. 4.3 b) and an oven (Fig. 4.3 d) are required. The minimum specifications for the balance are given as following:

- a) Romanian Standard STAS 1913/1-82 [14]
  - i) 0.01 g readability for masses of 20...100 g;
  - ii) 0.1 g readability for masses of 100...500 g;
  - iii) 1 g readability for masses over 500 g.
  
- b) British Standard BS 1377-2:1980 [11]
  - i) 0.01 g readability for fine-grained soils;
  - ii) 0.1 g readability for medium-grained soils;
  - iii) 1 g readability for coarse-grained soils.
  
- c) American Standard ASTM D 2216-98 [12]:
  - i) 0.01 g readability for masses up to 200 g;
  - ii) 0.1 g readability for masses over 200 g.

Next, the vessel is tarred (Fig. 4.3 b) and the sampled material is placed in the vessel and weighed (Fig. 4.3 c). The measured weight can be denoted by  $M_{ws}$ ,

which stands for the mass of the wet specimen. In the example from picture Fig. 4.3 c), the recorded mass is:

$$M_{ws} = 143.426 \text{ g} \quad (4.9)$$

The sample is then left to dry inside an oven (Fig. 4.3 d, e) at 105°C (Fig. 4.3 f). The drying shall take for as long as necessary (Fig. 4.3 g), until no more water evaporates from the sample. As a rule of thumb, samples should not be placed to dry if there are already other samples in the oven, since the resulted vapours may influence the drying process of the original samples.

Some standards specify a minimum time for drying, as following:

- a) Romanian Standard STAS 1913/1-82 [10]:
  - i) sands – 6 h;
  - ii) sandy soils – 10 h;
  - iii) clayey soils – 16 h;
  - iv) fat clays – 24 h;
  - v) soils with limestone or more than 5% organic matter – 24 h, at 80°C.
- b) British Standard BS 1377-2:1980 [11] states that the soil is “dry” when no further water can be removed at a temperature less than 110°C. Also, the standard recommends that the sample shall be deemed to be dry when the differences in successive weightings at intervals of 4 h do not exceed 0.1 % of the original mass of the sample.
- c) American Standard ASTM D 2216-98 [12] specifies that the time required to obtain constant mass will vary depending on the type of material, size of specimen, oven type and capacity, and other factors. The influence of these factors generally can be established by good judgment, and experience with materials being tested and the apparatus being used.



Fig. 4.4: Desiccator [15]

When taking the sample out of the oven, it should be left to cool in a desiccator (Fig. 4.4), which is a glass vessel that keeps the sample isolated from the environment, preventing it to dry or moist. After drying and cooling, the sample is weighed and the value may be recorded as  $M_s$ , which stands for the mass of the solid particles in the sample. In the example from picture Fig. 4.3 h), the recorded dry mass is:

$$M_s = 115.014 \text{ g} \quad (4.10)$$

Having both the mass of the wet sample (4.9), and the mass of the dry sample (4.10), one can proceed with the computations (Fig. 4.3 i), first determining the mass of water in the original sample as the difference between the two recorded masses:

$$M_w = M_{ws} - M_s \quad (4.11)$$

In the given example, the mass of water in the sample is:

$$M_w = 143.426 \text{ g} - 115.014 \text{ g} = 28.412 \text{ g} \quad (4.12)$$

and the resulted moisture content, using (4.8) is:

$$w\% = \frac{M_w}{M_s} \cdot 100 = \frac{28.412}{115.014} \cdot 100 = 24.70\% \quad (4.13)$$

The reported value of the moisture content is given after repeating the described procedure at least three times. Generally, studying the soil properties can yield different results on the same specimen due to multiple factors such as soil heterogeneity and testing errors, so tests are repeated at least three times to report reliable values.

### **4.3 Unit weight and density**

Engineering practice requires handling forces acting on the system of interest. A great deal of these forces is gravity generated, so evaluating the weights is an important step in understanding a phenomenon. In order to easily assess these weights one should first describe the weight of a unit volume and then extrapolate that to the analysed system. To this respect, a useful characterization of soil is describing its unit.

Since soil is a mixture of different phases (Fig. 4.1) it's useful to describe the unit weight in different conditions, depending on how much of each phase is present in the analysed sample.

#### **4.3.1 Particle density**

The particle density, denoted by “ $\rho_s$ ” and usually expressed in g/cm<sup>3</sup>, is defined by the ratio between the mass of the solid phase of soil ( $M_s$ ) and its volume ( $V_s$ ):

$$\rho_s = \frac{M_s}{V_s} \quad (4.14)$$

Similarly, the particle unit weight, denoted by “ $\gamma_s$ ” and usually expressed in kN/m<sup>3</sup>, is defined by the ratio between the weight of the solid phase of soil ( $W_s$ ) and its volume ( $V_s$ ):

$$\gamma_s = \frac{W_s}{V_s} \quad (4.15)$$

Since the weight depends on the mass by the gravitational acceleration, the density and unit weight of the particles can be expressed one function of the other:

$$\gamma_s = \frac{W_s}{V_s} = \frac{M_s \cdot g}{V_s} = \rho_s \cdot g \quad (4.16)$$

or

$$\rho_s = \frac{\gamma_s}{g} \quad (4.17)$$

where “g” is the gravitational acceleration.

A widely used form of  $\gamma_s$  and  $\rho_s$  is the specific gravity of soil, usually denoted by “ $G_s$ ”, representing the ratio between the particle unit weight ( $\gamma_s$ ) and the unit weight of water ( $\gamma_w$ ), or the particle density ( $\rho_s$ ) and the density of water ( $\rho_w$ ):

$$G_s = \frac{\gamma_s}{\gamma_w} = \frac{\rho_s}{\rho_w} \quad (4.18)$$

It actually expresses how much heavier or lighter the solid phase of the soil is compared to water.

The specific gravity is dimensionless, hence an advantage of using it as opposed to unit weight or density. Since the density of water can be approximated to be of unit value, the value of the specific gravity is basically the same as the value of the density of the solid skeleton, so actually no information is lost when using either terms.

Generally, the values of  $G_s$  may vary between 1 and 5.2 depending on the type of mineral of the soil, but the most common values vary between 2.65 (sand) and 2.72 (fat clay).

Finding the particle density of soil is a common practice in civil engineering, and is easily performed in the laboratory by means of the pycnometer test

(Fig. 4.5) (also known as the small pycnometer method – BS 1377-2:1990 [11] and STAS 1913/2-76 [8]).



Fig. 4.5: Examples of pycnometers

The pycnometer test (Fig. 4.6) is described by various national or international standards: STAS 1913/2-76 [8], BS 1377-2:1990 [11] and ASTM D 854-2010 [16] and provides an average particle density for the tested material. According to the Romanian and British standards, this method is suitable for soils with particles smaller than 2.0mm, but larger particles can be ground down to sizes smaller than 2.0mm. The American standard, however, requires particles smaller than 4.75mm. In the same time, the test cannot be performed on soils that are soluble in water.

The three mentioned standards have significant differences, so we will just focus on the national Romanian standard. Performing the test requires distilled water, ceramic mortar and pestle mill, 2.0mm and 0.2mm wire sieves, electric oven, glass funnel, electric sand bath, grater, thermometer, desiccator and electric balance. The samples to be used may be either disturbed or undisturbed, since their structure is to be destroyed anyway and will not influence the test results.

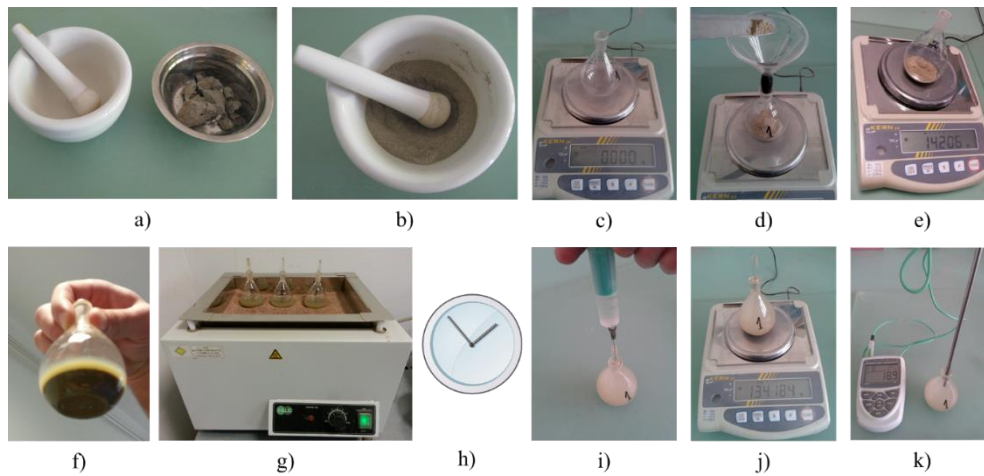


Fig. 4.6: Steps in performing the pycnometer test

In preparation for performing the test, the sample will be dried in the electric oven at  $105\pm 2^{\circ}\text{C}$  and then grounded using the ceramic mortar and pestle mill (Fig. 4.6 a), resulting in about 100g of powder smaller than 0.2mm (Fig. 4.6 b). If the initial material has particles larger than 2.0mm, it will be crushed into smaller grains prior to testing.

A calibrated pycnometer (with known mass and volume) is then placed on the balance and tared (Fig. 4.6 c) and about 12-20g of powder is poured inside the pycnometer through a funnel (Fig. 4.6 d). In the provided picture example (Fig. 4.6 e), the dry soil mass ( $m_1$ ) is:

$$m_1 = 14.206\text{g} \quad (4.19)$$

Distilled water is then added (Fig. 4.6 f) to the pycnometer. The procedure from (Fig. 4.6 c) to (Fig. 4.6 f) is repeated until three pycnometers are obtained. Afterwards, the pycnometers are placed on a sand bath to ensure a slow and steady boil for about 15 minutes. This will allow the trapped air bubbles inside the sample to slowly evacuate without having a violent boiling disturbing the sample and producing loss of material.

The pycnometers are then filled with water to their maximum capacity (Fig. 4.6 i) and weighted on the scale. The given example (Fig. 4.6 j) shows a mass of soil and water ( $m_3$ ):



$$m_3 = 134.184\text{g} - m_{\text{pyknometer}} = 108.447\text{g} \quad (4.20)$$

It is also important to measure the temperature of the water in the pyknometer (Fig. 4.6 k), to be able to assess a correct value of the water density:

$$T = 18.9^\circ\text{C} \quad (4.21)$$

The purpose of the test is to determine the particle density of the soil, which is defined by equation (4.14). The mass of the solid particles is easily determined, because we can weigh the dry sample, but the volume of the particles is more difficult to assess. The principles of the pyknometer test are described graphically in Fig. 4.7. Therefore, we can note that the sum between the initial dry mass (denoted by  $m_1$ ) and the mass of the water that the pyknometer can hold (denoted by  $m_2$ ) is equal to the mass of the pyknometer with the solid particles and water to its maximum capacity (denoted by  $m_3$ ) and the mass of the excess water (denoted by  $m_4$ ), having the volume equal to the volume of all the solid particles. Mathematically, this is:

$$m_1 + m_2 = m_3 + m_4 \quad (4.22)$$

so

$$m_4 = m_1 + m_2 - m_3 \quad (4.23)$$

Now that we know the mass of the volume of water equal to the volume of the solid particles, we can assess the volume of the particles, function of the water density:

$$V_s = V_4 \quad (4.24)$$

where

$$V_4 = \frac{m_4}{\rho_w} \quad (4.25)$$

so

$$V_s = \frac{m_1 + m_2 - m_3}{\rho_w} \quad (4.26)$$

Replacing this in expression (4.14):

$$\rho_s = \frac{m_1}{m_1 + m_2 - m_3} \rho_w \quad (4.27)$$

It is a common procedure to make corrections to the density of water depending on the recorded temperature, since a high accuracy is required:

$$\rho_s = \frac{m_1}{m_1 + m_2 - m_3} \rho_w^T \psi \quad (4.28)$$

where

$\rho_w^T$  – the density of water at the temperature T;

$\psi$  – density correction factor at temperature T.

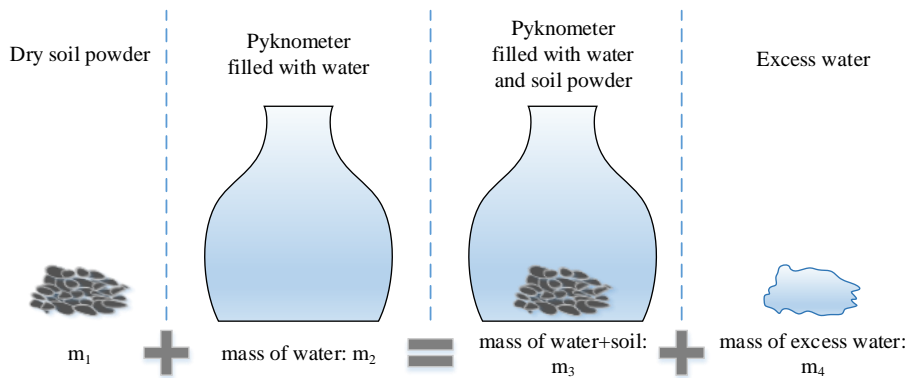


Fig. 4.7: Pycnometer test principles

In the given example, the particle density would be computed as:

$$\rho_s = \frac{14.206\text{g}}{14.206\text{g} + 99.491\text{g} - 108.447\text{g}} 0.998204 \frac{\text{g}}{\text{cm}^3} \cdot 1.000218 = 2.70\text{g/cm}^3 \quad (4.29)$$

### 4.3.2 Dry density

Another useful index of soil is its dry density, denoted by “ $\rho_d$ ” and usually expressed in  $\text{g/cm}^3$ , computed as the ratio between the mass of a dried sample of soil ( $M_s$ ) and its total volume ( $V$ ):

$$\rho_d = \frac{M_s}{V} \quad (4.30)$$

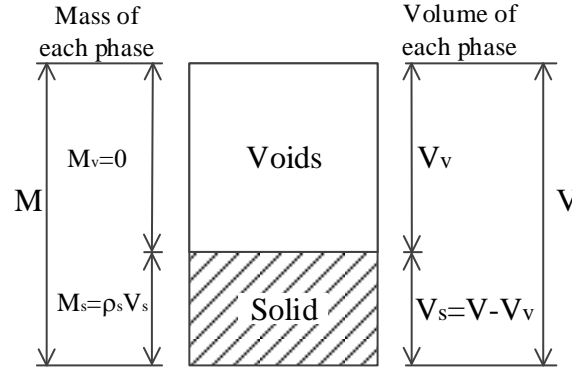


Fig. 4.8: Phase diagram for dry soil

In dry state, the soil is considered to be water free ( $V_w=0$ ), so the voids have no real weight, thus only the weight of the solid particles are taken into account. Replacing (4.15) into the above equation, and rewriting it with respect to the volume components, one can obtain:

$$\rho_d = \frac{\rho_s \cdot V_s}{V} = \rho_s \frac{V - V_v}{V} = \rho_s \left(1 - \frac{V_v}{V}\right) \quad (4.31)$$

Finally, the above result can be conveniently rewritten using (4.3) as:

$$\rho_d = \rho_s \left(1 - \frac{n}{100}\right)$$

or

$$(4.32)$$

$$\gamma_d = \gamma_s \left(1 - \frac{n}{100}\right)$$

This equation is proven to be more useful than (4.30) when describing the properties of the soil, because it relates to the porosity (an index that cannot be determined directly) and the density of the solid skeleton (an index that can be determined in the laboratory).

We can also express relations (4.32) function of the voids ratio, using equation (4.7), and it follows:

$$\rho_d = \frac{\rho_s}{1+e}$$

or (4.33)

$$\gamma_d = \frac{\gamma_s}{1+e}$$

### 4.3.3 Saturated density

As opposed to the dry density, when computing the saturated density, denoted by “ $\rho_{sat}$ ” and usually expressed in  $g/cm^3$ , one assumes that all the voids in the sample are filled with water ( $V_a=0$ ), and the term is computed as the ratio between the mass of the saturated sample ( $M_{sat}$ ) and its total volume ( $V$ ):

$$\rho_{sat} = \frac{M_{sat}}{V} \tag{4.34}$$

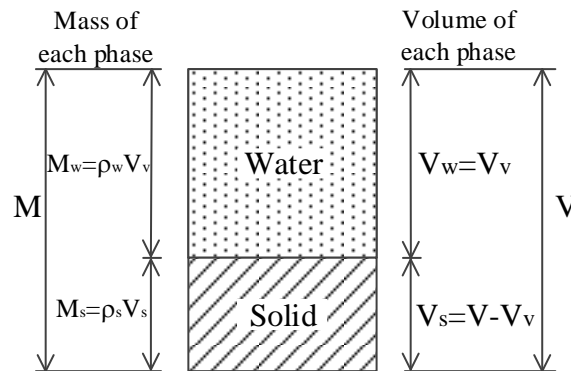


Fig. 4.9: Phase diagram for saturated soil

Using the provided assumption, the equation can be rewritten as:

$$\rho_{sat} = \frac{M_s + M_w}{V} \tag{4.35}$$

where  $M_s$  is the mass of the solid phase and  $M_w$  is the mass of the water phase. Rewriting the above equation using the same judgment as for (4.31), results:

$$\rho_{\text{sat}} = \frac{\rho_s \cdot V_s + \rho_w \cdot V_v}{V} = \rho_s \frac{V - V_v}{V} + \rho_w \frac{V_v}{V} = \rho_s \left(1 - \frac{V_v}{V}\right) + \rho_w \frac{V_v}{V} \quad (4.36)$$

Finally, using the definition of porosity provided in equation (4.3), one obtains:

$$\rho_{\text{sat}} = \rho_s \left(1 - \frac{n}{100}\right) + \rho_w \frac{n}{100}$$

or (4.37)

$$\gamma_{\text{sat}} = \gamma_s \left(1 - \frac{n}{100}\right) + \gamma_w \frac{n}{100}$$

#### 4.3.4 Bulk density

The **bulk density**, denoted by “ $\rho$ ” and usually expressed in  $\text{g/cm}^3$ , describes the density of the soil in its natural state, which is actually an arbitrary combination between the three phases. This index is defined as the ratio between the weight of the soil ( $M$ ) and its total volume ( $V$ ):

$$\rho = \frac{M}{V} \quad (4.38)$$

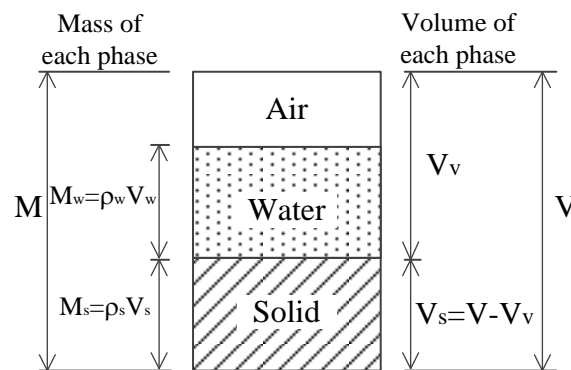


Fig. 4.10: General phase diagram

Rewriting the mass in (4.38) and using the definition of the moisture content in (4.8) the following relation can be obtained:

$$\rho = \frac{M}{V} = \frac{M_s + M_w}{V} = \frac{M_s + \frac{w}{100} \cdot M_s}{V} = \frac{M_s}{V} \left(1 + \frac{w}{100}\right) \quad (4.39)$$

The left term of the equation is the definition of the dry density ( $\rho_d$ ) from relation (4.30), which was already established to be written as expressed in equation (4.32), so it is more convenient to rewrite (4.39) as:

$$\rho = \rho_s \left(1 - \frac{n}{100}\right) \left(1 + \frac{w}{100}\right)$$

or (4.40)

$$\gamma = \gamma_s \left(1 - \frac{n}{100}\right) \left(1 + \frac{w}{100}\right)$$

In order to preserve the state of the soil, only undisturbed samples are suitable for use when finding the bulk density. The most common laboratory method to determine it is to use the so-called “mould method”. A mould is basically a vessel with known inner volume. To determine the interior volume of the mould we could simply measure it (Fig. 4.11) or fill it with water and assess the volume of water that is required to fill the mould.



Fig. 4.11: Measuring the interior dimensions of the mould

The basic steps in performing this test are briefly described in Fig. 4.12. Some reference standards that give instructions on how to perform this test are STAS 1913/3-76 [17] and BS 1377-2:1990 [11]. The materials needed for the

test are a mould, a sharp thin-bladed trimming knife, a spatula, a flat glass plate and a scale.

According to STAS 1913/3-76 [8], the mould should have a minimum volume of  $50\text{cm}^3$ , with the following dimensions:

- Diameter,  $d$ :
  - at least 40mm, for cohesive soils;
  - at least 70mm, for slightly cohesive soils;
  - at least 100mm for cohesionless soils (for in-situ testing).
- Height,  $h = 0.5d \div 1.3d$ ;
- Thickness,  $t = 1.5 \div 3\text{mm}$ .

Both Romanian and British standards require the balance to be readable to 0.01g and the measurements of the mould dimensions to be made to the nearest 0.1mm.

As the images describe in Fig. 4.12, after having an undisturbed sample ready (Fig. 4.12 a), the mould is carefully filled with soil, without disturbing its structure (Fig. 4.12 b). A thin knife can be used to trim the sample in front of the mould so it can advance more easily. After filling the mould, the excess soil will be trimmed so that the volume of the obtained sample is equal to the interior volume of the mould (Fig. 4.12 c). Finally, the soil is weighted (Fig. 4.12 e) and the bulk density is computed using relation (4.38).

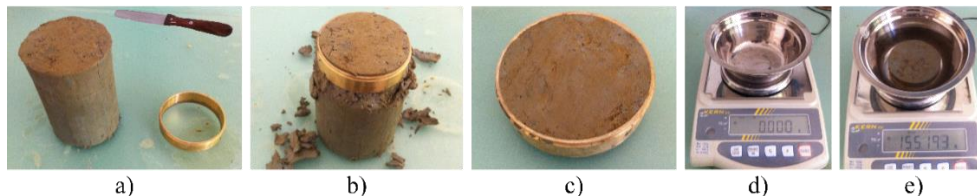


Fig. 4.12: Steps in finding the bulk density

The standards also mention that the dry density,  $\rho_d$ , can be computed if the sample is dried in the oven and then the dry mass is obtained (Fig. 4.13). Equation (4.30) can be used for this purpose, where  $M_s$  would be the mass of the dry sample. At the same time, the moisture content,  $w$ , can be determined using relation (4.8) where the mass of water in the sample,  $M_w$ , can be determined as the difference between the mass of the natural sample and the mass of the dry sample.

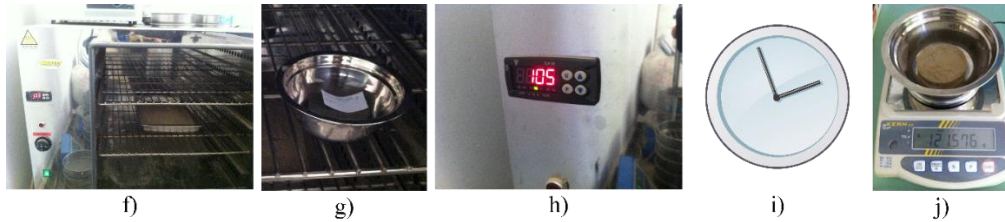


Fig. 4.13: Optional additional steps after finding the bulk density

#### 4.3.5 Submerged density

The submerged density of soil is denoted by “ $\rho'$ ” and is usually expressed in  $\text{g/cm}^3$ . It may be defined as the apparent density of soil when submerged in water. When under water, the soil will also be acted by Archimedes’ force, so the most convenient way to study its effect is by using forces instead of masses. Therefore, let’s introduce the notion of submerged unit weight, which is denoted by “ $\gamma'$ ”, is usually expressed in  $\text{kN/m}^3$ , and is defined as the ratio between the weight of soil in submerged state ( $W'$ ) and its total volume ( $V$ ):

$$\gamma' = \frac{W'}{V} \quad (4.41)$$

In this case, the soil sample is considered to be submerged in water, so the sample has no air phase. The Archimedes’ force acts on the sample, so the weight of each phase is reduced by the weight of a volume of water equal to the volume of the corresponding phase Fig. 4.14.



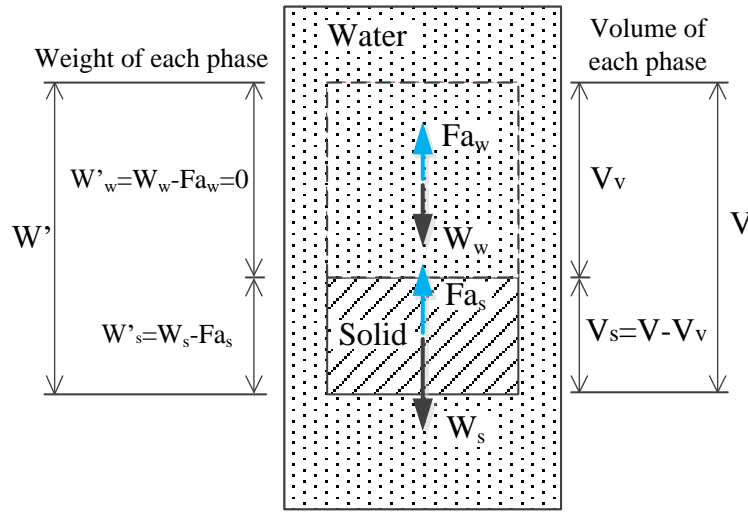


Fig. 4.14: Phase diagram for soil in submerged conditions

Therefore, the weight of the water phase is reduced to zero, ( $Fa_w = W_w$ ) and the weight of the solid particles is reduced by the weight of the Archimedes force:

$$W'_w = W_w - Fa_w = 0 \quad (4.42)$$

$$W'_s = W_s - Fa_s = \gamma_s \cdot V_s - \gamma_w \cdot V_s = V_s(\gamma_s - \gamma_w) \quad (4.43)$$

Merging the above result into equation (4.41) it results:

$$\begin{aligned} \gamma' &= \frac{W'}{V} = (\gamma_s - \gamma_w) \frac{V_s}{V} = (\gamma_s - \gamma_w) \frac{V - V_v}{V} = \\ &= (\gamma_s - \gamma_w) \left(1 - \frac{V_v}{V}\right) = (\gamma_s - \gamma_w) \left(1 - \frac{n}{100}\right) \end{aligned} \quad (4.44)$$

or

$$\rho' = (\rho_s - \rho_w) \left(1 - \frac{n}{100}\right)$$

Considering the expression (4.37) for the density of saturated soil, we can express the above relation as:

$$\gamma' = \gamma_{\text{sat}} - \gamma_w$$

or (4.45)

$$\rho' = \rho_{\text{sat}} - \rho_w$$

#### **4.3.6 Saturation ratio**

The saturation ratio of soil, denoted by “ $S_r$ ”, is a dimensionless index defined as the ratio between the volume of water ( $V_w$ ) and the volume of voids ( $V_v$ ):

$$S_r = \frac{V_w}{V_v} \tag{4.46}$$

It basically describes to what extent are the voids filled with water. This would mean that  $S_r$  can vary from 0, for completely dry materials, to 1, for fully saturated soils. We can express the volume of water ( $V_w$ ) as the ratio between the mass of water ( $m_w$ ) and its density ( $\rho_w$ ):

$$S_r = \frac{1}{V_v} \frac{m_w}{\rho_w} \tag{4.47}$$

But the mass of water ( $m_w$ ) can also be express using the moisture content ( $w$ ) relation:

$$S_r = \frac{1}{V_v} \frac{m_s \frac{w}{100}}{\rho_w} \tag{4.48}$$

and we know that the mass of solids is equal to the product between the density of the solid skeleton ( $\rho_s$ ) and the volume of solids ( $V_s$ ):

$$S_r = \frac{1}{V_v} \frac{V_s \rho_s \frac{w}{100}}{\rho_w} \tag{4.49}$$

Using equation (4.4), we can replace the ratio of volumes by the voids ratio, therefore:

$$S_r = \frac{\rho_s \frac{w}{100}}{\rho_w e} \quad (4.50)$$

The above equation describes the saturation ratio as a function of known indices, so we can actually compute  $S_r$  for a given sample, knowing the moisture content, the density of the solid skeleton (values which can be determined by laboratory tests) and the voids ratio (which can be determined from other indices).

#### 4.4 Density index

So far, we have dealt with simple indices of soils, which are valid for any type of soil. Some indices, however, can be employed only for certain types of soils. For instance, later on we will discuss about plasticity index and consistency index, which are parameters describing the nature or state of cohesive soils. Right now, we will introduce the density index (also called relative density), which is characteristic to cohesionless soils and describes their state of compaction.

The **density index** is denoted by “ $I_D$ ” and is defined as the ratio of the difference between the voids ratio of the soil in its loosest state ( $e_{max}$ ) and the voids ratio in its natural state ( $e$ ) to the difference between the voids ratios in its loosest ( $e_{max}$ ) and densest ( $e_{min}$ ) states. In less words, that is mathematically described as:

$$I_D = \frac{e_{max} - e}{e_{max} - e_{min}} \quad (4.51)$$

where

- $e_{max}$  – voids ratio in loosest state;
- $e_{min}$  – voids ratio in densest state;
- $e$  – voids ratio in natural state.

Because the porosity (hence the voids ratio) of a soil is not an accurate indicator of the looseness of a soil, since it depends on many factors (e.g. grain size distribution and shape, sedimentation etc.), the state of compactness of the soil must be characterized comparing to how much the porosity (or voids ratio) can vary for that given soil. This is particularly useful when establishing if a given granular soil on site can be further compacted or not, and to what extent. It can also be an indicator of the bearing capacity of that

soil. Therefore, we must compact the soil sample as much as possible, to obtain the minimum voids ratio that it can manifest, and also loosen the soil as much as possible, to find the maximum voids ratio that the soil can have. We then compare the natural state with the extreme possible states to describe the relative compactness of the soil, i.e. the density index.

Using equation (4.33) we can express the voids ratio function of the densities  $\rho_s$  and  $\rho_d$ :

$$e = \frac{\rho_s}{\rho_d} - 1 \quad (4.52)$$

so, we can rewrite the expression (4.51) as:

$$I_D = \frac{\left(\frac{\rho_s}{\rho_{d\min}} - 1\right) - \left(\frac{\rho_s}{\rho_d} - 1\right)}{\left(\frac{\rho_s}{\rho_{d\min}} - 1\right) - \left(\frac{\rho_s}{\rho_{d\max}} - 1\right)} \quad (4.53)$$

or

$$I_D = \frac{\frac{1}{\rho_{d\min}} - \frac{1}{\rho_d}}{\frac{1}{\rho_{d\min}} - \frac{1}{\rho_{d\max}}} = \frac{\rho_{d\max}(\rho_d - \rho_{d\min})}{\rho_d(\rho_{d\max} - \rho_{d\min})} \quad (4.54)$$

where

$\rho_{d\min}$  – the minimum dry density of the material (that is in the loosest state);

$\rho_{d\max}$  – the maximum dry density of the material (that is in the densest state);

$\rho_d$  – the dry density of the material in a natural state of compaction.

The maximum density can be determined by compacting a dry granular soil sample through vibrating in a mould under a surcharge of 14kPa. Then the density is computed measuring the weight of the sample and dividing by the volume, determined as the product between the average height of the sample and the cross-section area of the mould. This test procedure is described by Romanian standard STAS 13006-91 [18] and American standard ASTM D 4253-00.

The minimum density can be determined by pouring the sand in a mould through a funnel from a constant height by moving the pouring device in a spiral path from the outside to the centre of the mould to form each layer of nearly uniform thickness. The mould is to be filled approximately 2cm above the top and then the sample be trimmed carefully. The sample is then weighted and the minimum density is obtained by dividing the mass to the volume of the sample. A more accurate procedure description can be found in the Romanian standard STAS 13021-91 and American standard ASTM D 4254-00.

#### 4.5 Test your understanding

##### Problem 4.1

A dry soil sample has the following known data:

- mass  $m_d = 260$  g;
- volume before drying  $V = 150$  cm<sup>3</sup>;
- particle density  $\rho_s = 2.68$  g/cm<sup>3</sup>.

Compute the voids ratio,  $e$ .

##### Problem 4.2

A moist soil sample has the following known data:

- density  $\rho = 1.9$  g/cm<sup>3</sup>;
- dry density  $\rho_d = 1.7$  g/cm<sup>3</sup>;
- porosity  $n = 39\%$ .

Compute the saturation ratio,  $S_r$ .

##### Problem 4.3

A moist soil sample has the following known data:

- volume  $V = 157$  cm<sup>3</sup>;
- mass  $m = 310.0$  g;
- particle density  $\rho_s = 2.69$  g/cm<sup>3</sup>.
- dry density  $\rho_d = 1.66$  g/cm<sup>3</sup>.

Find the moisture content,  $S_r$ , and the moisture content,  $w$ .

##### Problem 4.4

A saturated soil sample has the following known data:

- particle density  $\rho_s = 2.66 \text{ g/cm}^3$ ;
- moisture content  $w = 3\%$ .

Find the following:

- a) voids ratio,  $e$ ;
- b) porosity,  $n$ ;
- c) bulk density,  $\rho$ ;
- d) saturated density,  $\rho_{\text{sat}}$ ;
- e) dry density,  $\rho_d$ ;
- f) submerged density,  $\rho'$ .

---

**Problem 4.5**

A moist soil sample has the following known data:

- porosity  $n = 37\%$ ;
- particle density  $\rho = 2.71 \text{ g/cm}^3$ ;
- moisture content  $w = 9\%$ .

Find the mass of water to be added to fully saturate  $1 \text{ m}^3$  of soil.



## **5 CLAY MINERALS**

### **5.1 Generalities**

The soil is a composite material, which contains an inhomogeneous mixture of solid particles in a fluid media that is in turn made of water, dissolved electrolytes and other liquid substances, air and other gases. Chemical and physical bonding always takes place between the solid, liquid and gaseous phase, in a dynamic rate, depending on the nature and percentage in which they are each found.

### **5.2 Electro-chemical bonds**

Depending on the interaction phenomena and the intra or inter phases that occur within the soil, some of these bonds are briefly presented below.

The primary chemical bonds are the ones that engage the electrons from the last electrical layer, which are also called "valence electrons". These are generally strong bonds. The three primary types of bonding are:

- covalent bond - one or more electrons from the valence electrons is or are put in common by two atomic nuclei. The covalent bond is specific for gases. In general, non-metallic atoms are the ones that form covalent bonds in the case of solid substances. Keeping in mind that only some electrons take part in the bond, covalent molecules have predefined positions, being directed after precise and fixed angles;

- ionic bond - it forms between differently charged atoms, as a result of gaining or losing electrons. The cations (positive ions) are formed by losing electrons from the last electrical layer of the atom. The anions (negative ions) are ions that need a smaller number of electrons in order to complete the valence layer. Because of this, namely, the last electrical layer of the atom is complete, covalent bonds cannot form, but its electrical charge is negative. As a result, the cations will electrostatically attract all the anions in its vicinity, thus, the ionic bond is governed only by electric polarity and geometric considerations. For example, in the case of the sodium chloride,



the sodium attracts as many chloride anions as would fit around it. A separation between the positively and negatively charged centres will exist in the molecule formed by the ionic bond, which will enable it to have a dipolar behaviour, being able to orientate in an electric field.

- metallic bond - the metallic atoms have weakly bonded electrons that can easily pass from one to the other. This type of bond is non-directional and it can be established only when there is a high enough number of metallic atoms.

Ionic and covalent bonds will both occur at once in the minerals that make up the solid phase of the soil, as it is very rare to have pure ionic or pure covalent bonds. For example, the silica oxide has a structure that is half ionic and half covalent.

The secondary bonds are weak in comparison with the principal bonds and may be formed between molecules and atoms. These are not bonds that are related with the addition of electrons on an atom's valence layer, and appear because of electrostatic and interaction forces between the atoms. The two types of secondary bonds that occur between water molecules and at the solid-liquid interface are:

-hydrogen bond - if the hydrogen is the positive end of a dipolar molecule, the attraction force that it exerts over the molecules around it is called a hydrogen bond. This kind of bond forms only with strong electronegative atoms, such as oxygen and fluoride. Because the electron is most of the time found (probabilistically) between the oxygen and hydrogen atoms, the latter will become the positive end of the dipole. The hydrogen bond is the most powerful among the secondary bonds. It has a determinant factor in the formation of ice crystals and it is of great importance in the case of solid-adsorbed water interface phenomena.

- van der Waals bond - it appears as an attraction between the in-phase or out-phase dipoles. It is much weaker than the hydrogen bond and non-directional, but overall it influences the water dipole retention capability at the surface of the solid.

The primary bond types are interatomic, while the secondary bonds appear between molecules or between particles. As a conclusion, it might be noticed that the secondary bonds are weaker than the primary ones, the deformations that appear in soil being actually the reconfiguration of the solid fragments,

rather than their own strain. Also, the secondary type bonds determine the resistance parameters of the soil.

### **5.3 Solid phase**

The soil solid phase is mainly made out of crystalline fragments that are the result of rock masses disintegration, as amorphous excerpts, organic matter or precipitated salts. The most common minerals are the silicates. The silicates organisation forms are presented in Table 5.1. The tetrahedron structures are formed only by their union through the corners.

In the case of isolated tetrahedral formations, the tetrahedral crystals are not united, but the four excess electrons of the oxygen atoms can bond with the positive ions within the crystal.


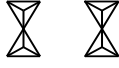

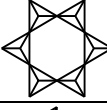

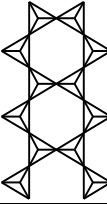
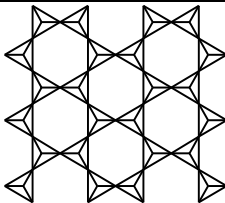
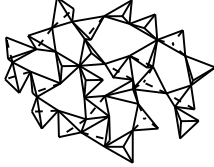
In the case of strip or ring structures, the tetrahedrons are linked in corners. Isomorphic substitution phenomena can appear, through which a  $\text{Si}^{4+}$  is replaced by  $\text{Al}^{3+}$ . The isomorphous substitution is the replacement of an ion with another that has the valence equal or different than the first, but keeps the crystalline structure unchanged.

The sheet type formation appears when the tetrahedrons have three corners shared in common.

Network type formations are characterised by the fact that all four corners of the tetrahedron are shared in common. Isomorphic substitution is frequent, and the excess negative charges are balanced by attracting potassium, calcium or sodium cations, and so on.

Knowing the crystalline structure is very important when appreciating the solid-solid and solid-liquid interaction forces, which strongly influences the global behaviour of granular materials. For example, the montmorillonite mineral can unfold into units with thickness of down to 1nm, reaching that way a specific surface of up to  $800\text{m}^2/\text{g}$ . Thus, reported to the weight of the solid particle, the global properties of the material are governed by the interaction forces.

Table 5.1: Various types of silica structures [19]

Tetrahedron combination	Structure organisation	Si-O radical and electrical charge	Example
Independent crystals		$(\text{SiO}_4)^{4-}$	Olivine $(\text{Mg, Fe})_2\text{SiO}_4$
Double crystals		$(\text{Si}_2\text{O}_7)^{6-}$	Akermanite $\text{Ca}_2\text{Mg}_2\text{Si}_2\text{O}_7$
Rings		$(\text{Si}_3\text{O}_9)^{6-}$	Benitoite $\text{BaTiSi}_3\text{O}_9$
		$(\text{Si}_6\text{O}_{18})^{12-}$	Beryl $\text{Be}_3\text{Al}_2\text{Si}_6\text{O}_{18}$
Strings		$(\text{SiO}_3)_n^{2-}$	Pyroxene
Bands		$(\text{Si}_4\text{O}_{11})_n^{6-}$	Amphibole
Sheets		$(\text{Si}_4\text{O}_{10})_n^{4-}$	Mica
Networks		$(\text{SiO}_2)_n$	Quartz $\text{SiO}_2$

The non-clayey minerals are usually structured in physically and chemically stable lattices (networks) that are hard to destroy. Such an example is the quartz mineral, which is chemically very stable, as it is an oxide (does not have weakly bonded ions), and also resilient to mechanical actions. Another

example is the fly ash, because although the particle dimension is in the clay-silt interval, it does not have cohesion.

The clayey minerals are part of the phyllosilicates mineral family. The particles are of colloidal dimensions and have negative residual charges. The most common structure has "lamellar" shape, made up of tetrahedron or octahedral crystal layers (silica oxides or magnesium and aluminium hydroxides respectively), illustrated in Figure 5.1.

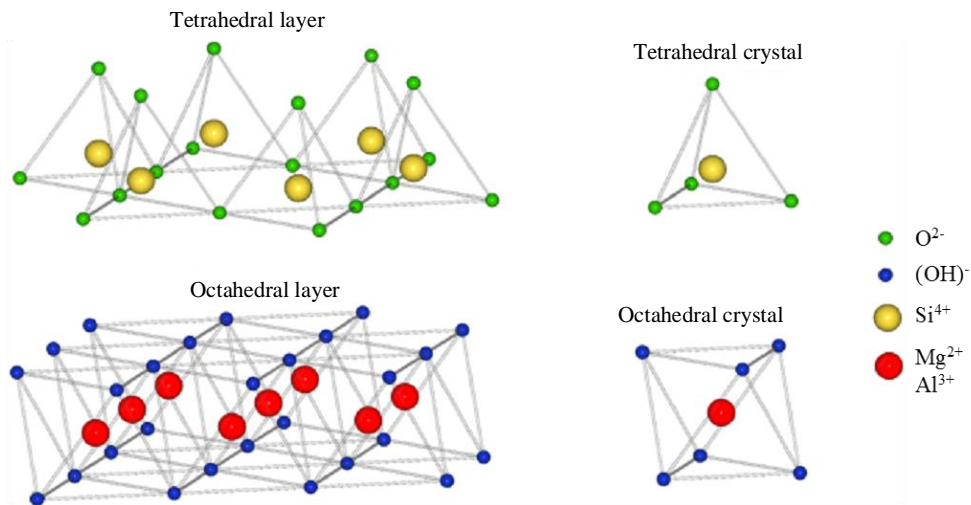


Figure 5.1: Tetrahedral and octahedral layers example [19]

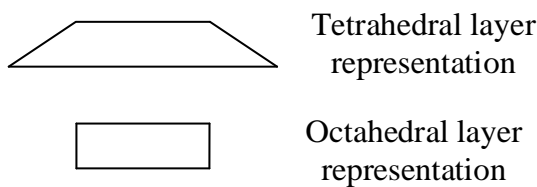


Figure 5.2: The symbols for the two layer types

Figure 5.2 illustrates the symbols for the tetrahedral and octahedral layers. The representation comes from the fact that both lamellae-sheet types have the same thickness (approximately 0.24nm), and that the side view of the sheets resembles a trapezoid in the case of tetrahedral sheets and a rectangle in the case of octahedral sheets.

The main difference between clayey minerals is the number of layers in the sheets (bi-layer, tri-layer, tri-layer with interstitial cations, etc.), and the number of isomorphic substitutions within the crystal.

The tetrahedron layer is made up of silica oxide tetrahedrons with all the corners of the base joined in hexagonal shape and with all the tips on the same side of the base plane. In theory, this structure  $(\text{Si}_4\text{O}_{10})^{4-}$  may repeat itself indefinitely. The electric neutrality may be obtained by replacing the four oxygen ions with hydroxyls or by joining with other layers. The distance between oxygen-oxygen atoms is 0.225nm, the available space for the silica ion is 0.055nm, and the thickness of the tetrahedral layer of the clayey mineral is 0.463nm.

The octahedral layer contains oxides, magnesium or aluminium hydroxides. There are cases when instead of  $\text{Al}^{3+}$  or  $\text{Mg}^{2+}$  cations there may exist  $\text{Fe}^{2+}$ ,  $\text{Fe}^{3+}$ ,  $\text{Mn}^{2+}$ ,  $\text{Ti}^{4+}$ ,  $\text{Ni}^{2+}$ ,  $\text{Cr}^{3+}$  or  $\text{Li}^+$  octahedrons. The distance between oxygen-oxygen atoms is 0.260nm, the available space for the central cation is 0.061nm, and the thickness of the octahedral layer of the clayey mineral is 0.505nm.

There are five types of forces that may appear between layers (Marshall, 1964):

- van der Waals bonding forces that appear between parallel, electrostatically neutral layers. The bond is weak, but large crystals may form in such a way (talcum -for example);
- hydrogen and van der Waals bonding forces that appear between adjacent faces which are oxygen-hydroxyl or hydroxyl- hydroxyl. The hydrogen bonds remain stable in the presence of water;
- quasi-neutral electric layers that are separated by water layers and have hydrogen bonds;
- tetrahedral or octahedral layers into which isomorphous substitutions appeared may gain back their electrical neutrality if cations are attracted between the layers. This bond (that occurs in mica for example) may cause cleavage phenomena (the electrostatic bond from the cations is weaker than the covalent inter-crystal bond), but it is not sensible to water or polar liquids;
- when the surface electrical density is moderate, the ions adsorbed at the layers interface may hydrate, which will lead to the layer separation and expansion phenomena. This bond is weak and is mainly dependent on the

adsorbed cations characteristics, required hydration energy and electrical charge distribution.

Bi-layer sheets are made of a tetrahedral layer and an octahedral layer. As mentioned before, the tetrahedral layers has free tips ( $O^{2-}$ ), orientated in a single direction, so that when it comes into contact with an octahedral layer, two thirds of the oxygen atoms are shared for both layer types (Figure 5.2). The hydroxyls will be found in the plane, exactly above the tetrahedral layer, in the hexagonal space.

The bonds between two sheets are both hydrogen and van de Waals bonds. The bond is strong enough so that there will be no sheets separation.

Deviations from the ideal tetrahedral lattice exist though, because of the small difference between the distance oxygen-oxygen in the tetrahedral layer versus the same distance in the octahedral layers. The thickness of the bi-layer lamella varies between 0.72nm (kaolinite) and 1.01nm (hydrated halides). The halides contain water dipoles between the bi-layer sheets. By dehydrating (which occurs even at relatively low temperatures) it can also reach a 0.72nm thickness. Dehydration is an irreversible process.

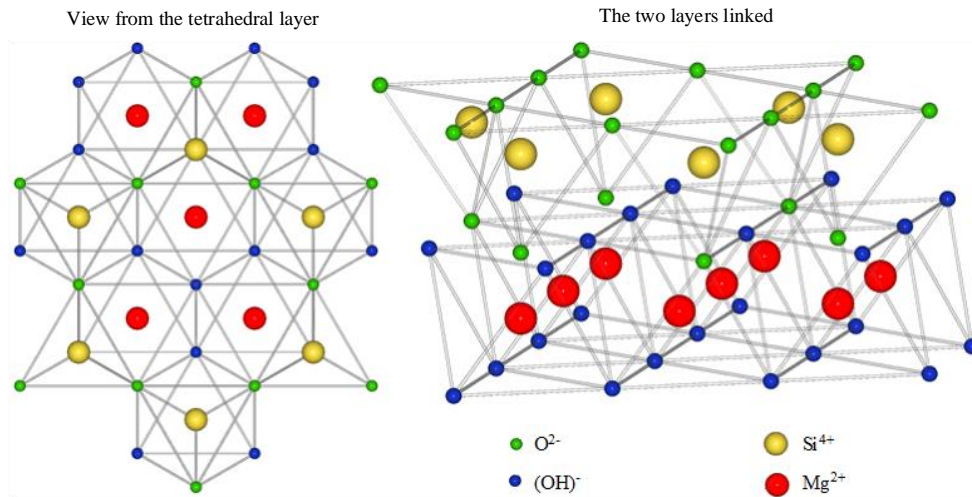


Figure 5.3: Bi-layer sheet [19]

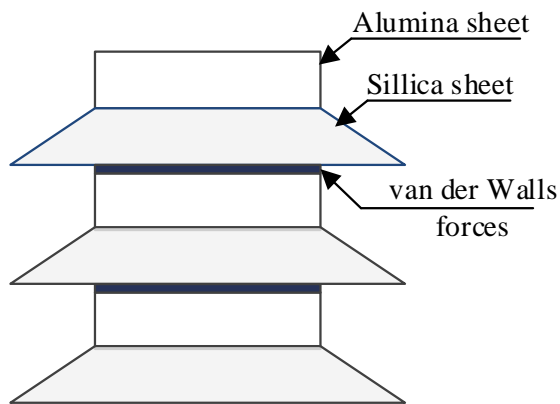


Figure 5.4: Bi-layer sheet schematic representation (Kaolinite)

Figure 5.4 illustrates the schematic representation for a bi-layer sheet structure, mineral which is known as kaolinite  $[\text{Al}_2[\text{Si}_2\text{O}_5](\text{OH})_4]$ . Because of this crystalline structure, the clays that contain kaolinite have a reduced sensibility to water, which translates into small swelling pressures and low water retention. Kaolinite was named after the Chinese town Kao-Ling.

If instead of the alumina sheet there is a magnesium sheet, the mineral is called serpentine  $[\text{Mg}_3[\text{Si}_2\text{O}_5](\text{OH})_4]$ .

The tri-layer sheets contain an octahedral layer and is bordered by two tetrahedral layers with the tips orientated towards the former. The tetrahedron's oxygen atoms are common for the octahedral layer also. As for the bi-layer sheets, the octahedral layer's corners which are hydroxyls will be found exactly above the tetrahedral layer, in the hexagonal space (Figure 5.5).

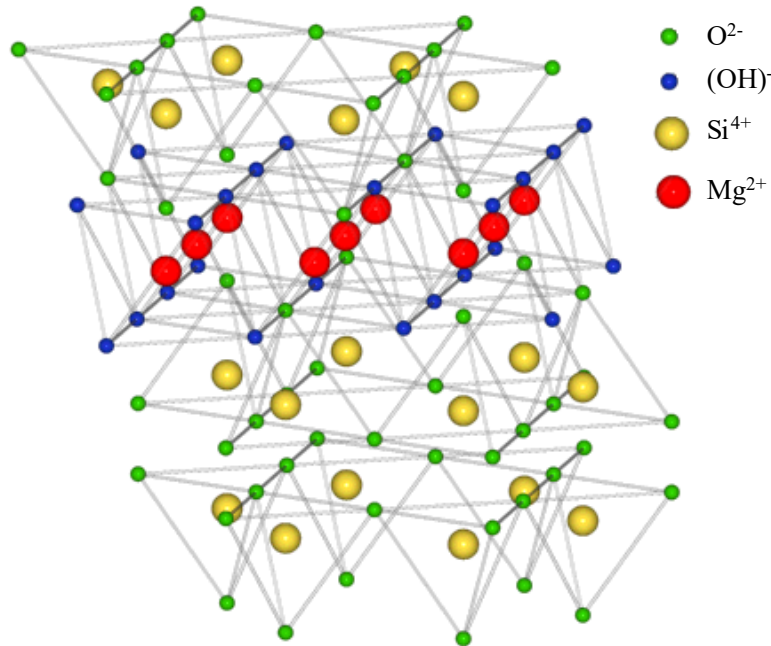


Figure 5.5: Three-dimensional structure of the tri-layer sheets. Interaction between the sheets [19]

The bonds between two tri-layer sheets are made either through van der Waals forces or through the cations that are found between the sheets in order to balance the electric charges. These bonds are very weak and can be easily destroyed through cleavage or hydration of the bonded cations. The thickness of the lamella, including the inter-sheets gap, varies from 0.96nm up to complete separation.

Depending on the type of bond between the tri-layer sheets, we can distinguish the montmorillonite  $[(\text{Na},\text{Ca})_{0.33}(\text{Al},\text{Mg})_2[\text{Si}_4\text{O}_{10}](\text{OH})_2 \cdot n\text{H}_2\text{O}]$  or the illite  $[\text{KAl}_2[\text{Si}_3\text{AlO}_{10}](\text{OH})_2]$  or  $[\text{KMg}_3[\text{Si}_3\text{AlO}_{10}](\text{OH})_2]$  minerals.



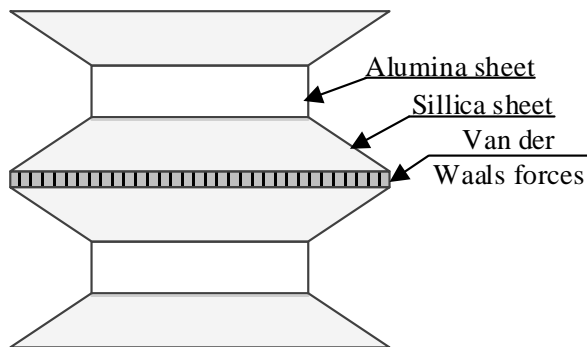


Figure 5.6: Tri-layer sheet schematic representation (Montmorillonite)

The montmorillonite (Figure 5.6) is a part of the smectite family. The accumulation of this mineral is called bentonite, which can be calcic, potassic or sodic, depending on the dominant element in its structure (Ca, K and Na respectively). It bears the name of a French town, Montmorillon, where it was discovered in 1847.

The bonds are relatively weak, so the water molecules can easily penetrate between the sheets, which in turn will cause the mineral to expand (or contract when the water is not there anymore). This mineral is widely used for the drilling slurry or in the geocomposites industry.

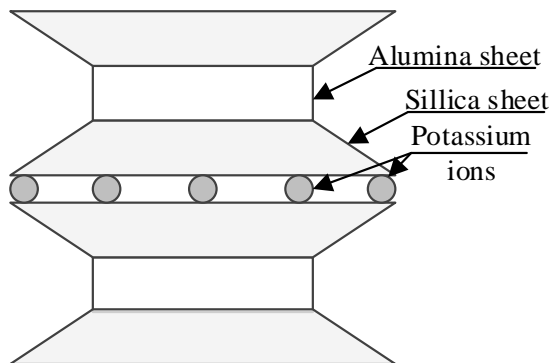


Figure 5.7: Tri-layer sheet schematic representation (Illite)

Illite (Figure 5.7) is formed from altered muscovite (white mica) and feldspars. It bears the name of the Illinois state, where it was discovered in 1937. Through isomorphic substitution, a part of the cations ( $Al^{3+}$  for example) are replaced with atoms that have the same atomic mass, but inferior valence ( $Mg^{2+}$  for example). Because of the positive charges deficit, potassium (K)

ions will be attracted from the environment, which will form bonds between the sheets. In this way, the illite has a structure that is more stable than the one of montmorillonite but not as rigid as for kaolinite.

#### **5.4 The clay-water electrolyte system**

As in the case of ionic solutions, the hydrophobic sols do not have a net electric charge, so the electrostatically charged particles must compensate the charges between them. The internal balance of the charges in a sol is characterised by the "electric double layer" (Gouy, 1910 - Chapman 1913). The electric double layer is made of electrically charged particles and an equivalent quantity of punctual charges that accumulate in the liquid surrounding the particles. These punctual charges are also known as counter-ions. When the clay is dry, these counter-ions remain attached to the clay particle. That is why when the clay is damped, the electrical double layer is created spontaneously.

The hypotheses of this model are:

- the ions that make up the system are considered punctual charges, with no interaction between the ions with the same sign;
- the charge is uniformly distributed on the surface;
- the surface of the particle is plane;
- the media permittivity ( $\epsilon$ ) is constant in the considered environment.

#### **5.5 Attraction and rejection forces equilibrium**

Keeping in mind that the clay particles have the same electrical charge sign on their surface (usually negative), rejection forces will appear between the particles. This rejection forces are electrostatic, so that they vary exponentially with the distance between the particle and with their unbalanced electrical charge.

Also, knowing that the electrolytic system of clayey soils contains a relatively large number of free ions, the rejection forces between the particles are small. If for a reason of the other, the free ions found in the clay are not in high enough number in order to satisfy the free charges from the clay particles, a rejection phenomenon will appear between them. The rejection force will

decrease exponentially with the increase of the distance between the particles (Figure 5.8).

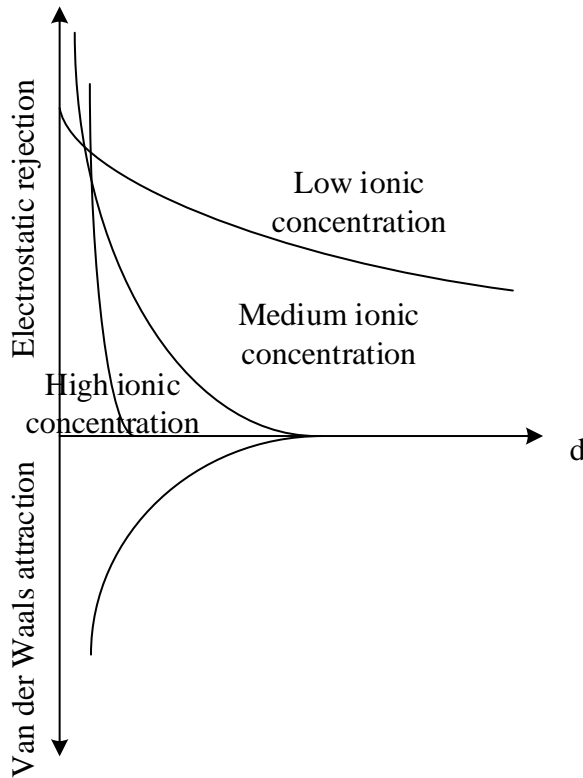


Figure 5.8: The variation of the attraction and rejection forces between the clay particles with the distance, for high, medium and low free ions concentration [19]

The coagulation proves the existence of attraction forces between particles. At first glance, van der Waals forces do not seem strong enough or acting at a large enough distance in order to induce clay particles proximity. These forces have a small magnitude and rapidly decrease with the increase in the distance between particles. Yet, they are additive in nature, meaning that the attraction force of a group of particles will be the sum of the attractions of each particle. By adding up these forces one may observe that not only that the attraction force is much larger in modulus, but that it also decreases a lot less with the increase of distance. For two atoms, the van der Waals attraction forces are inversely proportional with the seventh power of the distance

between them, but for two large particles it is inversely proportional with the third power of the distance.

The summation of the attraction and rejection forces shows that for relatively large electrolytic concentrations, the rejection will be larger only for very small distances between the particles, and that in the rest, the rejection force effect is very small.

For low electrolytic concentrations, the rejection forces are large, and the clay will become a "quasi-stable sol", because the hydrophobic sols can never be stable. Sooner or later they will coagulate.

## **5.6 Test your understanding**

### **Problem 5.1**

Which are the main types of clay minerals?

### **Problem 5.2**

What types of weathering lead to the formation of clay minerals?

### **Problem 5.3**

How does the ionic content influence the attraction forces between clay particles?

### **Problem 5.4**

Specify three types of electro-chemical bonds that occur within the soil.



## **6 BONDED WATER**

It is well known that due to the reduced particle size, the physical and mechanical behaviour of the soils containing large amount of fines, is deeply influenced by the ionic and electrolytic bonds that are established between them.

In the soil there are three types of water:

- strongly bonded water;
- weakly bonded water;
- free water

Strongly bonded water is formed by water dipoles packed together near the solid surface on about 2-3 molecules thickness. This is virtually the hydration water and it may not be removed unless extremely high temperatures are applied. This kind of water is in a solid state due to the electrostatic attraction, yet no bonds specific to water freezing are present, where hydrogen bonds are formed. From the geotechnical point of view, it may be considered as a part of the solid with no engineering importance.

Weakly bonded water is represented by the water dipoles ensuring the plasticity related properties of clays. The amount of this kind of water governs the distance between solid particles, as well as the bond strength. It may be removed by oven drying at 105°C. It is the most important type of water for clays from the engineering point of view.

Free water is the water unbound to solids, filling the soil voids. It is very important for sands and it may be acted by two kinds of forces: gravity and capillary rise.

The weakly bonded water forms the adsorption complex or the electrical double layer of clays (Fig. 6.1).

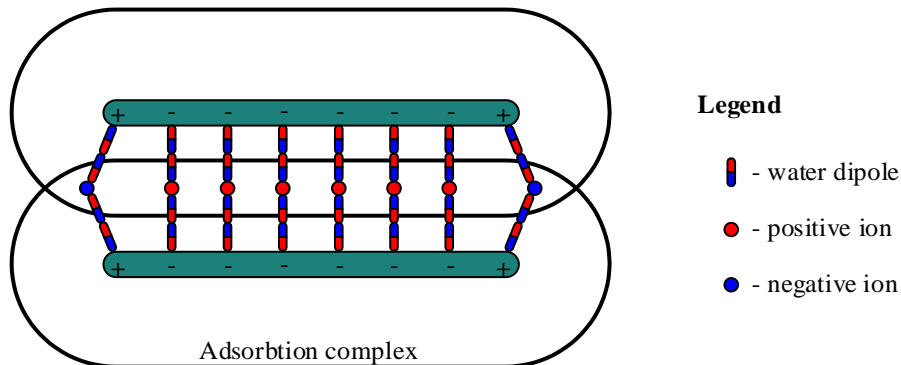


Fig. 6.1: The adorption complex of clay minerals

The meaning of the electrical double layer is on one hand the physical layering in the adsorption complex of the positive charges given by the free ions making water dipole bridges between two adjacent negatively charged clay particles. The distance between two clay particles is governed by the so-called potential pit principle, since simultaneously a repelling force of electrostatic type and an attraction force through the dipole and ion bridges are exerted between two neighbouring particles.

The suction curve, known in the literature as the Soil-Water Characteristic Curve (SWCC) (Fig. 6.2), describes the influence of the solid clay mineral on the water dipole. The suction is described in terms of suction index pF, having the meaning of the negative pressure exerted by the solid, expressed in logarithmic centimetre water column; the largest value recorded being pF 7 (meaning  $10^7$  cm water column =  $10^5$  m water column = 100 kN =  $10^4$  atm =  $10^6$  kPa). This is an equivalent mechanical pressure due to the presence of electrostatic forces and capillarity phenomena and has no meaning with respect to the mechanical limit of 7 atm.

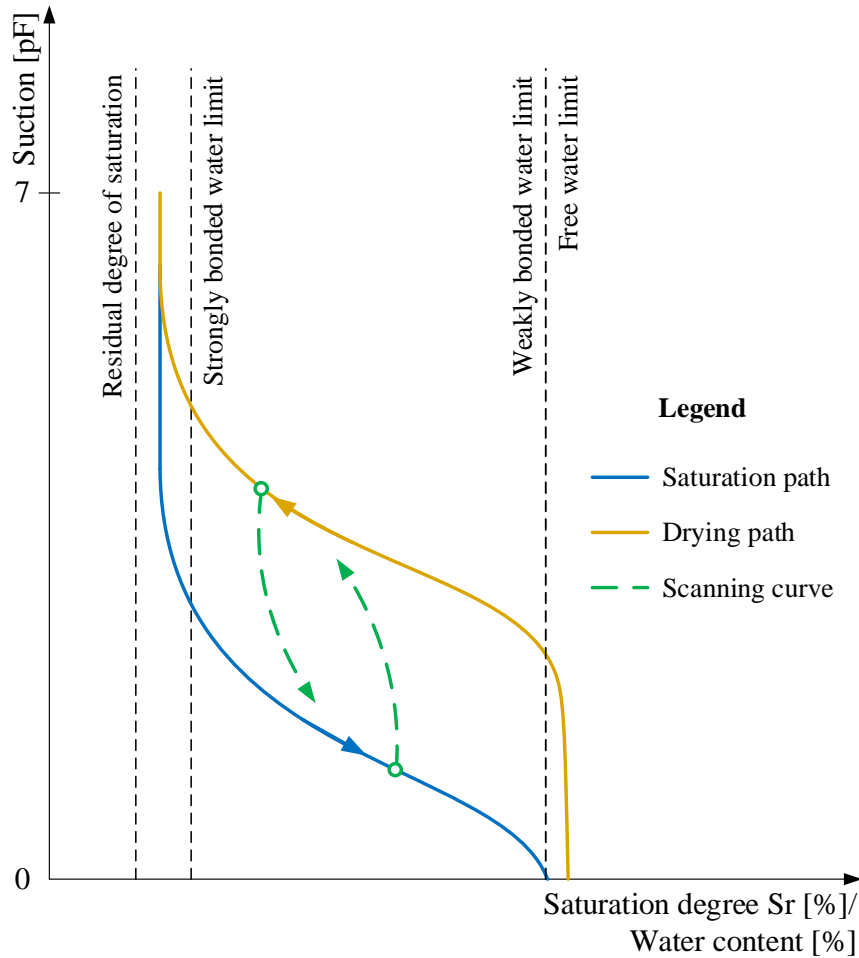


Fig. 6.2: Soil-water characteristic curve

On the graph there are three main zones. The closest to the solid surface are the water dipoles kept with pF 7 to pF 5 almost in a solid state.

The governing bond between solids is Van de Waals. The electrical bonding synchronises up until the particles are mechanically taken apart. If the moisture content is high enough, putting them together will make them resynchronise. If the moisture content is too low, the repellent force will prevent the parts to stick together.



## 6.1 Consistency limits of cohesive soils

The cohesive soil heave may have two causes:

- water migration due to saturation or evaporation;
- water migration due to freezing.

In the first case, due to the electrical double layer contact from particle to particle, the top surface clay particles will have an extra adsorption potential due to water evaporation, so that the water particles migrate from the lower layer to the upper one. The same thing happens when a clay layer comes in contact with a saturation sand layer (Fig. 6.3 a.)

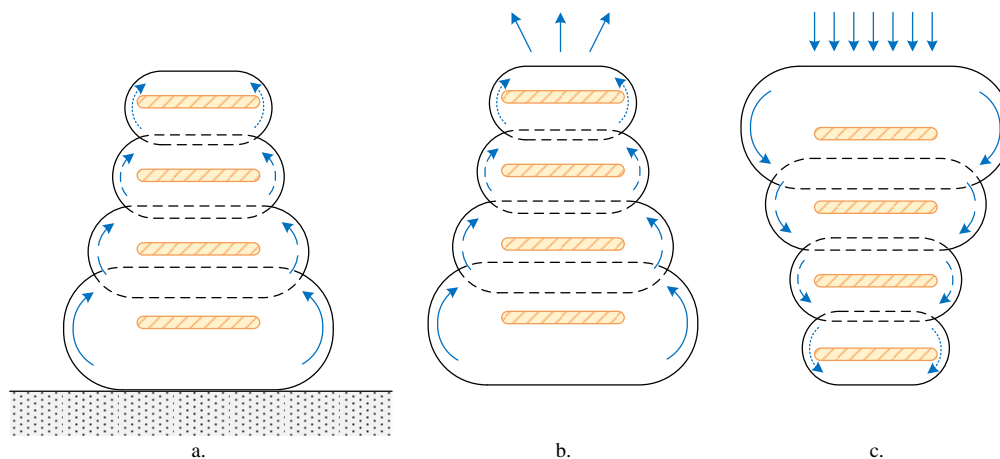


Fig. 6.3: Water movement across the adsorption complex

In the winter time, the water from the top clay particles freezes and does not participate to the electrical double layer complex anymore. Because of this, the water will migrate from the lower clay layers in order to balance the adsorption potential. This process is repeated until the frozen water creates large ice lenses that block the liquid flow (Fig. 6.3 b.).

During the spring time, when water thaws, it is impossible to develop the same adsorption gradient to draw down all the water attracted when freezing. This phenomenon, along with uneven thawing, will induce settlements for all foundations above frost depth (Fig. 6.3 c.). For Bucharest, frost penetration depth is about 90cm.

The clayey soils' electrical double layer is greatly expanded, but maintains a low permeability of the material. The sands have high permeability and low adsorption complex, making the silts the most frost sensitive soils having both high permeability and an important adsorption complex.

A consequence of balance between ionic and Van der Waals bonds is the minimum volume of the soil when drained. When the water content decreases at a certain point, the repelling force will prevent the solids coming closer together.

In the graph of volume variation with moisture content (Fig. 6.4) there is a plateau zone for low moisture contents and a linear part for bigger moisture content. The break point is denoted  $w_s$  and is called shrinkage limit of soil passing from a solid state into a semi-solid state. Generally, for a moisture content less than  $w_s$ , the colour of the solid is lighter.

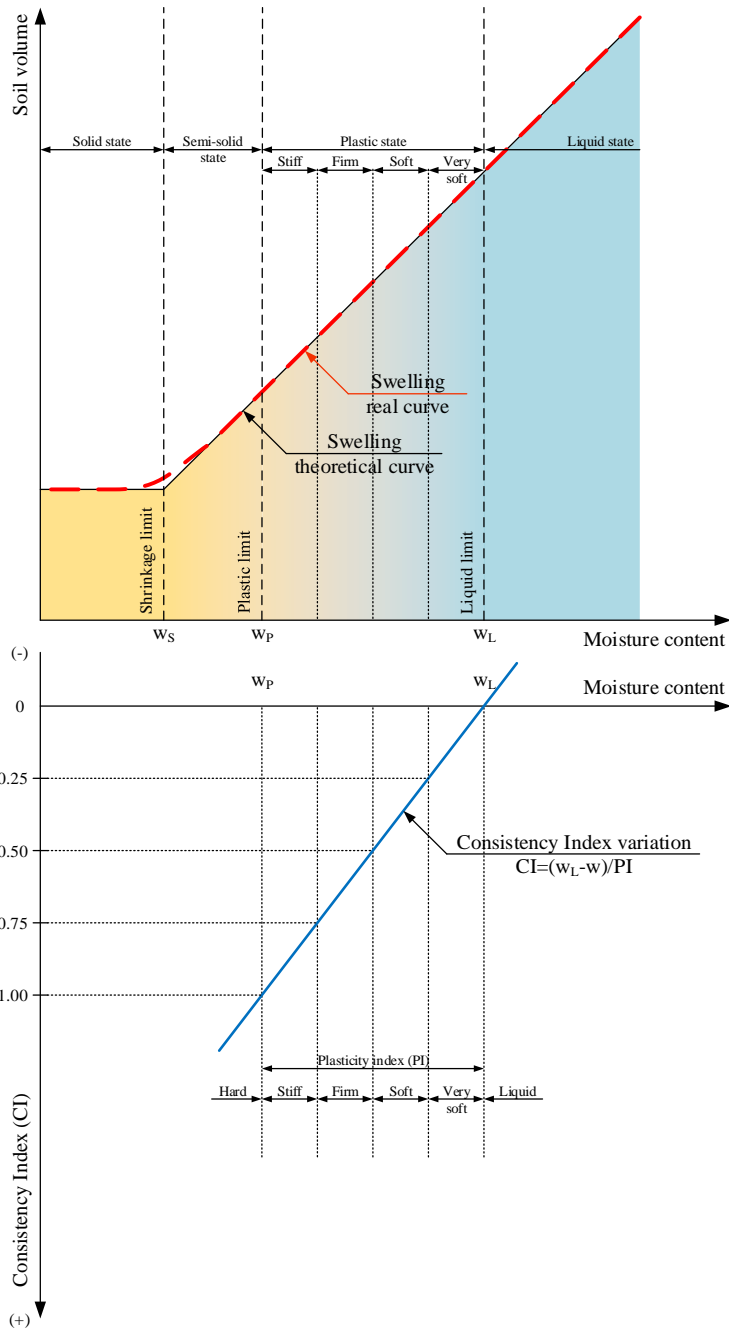


Fig. 6.4: Soil's volume and consistency index variation as functions of the moisture content

The soil generally may be found in one of these physical states:

- solid state – a very dry soil with strong bonds with whom impossible to be worked with;
- semisolid state – the soil is hardly workable and brittle, as it cracks or crumbles;
- plastic state – the soil may be remoulded without cracking;
- liquid state – the water content of the soil renders it impossible to keep its own shape under the load of its weight.

If we continue increasing the moisture content, the electrostatic bonds become weaker and weaker up to a point when the soil is unable to hold its shape anymore and it is considered liquid. The moisture content for which the soil turns from plastic to liquid is denoted  $w_L$ .

In the colloquial geotechnical engineering language, there is often used the notion of “plastic state” or “plastic domain”. It represents an obstruction of the correct usage, as, from the mechanical point of view, even the hardest soil is in fact behaving as a plastic material. Thus, even taking into consideration the classic definition of this domain’s limits, it is not referred as “plastic domain”, but as “ductile plastic domain”.

$w_P$  and  $w_L$  are commonly known as Atterberg limits, plasticity limits or upper and lower plastic limit. These two values that are defining the range when the soil is workable depend mostly on the soil solid specific surface (described by grading) and the type and activity of the clay mineral. The most active clay mineral is montmorillonite, followed by illite and then kaolinite.

For the same clay mineral, drawing the variation of Atterberg limits with different soils having various percentage of the same type of clay, we obtain the variation displayed in Fig. 6.6. The plasticity range width is described by an index referred to as the plasticity index:

$$PI = w_L - w_P \quad (6.1)$$

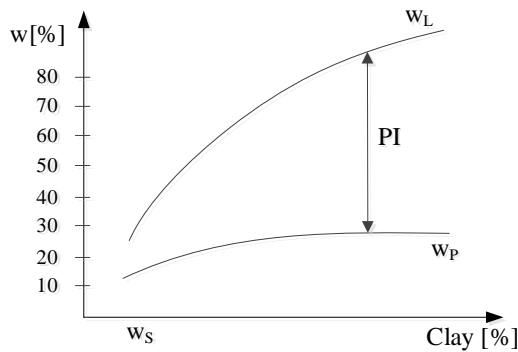


Fig. 6.5: Plasticity limit variation as functions of the clay percentage

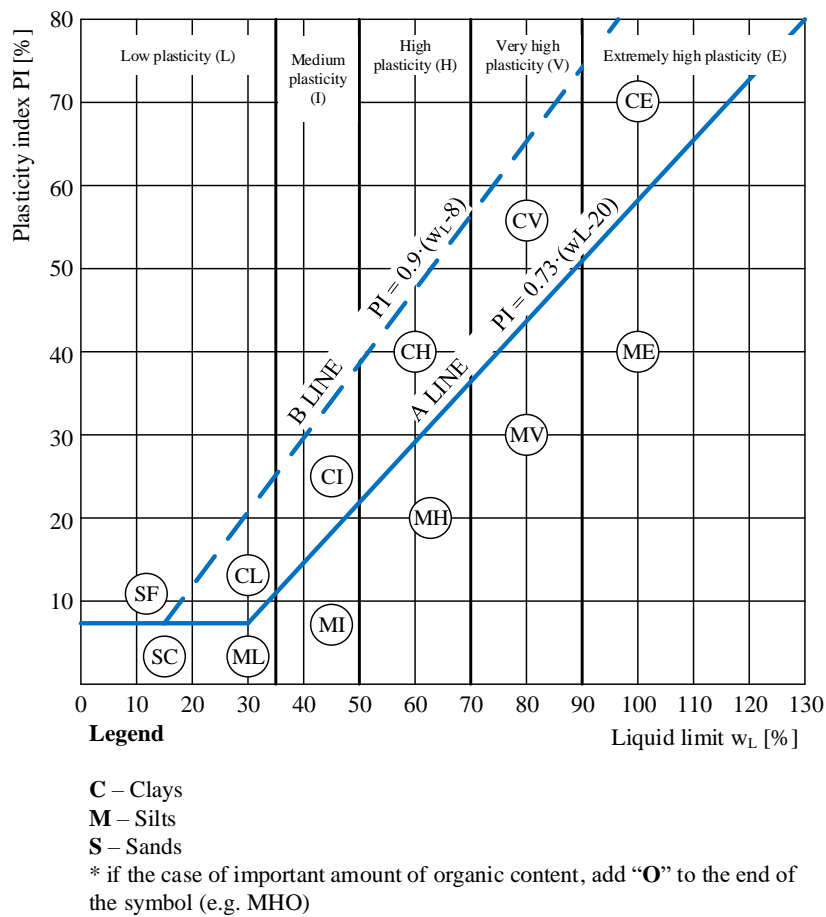


Fig. 6.6: Plasticity chart (Unified Soil Classification System)

There are many soil classifications function of the plasticity index, among which there may be mentioned the Romanian norms, displayed in Tab. 6.1, and the USCS, depicted in Fig. 6.6.

Tab. 6.1: Soil classification according to the plasticity index

Activity index $I_A$ [-]	Soil classification
0	Soil with no plasticity
0÷10	Low plasticity soil
10÷20	Medium plasticity soil
20÷35	High plasticity soil
35>	Very high plasticity soil

An important observation to always bear in mind is that granular soils, such as fine sands or coarser, have no plasticity, passing directly from solid to liquid.

In order to characterize the clay mineral mixture of a certain soil it is used an index called activity index:

$$A = \frac{PI}{\%Clay} \quad (6.2)$$

Using the activity index, the soils may be classified as presented in Tab. 6.2.

Tab. 6.2: Soil classification according to the activity index

Activity index $I_A$ [-]	Soil classification
<0.75	Inactive soil
0.75÷1.00	Low activity soil
1.00÷1.25	Active soil
1.25>	Very active soil

The plasticity index is actually used to describe the cohesive soil nature, correlate soil strata and investigate in detail the variation of soil properties. In order to describe the state, it is used an index called consistency index (CI):

$$I_C = \frac{w_L - w}{w_L - w_p} \quad (6.3)$$

where  $w$  is the moisture content in natural state.

## **6.2 Shrinkage limit**

In order to obtain the shrinkage limit, one has to determine the variation of the sample's volume as it dries, using a reference volume (possibly a mould) and mercury. The required fluid is mercury, because it cannot bond to, stick to, fill the voids, saturate or dissolve the soil sample. If a sample's moisture content is less than the shrinkage limit, it will disintegrate during saturation in the oedometer (see chapter 9.3) or direct shear equipment (see chapter 10.2.1), due to the increase of air pressure inside it.

## **6.3 Laboratory methods of determining the Atterberg limits**

The standardized methods for finding the plastic limits are given in STAS 1913/4 [20] and are briefly described below.

### **6.3.1 Plastic limit**

Terzaghi considered the plastic limit as the moisture content limit beneath which the free water's properties are not similar to the commonly known ones. The most acknowledged definition of the plastic limit is still the boundary moisture content above which the behaviour is ductile plastic, which implies the fact that the soil will deform without volume modifications or cracks or splits appearing.

- Method of soil cylinders

A mass of soil in plastic is rolled by hand on a porous glass sheet into cylinders of 7 cm length and 3÷4 mm diameter. By rolling, the soil gradually loses moisture content until cracks appear on the cylinder surface, showing that the soil becomes semi-solid. If the cylinders are not cracked, the samples are remixed and the procedure is repeated. When the soil is brought to a semi-solid state, three samples are taken and their average moisture content is  $w_P$ .



Fig. 6.7: Rolling the soil cylinders against the sandblasted glass

- Method of absorbing media

A soil disc of 2 mm thickness and 5 cm diameter in plastic state is pressed under a constant stress 6420kPa between two sets of filter paper pieces (absorbing media) for 30minutes. The water is thus slowly drawn out. Following the compression stage, the disc is kept from the edge and if it bends, when pressed a concave glass form, the procedure is repeated. If it cracks, it is considered that its moisture content reached  $w_p$ , and the moisture content is measured. The average moisture content of three samples prepared as such is  $w_p$ .

### **6.3.2 Liquid limit**

In order to determine the liquid limit, Casagrande proposed a method consisting of a cup that, filled with a soil paste, is to be struck against a support. Later, more engineers studied the problem, resulting in more types of determination of the liquid limit.

Nagaraj (1990) explains that for all the soils, near the liquid limit, the permeability coefficient is almost equal (Tab. 6.3), due to the fact that the voids' sizes are approximately equal, which may be transposed into the idea that clays will coagulate the same manner as the silts (Fig. 6.8). This model takes into consideration only the dimensions of the voids between the particle clusters.



Tab. 6.3: Liquid limit and permeability coefficient of different soil types (Nagaraj)

Soil type	wL [%]	eL [-]	k [ $\cdot 10^{-9}$ m/s]
Bentonite	330	9.240	1.28
Bentonite mixed with sand	215	5.910	2.65
Marine clay	106	2.798	2.56
Brown common clay	62	1.674	2.83

In general, the liquid limit depends on the specific surface of the analysed soil and the electrostatic force between the particle surface and the ions of the double electrical layer.

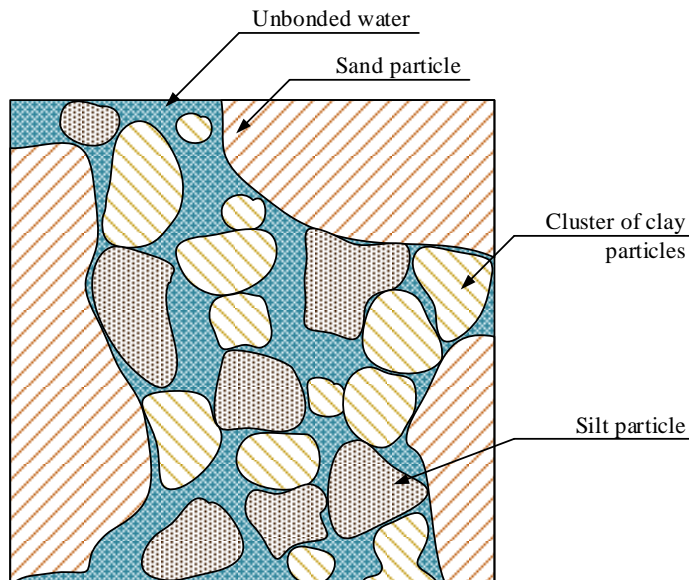


Fig. 6.8: The Nagaraj model of the soil's structure near the liquid limit [19]

- Casagrande's cup method

Casagrande device is a mechanism rising a cup to 1cm height and letting it suddenly fall. The cup is filled with soil paste for about 2/3 of its volume (the paste has to be horizontal while the cup is resting on its support) and with a template a groove is drawn at the surface. It is counted the number of falls

necessary for closing the groove on a 1.2cm distance measured with the template. For each sample the moisture content is found and the process is repeated four times so that two samples to be slightly above and two slightly below the closing number of 25 blows corresponding to the liquid limit  $w_L$ . If a sample closed at exactly 25 blows, the value is disregarded. It is drawn a semilogarithmic graph of the number of blows with moisture content. From the point where the line between four points intersects the 25 blows horizontal it is found on the axis  $w_L$ . If three points are not collinear, the test is repeated.

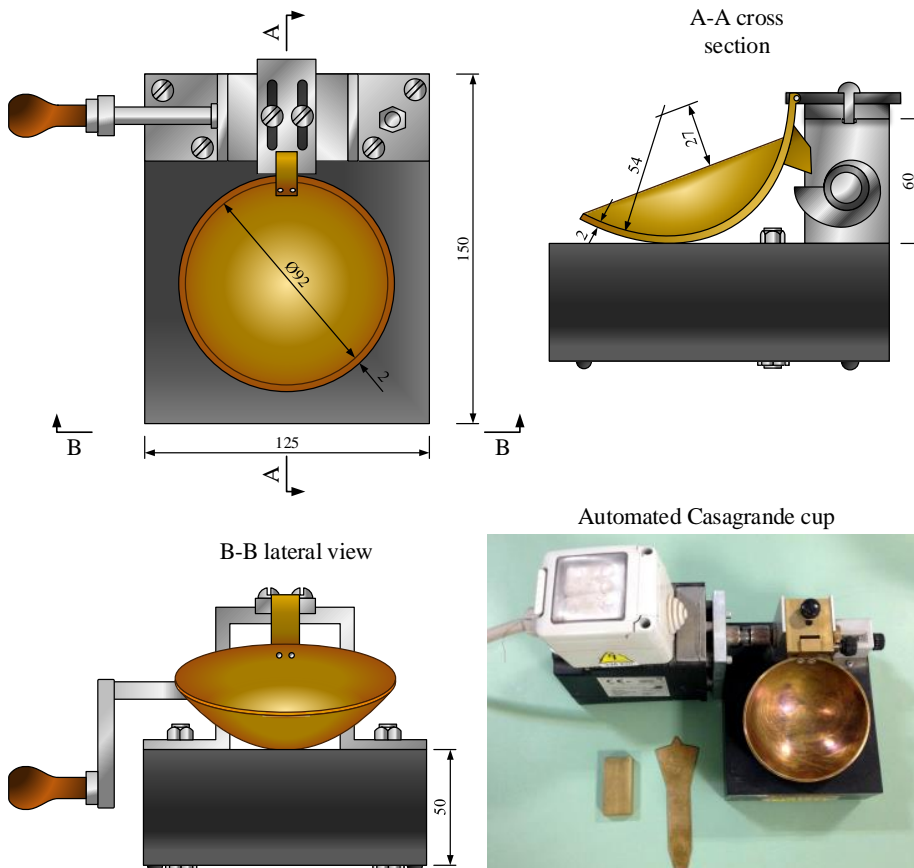


Fig. 6.9: The Casagrande cup

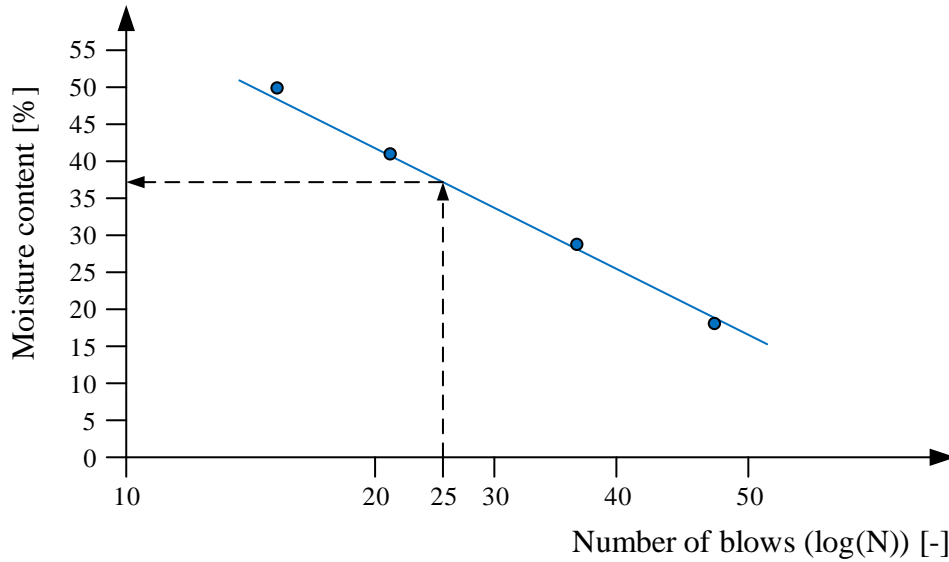
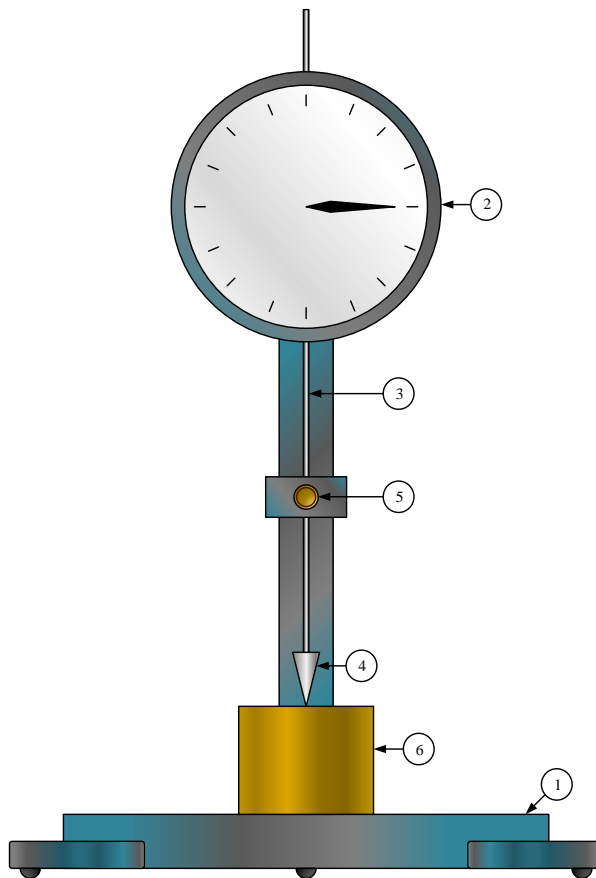


Fig. 6.10: Flow curve for determining the liquid limit by Casagrande cup method

- Cone method (not covered in the STAS 1913/4)

A rod with a cone scaling 80g is left to fall freely for 12 seconds from a soil sample surface. The cone has the tip angle of 30° and for each test is measured the penetration depth as the difference between the rod's end before being left to fall and after penetration. The moisture content of the soil paste is also found.



Legend

- |               |                           |
|---------------|---------------------------|
| 1. Body       | 4. Cone                   |
| 2. Micrometer | 5. Stopper                |
| 3. Rod        | 6. Mould with soil sample |

Fig. 6.11: The penetrometer apparatus

Four sample are tested with the moisture content set to have two penetrations slightly above and two slightly below 20mm. A graph is drawn in decimal scale with the penetration depth and moisture content. The intersection with the 20mm horizontal is considered to be  $w_L$ .

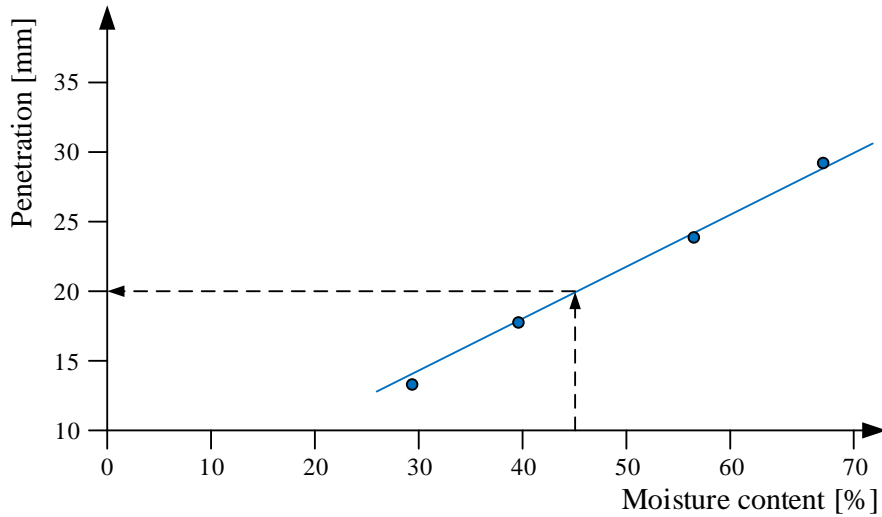


Fig. 6.12: Flow curve for determining the liquid limit by free fall cone method

#### 6.4 Test your understanding

##### Problem 6.1

How can one assess the activity of a clay mineral?

##### Problem 6.2

How does the plasticity of a soil vary with the content of fines?

##### Problem 6.3

How is soil plasticity influenced by the mineral type?

##### Problem 6.4

Testing a soil sample using the cylinders method has yielded the following results:

wet mass [g]	dry mass [g]
14.05	12.07
10.71	9.22
13.25	11.42

Determine the plastic limit.

**Problem 6.5**

Testing a soil sample using the Casagrande cup method has yielded the following results:

number of falls [-]	moist mass [g]	dry mass [g]
40	21.16	15.70
27	17.40	12.75
18	16.56	12.00
11	16.79	12.02

Compute the liquid limit.

**Problem 6.6**

Testing a soil sample using the cone method has yielded the following results:

cone penetration [mm]	moist mass [g]	dry mass [g]
23.7	16.82	12.50
30.2	12.48	8.87
35.4	14.56	10.00
38.9	18.54	12.50

Compute the liquid limit.

**Problem 6.7**

A moist soil sample has the following known data:

- moisture content  $w = 17\%$ ;
- liquid limit  $w_L = 38\%$ ;
- plastic limit  $w_P = 15\%$ .

Determine the following:

- a) plasticity index;
- b) consistency index;
- c) classify the soil based on consistency.



## **7 UNBONDED WATER**

### **7.1 Unbounded groundwater**

The free water in the ground represents all molecules that are not electrostatically bound by the solid minerals as hydration water or as a part of the electrical double layer. There are two main forces acting upon the free water dipoles, namely the superficial tension forces and the gravity. Other forces like the one induced by various types of osmosis (thermo-osmosis, electro-osmosis, chemo-osmosis and so on) shall not be the object of this book, the study of these kind of flows being a matter of intricate coupling phenomena.

The free water in the ground is distributed as shown in Fig. 7.3. By aquifers there are defined the fully or partially saturated high permeability soil layers that allow water flow. The aquifers must be bounded to the base by low permeability geological structures called aquitard. If an aquifer layer has an aquitard above it preventing water flow, the ground water table may rise to an artesian level.

When the aquifer communicates freely with the surface, it is considered to be unconfined (Fig. 7.1) and the upper limit of the water is known as ground water table. If an aquitard layer bounds the top surface of an aquifer then the aquifer is considered to be confined (Fig. 7.2). If a lithological pressure is applied to the aquitard, it acts like a piston upon the aquifer below, the applied pressure inducing a ground water level rise known as artesian.



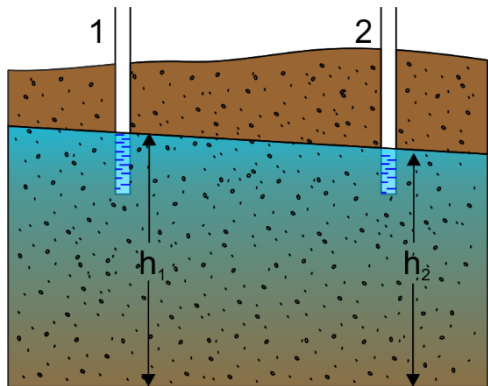


Fig. 7.1 Unconfined aquifer

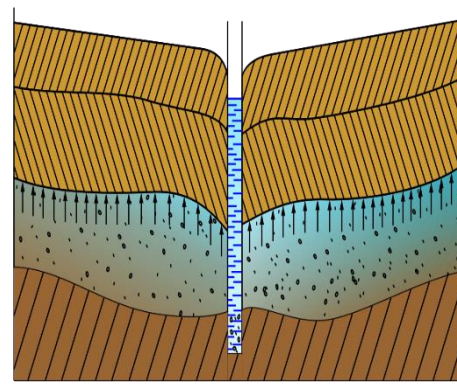


Fig. 7.2 Confined aquifer

Ground water level rise may also be produced by capillarity. In order to occur, the capillary rise needs an air-water interface and a set of narrow paths through the granular material similar to a bunch of tubes of various diameters. The part of the layer where the soil hosts the top end of the capillary tubes is the so called unsaturated capillary zone. Between this and the ground water table limit is the saturated capillary zone.

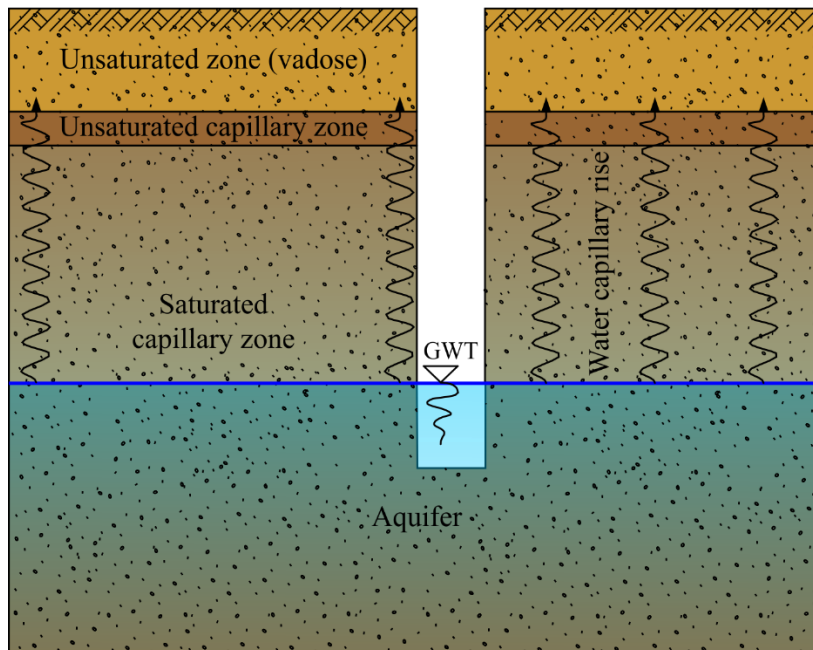


Fig. 7.3: Free water distribution in the ground

## 7.2 Capillary water

The soil grains are essentially hydrophilic substances, meaning that the adhesion forces between water and silicon-derived minerals are stronger than the cohesive bonds among water dipoles themselves. The capillary meniscus is formed adjacent to the wall due to the equilibrium of forces (adhesion, cohesion and gravity) rising the water on the hydrophilic surface. A dipole may be about the water-air interface, where the unbalancing of hydrostatic cohesive forces having as resultant the surface tension force maintain the flat surface by creating a layer of molecules subjected to tension forming a confining membrane for the rest of the mass (Fig. 7.4).

In the proximity of the hydrophilic wall, the water molecules “climb” one on top of the other until adhesive of each of them is balanced by the own weight and the superficial tension force forming an approximately circular shape. If the distance between two neighbouring walls is larger than the meniscus radius (Fig. 7.5), no capillary rise is recorded. The closer the walls are together (if the distance between them is smaller than  $2R$ ), the water climbs higher and higher pulled by the water tension force  $T$ . This means that the rise occurs only if there is an interface air-water surface. This phenomenon occurs in partially saturated sands (Fig. 7.5 b.), being called apparent cohesion, but not in saturated sands where no air-water interface is present and no superficial force may develop among the hydrophilic walls of solid grains.

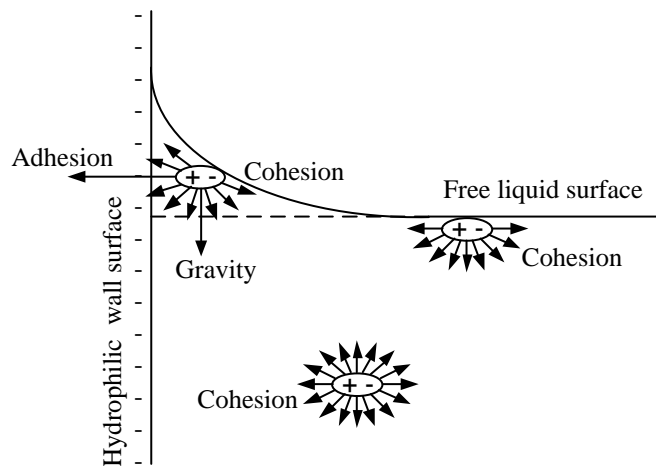


Fig. 7.4: Formation of the capillary meniscus

The sand own hygroscopic attraction draws from the environment air enough water to produce apparent cohesion at shallow depths under the sand mass surfaces where the material is dried by sun exposure. However, this mechanism which induces a certain amount of self-support for sand slopes steeper than the normal stable one, disappears as soon as sun exposure is stronger or during rainfalls and this is why no slope design may rely on this phenomenon.

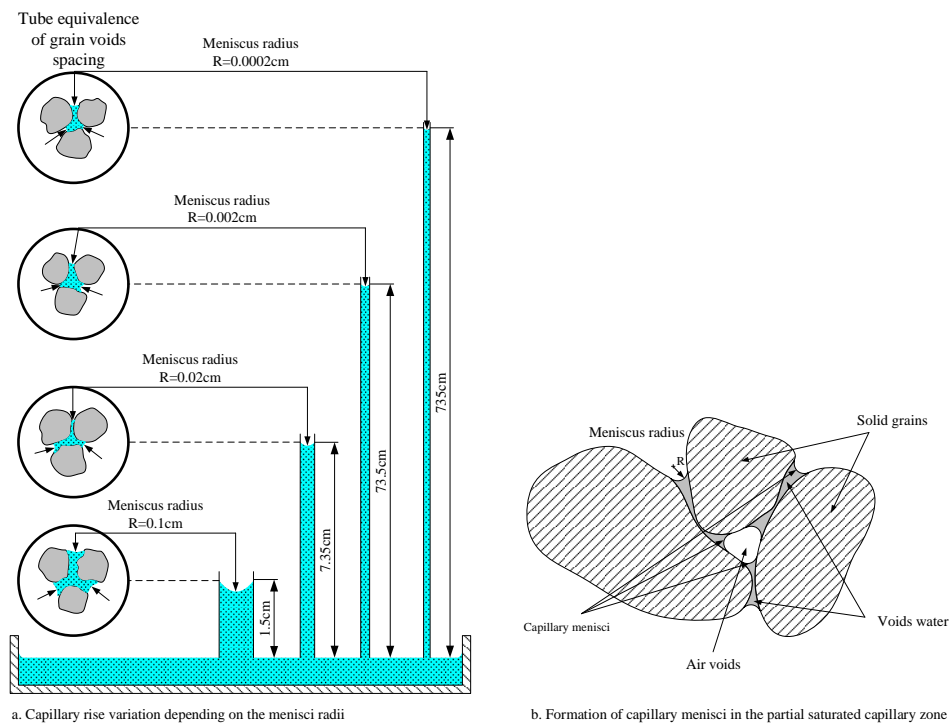


Fig. 7.5: Capillary rise depending on the relative distance between walls

If we consider the soil grains as forming a network of tube-like voids, an empirical approximation for the average tube radius,  $r$  is:

$$r = \frac{d_{50}}{5} \quad (7.1)$$

where  $d_{50}$  is the diameter for which 50% of the particles by mass are smaller.

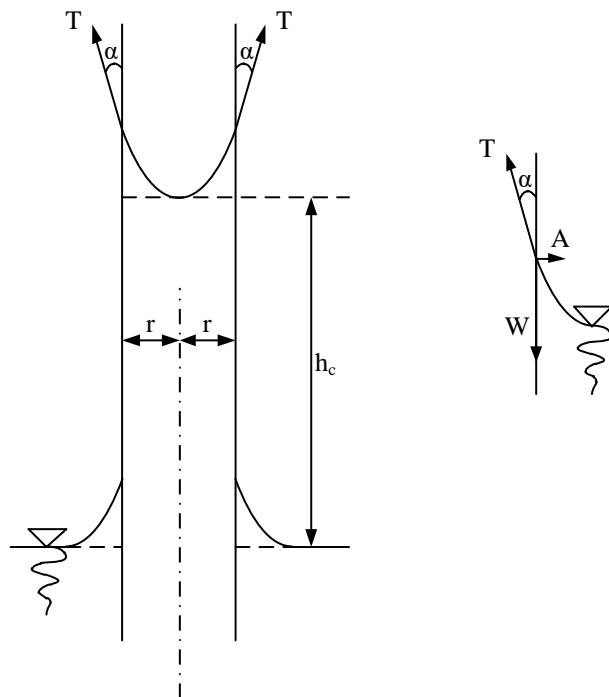


Fig. 7.6: Equilibrium of forces in a capillary tube

In order to assess the capillary rise  $h_c$  in an equivalent tube, we express the equilibrium of forces along the wall (Fig. 7.6). The adhesion force  $A$  acts on the horizontal direction and tends to shrink the tube diameter, being the force inducing the apparent cohesion of sands, but does not influence the capillary rise. The surface tension force vertical component acting on the tube perimeter has to be balanced on vertical direction by the own weight of the water in the tube, so:

$$T \cdot 2\pi r \cdot \cos \alpha = \pi r^2 \cdot h_c \cdot \gamma_w \quad (7.2)$$

The capillary rise is:

$$h_c = \frac{2 \cdot T \cdot \cos \alpha}{r \cdot \gamma_w} \quad (7.3)$$

Since the surface tension force is  $T = 72.8 \cdot 10^{-6} \text{ kN/m}$  and the angle  $\alpha \sim 0^\circ$ , it results that:

$$h_c = \frac{1.456 \cdot 10^{-6} \text{ m}^2}{r} \quad (7.4)$$

This means that the maximum capillary rise for a colloidal clay may be as much as about 7m, while for a sand it may be several centimetres. Even if the water flux of capillary water pumped by a clay material in contact with a concrete wall, is extremely low, the exerted pressure slowly destroys the unprotected buried structures. For the foundation bottom a simple layer of “capillary barrier” works very well in preventing capillary pumping, while for the foundation sides water tightening geomembranes (high density polyethylene sheets) are the best.

### 7.3 Gravitational water

In order to explain the behaviour of the gravitational water in soils, the term hydraulic head must be defined. The hydraulic head represents pressure in a liquid represented as hydrostatic rise above a chosen datum. Having two points with equal hydraulic head, between them there is no flow (Fig. 7.7). When between two points there is a difference of the hydraulic head, the flow occurs between those two points, from the higher pressure to the lower one (Fig. 7.8).

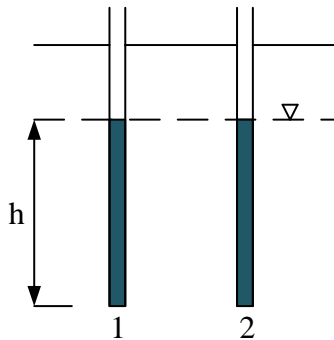


Fig. 7.7: Hydrostatic state

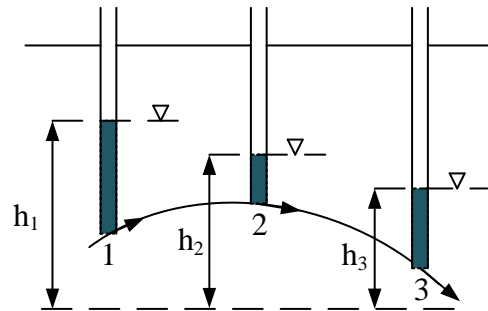


Fig. 7.8: Steady state seepage

The Bernoulli's principle states that the total mechanical energy of the fluid along a streamline is constant along each point of the streamline. This implies that the sum of the potential and kinetic energies remains constant.

$$E_h = z + \frac{p}{\gamma_w} + \frac{v^2}{2g} \quad (7.5)$$

where  $E_h$  is the total energy, also called total head,  $z$  is the elevation of the point where the equation is written in relation to a datum,  $p$  is the pressure in that point and  $v$  is the flow velocity.

The equation can be written using the hydraulic head  $h$  of the point, which can be associated with the potential energy component.

$$E_h = z + \frac{v^2}{2g} \quad (7.6)$$

The law that governs the flow of water through soils is the Darcy law. It was discovered in 1856 when the French engineer Henry Darcy was working to improve the water supply network of his birth town, Dijon. He noted that the velocity of the water passing through the soil is directly proportional with the difference in head ( $v \sim \Delta h$ ) and inverse proportional with the length of the path of water through the porous material ( $v \sim \frac{1}{L}$ ). The ratio between these two geometrical parameters influencing flow speed was denoted by  $i$  (7.7).

$$i = \frac{\Delta h}{L} \quad (7.7)$$

The coefficient of proportionality is a material constant known as coefficient of permeability and denoted by  $k$ . Darcy's law may be thus equated as:

$$v = k \cdot i \quad (7.8)$$

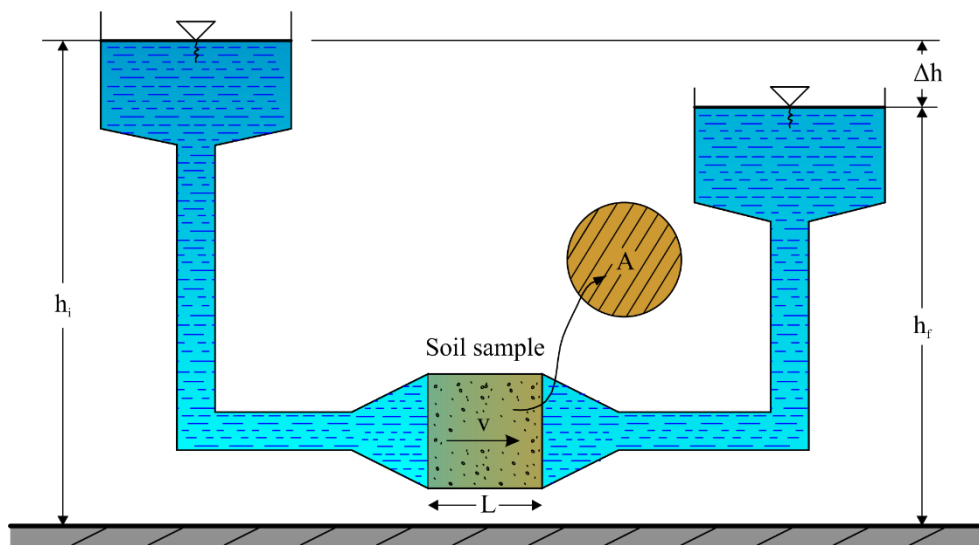


Fig. 7.9: Water flow through soils

The permeability coefficient may be approximated by empirical relationships only in few cases, starting based on the soil grading and sometimes corrected by voids ratio, yet valid only for cohesionless soils. The reason lays in the fact that cohesive soils have a certain electrostatic opposition to the water flow. So, if the cohesive soil state does not display a moisture content larger than the one of the liquid limit, most of the voids' water is actually bonded water for which displacement it requires a larger mechanical work than in the case of cohesionless soils (free water).

In order to find the value of the permeability coefficient  $k$  we may employ either laboratory tests using permeameters or in-situ tests. The two laboratory methods to determine it, according to STAS 1913/6 [21] are:

- constant head permeameter method;
- variable head permeameter method.

### 7.3.1 The constant head permeameter

The main feature of the method consists in maintaining a constant water pressure at the top of the sample. This means that the testing equipment properties are the head ( $\Delta h$ ), the length of the sample along the water path ( $L$ ) and the cross-sectional area of the sample ( $A$ ).

There are two builds for this type of permeameter: the dedicated type, shown in Fig. 7.10 and different equipment adapted for the test such as oedometer (which is an oedometer provided with drains to the soil sample top and bottom) or simply the triaxial compression cell (where in the cell it is applied a pressure to keep the membrane tight on the sample to avoid water infiltration outside the sample and the pressure gradient is imposed between the back-pressure line and the top line).

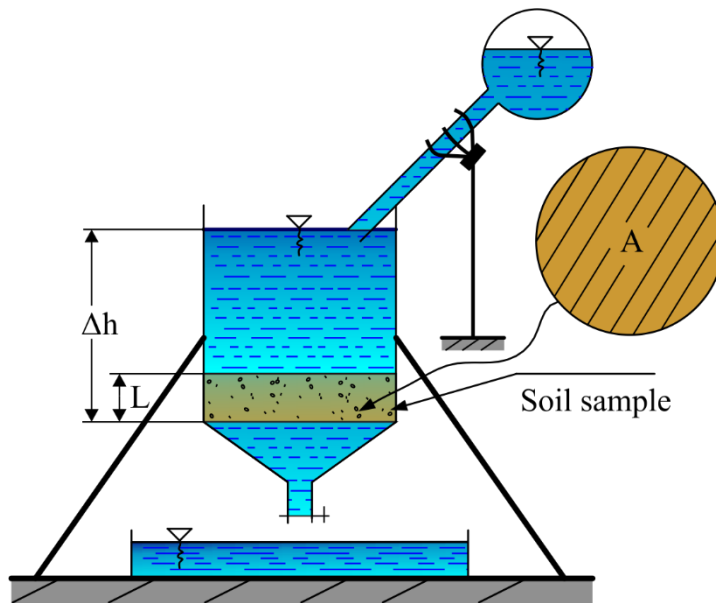


Fig. 7.10 The constant head permeameter

The discharge through the sample of area  $A$  of water flowing with the velocity  $v$  is:

$$q = v \cdot A \quad (7.9)$$

The total discharge or total volume of water passing in a given time  $t$  is:

$$Q = q \cdot t \quad (7.10)$$

Starting from (7.10) and replacing  $q$  according to (7.9) and then  $v$  as expressed by Darcy's law (7.8), we obtain:

$$Q = k \cdot A \cdot i \cdot t \quad (7.11)$$



In the previous equation, with respect to the constant head permeameter, the area  $A$  and the hydraulic gradient  $i$  are equipment constants, the time  $t$  is set according to the permeability of the soil sample for being able to record a measurable volume of water,  $Q$ . Based on these values, the permeability coefficient  $k$  is computed as:

$$k = \frac{Q}{A \cdot i \cdot t} \quad (7.12)$$

### 7.3.2 *The variable head permeameter*

The variable head permeameter consist of a cell or a mould where the soil sample is installed and a vertical water column induces the flow (Fig. 7.11). Generally, the water column is just a transparent tube or a hose mounted on a ruler so that the head variation to be recorded at certain moments of time. For the ease of computation, the pipe may have the area equal to the one of the specimen, yet most of the times is just a different one. In the computation here, the sample area is denoted by “ $A$ ”, while the one of the tube is “ $a$ ”.

Darcy’s Law is valid only for a constant head  $i$ . For the variable head permeameter we may consider that for an infinitesimal lapse  $dt$  the law is valid, so that the total discharge  $dQ$  flows through the sample. Even if the head varies by  $dh$  between  $h_{\text{initial}}$  and  $h_{\text{final}}$ , when computing the hydraulic gradient this change is so small that the head remains to a value  $h$ . So, the equation (7.11) becomes:

$$dQ = k \cdot A \cdot \frac{h}{L} \cdot dt \quad (7.13)$$

But the water passing through the sample must come from the tube above. Since the differential  $dh$  is defined as the difference between  $h_{\text{final}}$  and  $h_{\text{initial}}$  and the former is smaller than the latter, we have to apply the minus sign to the volume computation in order to avoid having a negative value. So, the amount of water out of the tube is:

$$dV = -a \cdot dh \quad (7.14)$$

The water volume out of the tube and the total discharge passing through the sample have to be equal:

$$dQ = dV \quad (7.15)$$

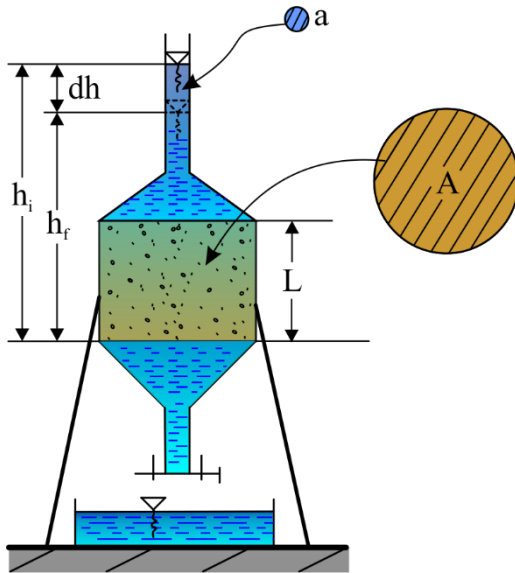


Fig. 7.11 The variable head permeameter

Replacing (7.13) and (7.14) in (7.15), we obtain:

$$k \cdot A \cdot \frac{h}{L} \cdot dt = -a \cdot dh \quad (7.16)$$

Separating the variables, we obtain:

$$\frac{A}{a} \cdot \frac{k}{L} \cdot dt = -\frac{dh}{h} \quad (7.17)$$

Integrating (7.17) on both sides of the equal sign over the whole domain and, to lose the minus sign, we flip the integration limits in the left side:

$$\int_0^t \frac{A}{a} \cdot \frac{k}{L} \cdot dt = \int_{h_{\text{final}}}^{h_{\text{initial}}} \frac{dh}{h} \quad (7.18)$$

Computing the integrals, we obtain:

$$\frac{A}{a} \cdot \frac{k}{L} \cdot t = \ln h_{\text{initial}} - \ln h_{\text{final}} \quad (7.19)$$

In the right-hand side, we transform the difference of logarithms into the logarithm of the two variables ratio and we change the base from  $e$  to  $10$  knowing that  $\ln x = 2.30 \cdot \log x$ . Equation (7.19) becomes:

$$\frac{A}{a} \cdot \frac{k}{L} \cdot t = 2.30 \cdot \log \frac{h_{\text{initial}}}{h_{\text{final}}} \quad (7.20)$$

In the equation (7.20)  $A$ ,  $a$  and  $L$  are known equipment geometrical properties. The time  $t$  is set to be able to easily record the head variation  $h_{\text{initial}}$  and  $h_{\text{final}}$  meaning that all the values for computing the permeability coefficient  $k$  are known:

$$k = 2.30 \frac{a}{A} \cdot \frac{L}{t} \cdot \log \frac{h_{\text{initial}}}{h_{\text{final}}} \quad (7.21)$$

#### **7.4 In-situ pumping tests**

In-situ tests are methods of finding the permeability coefficient as average value of the whole aquifer layer, without disturbing the soil structure as this happens in the case of the laboratory tests. If the layer to be tested is dry, then the procedure consists in pouring continuously water in a borehole until the steady regime is reached. The most general case is, however, when the aquifer has a free surface, the so-called ground water table, having the acronym G.W.T. For this layer a well is drilled and the water is pumped out until the steady regime is reached. If the drain crosses the whole thickness of the layer having the bottom in a low permeability layer, the well is called fully penetrated or perfect, otherwise is called partially penetrated or imperfect.

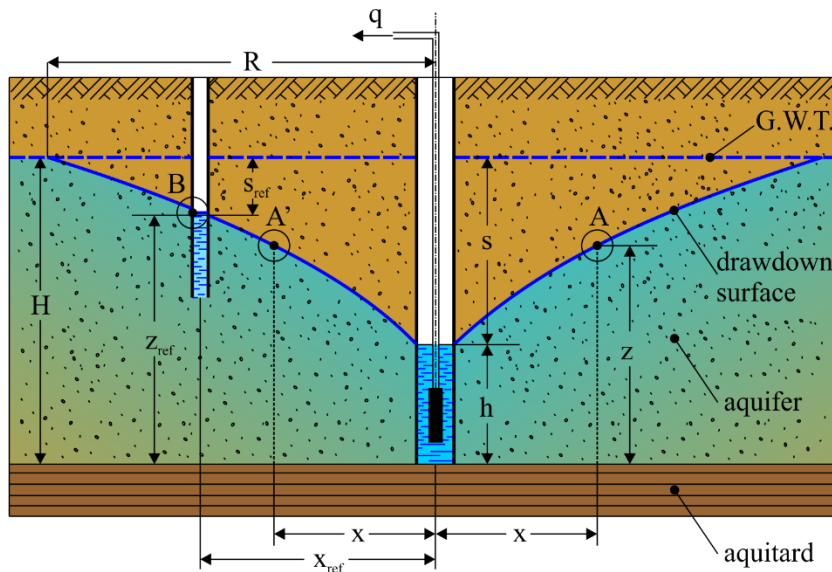


Fig. 7.12: Pumping test

We are going to present the in-situ pumping test on a fully penetrated well (Fig. 7.12). The well itself has the radius  $r$  and by draining water with the discharge  $q$  the water level stabilizes at the depth  $s$  with respect to GWT or at a height  $h$  with respect to the bottom. The lowered free water surface is called drawdown surface and for finding its exact shape it is necessary to drill a piezometer at the distance  $x_{ref}$  from the well axis, where the water level is found at the depth  $s_{ref}$  with respect to the initial GWT and  $h_{ref}$  with respect to the impervious base. The influence radius of the well,  $R$ , represents the distance from the well axis where the thickness of the aquifer is the same as the initial one,  $H$ .

For finding the equation of the drawdown surface we consider the assumption that the discharge over any cylindrical surface around the well axis has to be constant. We consider the general shape of this cylinder with the radius  $x$  and the wetted height  $z$ . For expressing the discharge, we use equation (7.9) where we replace  $v$  from Darcy's law (7.8):

$$q = k \cdot A \cdot i \quad (7.22)$$

The flow-in cylindrical area is:

$$A = 2\pi \cdot x \cdot z \quad (7.23)$$

The hydraulic gradient in the corresponding point A or A' on the drawdown surface should be:

$$i = \frac{dz}{dL} \quad (7.24)$$

But, since the surface is not very steep, we could approximate  $dL$  by  $dx$ . The equation (7.24) becomes:

$$i = \frac{dz}{dx} \quad (7.25)$$

Replacing (7.23) and (7.25) in (7.22) we obtain:

$$q = 2\pi k \cdot x \cdot z \cdot \frac{dz}{dx} \quad (7.26)$$

We separate the variables in (7.26):

$$z \, dz = \frac{q}{2\pi k} \cdot \frac{dx}{x} \quad (7.27)$$

Integrating both sides we obtain:

$$\frac{z^2}{2} = \frac{q}{2\pi k} \cdot \ln x + C \quad (7.28)$$

where  $C$  is the integration constant which may be obtained expressing the condition to the well limit where  $x = r$  and  $z = h$ , so that:

$$C = \frac{h^2}{2} - \frac{q}{2\pi k} \cdot \ln r \quad (7.29)$$

Replacing (7.29) in (7.28) we obtain:

$$z^2 - h^2 = \frac{q}{\pi k} \cdot \ln \frac{x}{r} \quad (7.30)$$

The equation (7.30) expressing the draw-down surface equation may be used to compute the permeability coefficient knowing the drawdown position in the piezometer tube at  $x = x_{\text{ref}}$ , namely  $z = z_{\text{ref}}$  and the pumping discharge  $q$  from the well. The permeability coefficient is:

$$k = \frac{q}{\pi(z_{\text{ref}}^2 - h^2)} \cdot \ln \frac{x_{\text{ref}}}{r} \quad (7.31)$$

Another method, if a piezometer tube is not available is to form a system of equations expressing the conditions at the influence zone limit where  $x = R$  and  $h = H$  along with an empirical relationship connecting the influence radius  $R$  with the permeability coefficient, namely:

$$R = 3000(H - h)\sqrt{k} \quad (7.32)$$

where  $R$ ,  $H$  and  $h$  are expressed in m and  $k$  in m/s.

### **7.5 Dynamic effect of water upon cohesionless soils**

When a water stream acts upon cohesionless soils it may have two effects: when the stream flows to the gravity direction and sense, it will densify the soil, while in case of having opposite sense, it will tend to pull particles away from the matrix or even induce liquefaction. If this phenomenon occurs on a horizontal direction, such as the case of a bridge pier foundation, the phenomenon is called scouring.

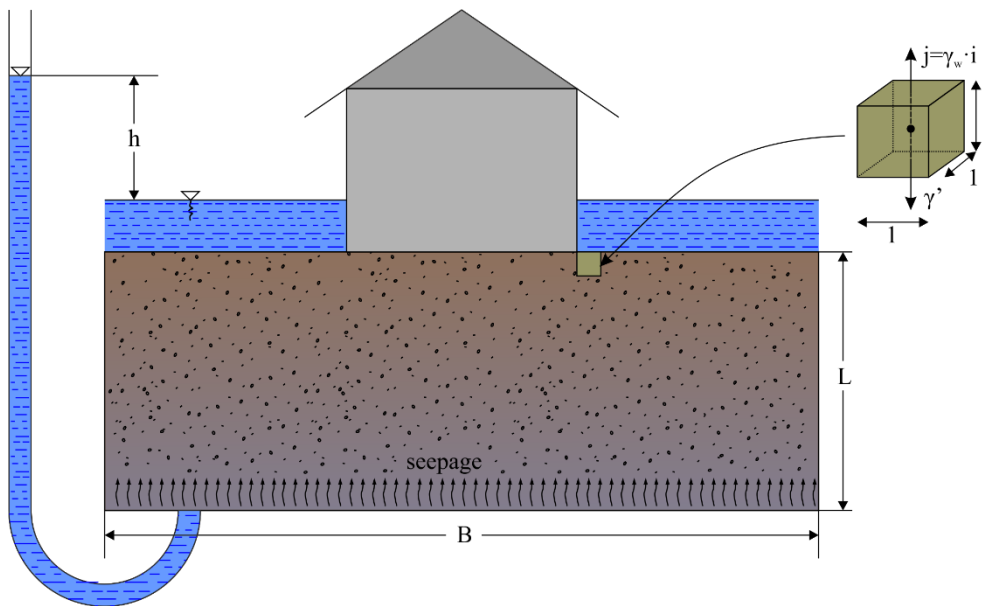


Fig. 7.13: Foundation liquefaction by vertical seepage

The most unfavourable situation occurs when the stream force, denoted by  $J$ , acts opposing gravity. The force  $J$  is expressed as the water pressure  $u$  acting on a certain area  $A$ .

$$J = u \cdot A \quad (7.33)$$

where the water pressure  $u$  is:

$$u = \gamma_w \cdot h \quad (7.34)$$

From the equations (7.33) and (7.34) we obtain that:

$$J = \gamma_w \cdot h \cdot A \quad (7.35)$$

In order to assess the effect of the stream upon the soil unit volume it is computed the so-called stream body force  $j$ :

$$j = \frac{J}{V} \quad (7.36)$$

Taking into account that the volume acted by the stream force is  $V = A \cdot L$ , the stream body force becomes:

$$j = \frac{\gamma_w \cdot h \cdot A}{A \cdot L} \quad (7.37)$$

But, in the equation (7.37),  $A$  vanishes and  $i = \frac{h}{L}$ , so the final shape of the stream body force becomes:

$$j = \gamma_w \cdot i \quad (7.38)$$

The solid particles become afloat when the stream body force ends up to be equal to the unit weight of the soil in submerged state, namely:

$$j = \gamma' \quad (7.39)$$

Since the only variable the body force depends on is the hydraulic gradient, the value for which liquefaction occurs is denoted by  $i_{cr}$ . Introducing (7.38) in (7.39) we obtain:

$$i_{cr} = \frac{\gamma'}{\gamma_w} \quad (7.40)$$

Since  $\gamma'$  and  $\gamma_w$  are both about  $10 \text{ kN/m}^3$ ,  $i_{cr}$  is about 1.

The safety factor approach defines the safety factor against liquefaction:

$$F_s^{\text{liquefaction}} = \frac{i_{cr}}{i_{\text{effective}}} \quad (7.41)$$

For  $F_s < 1$  liquefaction occurs.



## 7.6 Filters

There are two kinds of filters: direct and inverse.

The direct filters, aiming to catch all the solid particles until clogging, are not the object of soil mechanics, as the case of inverse filters, aiming to prevent scouring without clogging.

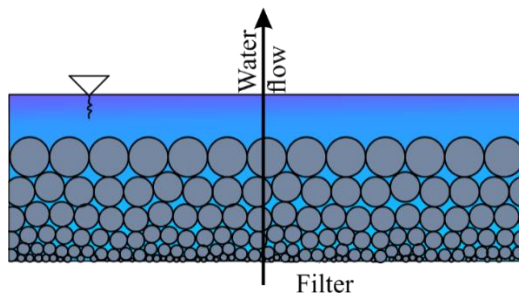


Fig. 7.14 Inverse filter

The purpose of filters is to have a progressive layering of particles, starting from finest towards the soil to be protected and the roughest to the exterior, preventing liquefaction with their own weight.

The material to be used as filter have to fulfil the following rules:

$$\begin{aligned} d_{15}^{\text{min filter}} &> 5 \cdot d_{15} \\ d_{15}^{\text{max filter}} &> 5 \cdot d_{85} \end{aligned} \quad (7.42)$$

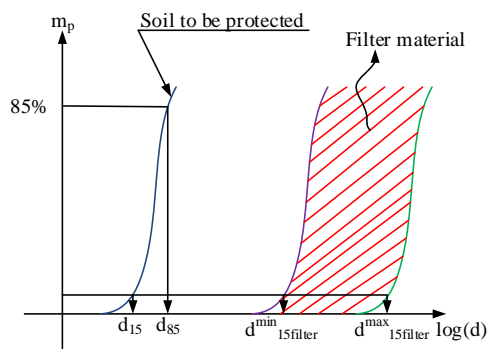


Fig. 7.15: Filter material rule

## **7.7 Test your understanding**

### **Problem 7.1**

What types of soils are considered practically impervious and why?

### **Problem 7.2**

How does the particle size influence permeability of soil?

### **Problem 7.3**

How can one obtain the permeability coefficient for soil?

### **Problem 7.4**

What are the disadvantages of permeability tests in the laboratory?

### **Problem 7.5**

Which are the 3 major types of aquifers?

### **Problem 7.6**

What is the influence of groundwater to an engineering project?

### **Problem 7.7**

What methods can be used to prevent groundwater flow effects to retaining structures for deep excavations?

### **Problem 7.8**

What methods can be used to build foundations below the groundwater table?

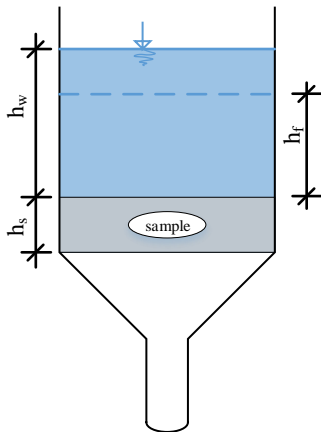
### **Problem 7.9**

Testing a soil concluded that the permeability coefficient is 0.04 cm/s. How much water can flow in an hour through a cross-section of 12m<sup>2</sup> if the hydraulic gradient is kept constant at 0.4?

**Problem 7.10**

A variable head permeameter test was conducted to find the permeability coefficient of a soil sample. The test conditions, as shown in the picture below, are the following:

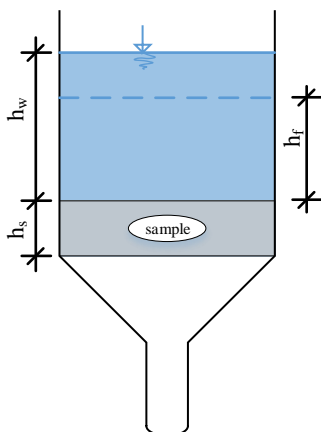
- Sample thickness:  $h_s=3\text{cm}$ ;
- Initial height of water measured from the top of the sample:  $h_w=50\text{cm}$ .



Find the permeability coefficient knowing that after 20 seconds of flow, the height of the water column becomes  $h_f=40\text{cm}$ .

**Problem 7.11**

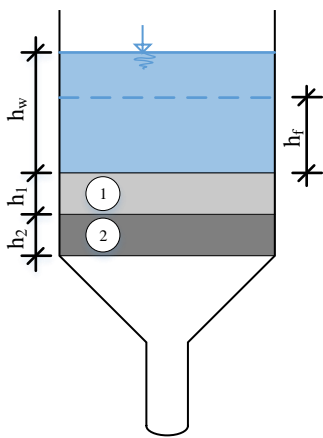
The setup in the figure below shows a soil sample of thickness  $h_s=3\text{cm}$  and a permeability coefficient  $k=5 \times 10^{-1}\text{cm/s}$ . The initial water thickness measured from the top of the sample is  $h_w=85\text{cm}$ .



Compute the water thickness  $h_f$  after 3 seconds of flow.

**Problem 7.12**

The setup in the figure below shows a soil sample composed of two distinct layers. The permeability coefficient of layer 1 is  $k_1=5 \times 10^{-1} \text{cm/s}$  and the overall equivalent permeability coefficient of the sample is  $k_{eq}=4 \times 10^{-1} \text{cm/s}$ . The thickness of the two soil layers are  $h_1=2 \text{cm}$  and  $h_2=2 \text{cm}$ . The initial water thickness measured from the top of the soil sample is  $h_w=7.5 \text{cm}$ .



The following are required:

- a) Compute the permeability of the second soil layer
- b) Estimate the water thickness  $h_f$  after 20 seconds of flow.

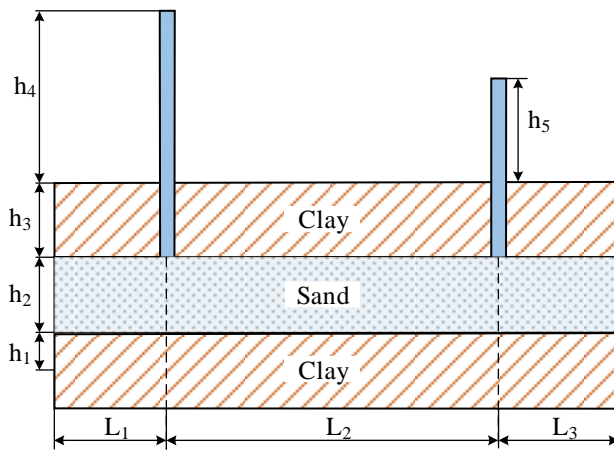
**Problem 7.13**

The figure below shows a hydrogeological cross-section describing the site conditions for a future construction. The geotechnical boreholes performed up to a depth  $h=14 \text{m}$  have shown that the site lithology is consisting of three layers parallel to the ground surface. The top clay layer of thickness  $h_3=5 \text{m}$  is followed by a sand layer of thickness  $h_2=5 \text{m}$  and a bottom clay layer of thickness  $h_1=4 \text{m}$ .

The sand layer contains a pressurized water, creating an artesian aquifer. The piezometric head of the aquifer was found to have different values, as follows: in a piezometric borehole at a distance  $L_1=51 \text{m}$  with respect to the left edge of the cross-section, the head is  $h_4=3 \text{m}$  with respect to the ground surface. In

a second piezometric borehole, at a distance  $L_2=102\text{m}$  from the first one, and  $L_3=51\text{m}$  from the right edge of the cross-section, the head is  $h_5=2\text{m}$  with respect to the ground surface.

Knowing that the average permeability coefficient of the sand layer was found to be  $k=0.01\text{cm/s}$ , determine the flow rate of water through the aquifer (expressed in  $\text{m}^3/\text{day}$ ) considering the thickness of the cross-section equal to 1 meter.



## **8 SHORT REVIEW OF STRENGTH OF MATERIALS, THEORY OF ELASTICITY AND PLASTICITY APPLIED TO SOIL MECHANICS**

### **8.1 State of stress**

Although in the literature concerning the Theory of Elasticity and Plasticity the tension stresses are considered to be positive, in the field of Geotechnical Engineering, where the majority of the loads are compressive, it would be counterproductive to work with this sign convention, thus hereinafter the compression stresses will be considered positive.

Consider a solid body (Fig. 8.1) with a random geometry in equilibrium under a set of exterior forces  $F_{e1} \dots F_{en}$ . As a reference, the position of the body is defined with respect to a global Cartesian coordinate system OXYZ. Consider now a random material point in the body and an arbitrary plane that passes through that point, sectioning the body. In order to keep the equilibrium, one of the two parts can be replaced by the equivalent internal force. In the considered point an orthogonal local system of axes OXYZ can be defined, having the z axis normal to the plane.

Sectioning the body following the directions of the OZX and OZY surfaces and isolating the material point, it is obtained a cube having infinitesimal dimensions and the sides parallel to the local system of coordinates (Fig. 8.2). The volume of the material point is  $\partial V$  and its lateral surfaces are  $\partial A_x$ ,  $\partial A_y$ , and  $\partial A_z$ .

In order to fulfil the equilibrium condition, on parallel faces of the material point, the corresponding resultant forces must form couples of equal forces having opposed sign. The internal force that acts on a face is denoted using as index the name of the normal axis, for instance  $\partial F_{i_z}$  is the force corresponding to the material point on the face having as normal the axis oz.

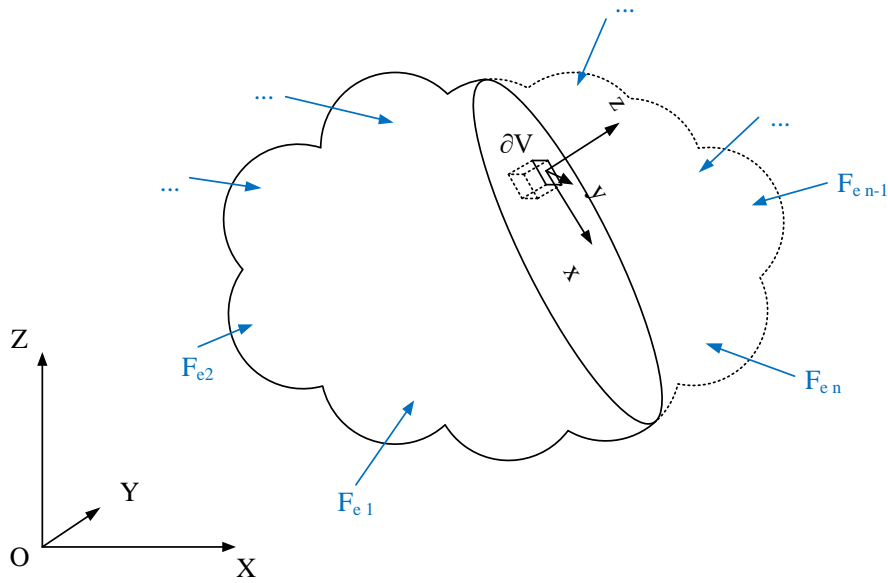


Fig. 8.1: Solid body in equilibrium under the action of a set of external forces

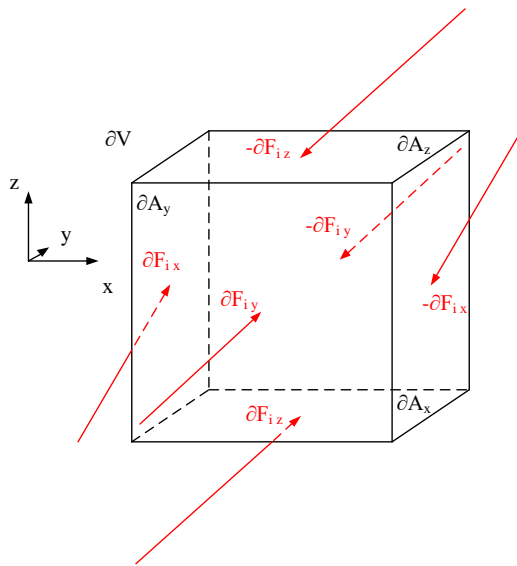


Fig. 8.2: Material point bounded by planes parallel with the local coordinate system of axes

Each force is then decomposed following the directions of the three axes and the name of the axis is used for the denomination of the parallel component to that direction. For example,  $\partial F_{i\ zz}$  is the normal component of  $\partial F_{i\ z}$  force, while  $\partial F_{i\ zx}$  is the component of  $\partial F_{i\ z}$  force on ox direction.

The stresses in the material point (Fig. 8.3) can be defined normalizing each component of the resultant force with the area on which they act.

$$\begin{aligned}\sigma_x &= \frac{\partial F_{i\ xx}}{\partial A_x} & \sigma_y &= \frac{\partial F_{i\ yy}}{\partial A_y} & \sigma_z &= \frac{\partial F_{i\ zz}}{\partial A_z} \\ \tau_{xy} &= \frac{\partial F_{i\ xy}}{\partial A_x} & \tau_{yz} &= \frac{\partial F_{i\ yz}}{\partial A_y} & \tau_{zx} &= \frac{\partial F_{i\ zx}}{\partial A_z} \\ \tau_{xz} &= \frac{\partial F_{i\ xz}}{\partial A_x} & \tau_{yz} &= \frac{\partial F_{i\ yz}}{\partial A_y} & \tau_{zy} &= \frac{\partial F_{i\ zy}}{\partial A_z}\end{aligned}\quad (8.1)$$

In order to have the material point in equilibrium, the components of the internal forces must be in equilibrium as well. This means that the normal stress  $\sigma_x$  on one face must be equal to the one on the parallel face and the tangential stress  $\tau_{xy}$  must be in the same relationship with the  $\tau_{xy}$  vector on the opposing face. Moreover, the  $\tau_{xy}$  vector on the adjacent face must produce the same couple, but of opposite sign to keep the equilibrium of the material point and to avoid its rotation.

It can be observed that the tendency of the couple formed by the normal components ( $\sigma$  stresses) is to modify the volume of the particle, while the tangential components ( $\tau$  stresses) tend to deform it. Generally, the stresses that induce volumetric strains are called spherical stresses and the ones that induce shape strains are called deviatoric stresses.



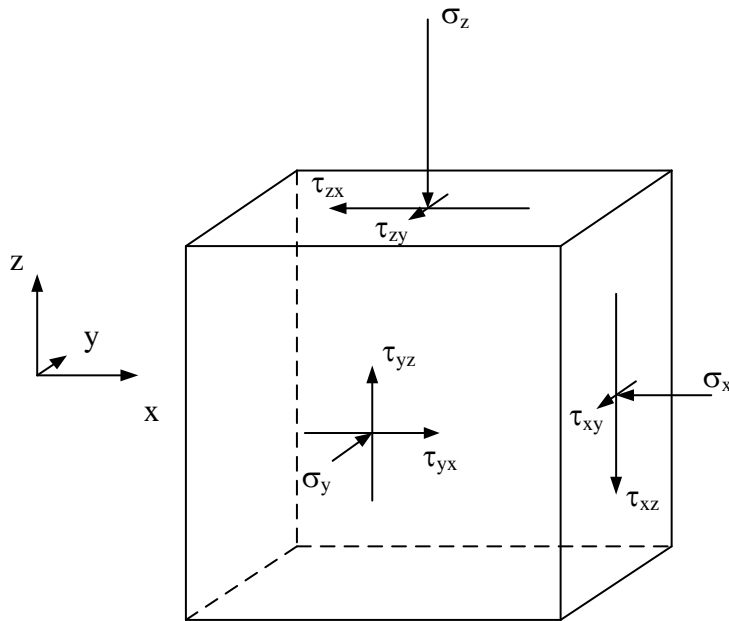


Fig. 8.3: Denomination of the stresses acting on the faces of the material point

After that, the normal vector of the OXYZ system of coordinates is denoted by  $\bar{n}$ , such that its components (unit vectors) are:

$$\bar{n} = [\bar{n}_x \quad \bar{n}_y \quad \bar{n}_z] \quad (8.2)$$

The tensor of the stresses in the point on OXYZ directions can be written as:

$$\bar{T} = \bar{n} \cdot \bar{\sigma} \quad (8.3)$$

where  $\bar{\sigma}$  is the matrix of the state of stress:

$$\bar{\sigma} = \begin{bmatrix} \sigma_x & \tau_{xy} & \tau_{xz} \\ \tau_{yx} & \sigma_y & \tau_{yz} \\ \tau_{zx} & \tau_{zy} & \sigma_z \end{bmatrix} \quad (8.4)$$

When one of the faces of the material point is oriented following the direction of the resultants of the internal forces in the point,  $F_{ix}$ ,  $F_{iy}$  and  $F_{iz}$ , their horizontal components are zero, meaning that the tangential stresses on these

directions are zero as well. The directions along which there is no tangential stress are called principal directions and the corresponding normal stresses are called principal stresses. Traditionally, the maximum value of the principal stresses is denoted by  $\sigma_1$ , the intermediary value by  $\sigma_2$  and the minimum with  $\sigma_3$ . The matrix of the stress state described by principal stresses can be written as follows:

$$\bar{\sigma} = \begin{bmatrix} \sigma_1 & 0 & 0 \\ 0 & \sigma_2 & 0 \\ 0 & 0 & \sigma_3 \end{bmatrix} \quad (8.5)$$

Comparing the definition of the matrix of the stress state (8.4) with (8.5) it can be observed that the use of principal stresses in describing the state of stress simplifies its expression from six distinct and non-null values to only three.

The expression of the stress state (8.4) is per se a simplification of the general case in which the unitary point would be considered as a parallelepipedal body with faces that are not parallel. In this case, the duality of the tangential stresses would no longer be applicable, meaning that the description of the state of stress would imply the use of nine distinct and non-null values, the tangential stresses on adjacent faces having different values. Obviously, the generalization could go on to a completely randomized expression of the shape, that would lead to a very complicated situation.

The above mentions were made for a better understanding of the principal stresses' role, namely that of minimizing the number of values through which the state of stress is described without losing any information. Obviously, the associated principal directions are used for a simplification in expressing the local coordinate system of the material point.

In this way, we consider an infinitesimal point having cubical shape, with the faces parallel to the direction  $Ox$  and  $Oy$  and it is to be analysed the stresses  $\sigma_x$  and  $\tau_{x'y'}$  that act on a plane inclined with angle  $\theta$  with respect to the  $Oy$  direction.

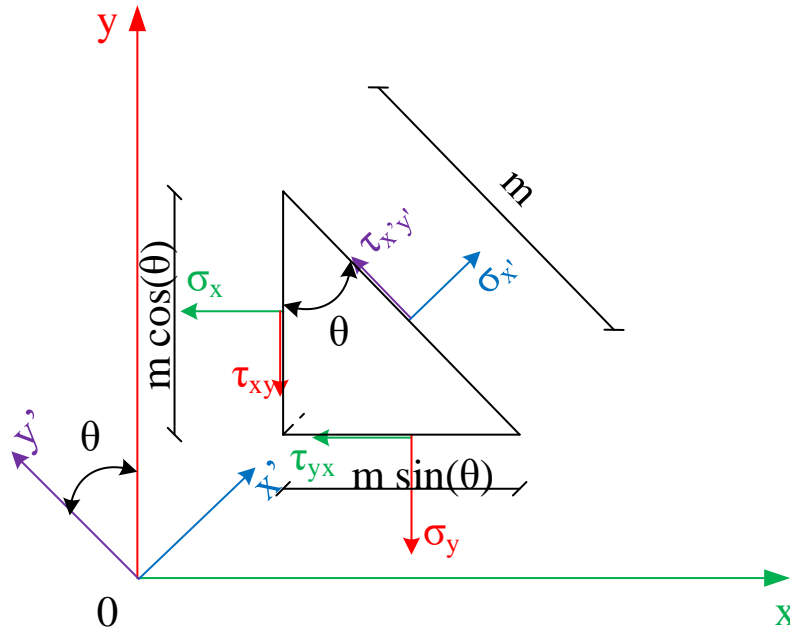


Fig. 8.4: Stresses on a plane inclined with angle  $\theta$  with respect to the direction  $Oy$

The dimensions of the face obtained through sectioning with a plane defined by the normal direction  $Ox'$  are infinitesimally small,  $m$  and  $1$ . The face perpendicular to  $Ox$  direction is equal to  $m \cos(\theta)$  and the face perpendicular to  $Oy$  direction is equal to  $m \sin(\theta)$ .

In order to express the force equilibrium on the sectioned part, the stresses will be multiplied with the areas on which they act. It will be taken into account the fact that the side of the element is unitary.

$$\begin{aligned}
 Ox': \sum F=0 &\Leftrightarrow \sigma_x' \cdot m \cdot 1 = \\
 &= \sigma_x \cdot m \cdot \cos(\theta) \cdot 1 \cdot \cos(\theta) + \tau_{xy} \cdot m \cdot \cos(\theta) \cdot 1 \cdot \sin(\theta) + \\
 &+ \sigma_y \cdot m \cdot \sin(\theta) \cdot 1 \cdot \sin(\theta) + \tau_{yx} \cdot m \cdot \sin(\theta) \cdot 1 \cdot \sin(\theta) \Leftrightarrow \\
 &\Leftrightarrow \sigma_x' = \sigma_x \cdot \cos(\theta)^2 + \sigma_y \cdot \sin(\theta)^2 + 2 \cdot \tau_{xy} \cdot \sin(\theta) \cos(\theta) \tag{8.6}
 \end{aligned}$$

$$\sigma_x \cdot \cos(\theta)^2 + \sigma_y \cdot \sin(\theta)^2 =$$

$$\begin{aligned}
 &= \frac{1}{2} \sigma_x \cdot (\cos(\theta)^2 + \cos(\theta)^2) + \frac{1}{2} \sigma_y \cdot (\sin(\theta)^2 + \sin(\theta)^2) = \\
 &= \frac{1}{2} \sigma_x \cdot (\cos(\theta)^2 + 1 - \sin(\theta)^2) + \frac{1}{2} \sigma_y \cdot (\sin(\theta)^2 + 1 - \cos(\theta)^2) = \\
 &= \frac{1}{2} (\sigma_x + \sigma_y) + \frac{1}{2} \sigma_x \cdot (\cos(\theta)^2 - \sin(\theta)^2) - \frac{1}{2} \sigma_y \cdot (\cos(\theta)^2 - \sin(\theta)^2) \Leftrightarrow \\
 &\cos(\theta)^2 - \sin(\theta)^2 = \cos(2\theta) \\
 &\Leftrightarrow \sigma_x \cdot \cos(\theta)^2 + \sigma_y \cdot \sin(\theta)^2 = \frac{1}{2} (\sigma_x + \sigma_y) + \frac{1}{2} (\sigma_x - \sigma_y) \cos(2\theta)
 \end{aligned}$$

$$\sigma_{x'} = \frac{1}{2} (\sigma_x + \sigma_y) + \frac{1}{2} (\sigma_x - \sigma_y) \cdot \cos(2\theta) + \tau_{xy} \cdot \sin(2\theta) \quad (8.7)$$

Oy':  $\sum F = 0 \Leftrightarrow$

$$\begin{aligned}
 \tau_{xy}' \cdot m \cdot 1 &= -\sigma_x \cdot m \cdot \cos(\theta) \cdot 1 \cdot \sin(\theta) + \sigma_y \cdot m \cdot \sin(\theta) \cdot 1 \cdot \cos(\theta) \\
 + \tau_{xy} \cdot m \cdot \cos(\theta) \cdot 1 \cdot \cos(\theta) - \tau_{yx} \cdot m \cdot \sin(\theta) \cdot 1 \cdot \sin(\theta) &\Leftrightarrow \\
 \tau_{xy}' &= -\frac{1}{2} \sigma_x \cdot \sin(2\theta) + \frac{1}{2} \sigma_y \cdot \sin(2\theta) + \tau_{xy} \cdot (\cos(\theta)^2 - \sin(\theta)^2)
 \end{aligned}$$

$$\tau_{xy}' = -\frac{1}{2} \cdot (\sigma_{xx} - \sigma_{yy}) \cdot \sin(2\theta) + \tau_{xy} \cdot \cos(2\theta) \quad (8.8)$$

The shear stress can be zero if:

$$\frac{1}{2} \cdot (\sigma_{xx} - \sigma_{yy}) \cdot \sin(2\theta) = \tau_{xy} \cdot \cos(2\theta) \Leftrightarrow$$

$$\begin{aligned}
 \tan(2\theta) &= \frac{2 \cdot \tau_{xy}}{(\sigma_x - \sigma_y)} \Leftrightarrow \theta = \frac{1}{2} \tan^{-1} \left( \frac{2 \cdot \tau_{xy}}{\sigma_x - \sigma_y} \right) \text{ or} \\
 \theta &= \frac{1}{2} \tan^{-1} \left( \frac{2 \cdot \tau_{xy}}{\sigma_x - \sigma_y} \right) + 90^\circ \quad (8.9)
 \end{aligned}$$

The maximum or minimum values of the normal stress are reached when the first derivative with respect to angle  $\theta$  is zero:

$$\frac{d\sigma_{x'}}{d\theta} = -\frac{2}{2} (\sigma_x - \sigma_y) \sin(2\theta) + 2\tau_{xy} \cos(2\theta)$$

$$\frac{\sin(2\theta)}{\cos(2\theta)} = \frac{2\tau_{xy}}{(\sigma_x - \sigma_y)} \Leftrightarrow \tan(2\theta) = \frac{2\tau_{xy}}{(\sigma_x - \sigma_y)} \quad (8.10)$$

As stated previously, are called principal directions the directions of the planes for with the shear stress is zero and the normal stresses acting on these planes are called principal stresses. It can be observed from (8.9) and (8.10) that the shear stresses are zero when the normal stresses have a maximum or a minimum value. It can be concluded that the normal stresses are also the maximum and the minimum values.

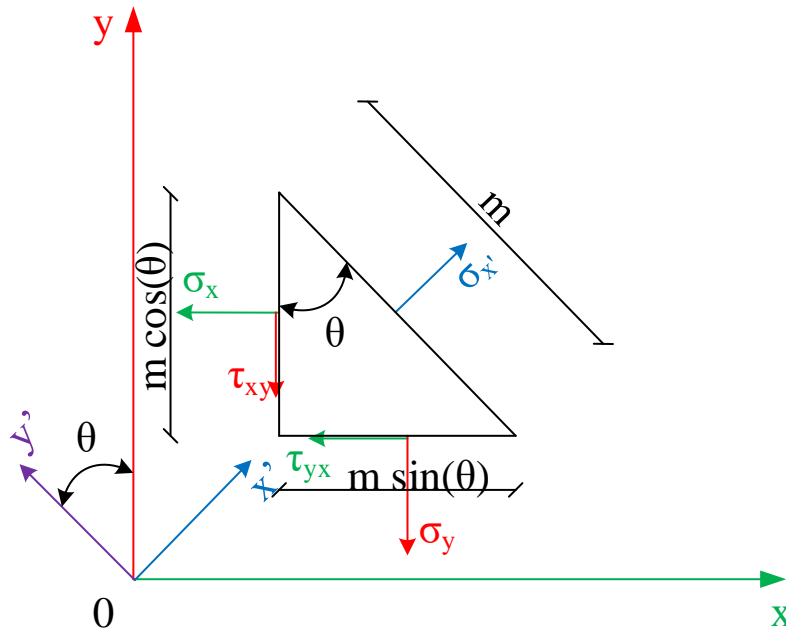


Fig. 8.5: Stresses on a principal plane having the direction Ox'

$$\begin{aligned} F_x=0 &\Leftrightarrow \sigma_x \cdot m \cdot \cos(\theta) \cdot 1 + \tau_{yx} \cdot m \cdot \sin(\theta) \cdot 1 - (\sigma_x' \cdot m \cdot 1) \cos(\theta) = 0 \\ &\Leftrightarrow (\sigma_x' - \sigma_x) \cdot \cos(\theta) = \tau_{yx} \cdot \sin(\theta) \Leftrightarrow \\ &\Leftrightarrow (\sigma_x' - \sigma_x) = \tau_{yx} \cdot \tan(\theta) \end{aligned} \quad (8.11)$$

$$\begin{aligned} F_y=0 &\Leftrightarrow \sigma_y \cdot m \cdot \sin(\theta) \cdot 1 + \tau_{xy} \cdot m \cdot \cos(\theta) \cdot 1 - (\sigma_x' \cdot m \cdot 1) \sin(\theta) = 0 \\ &\Leftrightarrow (\sigma_x' - \sigma_x) \cdot \sin(\theta) = \tau_{xy} \cdot \cos(\theta) \Leftrightarrow \end{aligned}$$

$$\Leftrightarrow (\sigma_{x'} - \sigma_x) = \tau_{xy} \cdot \cot(\theta) \quad (8.12)$$

Multiplying (8.11) and (8.12), one obtains:

$$(\sigma_{x'} - \sigma_x)(\sigma_{x'} - \sigma_{yy}) = \tau_{xy}^2 \Leftrightarrow \sigma_{x'}^2 - \sigma_{x'}(\sigma_x + \sigma_y) + \sigma_x \sigma_y - \tau_{xy}^2 = 0$$

$$ax^2 + bx + c = 0 \Rightarrow \Delta = b^2 - 4ac \Rightarrow x_{1,2} = \frac{-b \pm \sqrt{\Delta}}{2a}$$

$$\Delta = (\sigma_x + \sigma_y)^2 - 4\sigma_x \sigma_y + 4\tau_{xy}^2 = (\sigma_x - \sigma_y)^2 + 4\tau_{xy}^2$$

$$\sigma_{1,3} = \frac{\sigma_x + \sigma_y \pm \sqrt{(\sigma_x - \sigma_y)^2 + 4\tau_{xy}^2}}{2} \quad (8.13)$$

The maximum shear stress can be computed by deriving (8.8) (written using principal stresses) with respect to angle  $\theta$ :

$$\begin{aligned} \tau_{x'y'} &= -\frac{(\sigma_1 - \sigma_3)}{2} \sin(2\theta) \Leftrightarrow \frac{d\tau_{x'y'}}{d\theta} = -(\sigma_1 - \sigma_3) \cos(2\theta) = 0 \Leftrightarrow \\ &\Leftrightarrow \theta = 45^\circ \end{aligned}$$

The maximum shear stress is found on a plane inclined with  $45^\circ$  in relation to the principal planes.

$$\tau_{\max} = -\frac{(\sigma_1 - \sigma_3)}{2} \sin(2 \cdot 45^\circ) = -\frac{(\sigma_1 - \sigma_3)}{2} \quad (8.14)$$

$$\begin{aligned} \tau_{\max} &= -\frac{\sigma_1 - \sigma_3}{2} \xrightarrow{(8.13)} \\ \tau_{\max} &= \frac{\sqrt{(\sigma_x - \sigma_y)^2 + 4\tau_{xy}^2}}{2} = \sqrt{\left(\frac{\sigma_x - \sigma_y}{2}\right)^2 + \tau_{xy}^2} \end{aligned} \quad (8.15)$$

From equation (8.7) results:

$$\begin{aligned}
 \sigma - \frac{1}{2}(\sigma_x + \sigma_y) &= \frac{1}{2}(\sigma_x - \sigma_y)\cos(2\theta) + \tau_{xy}\sin(2\theta) \Leftrightarrow \\
 \Leftrightarrow \left( \sigma - \frac{1}{2}(\sigma_x + \sigma_y) \right)^2 &= \left( \frac{1}{2}(\sigma_x - \sigma_y)\cos(2\theta) \right)^2 + \\
 + \frac{1}{2}(\sigma_x - \sigma_y)\cos(2\theta) \tau_{xy}\sin(2\theta) &+ \left( \tau_{xy}\sin(2\theta) \right)^2
 \end{aligned} \tag{8.16}$$

From equation (8.8) results:

$$\begin{aligned}
 -\tau &= \frac{1}{2}(\sigma_x - \sigma_y) \cdot \sin(2\theta) - \tau_{xy}\cos(2\theta) \Leftrightarrow \\
 \Leftrightarrow \tau^2 &= \left( \frac{1}{2}(\sigma_x - \sigma_y) \cdot \sin(2\theta) \right)^2 - \frac{1}{2}(\sigma_x - \sigma_y) \cdot \\
 \cdot \sin(2\theta) \tau_{xy}\cos(2\theta) &+ \left( \tau_{xy}\cos(2\theta) \right)^2
 \end{aligned} \tag{8.17}$$

Adding the equations (8.16) and (8.17), the result is:

$$\begin{aligned}
 \left( \sigma - \frac{1}{2}(\sigma_x + \sigma_y) \right)^2 + \tau^2 &= \left( \frac{1}{2}(\sigma_x + \sigma_y) \right)^2 (\cos(2\theta)^2 + \sin(2\theta)^2) + \\
 + \tau_{xy}^2 (\cos(2\theta)^2 + \sin(2\theta)^2) &\Leftrightarrow \\
 \Leftrightarrow \left( \sigma - \frac{1}{2}(\sigma_x + \sigma_y) \right)^2 + \tau^2 &= \left( \frac{1}{2}(\sigma_x + \sigma_y) \right)^2 + \tau_{xy}^2
 \end{aligned} \tag{8.18}$$

The cartesian equation of a circle with the centre in point C(a,b) and having the radius r is:

$$(x-a)^2 + (y-b)^2 = r^2 \tag{8.19}$$

The equations (8.7) and (8.8), corresponding to a pair of values ( $\sigma$ ,  $\tau$ ) that act on a random plane, define a circle with the centre in  $(\frac{1}{2}(\sigma_{xx} + \sigma_{yy}), 0)$  and

having the radius  $\sqrt{\left(\frac{1}{2}(\sigma_{xx} + \sigma_{yy})\right)^2 + \tau_{xy}^2}$ . (which actually is the maximum

shear stress obtained in (8.15)). This circle is called Mohr's circle and represents all the pairs of values  $(\sigma, \tau)$  in a moment in time that act on any plane that pass through a point. It can be said that the Mohr's circle represents the stress state in a point at one moment in time.

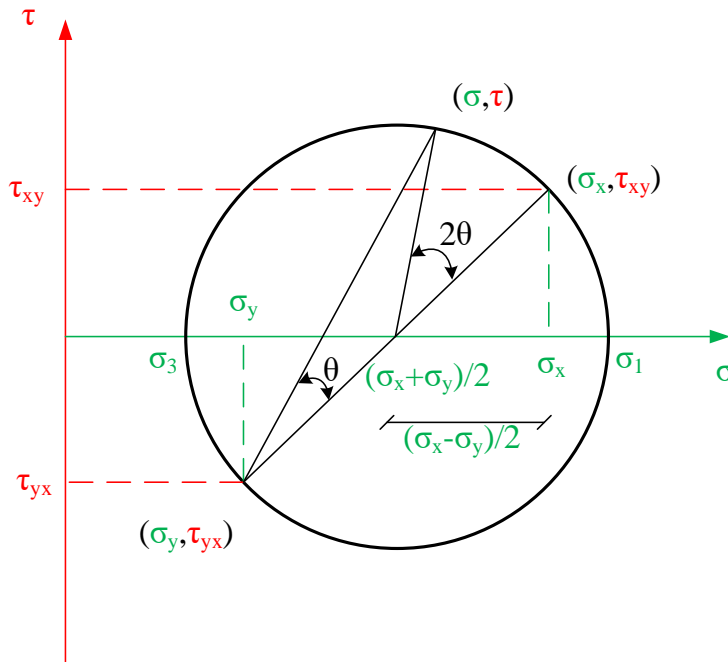


Fig. 8.6: Mohr's circle defined for two pairs of values acting on two perpendicular planes

The random plane on which the pair  $(\sigma, \tau)$  is inclined with angle  $\theta$  in relation with the plane on the pair  $(\sigma_x, \tau_{xy})$  acts. Representing the plane inclination with the centre in the centre of the circle, the angle will be  $2\theta$ . The inscribed angle theorem states that an angle inscribed in a circle is half of the centre angle that subtends the same arc of the circle.

Geometrically, in its most general form, the circle can be defined using two pairs of values  $(\sigma, \tau)$  that act on two general planes  $\alpha$  and  $\beta$ . For defining the stress state in its most general form four values are needed, grouped in two  $(\sigma, \tau)$  pairs.



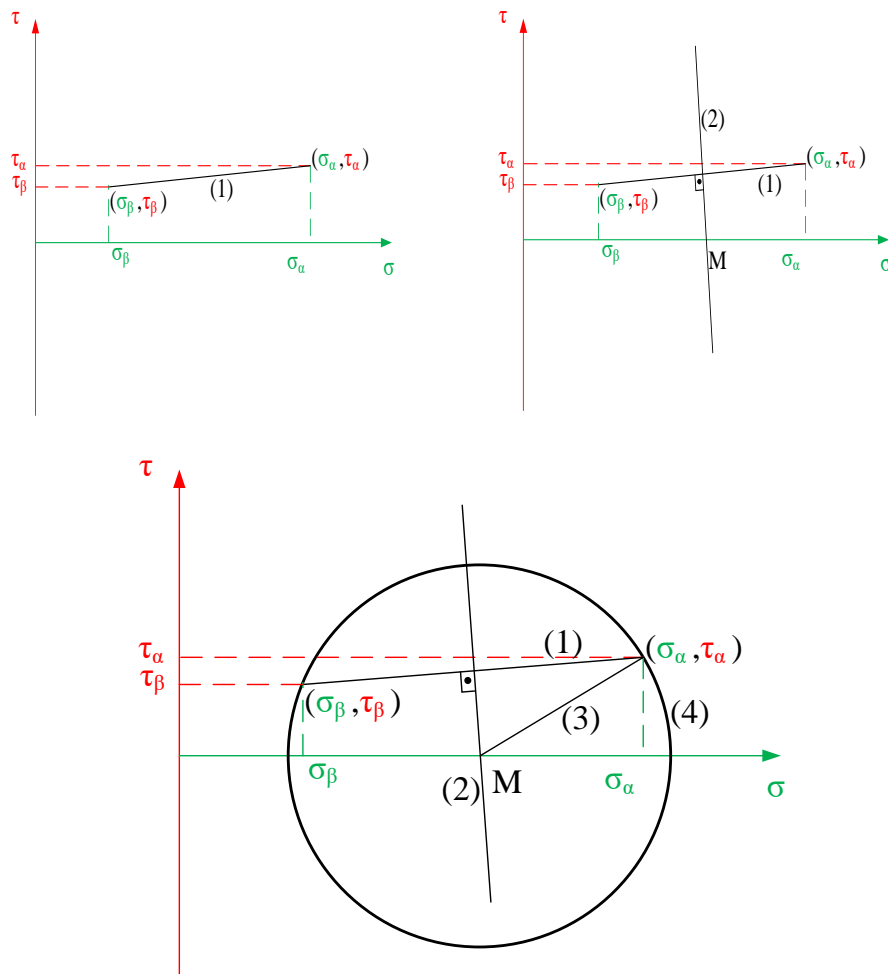


Fig. 8.7: Mohr's circle representation using two pairs of values acting on two random planes

The Mohr's circle representation algorithm using two general pairs of values  $(\sigma_\alpha, \tau_\alpha)$  and  $(\sigma_\beta, \tau_\beta)$  has the following steps:

- representing the two points  $(\sigma_\alpha, \tau_\alpha)$  and  $(\sigma_\beta, \tau_\beta)$  in  $(\sigma, \tau)$  coordinates;
- connecting the two points with a segment (1);
- drawing the perpendicular bisector (2) of the segment (1);
- intersecting the perpendicular bisector (2) with  $O\sigma$  axis, denoting the point obtained with M (this point is the centre of Mohr's circle);

- connecting the point M with one of the points having the coordinates  $(\sigma_\alpha, \tau_\alpha)$  and  $(\sigma_\beta, \tau_\beta)$  (3), this segment representing the radius of the Mohr's circle;
- using the centre M and the radius (3), the Mohr's circle (4) can be drawn.

Two points chosen randomly define an infinity of circles. All these circles have the property of having the centres on the perpendicular bisector of the segment connecting the two points. The intersection of the perpendicular bisector with the  $O\sigma$  axis is motivated by the fact that static equilibrium must be fulfilled in the point where the stress state is represented. The positive shear stresses must be equal with the negative shear stresses, resulting the circle being symmetrical with respect to the  $O\sigma$  axis – thus the centre must be on  $O\sigma$  axis. Because the centre of Mohr's circle is on the perpendicular bisector as well, the point can be found at the intersection of the perpendicular bisector with  $O\sigma$  axis. Because the points having the coordinates  $(\sigma_\alpha, \tau_\alpha)$  and  $(\sigma_\beta, \tau_\beta)$  are found on the circle, connecting one of these points with the centre of the circle defines the radius of the circle. The circle is drawn using the centre and the radius.

A particular case of the general representation appears when two pairs of values  $(\sigma_x, \tau_{xy})$  and  $(\sigma_y, \tau_{yx})$  that act on two perpendicular planes having the directions  $Ox$  and  $Oy$  are used. In this case, the middle of the segment connecting the two points is found on  $O\sigma$  axis. In this situation, three values are needed to define the stress state, because  $\tau_{xy} = \tau_{yx}$ .

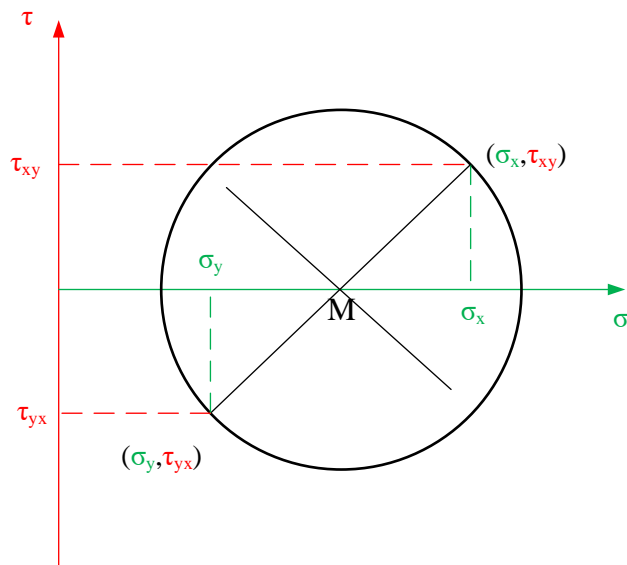


Fig. 8.8: Mohr's circle representation using two pairs of values that act on two perpendicular planes

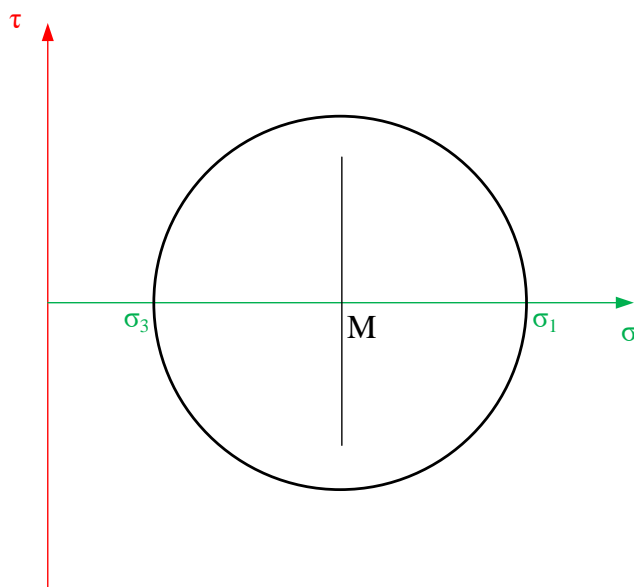


Fig. 8.9: Mohr's circle representation using principal stresses

A particular case of the situation in which the two pairs of stresses act on two perpendicular planes is when the shear stresses are zero. This case is equivalent with the usage of the principal stresses  $\sigma_1$  and  $\sigma_3$  to define the stress state. The centre of the circle M will be found at the middle of the segment that connects the two points and on O $\sigma$  axis. For the definition of the stress state in this case only two values are necessary since the shear stresses are zero.

If we generalize for three dimensions the previously described problem in two dimensions, the random plane is plotted as shown in Fig. 8.10. The dihedral angles formed between the random plane and the planes O12, O23 and O31 cannot be random, as the sum of the squares of cosines must be 1.

$$\cos^2 \alpha_1 + \cos^2 \alpha_2 + \cos^2 \alpha_3 = 1 \quad (8.20)$$

In these conditions, all the pairs of values  $\sigma - \tau$  corresponding to the three-dimensional stress state will be found on three circles, as it can be observed in Fig. 8.11.

As it will be shown in the following chapters, generally, in engineering problems it is done a simplified calculation in which the state of stress is considered plane. From the three-dimensional state of stress, by overlapping two axes, from the three circles remains only one on which we will choose the use of directions 1 and 3 corresponding to the maximum and minimum principal stresses.

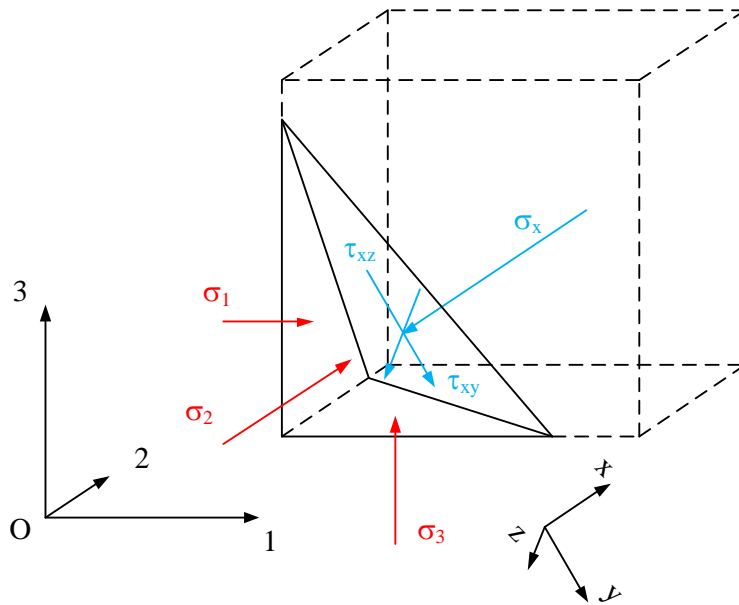


Fig. 8.10: Stresses on a random plane in a three-dimensional state of stress

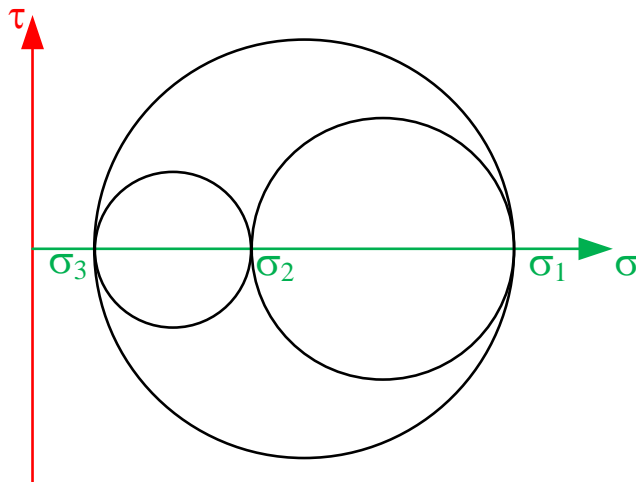


Fig. 8.11: Mohr's circles in a three-dimensional state of stress

For the determination of the stresses on a plane inclined with the angles  $\alpha_{xy}$ ,  $\alpha_{yz}$  and  $\alpha_{zx}$  of a random stress state defined through the coefficient matrix

(8.4), it is to be found the value of the  $\sigma$  resultant of the stresses on that direction, such that the system of equations can be written:

$$\begin{cases} (\sigma_x - \sigma)\cos\alpha_x + \tau_{xy}\cos\alpha_y + \tau_{xz}\cos\alpha_z = 0 \\ \tau_{yx}\cos\alpha_x + (\sigma_y - \sigma)\cos\alpha_y + \tau_{yz}\cos\alpha_z = 0 \\ \tau_{zx}\cos\alpha_x + \tau_{zy}\cos\alpha_y + (\sigma_z - \sigma)\cos\alpha_z = 0 \end{cases} \quad (8.21)$$

To this system of equations is added the equation (8.20). In order to avoid the trivial solution  $\cos\alpha_1 = \cos\alpha_2 = \cos\alpha_3 = 0$ , the determinant of the system (8.21) must be null, namely:

$$\begin{vmatrix} \sigma_x - \sigma & \tau_{xy} & \tau_{xz} \\ \tau_{yx} & \sigma_y - \sigma & \tau_{yz} \\ \tau_{zx} & \tau_{zy} & \sigma_z - \sigma \end{vmatrix} = 0 \quad (8.22)$$

Developing, a third-degree equation is obtained:

$$\sigma^3 - I_1\sigma^2 + I_2\sigma - I_3 = 0 \quad (8.23)$$

where:

$$\begin{aligned} I_1 &= \sigma_x + \sigma_y + \sigma_z \\ I_2 &= \begin{vmatrix} \sigma_x & \tau_{xy} \\ \tau_{yx} & \sigma_y \end{vmatrix} + \begin{vmatrix} \sigma_y & \tau_{yz} \\ \tau_{zy} & \sigma_z \end{vmatrix} + \begin{vmatrix} \sigma_z & \tau_{zx} \\ \tau_{xz} & \sigma_x \end{vmatrix} = \\ &= \sigma_x\sigma_y + \sigma_y\sigma_z + \sigma_z\sigma_x - \tau_{xy}^2 - \tau_{yz}^2 - \tau_{zx}^2 \\ I_3 &= \begin{vmatrix} \sigma_x & \tau_{xy} & \tau_{xz} \\ \tau_{yx} & \sigma_y & \tau_{yz} \\ \tau_{zx} & \tau_{zy} & \sigma_z \end{vmatrix} = \sigma_x\sigma_y\sigma_z + 2\tau_{xy}\tau_{yz}\tau_{zx} - \tau_{xy}^2\sigma_z - \tau_{yz}^2\sigma_x - \tau_{zx}^2\sigma_y \end{aligned} \quad (8.24)$$

But the value of  $\sigma$  is unique for the state of stress, having the value of the resultant of all external loadings, meaning that the values of the coefficients  $I_1$ ,  $I_2$  and  $I_3$ , referred further as invariants of the spherical tensor, must be

unique as well. The easiest way is to compute them starting from principal stresses, such that the values of the shearing stresses to be null. The equations (8.24) become:

$$\begin{aligned} I_1 &= \sigma_1 + \sigma_2 + \sigma_3 \\ I_2 &= \sigma_1\sigma_2 + \sigma_2\sigma_3 + \sigma_3\sigma_1 \\ I_3 &= \sigma_1\sigma_2\sigma_3 \end{aligned} \quad (8.25)$$

In the case of an isotropic state of stress, for instance the hydrostatic one, it would not exist shear stresses and the normal ones would be equal (this state being symmetrical on all directions). It can be concluded that the deviation from the loading symmetry is the one induced by deviatoric stresses. In order to emphasize the effect of each principal component to the anisotropy of the loading, there are defined the reduced principal stresses, these being components of the deviatoric tensor.

$$\begin{aligned} s_1 &= \sigma_1 - \frac{I_1}{3} \\ s_2 &= \sigma_2 - \frac{I_1}{3} \\ s_3 &= \sigma_3 - \frac{I_1}{3} \end{aligned} \quad (8.26)$$

If the expression of the deviatoric tensor invariants is desired in a way that is similar to the one of the spherical tensor invariants, we get:

$$\begin{aligned} J_1 &= s_1 + s_2 + s_3 = 0 \\ J_2 &= s_1s_2 + s_2s_3 + s_3s_1 \\ J_3 &= s_1s_2s_3 \end{aligned} \quad (8.27)$$

The  $J_1$  invariant is always null directly from the definition of the reduced deviatoric stresses definition.

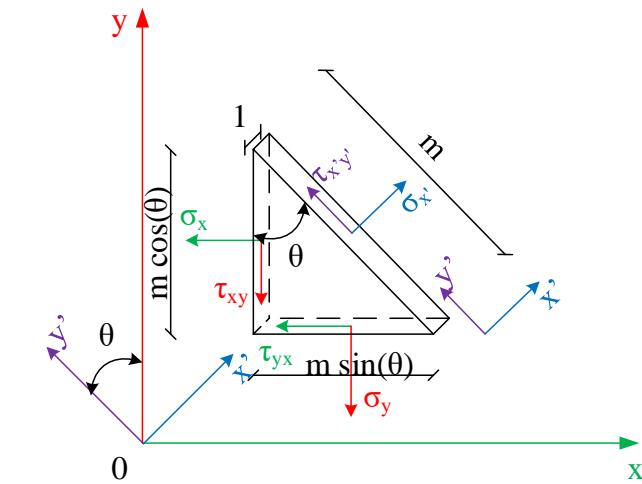
## **8.2 Pole of Mohr's circle**

The position of the pole of Mohr's circle is a unique point on the circle. This uniqueness is valid for a certain stress state. The position of the pole can change as the stress state changes, even if the represented stress state refers to the same point. If a line is drawn through the pole, the second point in which the line intersects the circle (the first one being the pole) will have the coordinates  $(\sigma, \tau)$  corresponding to the stresses that act on a plane parallel with the line drawn. A particular case is when the line is tangent to the circle at the pole. In this case the coordinates  $(\sigma, \tau)$  that define the pole are the values that act on the plane parallel with the drawn line. Alternatively, if the pole and a pair of values  $(\sigma, \tau)$  are known, connecting the two points provides the line that is parallel with the plane on which the pair  $(\sigma, \tau)$  act.

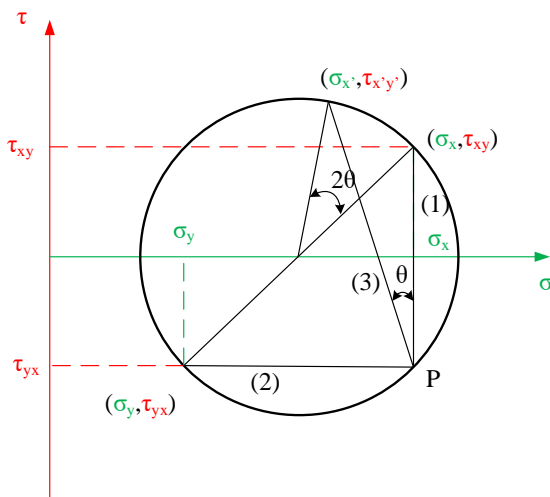
For determining the pole position, the points determined by the pairs of values  $(\sigma_x, \tau_{xy})$  or  $(\sigma_y, \tau_{yx})$  will be represented (Fig. 8.12). From the represented point a line is drawn, parallel with the plane on which the values that determine the point act. In Fig. 8.12 a) can be observed that the pair of values  $(\sigma_x, \tau_{xy})$  act on a vertical plane, so a vertical line (1) is drawn from the point defined by the coordinates  $(\sigma_x, \tau_{xy})$ . The second intersection point of the line with the circle represents the pole of the circle, denoted with P. Alternatively, the pair of values  $(\sigma_y, \tau_{yx})$  act on a horizontal plane. From the point defined by the coordinates  $(\sigma_y, \tau_{yx})$  a horizontal line (2) is drawn, the second point of intersection with the circle representing the pole.

One can notice that both lines intersect in the same point, the pole. Actually, all the lines drawn from a point defined by a pair of values  $(\sigma, \tau)$  parallel with the plane on which those values act will intersect in the pole. Consequently, if the position of the pole and the inclination of the plane is known, the pair of values that act on that plane can be determined. In Fig. 8.12 the position of the pole and the inclination of the plane are known. If a line is drawn, starting from the pole and having the inclination  $\theta$  with respect to the vertical (3), the second point of intersection with the circle represents a point defined by the pairs of values  $(\sigma_{x'}, \tau_{x'y'})$  that act on the plane with the direction  $Ox'$ .





a)



b)

Fig. 8.12: Pole position determination and the determination of a pair of values acting on a plane inclined with angle  $\theta$  with respect to the vertical

The pole of the circle is used either for obtaining a direction on which a certain  $\sigma - \tau$  pair of stresses act, for instance the failure stresses in the case of Rankine hypothesis of the Coulomb model of active thrust and passive resistance, or for assessing the unit stresses on a certain direction that passes through the point in which the state of stress is defined.

### **8.3 State of strain**

According to the definitions stated in chapter 8.1, the stresses that produce volume deformations are called spherical stresses, and those that produce deformations of shape are called deviatoric stresses. The stress-strain relations between the normal stress  $\sigma$  against the axial strain  $\varepsilon$ , and shearing stress  $\tau$  against the shearing strain  $\gamma$  respectively, are depicted in Fig. 8.13a. Considering these relations in the linear elastic domain, Hooke's law, reformulated by Young for spherical stresses and strains, and Lamé's equation for deviatoric stresses and strains may be stated as:

$$\begin{aligned}\sigma &= E\varepsilon \\ \tau &= G\gamma\end{aligned}\tag{8.28}$$

where  $E$  is Young's modulus, generally called "linear deformation modulus" in geotechnical engineering, and  $G$  is the shear modulus or "Lamé's second parameter". The significance of these moduli is described in (8.30).

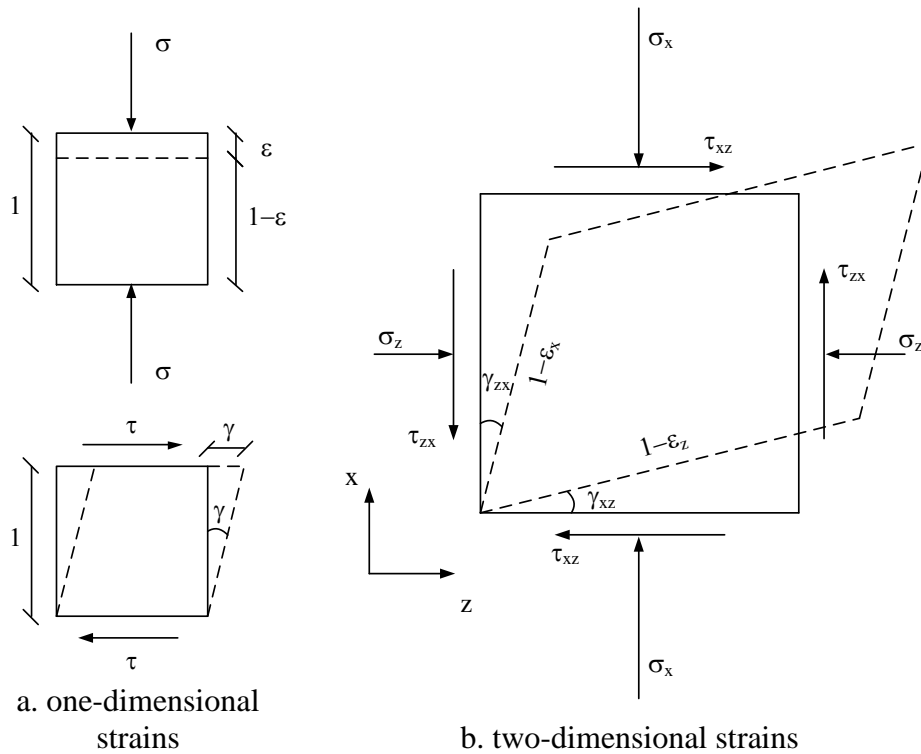


Fig. 8.13: One-dimensional and two-dimensional states of strains

For the two-dimensional and three-dimensional states of strain, it is necessary to consider the loading distribution on the directions rectangular to the one on which the loading is applied. This redistribution is performed based on the generalized Hooke's law, which quantifies the strain distribution through Poisson's coefficient,  $\nu$ :

$$\begin{aligned}
 \varepsilon_x &= \frac{1}{E}[\sigma_x - \nu(\sigma_y + \sigma_z)] \\
 \varepsilon_y &= \frac{1}{E}[\sigma_y - \nu(\sigma_z + \sigma_x)] \\
 \varepsilon_z &= \frac{1}{E}[\sigma_z - \nu(\sigma_x + \sigma_y)] \\
 \gamma_{xy} &= \frac{1}{G}\tau_{xy} \\
 \gamma_{yz} &= \frac{1}{G}\tau_{yz} \\
 \gamma_{zx} &= \frac{1}{G}\tau_{zx}
 \end{aligned} \tag{8.29}$$

Considering that the relation between E, G and  $\nu$  is:

$$G = \frac{E}{2(1 + \nu)} \tag{8.30}$$

The relation (8.29) can be rewritten in a compacted matrix form as:

$$\begin{pmatrix} \varepsilon_x \\ \varepsilon_y \\ \varepsilon_z \\ \gamma_{xy} \\ \gamma_{yz} \\ \gamma_{zx} \end{pmatrix} = \frac{1}{E} \begin{pmatrix} 1 & -\nu & -\nu & 0 & 0 & 0 \\ -\nu & 1 & -\nu & 0 & 0 & 0 \\ -\nu & -\nu & 1 & 0 & 0 & 0 \\ 0 & 0 & 0 & 2(1 + \nu) & 0 & 0 \\ 0 & 0 & 0 & 0 & 2(1 + \nu) & 0 \\ 0 & 0 & 0 & 0 & 0 & 2(1 + \nu) \end{pmatrix} \begin{pmatrix} \sigma_x \\ \sigma_y \\ \sigma_z \\ \tau_{xy} \\ \tau_{yz} \\ \tau_{zx} \end{pmatrix} \tag{8.31}$$

If one considers a linear relation between stresses and strains, it could be concluded that the relation between axial and shear strains is similar to the relation between normal and shear stresses. The state of strain could be represented as a circle according to Fig. 8.14. The strains determined for the example from Fig. 8.13 b are represented in the circle in the Fig. 8.14. The non-linearity of the relation between unit stresses and strains leads only to the scaling of the circles one with respect to the other.

The total volumic strain is equal to difference between the final volume computed as the product between the sides of the deformed element and the initial volume (unit wise):

$$\varepsilon_v = 1 - (1 - \varepsilon_x)(1 - \varepsilon_y)(1 - \varepsilon_z) \quad (8.32)$$

Taking into account that the strains are infinitesimal, so the product between two or three of them is negligible, the relation (8.32) can be rewritten as:

$$\varepsilon_v = \varepsilon_x + \varepsilon_y + \varepsilon_z \quad (8.33)$$

Studying Fig. 8.13, it may be noticed that the total shear strain of the element,  $\gamma$ , can be directly computed as the sum of the strains of the neighbouring faces:

$$\gamma = \gamma_{xz} + \gamma_{zx} = 2\gamma_{xz} \quad (8.34)$$

The linear deformation moduli that are mostly used in geotechnical engineering (8.30) are:

- for the linear behaviour model, Fig. 8.15a, the way of defining the slope of the  $\sigma - \varepsilon$  curve is irrelevant, because it is constant on the entire domain;
- for a non-linear behaviour model, for instance Fig. 8.15b, only two moduli are relevant, the initial one, tangent to the curve at the origin, denoted by  $E_{\text{tangent}}$  or  $E_0$  and the secant values, generally chosen between the loading limits to which the material is to be subjected. This modulus, denoted  $E_{\text{secant}}$ , approximates the arc of the curve that defines the  $\sigma - \varepsilon$  relation through a chord;
- in the case of cyclic loading on soils, the hysteresis curve has an initial arc, where the moduli presented previously are relevant, after which, through successive rearrangement of the solid particles in a denser state, the loading-unloading curves will tend to be more convergent with each cycle (if failure is not reached) to a stable shape, which has an average slope describe by  $E_{\text{resilient}}$ .

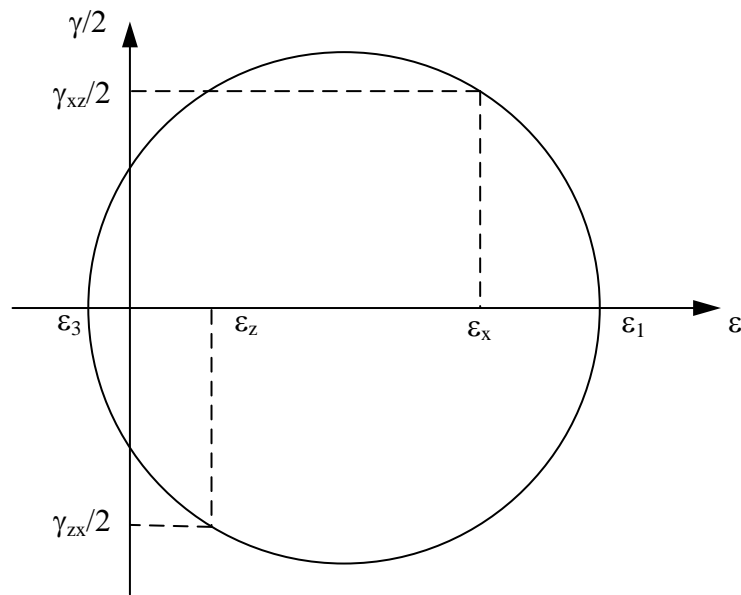


Fig. 8.14: Representation of the state of strain around a point

$$\begin{aligned}
 E_{\text{tangent}} &= \frac{d\sigma}{d\varepsilon} \\
 E_{\text{secant}} &= \frac{\Delta\sigma}{\Delta\varepsilon} \\
 E_{\text{resilient}} &= \frac{\sigma_{\text{max}} - \sigma_{\text{min}}}{\varepsilon_{\text{max}} - \varepsilon_{\text{min}}}
 \end{aligned}
 \tag{8.35}$$

The values of the linear deformation modulus may vary depending on the loading type, for instance, for cyclic loading, when the applied deformation range varies, the  $E - \varepsilon$  curve, or its analogous  $G - \gamma$  used for non-linear computations of seismic behaviour of soil masses, has the shape described in Fig. 8.16.

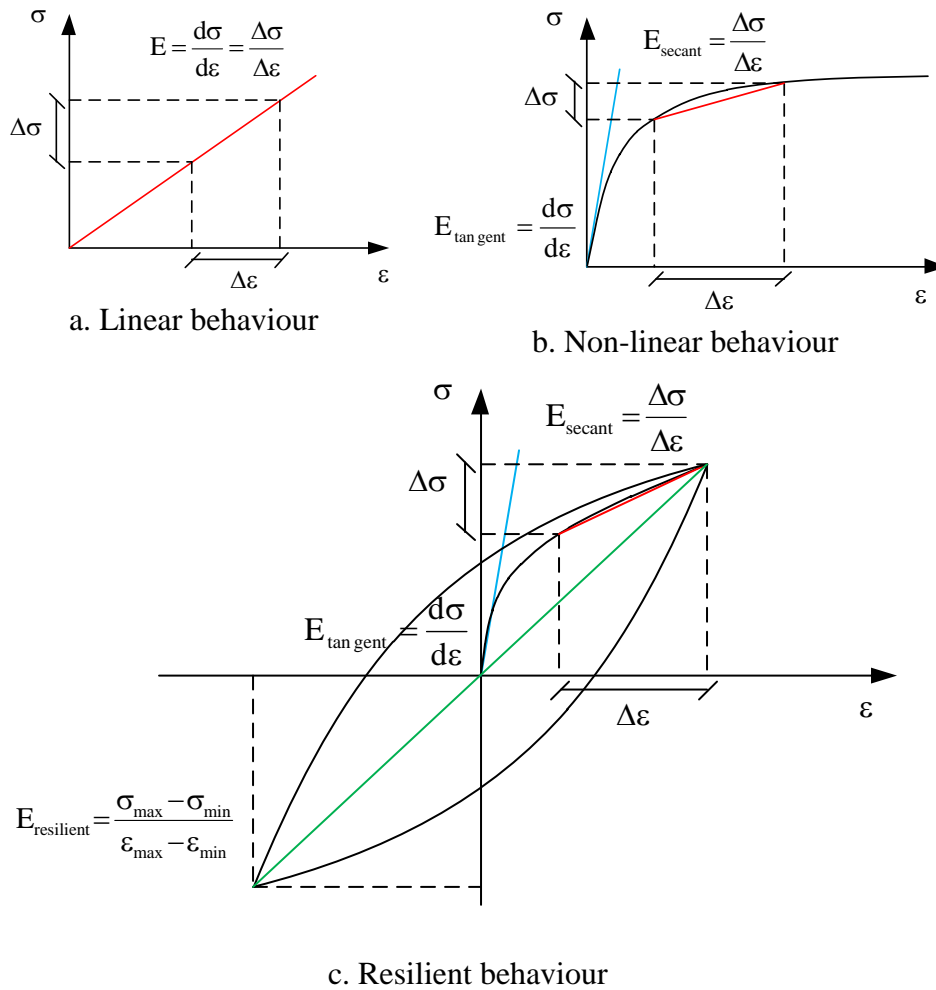


Fig. 8.15: Defining the linear deformation moduli function of the chosen material behaviour model

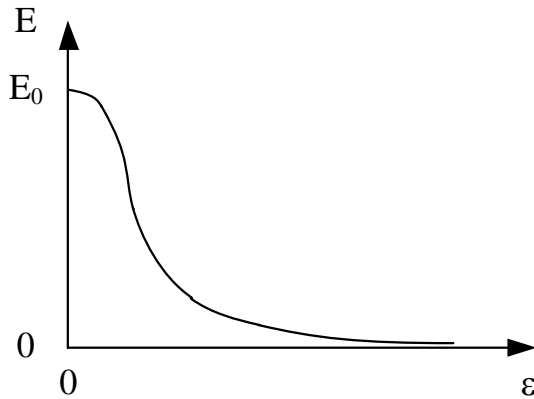


Fig. 8.16: Strain softening type relation

For simplifying the relations between different types of stresses and their corresponding strains, there are some elastic moduli less used or specific to certain types of applications.

One of these moduli is K, the volumetric strain modulus, which is defined by the relation between the spherical stress  $I_1$  and the volumic strain  $\varepsilon_v$ :

$$I_1 = K\varepsilon_v \quad (8.36)$$

which follows that:

$$K = \frac{I_1}{\varepsilon_v} = \frac{I_1}{\varepsilon_x + \varepsilon_y + \varepsilon_z} = \frac{(\sigma_x + \sigma_y + \sigma_z)}{\frac{1}{E}(1-2\nu)(\sigma_x + \sigma_y + \sigma_z)} = \frac{E}{1-2\nu} \quad (8.37)$$

The necessity for expressing a semi-logarithmic stress-strain relation for soils lead to the introduction of two more secant moduli for the loading curve (primary compression coefficient  $C_c$ ), and unloading curve respectively (unloading coefficient  $C_e$ ).



#### 8.4 Law of effective stresses

For emphasising the distribution of unit stresses in saturated soil masses, Karl Terzaghi published in 1924, in his fundamental book, “Erdbaumechnik”, the description of a mechanical model consisting in a cylinder full with water, having a piezometer tube attached to the base, in which a piston with a tap can slide. The cylinder and the piston are connected through a spring simulating the elastic behaviour of the solid skeleton in the soil (Fig. 8.17). The piston is loaded with a unit stress  $\sigma$ , called “total stress”, invariable in time.

At the initial time  $t_0$ , the tap is closed. The liquid in the piston, being incompressible and the drainage impossible, the piezometer tube will record an increase in the fluid pressure,  $u$ , and equal to the total applied stress. The spring is hydrostatically loaded, so that, without a differential loading at the ends, it will not deform. In conclusion, at time  $t_0$ , the stress equilibrium may be written as:

$$\sigma = u \quad (8.38)$$

The piston’s tap is then opened, so that after some time  $t$ , the water in the cylinder is evacuated, and its pressure,  $u$ , decreases. For maintaining the equilibrium, the difference between the total stress and the liquid pressure,  $u$ , is transferred to the spring that models the solid skeleton of the soil. The spring deforms, and the stress that produced this effect is denoted by  $\sigma'$  and is called “effective stress”. Therefore, at an intermediate time  $t$ , the equilibrium of stresses is:

$$\sigma = \sigma' + u \quad (8.39)$$

The equation (8.39) is called “the law of effective stresses”. The loading of the spring will continue in the same time with the drainage of the water, which is done in a non-steady state regime, caused by the decrease in water pressure. At the final time  $t_{100}$ , all the pressure taken by the fluid is transferred to the solid skeleton, which can be written as:

$$\sigma = \sigma' \quad (8.40)$$

Because the soil's pore water pressure, being a hydrostatic stress, does not lead to deformations, is sometimes also called "neutral pressure". The water cannot bear deviatoric stresses, but only spherical stresses, and in a point, its value is the same in all directions, so that, in matrix form, the law of effective stresses can be written as:

$$\begin{bmatrix} \sigma_x & \tau_{xy} & \tau_{xz} \\ \tau_{yx} & \sigma_y & \tau_{yz} \\ \tau_{zx} & \tau_{zy} & \sigma_z \end{bmatrix} = \begin{bmatrix} \sigma'_x & \tau_{xy} & \tau_{xz} \\ \tau_{yx} & \sigma'_y & \tau_{yz} \\ \tau_{zx} & \tau_{zy} & \sigma'_z \end{bmatrix} + \begin{bmatrix} u & 0 & 0 \\ 0 & u & 0 \\ 0 & 0 & u \end{bmatrix} \quad (8.41)$$

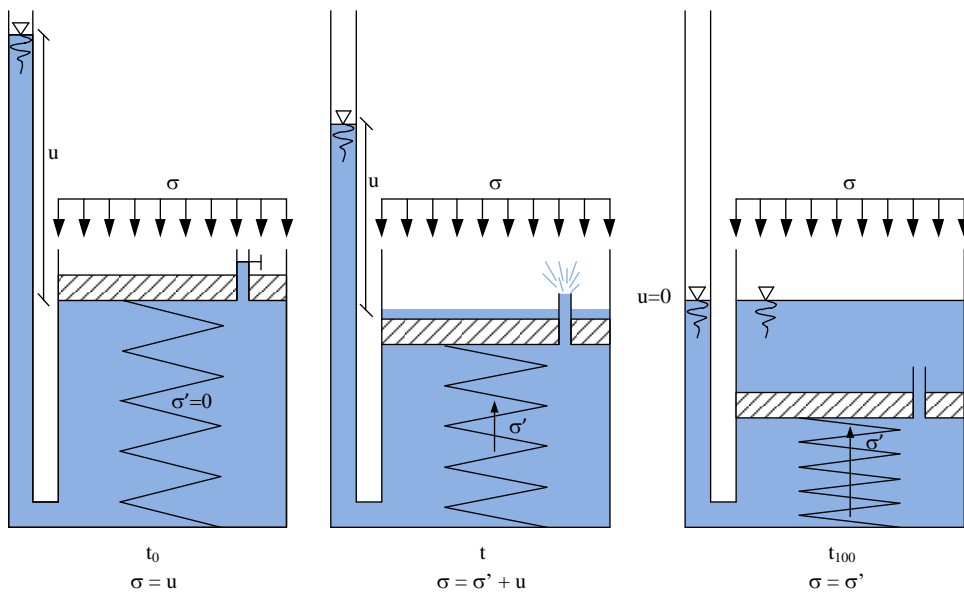


Fig. 8.17: Karl Terzaghi's one-dimensional consolidation mechanical model

The rheological (time dependant) phenomenon of transferring the total applied stress from the pore water pressure to the soil's solid skeleton is called "consolidation".

## 8.5 Plane problems

In some situations, one can consider the simplified models of the three-dimensional stress and strain states, as following

- plane stress state (or plane stress problem – PSS $\sigma$ ), in which we consider  $\sigma_z = 0$ ;
- plane strain state (or plane strain problem – PSS $\epsilon$ ), in which we consider  $\epsilon_z = 0$ ;

For example, when analysing a retaining wall loaded on the back surface, in perpendicular direction, by the soil thrust, one may assume that the longitudinal dimension will not be modified, or in other words  $\epsilon_z = 0$  which implies that the stresses in this direction will not vary.

An important characteristic of plane problems is that the thickness of the strip normal to the direction analysed is unitary. For the simplification for 3D to 2D problems, the conditions that need to be fulfilled are that the geometry, the loads and the material properties of the model that is simplified cannot vary on the direction of the simplification.

From the static point of view, a plane strain problem will have the deformations blocked on perpendicular direction (being simply supported on this direction or having restricted the translation degree of freedom), while the plane stress problem will have free translations on perpendicular direction.

Choosing the simplified model will be done generally according to the geometry of the deformable solid that is studied: PSS $\sigma$  is generally used to model small thickness structural elements (walls, diaphragms, thick plates etc.), while the PSS $\epsilon$  is generally used for structural elements that have larger longitudinal dimensions in comparison with transversal dimensions (retaining walls, dams, roads, etc.).

A special case of the plane strain problem is that of the half spaces or of the elements with a symmetry axis that is vertical in the soil (cylindrical shafts, cylindrical piles, etc.). The elements with a symmetry axis (let's suppose z axis) have the particularity that in each strip has an opening of one degree or one radian. Thus, in a perpendicular plane on the symmetry axis, two material

points shall be identically loaded, in such a way that the deformations are null, and the stresses are equal, namely  $\sigma_y = \sigma_x$ . On the vertical direction there are loading differences, especially from the soil mass' own weight

A particular situation of the axial symmetric problem is the one of the normal uniformly loaded half space and or gravity load acting on this direction. In this situation, any perpendicular line on the plane will be a symmetry axis. This problem bears the name "rest state". Minding that the vertical direction is a symmetry axis for the loading, it means that tangential stresses, as antisymmetric stresses, cannot act on this direction, so the vertical and horizontal axis are principal directions.

The third equation of the system (8.29) expressed on the principal directions:

$$\varepsilon_3 = \frac{1}{E} [\sigma_3 - \nu(\sigma_1 + \sigma_2)] \quad (8.42)$$

conditioning that  $\varepsilon_3 = 0$  and  $\sigma_2 = \sigma_3$  which is true for the rest state, we obtain:

$$\sigma_3 = \frac{\nu}{1-\nu} \sigma_1 \quad (8.43)$$

denoting

$$K_0 = \frac{\nu}{1-\nu} \quad (8.44)$$

so that the equation (8.43) becomes:

$$\sigma_3 = K_0 \sigma_1 \quad (8.45)$$

$K_0$  bears the name of thrust coefficient for soil at rest state and as it can be concluded from the demonstration above, it applies for the elastic state of soil masses.

## **8.6 Stress coordinates**

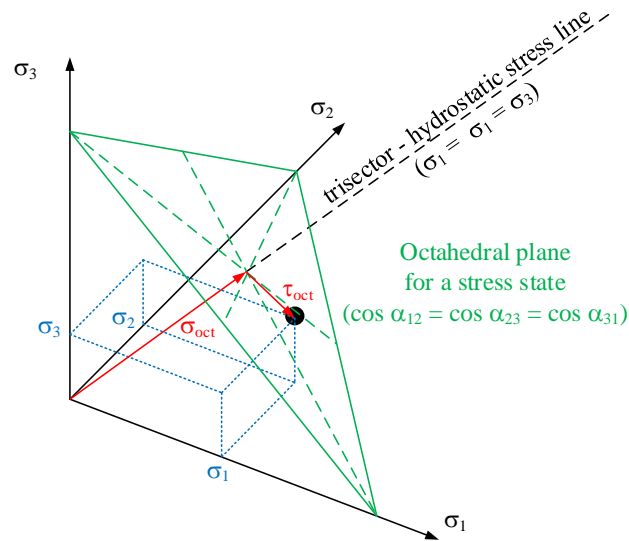
The stress states representation in the shape of Mohr circle has the advantage of describing all the  $\sigma - \tau$  stress pairs that can appear around a point from the analysed solid, as well as the possibility to find the action direction of the stresses through the Pole of the circle. If one desires to study a succession of stress states at which the material is subjected, the representation becomes far too expressive from the graphical point of view.

For this reason, only the information that can be used to reconstruct the more complex Mohr representation, without losing any data, are kept from the stress state. It is trivial to understand that all the representation must begin from the principal stresses, which must fulfil that condition.

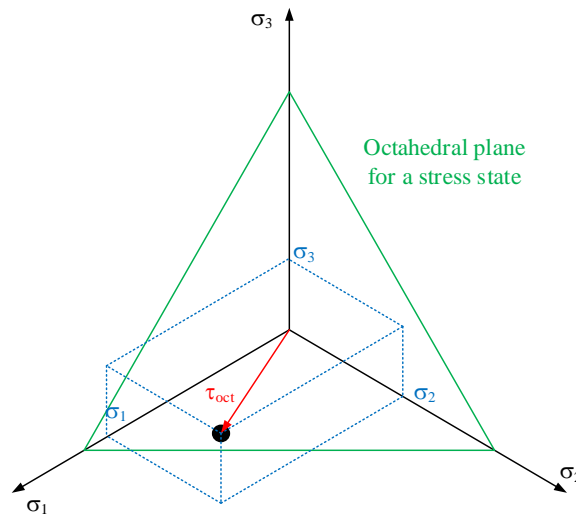
One coordinate option is exactly the principal stresses representation. If a three-dimensional stress state is studied, the representation in  $\sigma_1 - \sigma_2 - \sigma_3$  coordinate system is done through a point (Fig. 8.18).

In order to determine the spherical and deviatoric component of a stress state so that the invariants defined in equations (8.25) and (8.27) are similar, a cylindrical coordinate system is used. The longitudinal axis of the system, onto which the spherical components are plotted, will be the trisection of the Cartesian coordinate system  $\sigma_1 - \sigma_2 - \sigma_3$  and the deviatoric components will be described onto the polar axis. The azimuthal angle of the coordinate system has no special importance in the state description, so it will be ignored. The plane in which the representation of the stress state is found is an octahedral plane of the Cartesian system, perpendicular on the trisection.

Because of this, the height of the plane in relation with the origin or with the stress state longitudinal component will bear the name of octahedral spherical stress and is denoted with  $\sigma_{\text{oct}}$ , while the deviator, which in plane is the radial distance from the axis, is called the octahedral deviatoric stress and is denoted with  $\tau_{\text{oct}}$ .



a. Cartesian representation



b. Projection in the octahedral plane

Fig. 8.18: Stress state representation in the  $\sigma_1 - \sigma_2 - \sigma_3$  coordinate system

For determining  $\sigma_{oct}$ , one has to compute the addition of the values of the principal stresses projections on the trisection axis, in a tetrahedron that has three of the faces right isosceles triangles with the edges equal to "1". The height of the triangle will be  $1/3$ , as the hypotenuse is „ $1\sqrt{2}$ ”, thus the sum of the projections is:

$$\sigma_{\text{oct}} = \frac{\sigma_1}{3} + \frac{\sigma_2}{3} + \frac{\sigma_3}{3} = \frac{I_1}{3} \quad (8.46)$$

For computing  $\tau_{\text{oct}}$  we will use Pythagoras' theorem in the right triangle that has as hypotenuse the distance from the coordinate system origin to the Cartesian position of the stress state, equal to  $\sqrt{\sigma_1^2 + \sigma_2^2 + \sigma_3^2}$ , and one of the cathetus equal to  $\sigma_{\text{oct}}$ , thus

$$\begin{aligned} \tau_{\text{oct}} &= \sqrt{(\sigma_1^2 + \sigma_2^2 + \sigma_3^2) - \frac{I_1^2}{9}} = \\ &= \frac{1}{3} \sqrt{(\sigma_1 - \sigma_2)^2 + (\sigma_2 - \sigma_3)^2 + (\sigma_3 - \sigma_1)^2} = \sqrt{\frac{2J_2}{3}} \end{aligned} \quad (8.47)$$

One may simplify the stress state representation from three dimensions to two dimensions by using  $\sigma_{\text{oct}} - \tau_{\text{oct}}$  directly. By doing so for axial symmetric representation, or  $\sigma_2 = \sigma_3$ , we must keep the first non-null invariant of the respective tensor for the deviatoric axis, and in order to maintain the measuring units compatibility, it is necessary to multiply with 3 and extract the square root respectively. Thus the „Cambridge” stress coordinate system is obtained:

$$\begin{aligned} p &= \frac{I_1}{3} = \frac{\sigma_1 + \sigma_2 + \sigma_3}{3} = \frac{\sigma_1 + 2\sigma_3}{3} \\ q &= \sqrt{3J_2} = \sqrt{3(s_1s_2 + s_2s_3 + s_3s_1)} = \sqrt{3(2s_1s_3 + s_3^2)} = \sigma_1 - \sigma_3 \end{aligned} \quad (8.48)$$

Most of the British papers in the field use the  $p - q$  stress coordinates, but in order to maintain values that are closer to the values obtained for the Mohr circle representation, the M.I.T. researchers proposed a different coordinate system, in which the spherical stress component, denoted by  $s$ , is given on the  $O\sigma$  axis of the circle, while the deviatoric stress component, denoted with  $t$ , is the radius of the circle:

$$\begin{aligned} s &= \frac{\sigma_1 + \sigma_3}{2} \\ t &= \frac{\sigma_1 - \sigma_3}{2} \end{aligned} \tag{8.49}$$

As a general observation, both in  $\sigma_{\text{oct}} - \tau_{\text{oct}}$ , and  $p - q$ , as well as in  $s - t$  coordinate systems, a given stress state is reduced to a point, while there is always the possibility to convert it back to a Mohr circle representation. Another observation is that the effective stress law always remains valid, no matter what type of coordinate system is used. For  $\sigma - \tau$  coordinates, according to (8.41):

$$\begin{aligned} \sigma &= \sigma' + u \\ \tau &= \tau' \end{aligned} \tag{8.50}$$

in octahedral stresses:

$$\begin{aligned} \sigma_{\text{oct}} &= \frac{I_1}{3} = \frac{\sigma_1 + \sigma_2 + \sigma_3}{3} = \frac{(\sigma'_1 + u) + (\sigma'_2 + u) + (\sigma'_3 + u)}{3} = \sigma'_{\text{oct}} + u \\ \tau_{\text{oct}} &= \frac{\sqrt{(\sigma_1 - \sigma_2)^2 + (\sigma_2 - \sigma_3)^2 + (\sigma_3 - \sigma_1)^2}}{3} = \\ &= \frac{\sqrt{(\sigma'_1 - \sigma'_2)^2 + (\sigma'_2 - \sigma'_3)^2 + (\sigma'_3 - \sigma'_1)^2}}{3} = \tau'_{\text{oct}} \end{aligned} \tag{8.51}$$

in Cambridge coordinates:

$$\begin{aligned} p &= \frac{\sigma_1 + 2\sigma_3}{3} = \frac{(\sigma'_1 + u) + 2(\sigma'_3 + u)}{3} = p' + u \\ q &= \sigma_1 - \sigma_3 = (\sigma'_1 + u) - (\sigma'_3 + u) = q' \end{aligned} \tag{8.52}$$

and in MIT coordinates:



$$\begin{aligned}
 s &= \frac{\sigma_1 + \sigma_3}{3} = \frac{(\sigma'_1 + u) + (\sigma'_3 + u)}{2} = s' + u \\
 t &= \frac{\sigma_1 - \sigma_3}{2} = \frac{(\sigma'_1 + u) - (\sigma'_3 + u)}{2} = t'
 \end{aligned}
 \tag{8.53}$$

The stress coordinates that plot the principal directions are very useful especially when the stress state modification in a point under exterior loading is studied. This stress state succession is called "stress path".

In order to illustrate the stress path procedure, a plot of stress state succession both in  $\sigma - \tau$  and  $s - t$  coordinate systems is depicted below, for the case of monoaxial compression. In such a situation, the radial stress  $\sigma_3$  is null permanently, and the stress on the vertical direction,  $\sigma_1$ , is increasing from zero to the maximum value.

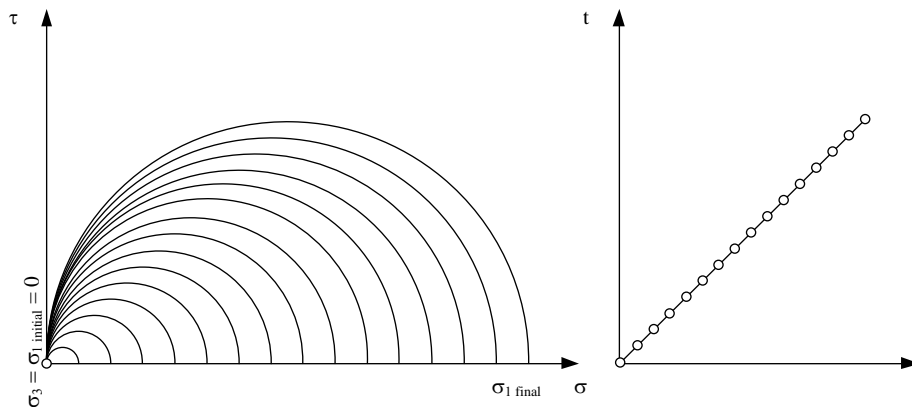


Fig. 8.19: Stress path representation example for the monoaxial compression test

### 8.7 Test your understanding

**Problem 8.1**

How can one express graphically the state of stress around a point?

**Problem 8.2**

What is the advantage of using MIT coordinates to express the state of stress?

**Problem 8.3**

What are the principle stresses?

**Problem 8.4**

What are only 2 principle stresses expressed to characterize the state of stress around a point in a soil mass?

**Problem 8.5**

What is a state of stress?

**Problem 8.6**

What is a state of strain?

**Problem 8.7**

State the law of effective stresses.

**Problem 8.8**

What is the Pole of Mohr's circle of stress?

**Problem 8.9**

What is a plane strain problem?



## **9 SOIL COMPRESSIBILITY AND CONSOLIDATION**

### **9.1 Compressibility**

Soil, as a material, presents a series of particularities that make difficult adopting a simplified approach when describing its behaviour under loads. It has been shown in the previous chapter through the law of effective stresses that soil can only deform when the pore water can be drained, so, without taking this component into account would result in breaking the principle of mass conservation. Moreover, soil is a material that exhibits “memory”. Considering that the volumetric deformations are only a result of rearrangement of the solid particles in a more compact state, capable of bearing the load, it may be assumed that this state is also kept when unloading, so the maximum load ever applied to the soil can be determined.

A soil that is subjected for the first time to a certain level of compressive stress and the pore water pressure has reached an equilibrium, is called “normally consolidated”. The study of the stress-strain relation of soils is generally required either for a state of stress at rest or isotropic, so that shearing strains be null or negligible. The isotropic state of stress does not naturally occur on soil, the deformability in these conditions being studied only when the technical conditions require it, specifically for the triaxial compression apparatus with imposed deformation. The study of the phenomenon affecting the state of the samples as little as possible, meaning the state of rest is kept, is performed using the oedometer, in which the soil is constrained within a steel ring that suppresses radial deformations, and the sample is loaded only axially. The same effect can be obtained following consolidation in triaxial compression apparatus with imposed stress, controlling the stress so that the deformations do not develop on radial direction. This chapter will only refer to consolidation in these conditions.

In decimal scale, the primary loading curve, also known as the normal consolidation curve, has a very small tangent modulus for small applied stresses, due to the large porosity of the soil so the particles have larger voids

to fill. Together with the increase in stresses, for each applied increment, the porosity gets smaller, as well as the voids available for rearranging. The solid particles suffer local crushing in the contact zones and fasten more to get into a denser state. In these conditions, the deformations become smaller and smaller. To summarize, in the range of small stresses, the deformations of the material are large, while they decrease with the increase of stresses. For having a balanced representation of the stress-strain curve, a semi-logarithmic scale is chosen, mainly decimal scale for deformations and logarithmic scale for stresses.

Generally, the obtained deformation modulus following an oedometric test, in which the state of stress is kept at rest, is called oedometric modulus and is denoted by M:

$$M = \frac{\Delta\sigma}{\Delta\varepsilon} = \frac{\sigma_f - \sigma_i}{\varepsilon_f - \varepsilon_i} \quad (9.1)$$

Considering the soil is in a state of stress at rest, the radial deformation is equal to zero, so  $\varepsilon_r = \varepsilon_3 = 0$ . This means that the cross-section of the sample is unchanged so its area, A, is constant, following:

$$\Delta\varepsilon_v = \frac{\Delta V}{V_0} = \frac{A \cdot \Delta h}{A \cdot h_0} = \Delta\varepsilon_a \quad (9.2)$$

where  $\varepsilon_a$  is the axial strain.

On the other hand, the variation of the volume of the sample is just a variation of the volume of voids,  $V_v$ , the volume of solids,  $V_s$ , remaining constant, since no material is lost or gained. Therefore:

$$\Delta\varepsilon_v = \frac{\Delta V}{V_0} = \frac{(V_s + V_{vf}) - (V_s + V_{v0})}{V_s + V_{v0}} = \frac{\frac{\Delta V_v}{V_s}}{\frac{V_s}{V_s} + \frac{V_{v0}}{V_s}} = \frac{\Delta e}{1 + e_0} \quad (9.3)$$

where e is the voids ratio. From equations (9.2) and (9.3) it follows that:

$$\Delta \varepsilon_a = \frac{\Delta e}{1 + e_0} \quad (9.4)$$

Replacing (9.4) into (9.1):

$$C = \frac{\Delta \sigma}{\Delta \varepsilon} = \frac{\Delta \sigma}{\frac{\Delta e}{1 + e_0}} = \frac{1 + e_0}{a_v} \quad (9.5)$$

By  $a_v$  is denoted the compressibility modulus. This modulus is determined as the slope of the  $e$ - $p$  graph, which can be obtained from Fig. 9.1a applying equation (9.4) and knowing the value of the initial voids ratio,  $e_0$ . In the model of one-dimensional consolidation model, described in chapter 9.2, the equivalent modulus,  $m_v$ , will be used, called modulus of volumetric compressibility, and being defined as:

$$m_v = \frac{1}{M} = \frac{a_v}{1 + e_0} \quad (9.6)$$

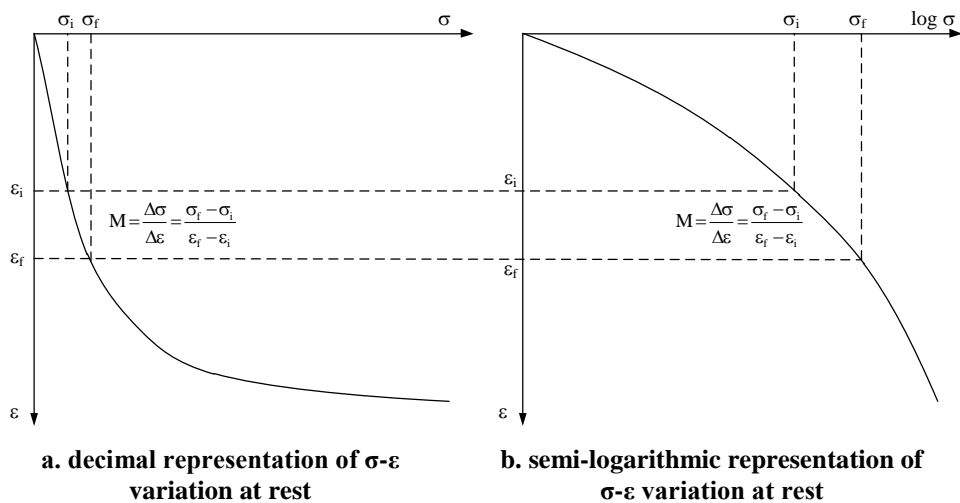


Fig. 9.1: Oedometric modulus representation in decimal and semi-logarithmic scales

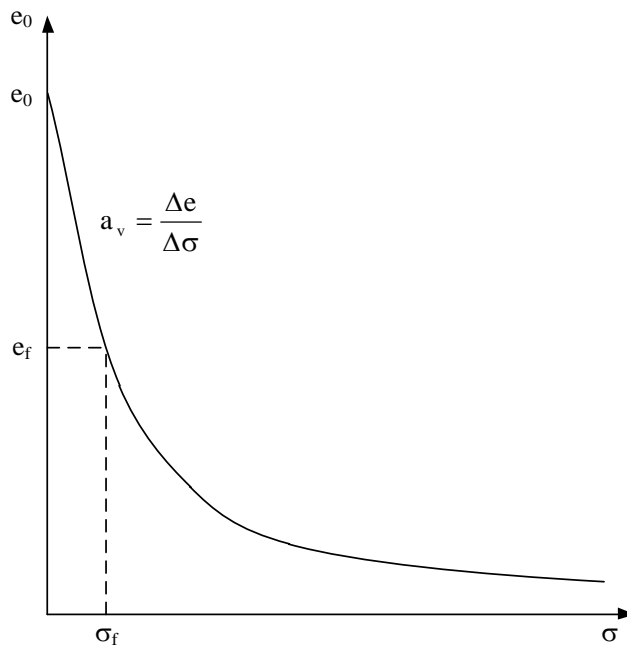


Fig. 9.2: Compressibility modulus representation using  $\sigma - e$  variation in decimal scale

Using a logarithmic scale for the stress axis of the  $\sigma - e$  curve shown in Fig. 9.2 a flattening effect on the small stresses range is obtained, similar to the compression-settlement curve from Fig. 9.1 a. This representation was proposed by Casagrande in 1936 for obtaining the maximum geological stress to which the sample was subjected in its geological history. In the critical state theory, instead of the voids ratio, the specific volume is preferred, defined as:

$$v = 1 + e \tag{9.7}$$

In this model, the stress axis is either naturally logarithmic, or decimal and replaced by the effective spherical stress  $p'$ .

Thanks to linearization, certain constitutive models prefer using secant moduli derived from the logarithmic expression. Thus, the following coefficients can be described for the compression-porosity or compression-settlement curves, all having the same expression, but being defined for different curve segments:

$$\left. \begin{array}{l}
 C_c - \text{compression coefficient} \\
 \text{(from normal consolidation curve)} \\
 \\
 C_e - \text{extension coefficient} \\
 \text{(from the unloading curve)} \\
 \\
 C_r - \text{reloading coefficient} \\
 \text{(from the reloading curve)}
 \end{array} \right\} = \frac{\log p_f - \log p_i}{e_i - e_f} \quad (9.8)$$

The same types of moduli are obtained from the compression-specific volume curve:

$$\left. \begin{array}{l}
 \lambda - \text{primary compression coefficient} \\
 \text{(from the normal consolidation curve)} \\
 \\
 \kappa - \text{secondary compression coefficient} \\
 \text{(from the reloading curve)}
 \end{array} \right\} = \frac{\ln p_f - \ln p_i}{v_i - v_f} \quad (9.9)$$

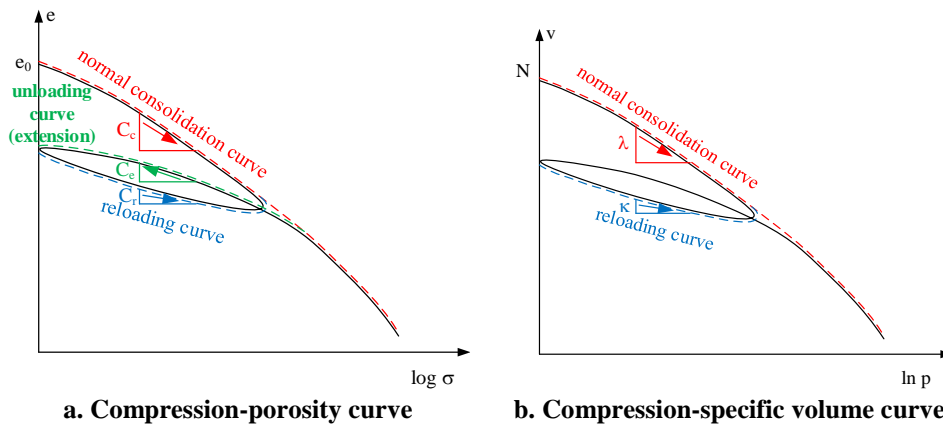


Fig. 9.3: Specific volume and voids ratio variations with the applied load

Denoting the initial specific volume by  $N$  and the initial voids ratio by  $e_0$ , the equation of the normal consolidation curve can be linearly approximated by:



$$\begin{aligned}v &= N - \lambda \ln p \\ e &= e_0 - C_c \lg \sigma_v\end{aligned}\tag{9.10}$$

In engineering practice, any sample with no cementation bonds taken from the site, when it is subjected to an oedometric test will have its first section of the compressibility curve on a loading path at least up to the geologic stress at the depth from which the sample was taken. The history of loading cannot be determined, but studying the inflexion point of the compression-porosity curve, the pre-consolidation stress,  $\sigma_c$ , can be determined, corresponding to the maximum stress to which the sample was subjected during its geological history (Fig. 9.4).

Taking into account that the geological stress  $\sigma_g$  to which the sample is currently subjected, the overconsolidation ratio can be determined. Denoted by OCR, the overconsolidation ratio is computed as the ratio between pre-consolidation stress and the geological stress:

$$\text{OCR} = \frac{\sigma_c}{\sigma_g}\tag{9.11}$$

The soils for which  $\text{OCR} = 1$  are called normally consolidated soils and they are found on the normal consolidation curve, meaning that never in the geological history of the soil has it been subjected to a load larger than the current one. This can be characteristic to samples deep within a layer that has never been subjected to additional loads that might have disappeared or to erosion phenomena, but is subjected to a lithological load that guarantees its resistance. The normal consolidation can also characterize the recently deposited soils, of soft or liquid consistency.

For small overconsolidation ratios (generally smaller than 5), the soil structure is not affected by unloading to the geological stress, however, for large values of OCR (e.g. larger than 15), the over-consolidated clays form micro-fissures, developing the so-called glomerular soils. The glomerular clay structures have a coarse-like soils mechanical behaviour, with degradable particles, and some properties characteristic to clays (e.g. low permeability) are altered by the development of the large voids between the aggregates. Micro-fissuring of the strongly over-consolidated clays is caused

by reaching the tensile strength of the material by decompression of the layer during the unloading stage.

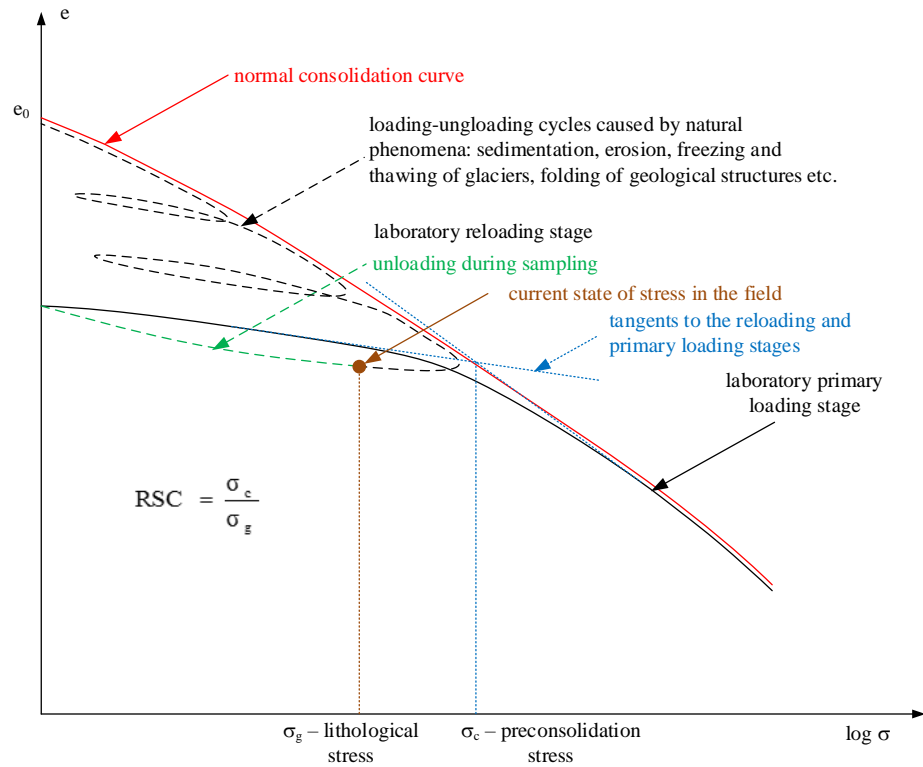


Fig. 9.4: Pre-consolidation stress – origin and determination method

## 9.2 Linear one-dimensional consolidation theory

The assumptions for developing the linear one-dimensional consolidation theory

1. The soil is homogenous and saturated.
2. The principle of effective stresses is valid.
3. Darcy's law is valid.
4. The pore water and the solid particles are incompressible.
5. Liquid flow and all solid particles displace one-dimensionally
6. The permeability coefficient ( $k$ ) and the volumic compressibility modulus ( $m_v$ ) are constant

Taking into account that the final assumption states the volumic compressibility modulus,  $m_v$ , is constant, the theory is valid for a relatively small stress increment.

Let's consider a soil layer of thickness  $2H$  placed between two infinitely pervious layers (Fig. 9.5). Following the increase of pore water pressure, assuming the pore water pressure in the infinitely pervious layers is zero, a flux of water will appear from the soil towards the pervious layers at the boundaries. As the hydrostatic gradient is the same for both pervious layers, the water drainage from each half of the soil layer will take place towards the closest pervious layer. Moreover, the water flow towards the pervious layers is symmetric with respect to the half of the distance between them (the axis of symmetry).

Let's consider an element of thickness  $dz$ , at a distance  $z$  with respect to the symmetry axis. The total stress with which the soil is loaded is denoted by  $\sigma$ . This stress is considered constant. Under the resulted effective stress  $d\sigma'$ , the element will suffer a deformation  $dl$ . The pore water pressure at the top of the element is  $u$ , and at the bottom is  $u+du$ .

The differential equation of one-dimensional consolidation can be proven to be:

$$c_v \frac{\partial^2 u}{\partial z^2} = \frac{\partial u}{\partial t} \quad (9.12)$$

where  $c_v$  is the consolidation coefficient, defined as:

$$c_v = \frac{k}{m_v \gamma_w} \quad (9.13)$$

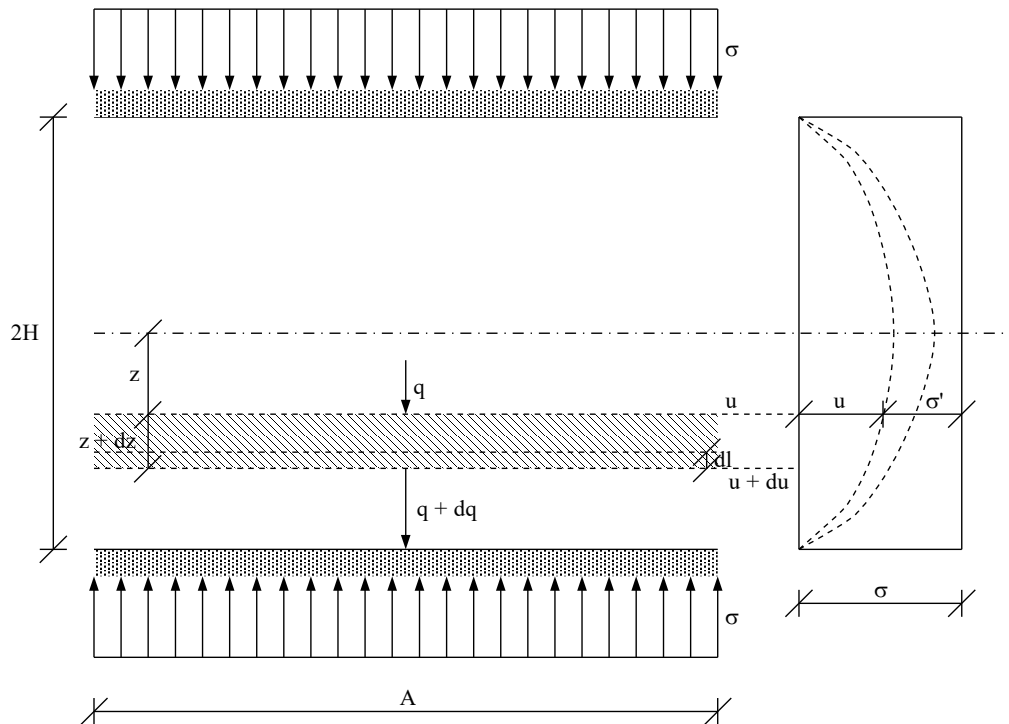


Fig. 9.5: Stress and drainage conditions for an infinitesimal element subjected to one-dimensional consolidation

The boundary conditions for the one-dimensional consolidation are:

$$\begin{array}{lll}
 t = 0 & 0 \leq z \leq H & u = \sigma' \\
 0 < t \leq \infty & z = 0 & u = 0 \\
 0 \leq t \leq \infty & z = H & \frac{\partial u}{\partial z} = 0 \\
 t = \infty & 0 \leq z \leq H & u = 0
 \end{array}$$

At a random time,  $t$ , the time factor  $T_v$  and the consolidation degree  $U_t$  can be defined as follows:

$$T_v = \frac{c_v t}{H^2} \tag{9.14}$$

$$U_t = \frac{s_t}{s_\infty} \quad (9.15)$$

where  $s_t$  is the settlement at time  $t$  over the height  $H$  of the soil layer that undergoes consolidation, and  $s_\infty$  is the final settlement of the soil. The limit values of the degree of consolidation are:

$$\begin{aligned} t = 0 & \quad U_0 = 0 \\ t = \infty & \quad U_\infty = 1 \end{aligned}$$

The local degree of consolidation at depth  $z$  can be expressed as:

$$U_t(z) = 1 - \frac{u(z,t)}{u(z,0)} \quad (9.16)$$

The solution of the equation (9.12), solved by means of Fourier series is:

$$u(z,t) = \sum_{m=0}^{\infty} \frac{2\sigma}{M} \sin\left(\frac{Mz}{H} e^{-M^2 T_v}\right) \quad (9.17)$$

where:  $M = \frac{\pi}{2}(2m + 1)$

Thus, the expression of the degree of consolidation is obtained:

$$U_t(z) = 1 - \sum_{m=0}^{\infty} \frac{2}{M} \sin\left(\frac{Mz}{H} e^{-M^2 T_v}\right) \quad (9.18)$$

and:

$$U_t = 1 - \sum_{m=0}^{\infty} \frac{2}{M^2} e^{-M^2 T_v} \quad (9.19)$$

For values  $U_t < 0.6$ , the degree of consolidation may be approximated as:

$$U_t = 2\sqrt{\frac{T_v}{\pi}} \quad (9.20)$$

### **9.3 Laboratory tests**

The study of soil compressibility is based on the use of the oedometer (Fig. 9.6), which is an apparatus that subjects the sample to vertical loadings, while keeping it confined.

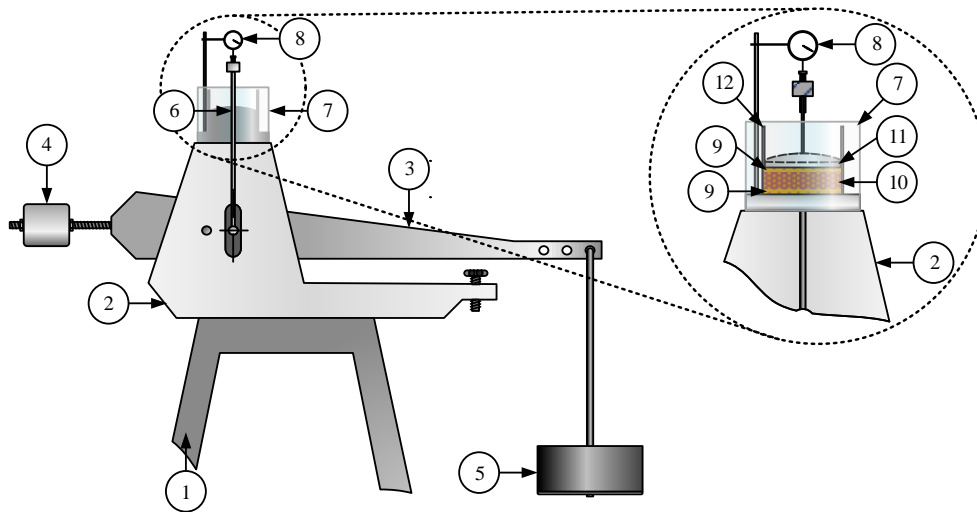
There are basically two main types of tests that can be performed (according to STAS 8942-1/1989 [22]):

- Compressibility tests, from which the data obtained offers the compressibility curves (settlement-loading curve, voids ratio-loading curve);
- Consolidation tests, which offer information on the amount of time a soil needs to consolidate under a certain loading.

The apparatus, as depicted by Fig. 9.6, is made of both mobile and fixed parts, as it follows:

1. Supporting frame – it forms the base upon the rest of the apparatus is built;
2. Body – it represents the real support upon which all the parts are resting;
3. Lever – it allows the user to change the loadings under which the soil sample is loaded;
4. Counter weight – this part allows the user to balance the lever (without any weights applied to it), so that the only loading applied to the soil sample is obtained by adding weights to it;
5. Loading weights – the various combinations of these weights allow the user to subject the sample to the desired loading; their position may vary along the lever, as function of the soil sample's diameter and required loading to be obtained;
6. Ram – this part will transfer the force from the loaded lever to the soil sample, by resting upon the loading plate;
7. Saturation cell – it allows the user to submerge and saturate the soil samples, according to the desired test procedure;
8. Dial gauge – it measures the settlement of the soils sample subjected to loading; it may be either mechanical, either electronic;
9. Porous stones – situated both on top and at the bottom of the sample, these parts allow the soil's water (moisture content) to be released, when the sample is subjected to loading;

10. Soil sample – it is a cylindrical specimen, having a diameter between 5 and 7.5cm and a thickness of 2cm;
11. Loading plate – situated on top of the porous stone, it allows the transformation of the punctual force transferred by the ram, into an equally distributed pressure;
12. Confining ring – this part limits the soil sample, so that no lateral displacements may appear, due to the ring's high rigidity.



Legend

- |                     |                   |                    |                    |
|---------------------|-------------------|--------------------|--------------------|
| 1. Supporting frame | 4. Counter weight | 7. Saturation cell | 10. Soil sample    |
| 2. Body             | 5. Loading weight | 8. Micrometer      | 11. Loading plate  |
| 3. Lever            | 6. Ram            | 9. Porous stone    | 12. Confining ring |

Fig. 9.6: The oedometer apparatus

**9.3.1 The procedure of the compressibility test**

In order to obtain the compressibility curve, these common steps are to be undertaken:

- first of all, the soil sample is to be cut under the form of the required cylindrical mould;
- the obtained cut sample is introduced inside the confining ring and into the saturation cell, having the two porous stones (plates) on the top and lower faces; also, on top of the upper porous stone the loading plate will be positioned;

- the cell containing the entire inner setup is to be placed on the body of the oedometer and place the ram to be in contact with the loading plate; the lever, at this moment will be loaded only with a 12.5 or 10kPa equivalent mass, known as “contact step”; this allows the ram to rest lightly on the sample, maintaining a continuous contact with it;
- for a period of 30 minutes, the setup will remain in this state, as the sample has to accommodate this stress state, from which the actual test will begin;
- although there are two possibilities of conducting the compressibility test – the first, by keeping the sample at its natural state from the point of view of the moisture content, while the second by saturating the sample, the procedure for advancing is the same: a loading step is considered complete if over 3 consecutive one hour apart readings, the sum of the settlement is below 0.01mm;
- the usual loading steps that are considered during the test are twice the magnitude of the one before; therefore, if considering the case of a 12.5kPa contact step, the loading sequence will be: 25kPa, 50kPa, 100kPa, 200kPa; these steps are considered as they are equally distributed along the logarithmic scale
- following the 200kPa loading step, the next interest loading, according to Romanian standards, is 300kPa; this allows the user to obtain the reference oedometric modulus upon which a soil classification from the point of view of the compressibility and most of the common design is conducted –  $E_{\text{oed}}$  or  $E_{200-300}$ ;
- after completing the 300kPa loading step, the next values of loadings are generally asked by the designer, in order to provide the needed data; sometimes, in the case of excavations, the designer might ask the geotechnical laboratory to provide also an unloading-reloading curve;
- the test is ended either by decreasing step-by-step the loading, down to the contact step, either decreasing directly to the contact step.

Although the basic principles aforementioned are applicable to all the compressibility tests, certain particularities may appear, according to the different aspects the design requires.

For example, in the case of loessial soils, according to the norm regarding the collapsible soils, two compressibility tests must be conducted – one maintaining the natural moisture content, and the second under saturated state



(Fig. 9.7a). If the case of low sampling, a single test may be conducted and, under the 300kPa loading step, after completing it for natural state moisture, the sample will be saturated and the collapse measured (Fig. 9.7b). This variation of the recommended test is deficient as it does not provide information regarding the compressibility of the soil in both states or about its variable collapsibility potential.

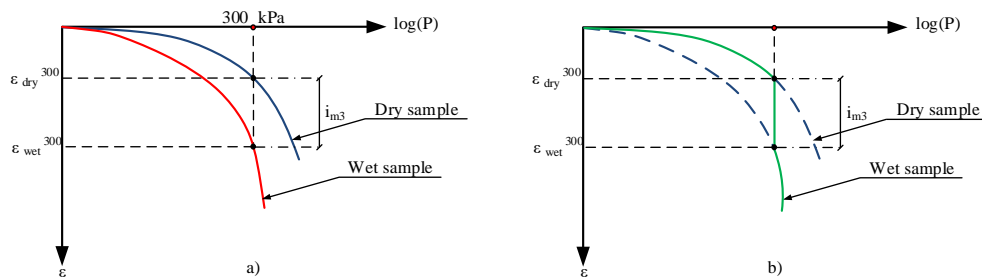


Fig. 9.7: Compressibility tests conducted on collapsible soils

In the case of the expansive soils (see STAS 1913/12 [23]), the compressibility test aims also at studying the swelling behaviour, and especially at determining the swelling pressure – value of the vertical stress for which the sample deformation is null. In order to conduct this type of test, following the setup of the cell onto the oedometer body and connecting the ram for a period of 30 minutes, the sample will be submerged by flooding the saturation cell. The sample will swell (Fig. 9.8) under this contact load and at obtaining a stabilization of the deformations, the test will be carried out as described herein.

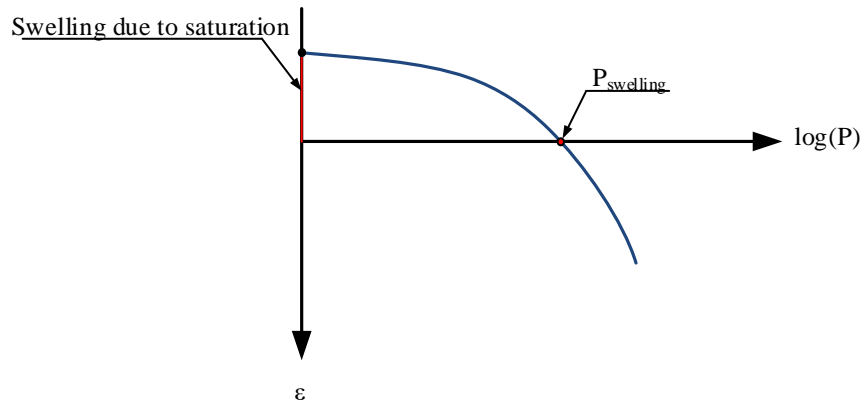


Fig. 9.8: Compressibility test conducted on expansive soils

### 9.3.2 The procedure of the consolidation test

The consolidation test, as mentioned before, implies the monitoring of the sample's settlement over time, under a constant load. Therefore, in order to perform the consolidation test, the following steps must be followed:

- the desired loading steps must be decided;
- during the compression test, at the end of the previous loading step, just before advancing to the loading under which the consolidation will be measured, the screw near the ram will be raised, so that the ram is supported by the first; the ram will be loaded with the extra weights, needed to obtain the desired vertical stress;
- after synchronizing the watch and setting it to 0seconds, the screw is to be lowered and the timer started;
- at 10s, 20s, 30s, 40s, 60s, 2min, 5min, 10min, 15min, 30min, 1h, 2h, 4h, 8h, 12h, and 24h, the settlement is recorded; in the case when the sample didn't reach equilibrium – the sum of the relative settlements between the last two readings is less than 0.01mm, the consolidation test will continue another 24h;
- at the end of the consolidation, the final settlement is recorded and may be used also in order to compute the compressibility curve and oedometric moduli.

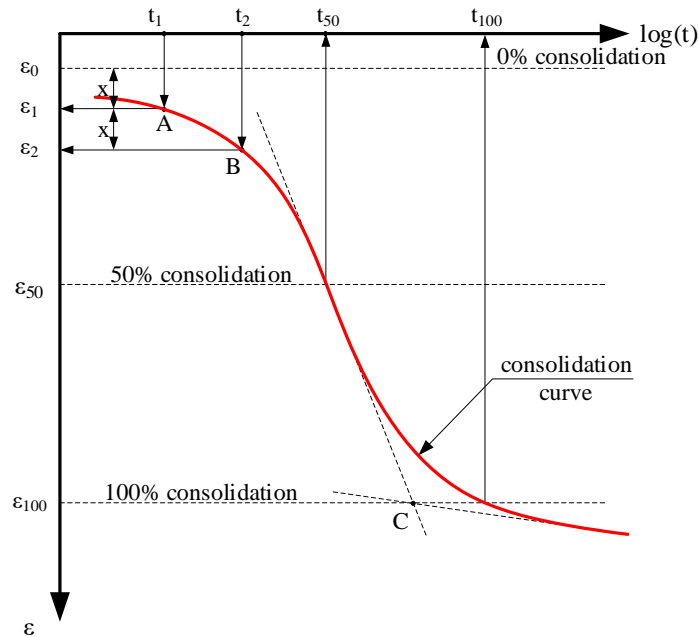


Fig. 9.9: The logarithm of time method for determining the coefficient of consolidation

In order to compute, based on the semi-logarithmic graphical variation of the strain as function of time (Fig. 9.9), the consolidation coefficient  $c_v$ , the following steps may be used:

- choose a time  $t_1$  and a time  $t_2$ , at the beginning of the test, so that  $t_2=4t_1$ ;
- at  $t_1$  find a point A on the curve and at  $t_2$  mark a point B on the curve;
- each of these points A and B have a given strain:  $\varepsilon_1$  and  $\varepsilon_2$  – the difference between them is  $\Delta\varepsilon$ ;
- find a point  $\varepsilon_0$  on the strain axis so that  $\varepsilon_0 = \varepsilon_1 - (\varepsilon_2 - \varepsilon_1) = 2\varepsilon_1 - \varepsilon_2$
- a horizontal line passing through  $\varepsilon_0$  is considered the 0% consolidation line;
- draw a tangent to the curve, passing through the inflexion point of the curve;
- draw a tangent to the last portion of the curve and intersect it to the tangent passing through the inflexion point, to find the point C;
- draw a horizontal line passing through point C and find the 100% consolidation line, with a strain  $\varepsilon_{100}$

- at the middle of the ( $\epsilon_0$ -  $\epsilon_{100}$ ) segment, lies  $\epsilon_{50}$ , from which a horizontal line shall be drawn – the 50% consolidation line
- the intersection between the 50% consolidation line with the consolidation curve marks a point with coordinates  $t_{50}$  and  $\epsilon_{50}$ .

Furthermore, considering the time factor  $T_v=0.197$ , which belongs to a degree of consolidation of 50%, compute the consolidation coefficient using the following relation:

$$c_v = \frac{0.197 \cdot H^2}{t_{50}} \quad (9.21)$$

where H is the longest drainage path (usually equal to half the sample's thickness as showed in Fig. 9.5).

#### **9.4 Test your understanding**

##### **Problem 9.1**

State three soil parameters that can be obtained using the oedometer compressibility test.

##### **Problem 9.2**

What is the difference between a compressibility and a consolidation test?

##### **Problem 9.3**

What deformations are allowed and what deformations are restricted during an oedometer compressibility test?

##### **Problem 9.4**

If the pressure is increased to an excessive value, can the soil specimen fail during the oedometer compressibility test?

##### **Problem 9.5**

How can we prevent failure of the specimen during a consolidation test?

##### **Problem 9.6**

Why are consolidation tests only relevant on clay samples?

**Problem 9.7**

How long does a consolidation test usually take?

**Problem 9.8**

What can be observed during the primary and secondary loading cycles during a compressibility test?

**Problem 9.9**

An oedometer specimen has the initial height 20mm, the diameter 70mm and the initial voids ratio  $e_0=0.44$ . Knowing that the oedometer modulus  $E_{\text{oad}}=7.5\text{MPa}$ , compute the compressibility coefficient,  $a_v$ .

**Problem 9.10**

An oedometer specimen has the initial height 2cm and the diameter 7cm. Knowing the oedometer test results shown in the table below, compute all the oedometric moduli.

Pressure [kPa]	Settlement [1/100 mm]
10	0
20	2
50	8
100	15
200	27
300	38
500	55

**Problem 9.11**

An oedometer specimen with the particle density  $2.72\text{g/cm}^3$  has the initial height 2.54cm, the area  $30.68\text{cm}^2$  and the dry mass 128g. Knowing the oedometer test results shown in the table below, draw the compression-porosity curve.

Pressure [kPa]	Specimen height [cm]
10	2.540
20	2.488
50	2.465
100	2.431

Pressure [kPa]	Specimen height [cm]
200	2.389
300	2.324
500	2.225
800	2.115

**Problem 9.12**

A clay layer with 5m thickness is confined between a sand layer to the top and bedrock at the bottom. During lab testing it was found that the consolidation coefficient of the clay is  $c_v = 1.5 \times 10^{-4} \text{cm}^2/\text{s}$ . Knowing  $T_{90} = 0.93$ , find the time required for 90% consolidation.

**Problem 9.13**

A soil specimen with initial diameter 7.14cm and height 2cm was tested in an oedometer. The initial voids ratio is 0.59. What is the voids ratio after a settlement of 0.35mm?

**Problem 9.14**

A soil specimen with initial diameter 7.14cm and height 2cm was tested in an oedometer. The particle density is  $2.71 \text{g/cm}^3$ , initial voids ratio is 0.82 and the moisture content is 22%. What would be the maximum settlement of the sample if no drainage is allowed during the test?



## **10 SOIL SHEARING STRENGTH**

### **10.1 Mohr-Coulomb failure criterion**

#### **10.1.1 Generalities**

Depending on the loads applied on a granular material, different types of stress states representations were broadly presented in the second chapter.

Coulomb demonstrates that a soil will reach failure in shear on a random plane when, due to the applied loads, the tangential stress varies with a unique and soil dependent linear expression of the normal stress. In this manner, the following expressions are identified:

- cohesionless soil - Fig. 10.1 a., is characteristic for coarse grained soils (sand and gravel);
- cohesive soil - Fig. 10.1 b., specific either for fine grained soils, for which the adsorption complex (or electrical double layer) induces large electrostatic forces, either for soils that have cementation bonds;
- pure cohesive soil - Fig. 10.1 c., is used only for high plasticity soils (clays), loaded in undrained conditions, for which the internal friction angle has a small enough value to be ignored. This model may also be used when mechanical tests are available for a given site that characterized mainly by clayey soils, for which in situ tests are made in order to make empirical correlations so that the undrained cohesion " $c_u$ " is obtained.



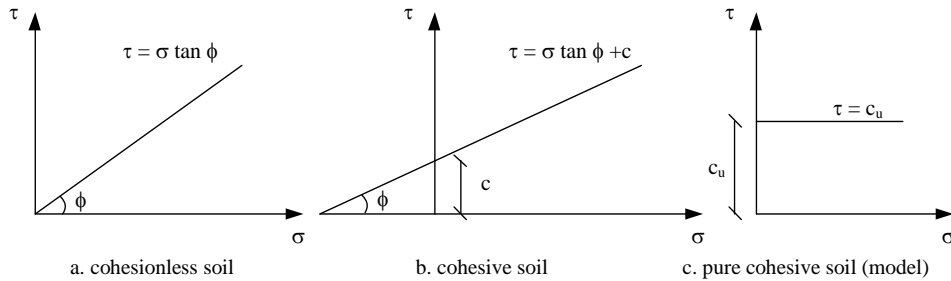


Fig. 10.1: Shear resistance models

Keeping in mind that the Coulomb line is generally expressed in the canonical form of a straight line equation, we can describe the function  $\tau(\sigma)$  having as parameters the slope  $\tan \phi$  and cut  $c$ . The parameters  $\phi$  and  $c$  are also known as the "shear resistance parameters", and the general equation is:

$$\tau = \sigma \tan \phi + c \quad (10.1)$$

Mohr's fundamental contribution to the expression of the shear resistance was the fact that he made a parametric study of many stress states that led to the shear failure of a given soil. By doing so, he noticed that those stress states have a common envelope, which is known as the "Mohr envelope". For the states of stresses commonly used in engineering practice, this envelope may be approximated with a straight line, which is known as the Coulomb line. As it is approximated to be the common tangent of the stress state circles, and thus characterising the failure, it is also called the "intrinsic line". The linear expression of the relation is not proper for small stresses in the case of normally consolidated soils or for very high stresses in the case of highly over-consolidated soils.

In order to determine the shear resistance parameters using the stress states it is necessary to know at least three different states (a common tangent for two circles is always possible, but not for three circles). Because of the curvature of the real failure criterion, if the circles are not perfectly cotangent to the Coulomb line, determining the parameters will be done using the extreme stress states. This may be done only if the circle that corresponds to the intermediate stress state is slightly above the line. If in reality the criterion was linear, this slight overpass of the failure line should not have been

possible, as after failure, the sample could not undertake the applied deviatoric stress.

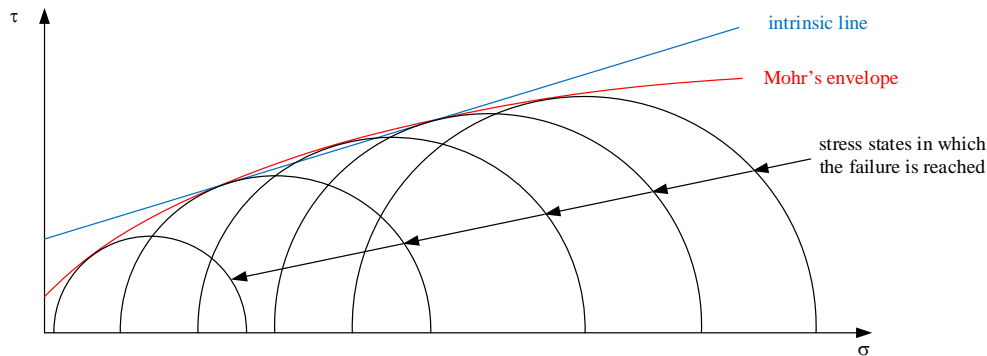


Fig. 10.2: Approximation of Mohr's envelope through the intrinsic line

The main disadvantage of the  $\sigma - \tau$  coordinate representation for the failure criterion is that the Mohr-Coulomb line is difficult to be computed and plotted as a common tangent for a set of circles. It is also impossible to track the stress state development that leads to failure.

Thus, it is better to obtain the shear resistance parameters from the representation of the failure criterion in the simplified  $s - t$  or  $p - q$  coordinates. As the interpretation of triaxial compression test results is more intuitive in this case, we will illustrate the advantages of using such a representation for a few common scenarios.

### ***10.1.2 The effect of overconsolidation over the shear resistance parameters***

If one will plot the variation of the deviatoric stress  $\tau$  against the shear displacement  $\delta$  (Fig. 10.3) in the case of the direct shear test, or for the case of the triaxial compression test, the deviatoric stress  $q$  against the axial strain  $\epsilon_a$ , it may be noticed the following:

- for dense cohesionless soils and for overconsolidated soils the curve will have the shape similar to the one depicted in Fig. 10.5a.
- for loose cohesionless soils or normally consolidated cohesive soils, the  $q - \epsilon_a$  curve will have the shape similar to the one depicted in Fig. 10.5b.

In the first case, the effect is due to clenching between the soil's particles. The grains that make up the soil's solid skeleton (up to coarse sands from the

granulometric perspective) are very rigid and resistant to the shear loads, so that in order for the shear plane to exist, it is necessary to overcome the inter-particle interaction forces and also to push them away from the shearing plane. At macroscopic scale, these phenomena are translated as extra stresses necessary to trigger the shear failure (the "peak" of the  $q - \varepsilon_a$  mobilization curve) and by a rise in volume due to mechanical considerations, called "dilatancy". The concept must not be mistaken with the "dilatation", which refers to thermal expand, nor to the swelling process that is related to the rise in volume due to water adsorption.

After the peak shear resistance value has been exceeded, which is characterized for a given stress state by the deviatoric stress  $q_{\text{peak}}$  or  $q_f$ , the solid grains will be reoriented in the failure surface. This phenomena is accompanied by a slight volume increase, and the deviatoric stress for which the sample resists the mechanical shear falls down to a value  $q_{\text{rez}}$ , which is called the residual value, and its origin is either due to friction between the coarse particles around the shear plane, either due to electrostatic interaction between the clay particles' adsorption complex.

The peak value of the deviator is larger as the clenching between the particles is higher, especially for the coarse soils, and as long as there are additional cementation bonds between the solid grains of the soil.

In the case of normally consolidated soil or for loose sands (Fig. 10.5b.), the internal configuration of the solid grains corresponds to the initial layout as arches that are built during the sedimentation stage. As the stress grows, the weaker arches are collapsing and the inner structure becomes denser. In the area next to the failure plane, the arches are loaded perpendicularly to the forming direction, so that a compression of the particles will appear, which are trying to resist efficiently to the shearing stress. On a macroscopic level, this diminishing of the sample's volume is called "contractancy", which is a different notion than "contraction" or "constriction".

In order to quantify the dilatancy or contractance value, the  $\psi$  angle is defined in the space determined by the volumetric and the axial variation:

$$\tan \psi = \frac{d\varepsilon_v}{d\varepsilon_a} \quad (10.2)$$

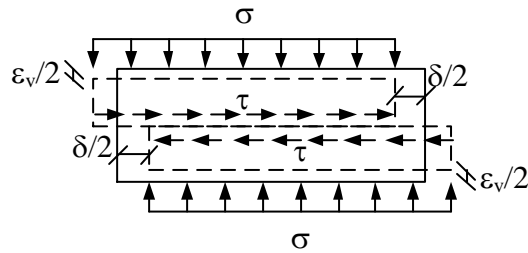


Fig. 10.3: Stresses, strains and displacements necessary to determine the dilatancy/contraction parameters for the direct shear test

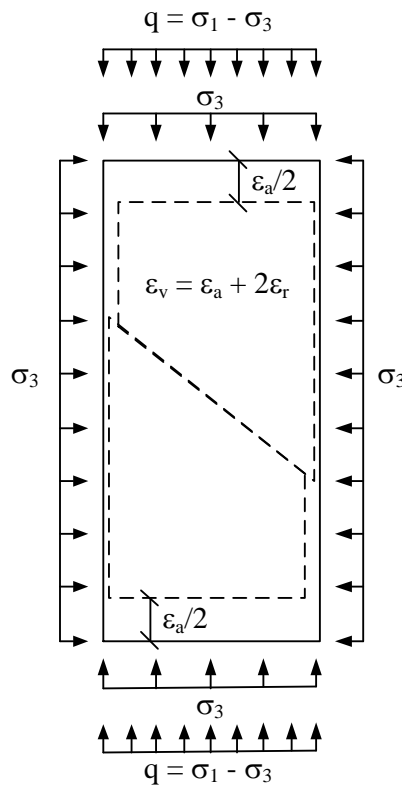
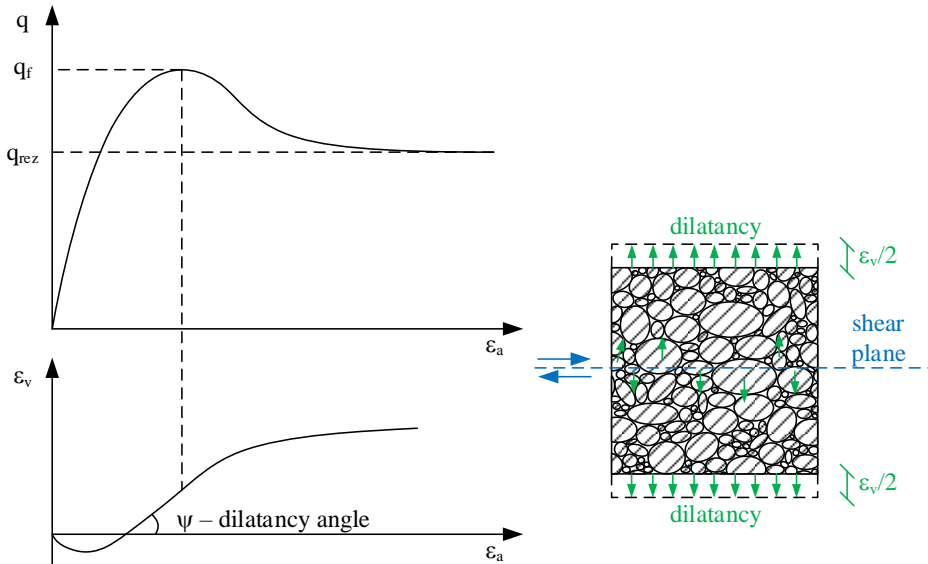
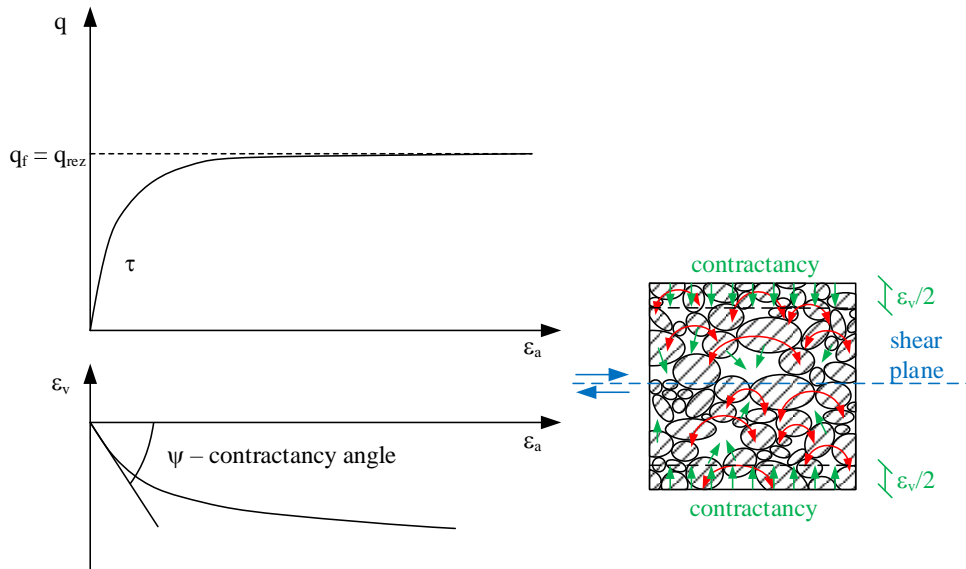


Fig. 10.4: Stresses, strains and displacements necessary to determine the dilatancy/contraction parameters for the triaxial shear test



a. Dense sands and overconsolidated cohesive soils



b. Loose sands and normally consolidated cohesive soils

Fig. 10.5: Shear stress variation against axial strain

Taking into account that following the failure, the solid particles will rotate and turn so that, indifferent whether the initial state was dense (overconsolidated) or loose (normal consolidated), the residual value of the deviator stress becomes the same.

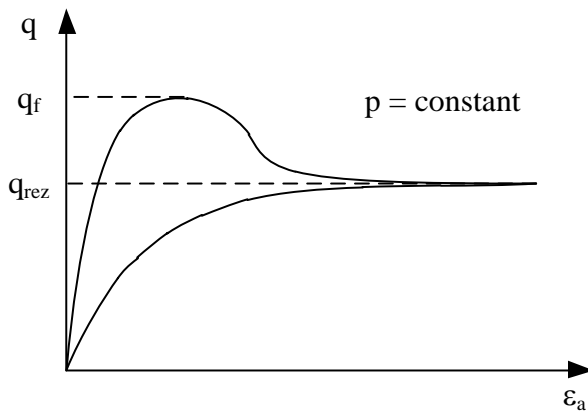


Fig. 10.6: The convergence of the mobilization curves for an overconsolidated soil and normally consolidated soil for the same value of the deviatoric stress to the same value of the deviator for large mobilizations, considering a constant spherical stress

If one takes into account that the residual behaviour is always characterized by an almost null cohesion and a very small value of the internal friction angle (e.g. a soft or very soft clay, normal consolidated, which cannot maintain its form under its own weight or be excavated vertically), one can point out that the cohesion source of the soils may be obtained either under the form of overconsolidation, either it is given by the cementation effects (Fig. 10.7). This is valid especially in the case of pre-consolidation stresses larger than the consolidation stress from which the shearing path starts, in order to determine the resistance parameters. Contrarily, the situation depicted in Fig. 10.8 may be obtained, where the loading history may influence the results of the deviatoric peak values, the samples having different overconsolidation ratios behaving as different materials.

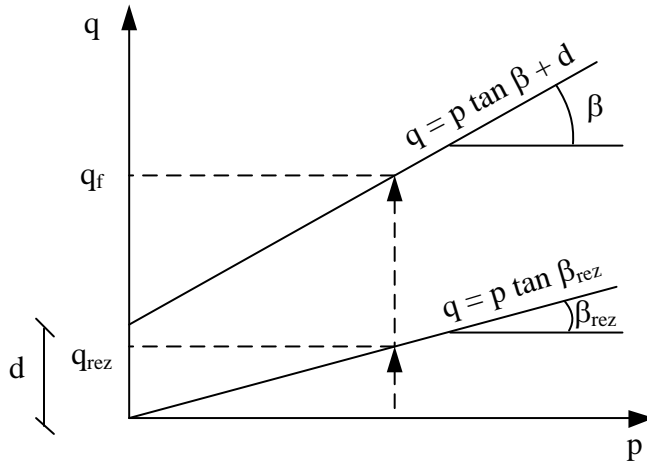


Fig. 10.7: Peak failure criterion vs. residual failure criterion

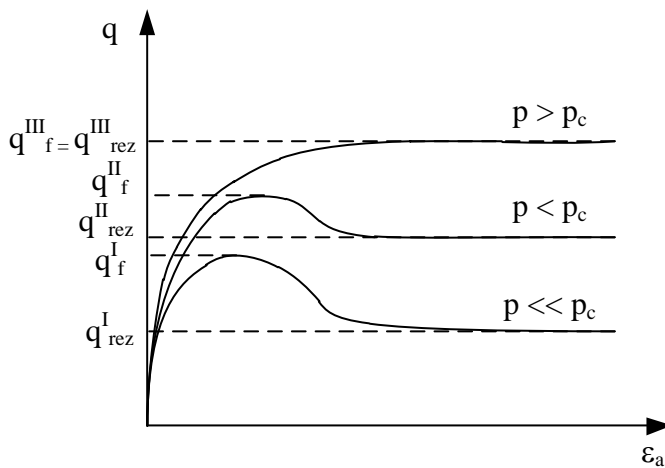


Fig. 10.8: Peak and residual values obtained for different overconsolidation ratios

An important consequence of the existence of the peak and residual parameters is represented by the fact that in the case of certain phenomenon (e.g. landslides). In this case, the peak resistance value has been overpassed and the solid particles in the area of the failure plane have rotated, making it a prone area to fail again, the resistance parameters not recovering to the peak values. The same phenomenon appears at some of the heavily overconsolidated clays (glomerular clays), where prone to fail surfaces are

spread across the soil mass. This proves the positive influence of the overconsolidation ratio on the shear resistance, which acts up to a certain value of OCR, at which the tension resistance due to unloading is reached.

### **10.1.3 Shear stress paths in $s - t$ total coordinates**

#### **Example 1 – the triaxial compression test along the isotropic consolidation path, followed by a shearing stage obtained by increasing the deviatoric stress**

During the consolidation stage, the sample is isotropically loaded by increasing the cell pressure, without activating the axial ram. The description of this example has been started during the 8.6 chapter.

As it has been shown, during the consolidation stage the normal stresses to which the sample is subjected is equal on all directions, therefore:

$$\begin{aligned} s &= \frac{\sigma_1 + \sigma_3}{2} = \sigma_3 \\ t &= \frac{\sigma_1 - \sigma_3}{2} = 0 \end{aligned} \tag{10.3}$$

During the next stage, the cell pressure is to be kept constant ( $\sigma_3 = \text{constant}$ ), and by using the ram, a compression deviatoric stress is applied, equal to the difference between the desired  $s_1$  value and the existing  $s_3$  (see (10.4) equation, where by using arrows, the overall tendencies of  $s$  and  $t$  are denoted). The evolution of the stress state depicted as Mohr circles is presented in Fig. 10.9.

$$\begin{aligned} s &= \frac{\sigma_1 + \sigma_3^{\text{consolidation}}}{2} \uparrow \\ t &= \frac{\sigma_1 - \sigma_3^{\text{consolidation}}}{2} \uparrow \end{aligned} \tag{10.4}$$

It is to be observed that, due to maintaining the constant value of  $\sigma_3$ , both  $s$  and  $t$  are rising with the same increment value -  $\frac{\sigma_1}{2}$  (Fig. 10.10). The stress



state will progress on an ascendant path, having a slope of 1L1 ( $45^\circ$ ). In a similar manner, in the  $p - q$  coordinate system, the same path will have a 1:3 slope (Fig. 10.11). The failure criterion in the  $s - t$  coordinate system is called „the  $k_f$  line”, while in  $p - q$  coordinate system is referred to as „the critical state line”. The latter coordinate system has been initially enunciated for the soft clays by Roscoe, being followed by a development for the overconsolidated soils by Hvorslev. Although the later has normalized the failure criterion with the pre-consolidation stress, the unmodified form is still called critical state line.

The shear resistance parameters in  $\sigma - \tau$  coordinate system,  $\phi$  and  $c$  are unequivocal associated to the intrinsic line. The  $\beta$  and  $d$  parameters are still generally used as internal friction angle and cohesion, in almost every coordinate system, other than  $\sigma - \tau$ . One such failure criterion is Drucker-Prager for example.

Although for the engineering practice the shear resistance parameters are considered as being material constants, although the testing procedure and the conditions of the test have a significant influence on the obtained results. Another aspect, which does not represent the subject of this book is the influence of the saturation degree of the samples, the assumption of the partially saturated soil introducing important negative pressures (suction) inside the soil mass.

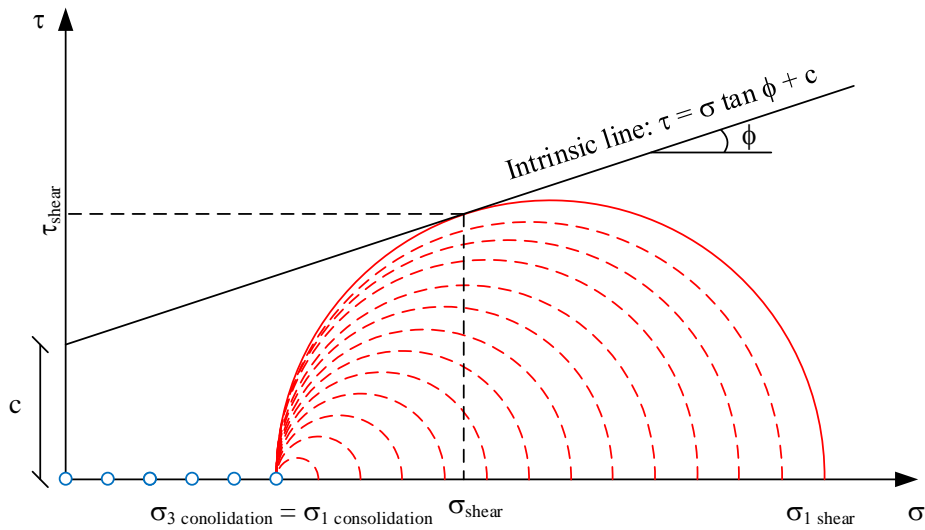


Fig. 10.9: Intrinsic line for an isotropic consolidated sample - sheared by axial loading

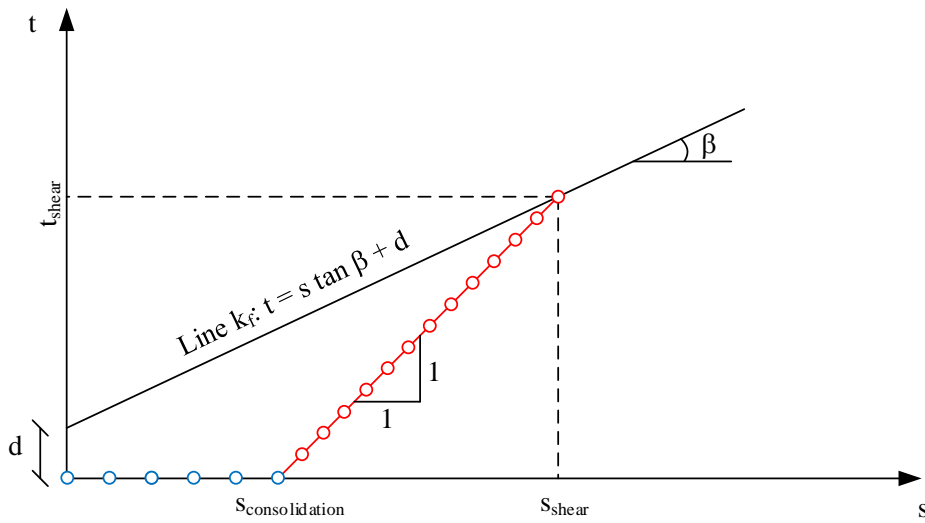


Fig. 10.10: The  $k_f$  line for an isotropic consolidated sample - sheared by axial loading

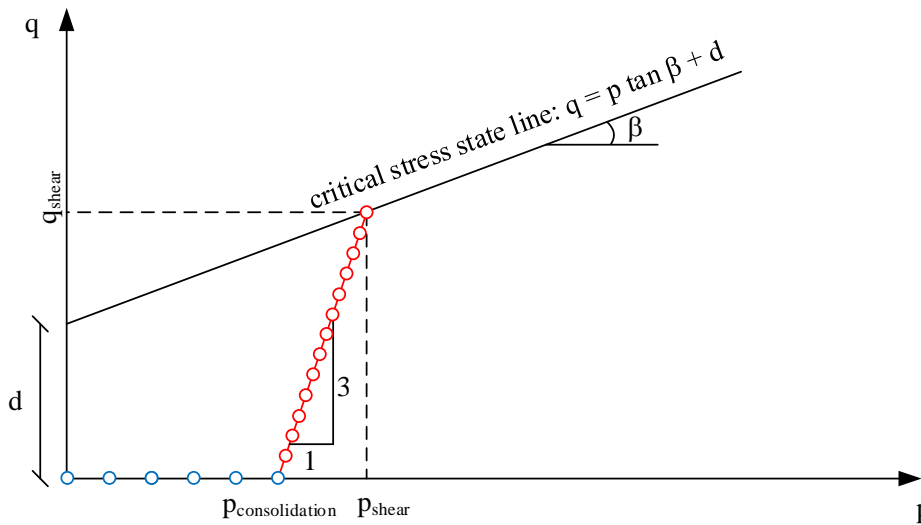


Fig. 10.11: Critical stress state line for an isotropic consolidated sample - sheared by axial loading

The  $\beta$  and  $d$  shear resistance parameters in the  $s - t$  coordinate system are derived from the ones of the intrinsic line, starting from the study of a failure stress state using the  $\sigma - \tau$  coordinate system.

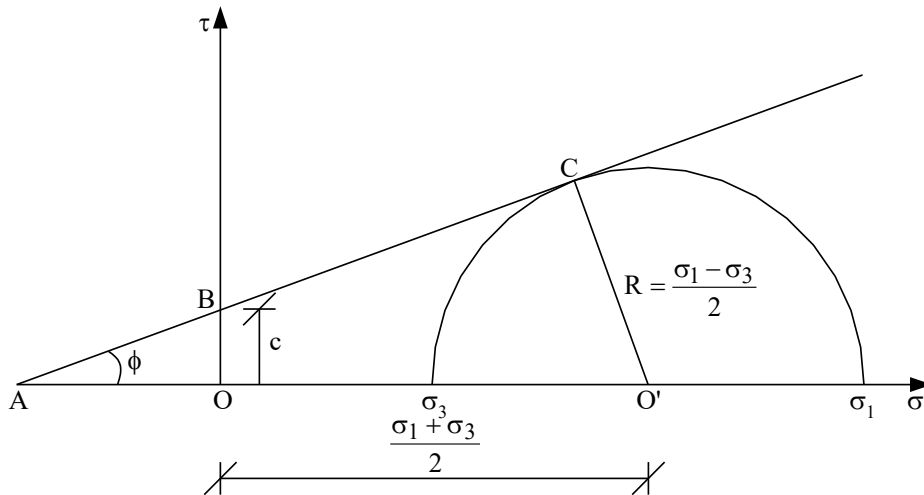


Fig. 10.12: Stress state tangent to the intrinsic line

From Fig. 10.12, it can be noticed that  $\Delta ABO \sim \Delta AO'C$ , thus:

$$\frac{AB}{AO'} = \frac{BO}{O'C} \quad (10.5)$$

meaning:

$$\frac{\frac{c}{\sin \phi}}{\frac{c}{\operatorname{tg} \phi} + \frac{\sigma_1 + \sigma_3}{2}} = \frac{c}{\frac{\sigma_1 - \sigma_3}{2}} \quad (10.6)$$

From which:

$$t = s \sin \phi + c \cos \phi \quad (10.7)$$

But:

$$t = s \operatorname{tg} \beta + d \quad (10.8)$$

From the equality of (10.8) and (10.9) it may be demonstrated that:

$$\begin{aligned} \operatorname{tg} \beta &= \sin \phi \\ d &= c \cos \phi \end{aligned} \quad (10.9)$$

### **Example 2 – the evolution of soil's lateral thrust starting from the stress state at rest**

During the first stage of the loading history, the stress state evolution starting from the sedimentation moment must be analysed. Basically, this can be considered as the starting moment, the stresses on all directions being null. Once with the sedimentation of other solid particles on top of the reference point, the loading begins, following the conditions described in the 8.5 chapter. The ratio between the vertical stress  $\sigma_1$  and radial  $\sigma_3$  is described using the (8.45) equation, where the distribution coefficient  $k_0$  is defined by the (8.46) relationship.

The stress state consolidation path in  $s - t$  coordinates will be:

$$\tan \alpha_{k_0} = \frac{t_{k_0}}{s_{k_0}} \quad (10.10)$$

Where  $t_{k_0}$  and  $s_{k_0}$  are depicted in Fig. 10.14. By replacing the (8.45) equation in the (10.10) relationship, one can obtain:

$$\begin{aligned} \tan \alpha_{k_0} &= \frac{\sigma_1^{\text{consk}_0} - \sigma_3^{\text{consk}_0}}{2} \frac{2}{\sigma_1^{\text{consk}_0} + \sigma_3^{\text{consk}_0}} = \frac{\sigma_1^{\text{consk}_0} - k_0 \sigma_1^{\text{consk}_0}}{\sigma_1^{\text{consk}_0} + k_0 \sigma_1^{\text{consk}_0}} = \\ &= \frac{1 - k_0}{1 + k_0} \end{aligned} \quad (10.11)$$

On reaching the end of the anisotropic  $k_0$  consolidation path, the test continues along a new path in order to shear the sample for the condition of the active Rankine thrust, which is translated in keeping constant the axial stress obtained at the of the consolidation stage,  $\sigma_1^{\text{consk}_0}$  and lowering the radial  $s_3$ , due to the equivalent lateral displacement of the retaining structure up to reaching the failure state. In these conditions, the spherical stress decreases with the same  $\frac{\sigma_3}{2}$  value, with which the deviatoric stress  $t$  is increasing, thus having an unloading  $45^\circ$  degrees sloped stress path.

$$\begin{aligned} s &= \frac{\sigma_1^{\text{consk}_0} + \sigma_3}{2} \downarrow \\ t &= \frac{\sigma_1^{\text{consk}_0} - \sigma_3}{2} \uparrow \end{aligned} \quad (10.12)$$

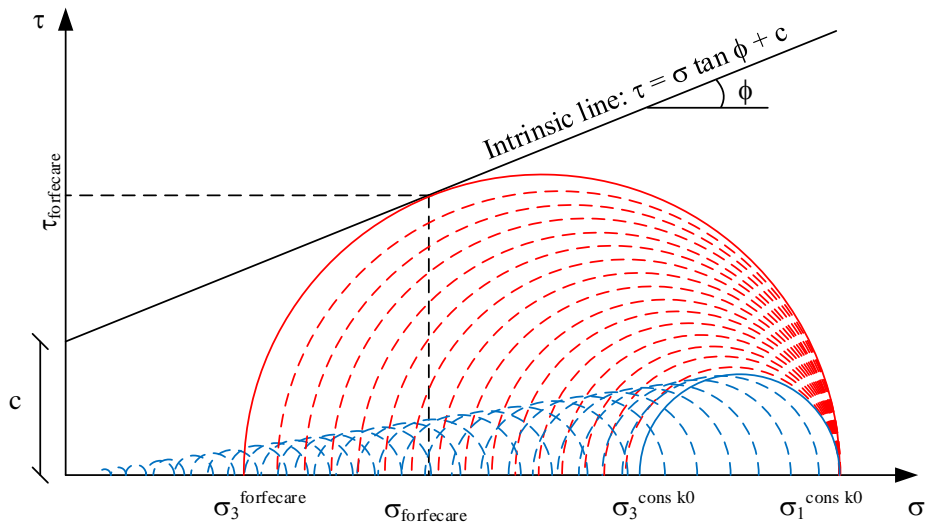


Fig. 10.13: The intrinsic line of a sample anisotropically  $k_0$  consolidated and sheared along an unloading stress path, appropriate to the active thrust case

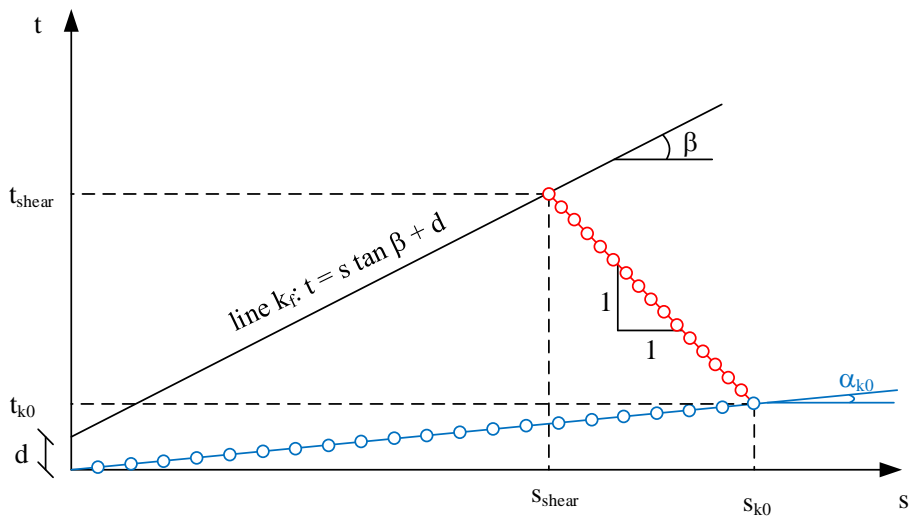


Fig. 10.14: The  $k_f$  line of a sample anisotropically  $k_0$  consolidated and sheared along an unloading stress path, appropriate to the active thrust case

An important observation is that in the case of cohesive soils with low value stress states, the failure may not be reached because of the compression zone

limit (Fig. 10.15). The active thrust does not lead to failure in tension, and the vertical slope is stable (Taylor condition  $h < h_{cr} = \frac{4c}{\gamma}$ ).

Another observation is that the final values of the shear parameters do not depend on the method used to determinate them if the drainage conditions were met (for example, a shear test done in drained conditions shall reach the same failure criteria as a shear test done in undrained conditions for which the effective parameters are computed by subtracting the pore water pressure from the total stresses), but depend of the degree of overconsolidation from which the shear test is started. It may be concluded that in some situations the obtained shear resistance parameters are closer to the real behaviour of the material if the test is done starting from the same consolidation stress and performing the shear on different stress paths in order to obtain different points on the  $k_f$  line.

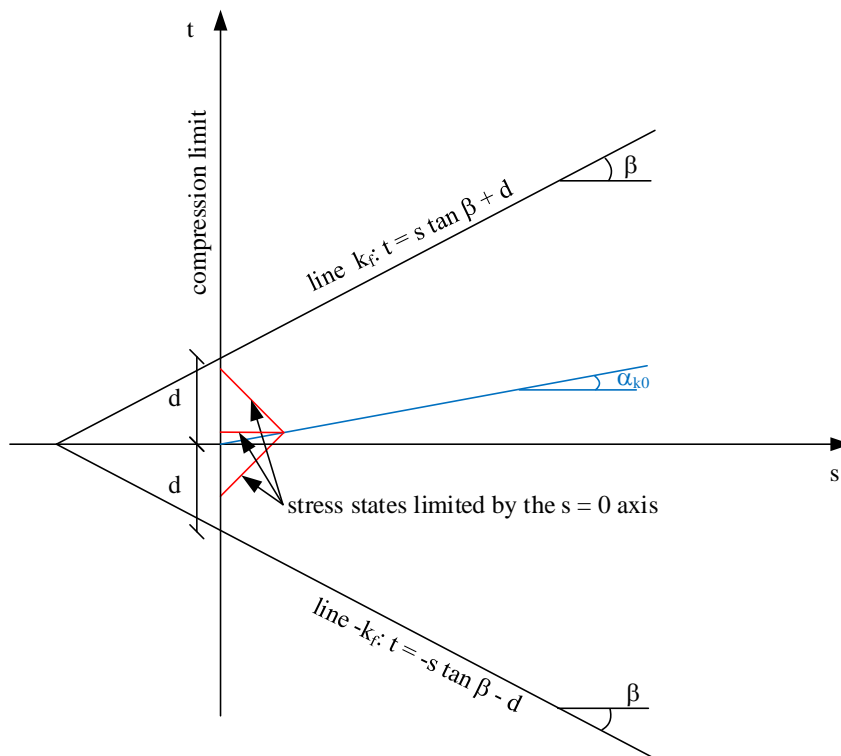


Fig. 10.15: Stress paths that do not lead to failure due to the compression limit

Obviously, the shear stress paths presented in example 1 may be obtained starting from the anisotropic consolidation  $k_0$  (Fig. 10.16). The 45° loading path (example 1), the vertical one (example 4) and the 45° unloading path (example 2) are the most commonly used stress paths combinations, when the shear strength parameters are obtained from the same consolidation value and different stress paths (Fig. 10.17).

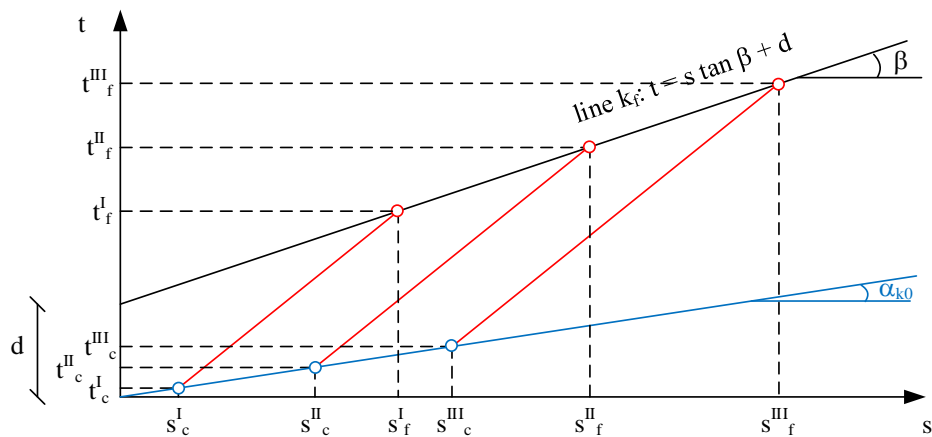


Fig. 10.16: Obtaining the shear resistance parameters from three values of the consolidation stress and one type of stress path

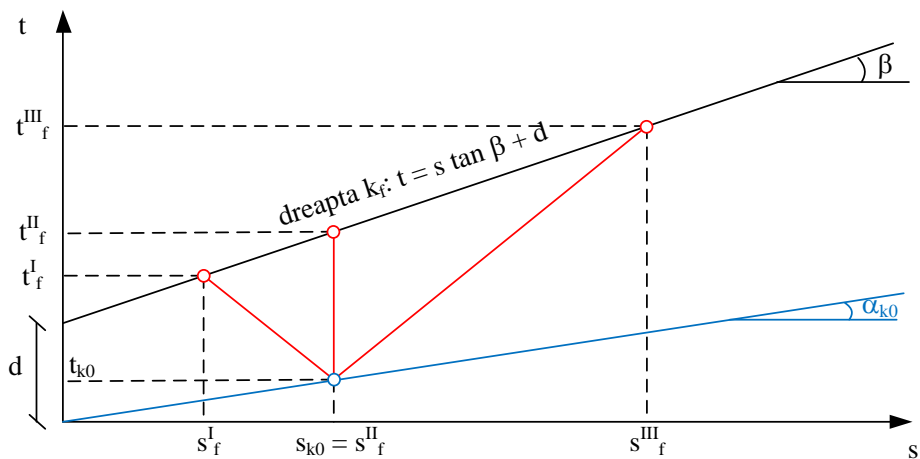


Fig. 10.17: Obtaining the shear strength parameters using one value of the consolidation stress and three types of stress paths



**Example 3 - the stress state progress in the case of the passive resistance mobilization starting from the state of rest**

This example is similar to the previous one as far as the consolidation phase is concerned, reaching a consolidation stress state that corresponds to the state of rest.

Regarding the shear phase, the equivalent displacement of a retaining structure, using Rankine hypothesis, will induce a rise in the values of the stress on radial direction (principal direction 3) and maintain the unitary stresses on axial direction ( $\sigma_1 = \text{constant}$ ). The rise in the value of  $\sigma_3$  will cause a decrease of the deviatoric stress  $t$  value and to an increase of the spherical stress value  $s$ , so that the failure occurs when the  $-k_f$  line is reached, after which the deviatoric stress passes through zero.

$$\begin{aligned}
 s &= \frac{\sigma_1^{\text{cons}k_0} + \sigma_3}{2} \uparrow \\
 t &= \frac{\sigma_1^{\text{cons}k_0} - \sigma_3}{2} \downarrow
 \end{aligned}
 \tag{10.13}$$

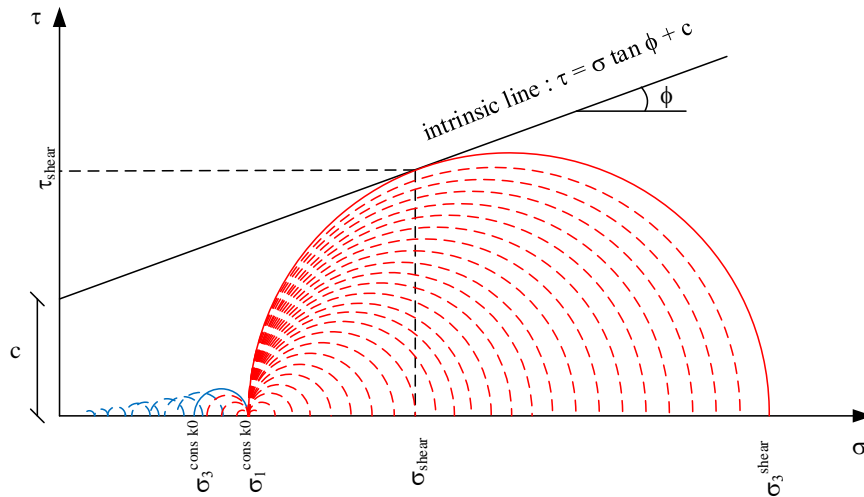


Fig. 10.18: Intrinsic line for a  $k_0$  anisotropically consolidated sample that is sheared on an unloading stress path, specific for the passive resistance

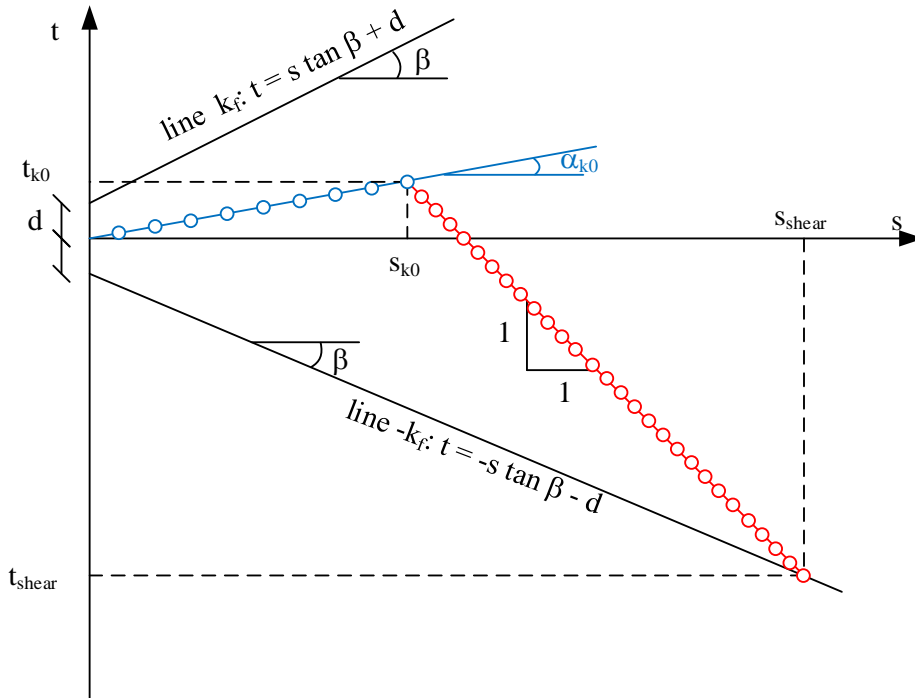


Fig. 10.19:  $K_f$  line for a  $k_0$  anisotropically consolidated sample, sheared on an unloading stress path, which is specific for the passive resistance

#### Example 4 - vertical stress path

This type of stress path does not necessarily simulate a real situation, being close to the situation in which the soil excavated from an enclosure is deposited on the edge of the hole, so that the increase in axial stress is equal with the decrease in the radial stress. In this situation, the spherical stress  $s$  is maintained constant while the deviatoric stress  $t$  increase.

$$s = \frac{\sigma_1^{\text{consk0}} + \sigma_3^{\text{consk0}}}{2} \text{ constant} \tag{10.14}$$

$$t = \frac{\sigma_1^{\text{consk0}} - \sigma_3^{\text{consk0}}}{2} \downarrow$$

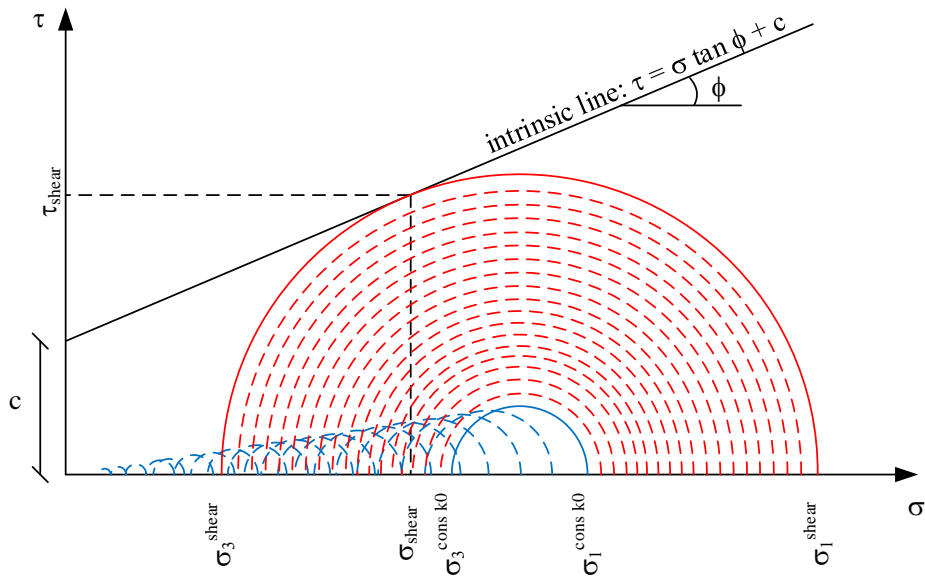


Fig. 10.20: Intrinsic line for a  $k_0$  anisotropically consolidated sample, sheared on a vertical stress path

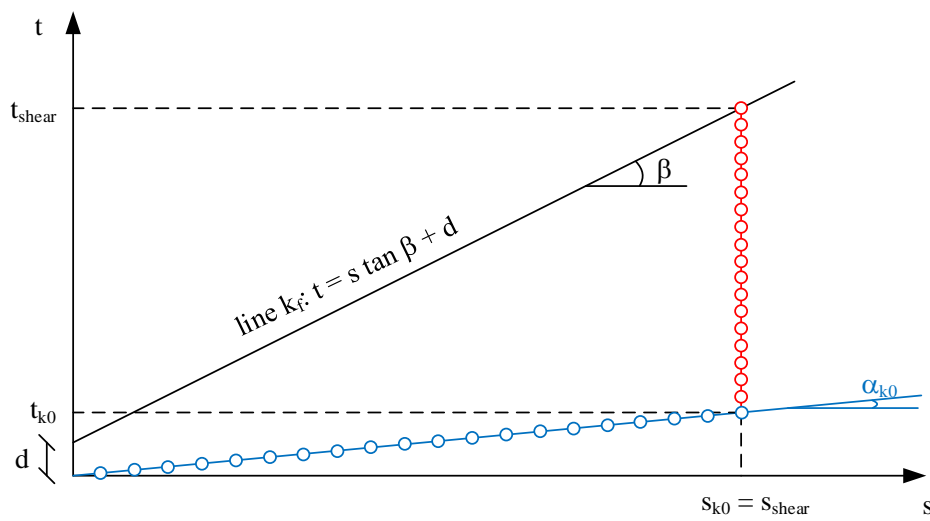


Fig. 10.21:  $K_f$  line for a  $k_0$  anisotropically consolidated sample, sheared on a vertical stress path

### 10.1.4 Stress paths in total vs effective coordinates

As it was mentioned earlier in this chapter, the test method used to obtain the shear resistance parameters may be reflected in the obtained values. For example (Fig. 10.22), in the case of a CU triaxial compression test, if one can record the pore water pressure variation, then the shear resistance parameters may be computed for both total and effective stresses. For this type of test, from the measured values (the total stress path - continuous red line) the value that corresponds to the pore water pressure was subtracted. In this manner the path expressed in effective stresses was plotted (represented with red dashed line).

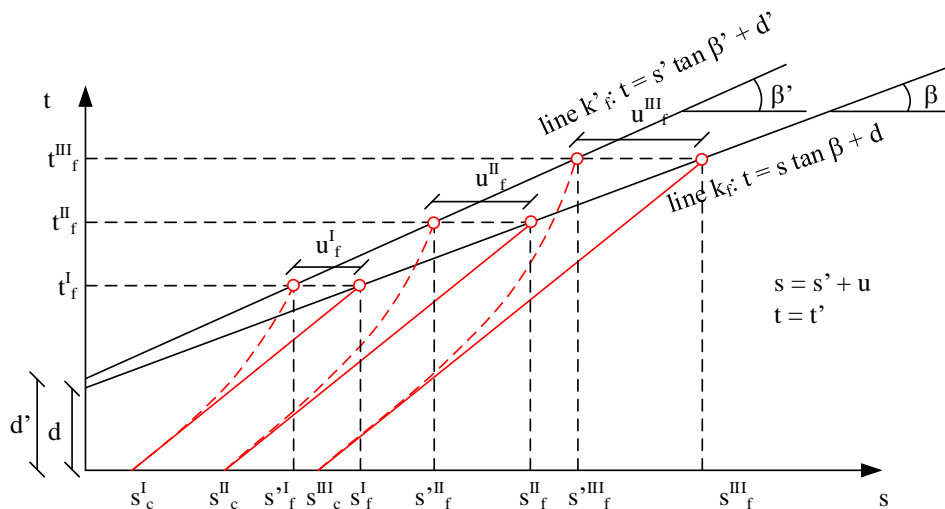


Fig. 10.22: Total and effective stress representation for the results of a CU type triaxial test

One may observe that the shear strength parameters for the total stresses hypothesis lead to smaller values for  $\beta$  (and by default for  $\phi$ ) than for the effective stresses hypothesis.

### 10.1.5 Mohr-Coulomb failure criterion in principal stresses

In the paragraph 8.6 it was shown the  $\sigma_1 - \sigma_2 - \sigma_3$  coordinate representation for a given stress state. In order to express the existence of a stress state limited by the Mohr-Coulomb failure criterion, we will study the geometric locus described by this at the intersection with the plane for which  $\sigma_2 = 0$ .

By writing the  $k_f$  and  $-k_f$  lines (Fig. 10.15) we obtain:

$$\begin{aligned}t &= s \tan \beta + d \quad k_f \text{ line} \\t &= -s \tan \beta - d - k_f \text{ line}\end{aligned}\tag{10.15}$$

or, applying the relations from (10.9):

$$\begin{aligned}t &= s \sin \phi + c \cos \phi \\t &= -s \sin \phi - c \cos \phi\end{aligned}\tag{10.16}$$

Knowing (8.49), we obtain:

$$\begin{aligned}\frac{\sigma_1 - \sigma_3}{2} &= \frac{\sigma_1 + \sigma_3}{2} \sin \phi + c \cos \phi \\ \frac{\sigma_1 - \sigma_3}{2} &= -\frac{\sigma_1 + \sigma_3}{2} \sin \phi - c \cos \phi\end{aligned}\tag{10.17}$$

Considering  $\sigma_1$  as a function of  $\sigma_3$ , the Mohr-Coulomb failure criterion in  $\sigma_2 = 0$  becomes:

$$\begin{aligned}\sigma_1 &= \sigma_3 \frac{1 + \sin \phi}{1 - \sin \phi} + 2c \frac{\cos \phi}{1 - \sin \phi} \\ \sigma_1 &= \sigma_3 \frac{1 - \sin \phi}{1 + \sin \phi} - 2c \frac{\cos \phi}{1 + \sin \phi}\end{aligned}\tag{10.18}$$

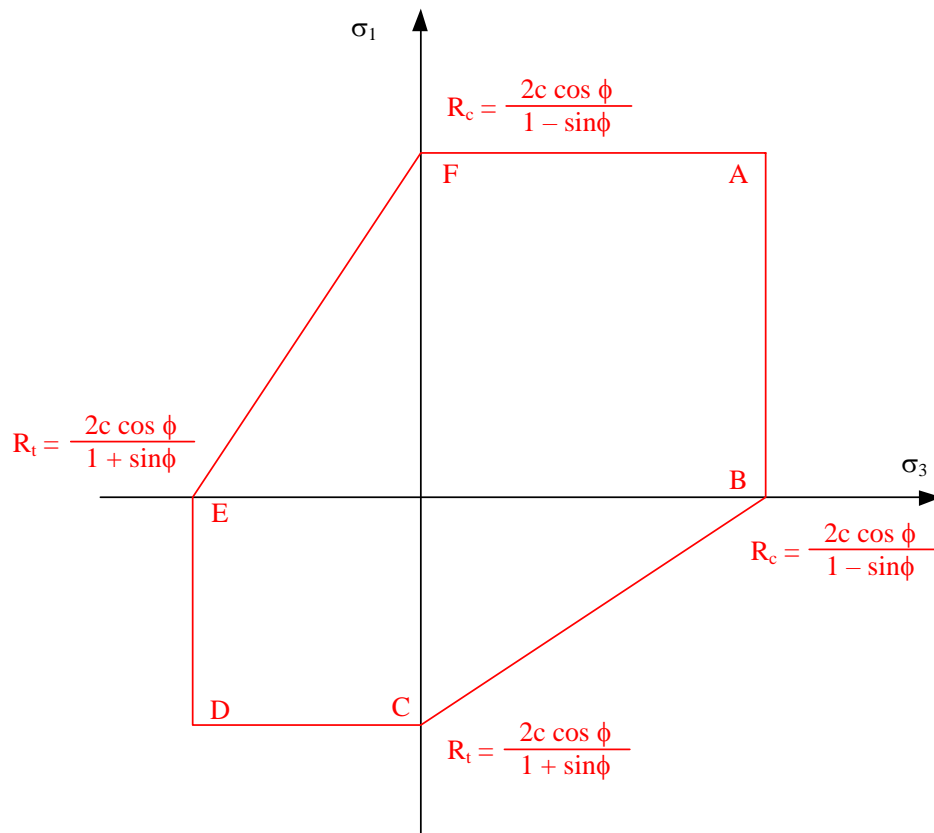


Fig. 10.23: Mohr-Coulomb representation in  $\sigma_2 = 0$  plane

The equations from (10.18) are the relations for failure in shear from the II<sup>nd</sup> and IV<sup>th</sup> quadrants, presented in Fig. 10.23, or to be more exact, the BC and EF line equations. If one considers that  $\sigma_2 = 0$ , in order to develop a deviatoric stress that will lead to failure in shear,  $\sigma_1$  and  $\sigma_3$  must have opposing signs. In the case that one of the two planar principal stresses is null, the failure will be in compression (I<sup>st</sup> quadrant) or in tension (III<sup>rd</sup> quadrant) under the stress that is zero, which means that the value of the failure stress is the following:

$$\begin{aligned}
 R_c &= 2c \frac{\cos \phi}{1 - \sin \phi} && \text{resistance in compression} \\
 R_t &= 2c \frac{\cos \phi}{1 + \sin \phi} && \text{resistance in tension}
 \end{aligned}
 \tag{10.19}$$

In the  $\sigma_1 - \sigma_2 - \sigma_3$  space, a stress state will not lead to failure if this is found inside the surface.

An important remark that can be deduced from (10.19) is that for pure cohesive materials the resistance in compression is equal to the resistance in tension, which is far away from truth in the case of soils, thus the purely cohesive material model must be used with caution.

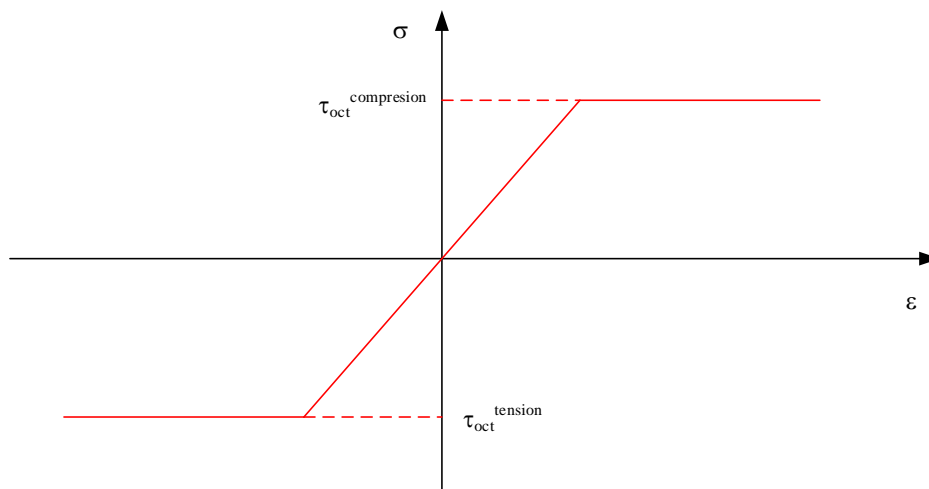


Fig. 10.24: Elastic-perfect plastic strain model with equal tension and compression resistances

## 10.2 Tests for assessing the shearing strength parameters

As it has been previously presented, soil's shearing resistance parameters may be determined by considering one of these two types of laboratory tests:

- Direct shear test – a common and very simple test, that controls the position of the failure surface and the normal stress acting on it, while assessing the maximum tangential stress at failure;
- Triaxial compression test – an advanced and more complex test, which is based on obtaining different stress states, in total and/or effective stresses, useful to model the stress evolution of a point in the soil mass.

In order to find the shearing strength parameters, it is necessary to have a set of known spherical-deviatoric stress pairs, used to generate an interpolated failure curve by regression. The number of tests, translated in known points in the spherical-deviatoric graph has to fulfil the mathematical condition for being able to equate the regression line. Thus, if only one point is known, an infinity of lines pass through it (Fig. 10.25 a.), so we have indeterminacy. If two points are known, there is a unique line defined by them, however, if one test was mistaken, there is no way of revealing it (Fig. 10.25 b.). This is why it is necessary to have at least three known points, since co-linearity shows the reliability of tests (Fig. 10.25 c'.). However, if the three points are not co-linear, it is not possible to identify the faulty one (Fig. 10.25 c''). In this case, it is compulsory to perform an extra test, or as many as necessary, to choose a set of test values that properly align.

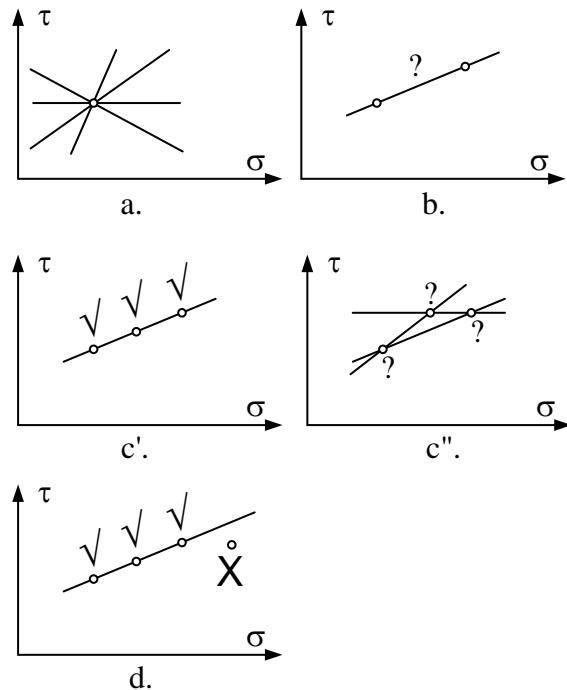


Fig. 10.25: The necessary number of tests for the direct shearing test

If the shearing strength parameters have to be computed from the common tangent to the states of stress leading to failure, expressed by Mohr's circle, the requirements are similar to the case where the line is drawn through points. In the case of a single sample (Fig. 10.26 a.), an infinite number of o



lines may be drawn tangent to the circle. If two samples are used, it is always possible to draw an unique common tangent to the two Mohr's circles (Fig. 10.26 b.), of course, as an exterior common tangent, on the positive side of the tangential stresses, so, in the case when one of the tests is bad, there is no possible verification. If three samples are used, and it is possible to build a common tangent then the results are confirmed and may be used as such (Fig. 10.26 c'.). However, if one test provided unreliable information, it is impossible to identify which one (Fig. 10.26 c''), in this case being necessary to perform four or more tests to have systematic values.

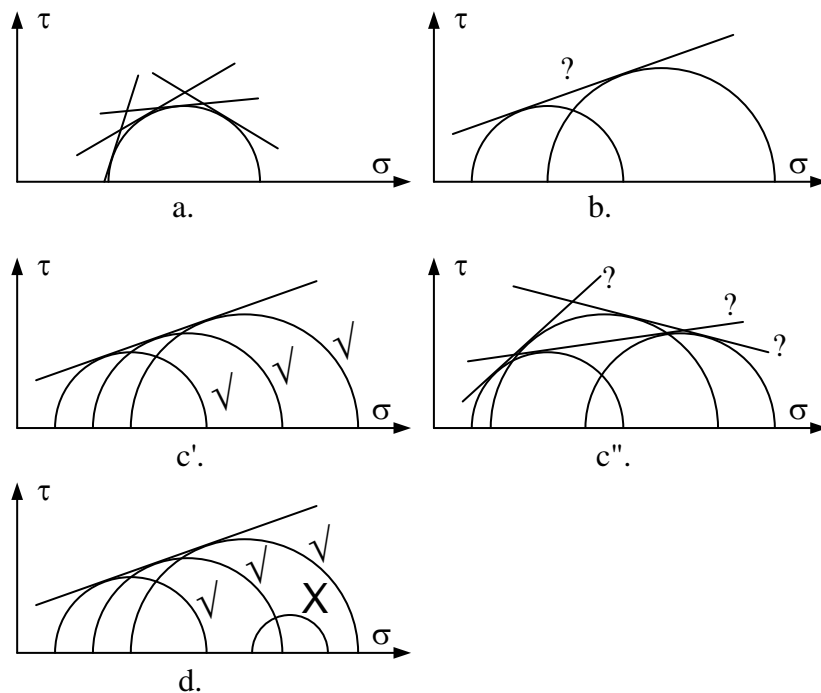


Fig. 10.26: The necessary number of tests for the triaxial test

Usually, since the cost of shearing tests is higher than the other geotechnical investigations and the fact that it is necessary a larger mass of undisturbed soil, in common engineering practice only three samples are tested, a fourth being employed only in the case of inconsistency.

The test procedure has to be chosen depending on the site destination and conditions. The first procedure in any type of shearing test, except for very rare cases (such as the dry loess where the soluble cementation bonds influence is studied), is saturation. This procedure is approached differently

in the two types of tests. In the case of the direct shearing test, the only way to saturate the sample is to submerge it in the floodable cassette.

In the Fig. 10.28, the detail 16 shows that the sample is provided on the top and bottom with porous stone so the water infiltrates into the soil. The disadvantage of this method is that there is no possibility of applying a saturation pressure, so that the soils of low permeability (such as clays) draw water only by matrix suction. Another disadvantage is the fact that the saturation of the sample occurs simultaneously from the outside towards the inside, being possible to disaggregate a cohesive sample with moisture content less than  $w_s$ . (see chapter 6.2). Moreover, the sample becomes softer towards the ends with respect to the median plane, where the imposed shearing surface produces.

The saturation of the triaxial test sample is carried out in a controlled manner. The water is injected in the base using the back pressure (BP) line (Fig. 10.31, item 16) while left to flush through the soil and be exhausted through the “u” top (UT) line (Fig. 10.31, item 18). In order to avoid the infiltration of water through the space between the rubber membrane and the sample, bypassing the latter, it is necessary to impose a pressure in the triaxial cell through the cell pressure line CP (Fig. 10.31, item 19) larger than the value imposed on BP. It may be noticed that this procedure for saturation is technically the same as the constant head permeameter test (see chapter 7.3.1), so that this stage of the triaxial test may be used for finding the permeability, especially since the equipment allows the use of very large hydraulic gradients.

Another advantage of the saturation procedure is the possibility of checking the degree of saturation. The method, proposed by Skempton [24] is based on the fact that both the soil grains and the pore water in the sample are virtually incompressible under the effect of hydrostatic stress, so that, for a perfectly saturated sample, any increase in the cell pressure stress,  $\Delta\sigma_3$ , has to be recorded as an increase of the pore water pressure  $\Delta u$  in an equal amount. If the sample is just partially saturated, the air being compressible, the increase in the pore pressure has to be less than that. So, the pore pressure coefficient  $B$ , is defined as:

$$B = \frac{\Delta u}{\Delta\sigma_3} \quad (10.20)$$

Theoretically, in the case of saturation, the value of  $B$  has to be 1, while for partially saturated samples,  $B$  has to be less than 1, accordingly. In reality, due to the head loss along the drain line, the permeability of the soil that delays substantially the dissipation of the pore water pressure in the sample and the deformability of the soil that may prevent the transfer of the cell pressure load, through the membrane, to the pore liquid, it may be considered that the soil is saturated for values of  $B$ . For instance, in low compressible sandstone, saturation may be considered achieved for  $B$  values as low as 0.58 [25]. For some porous and deformable soils, such as silts, the value of 0.98 may be attained, while low permeability soils, such as over-consolidated fat clays, may be regarded as saturated for  $B \sim 0.7$ .

After saturation, the test stages have to be chosen in accordance with the future evolution of stresses that are going to load the area the sample was taken.

One example is the case of the soils from the lake shores when the water level is suddenly dropped. Initially, the only loading the soil in the river bank is subjected to, is its own weight, given by the unit weight of the soil in submerged state,  $\gamma'$ . When the water level in the lake is suddenly dropped, there is no time for the water to drain, ensuring the consolidation of the ground, so the process is unconsolidated (U), followed by the fast development of the shearing stresses, namely to an undrained (U) shearing. To replicate this process in the shearing equipment (direct shearing or triaxial), the sample is loaded with the initial stress state, followed immediately by shearing, so the test progresses UU (unconsolidated-undrained).

The future loading may be applied slowly to a certain degree after which a sudden increase of loads may lead to failure of the soil. An example is the construction of a precast structure on a built in-place foundation system. The soil under the foundation is allowed time to consolidate (C) under the own weight of the supporting structure, after which, a large load is applied from the fast-installed superstructure, subjecting the respective ground area to an undrained (U) shearing. Accordingly, the test has to be CU (consolidated-undrained).

However, there is also the possibility for the soil to be loaded very slowly by the future structure allowing time to dissipate the pore water pressure both in

an initial stage of consolidation (C) and allowing drainage (D) during the application of the shearing stresses. A good example is the building of an embankment, where the foundation soil is loaded slowly, compacted layer by compacted layer. To simulate this type of behaviour, the test has to be carried-out CD (consolidated-drained).

Recapitulating, after the saturation, which is not mentioned in the test type name since it is done almost every time, the soil sample is subjected to an initial state of stress in order to induce the differentiated failure required to obtain at least three points out of which to regress the Mohr-Coulomb line. After applying this initial stress, the soil may be allowed to consolidate (C) or it is left unconsolidated (U), passing directly to the next step. Depending on the way the failure occurs, the following up shearing process may be undrained (U) or drained (D). Combining the relevant two stages, the test may be UU, CU or CD. It is obvious that there cannot be a UD test, because the drainage should occur uncontrollable during the shearing stage, after not being permitted during the consolidation one.

### 10.2.1 Direct shearing test

The easiest way to obtain the shear resistance parameters in the lab is by means of direct shearing test. The principle that lays the basis of this test is that a confined soil sample subjected to constant vertical stress is displaced horizontally on an imposed plane at half of the sample height.

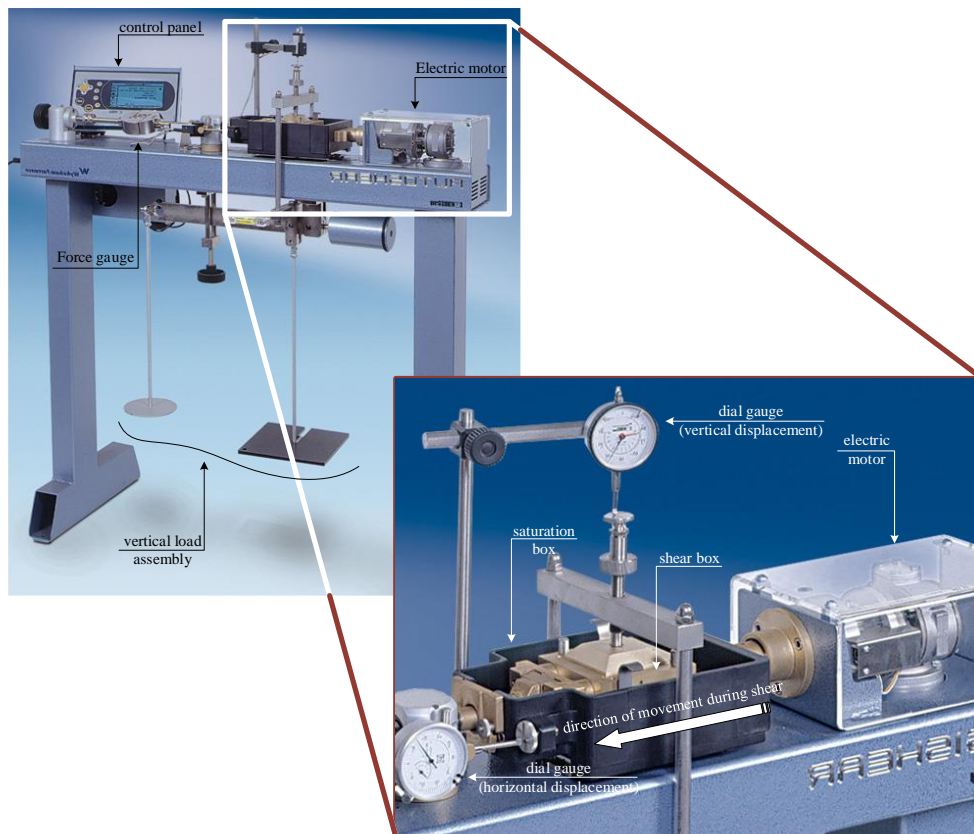


Fig. 10.27: Direct shear device major components [26] [27]

The direct shearing apparatus has the following components (see Fig. 10.27 and Fig. 10.28):

1. Supporting frame
2. Body – it represents the real support upon which all the parts are resting;
3. Lever – it allows the user to change the loadings under which the soil sample is loaded;

4. Counter weight – this part allows the user to balance the lever (without any weights applied to it), so that the vertical loading applied to the soil sample is obtained by adding weights to it;
5. Loading weight – the various combinations of these weights allow the user to subject the sample to the desired loading; their position may vary along the lever, as function of the soil sample's diameter and required loading to be obtained;
6. Ram – this part will transfer the force from the loaded lever to the soil sample, by resting upon the loading plate;
7. Saturation box – this part has a double role: it allows the lower part of the shearing box to move, while permits the user to flood the sample;
8. Vertical displacement dial gauge – it measures the vertical displacement of the sample during both the shearing process, and the optional consolidation stage;
9. Horizontal displacement dial gauge – it measures the horizontal displacement of the sample during the shearing process;
10. Dynamometer ring – this part represents a metal ring whose rigidity is well known, so that its deformation implies a known force; this force is the sample's resistance to shearing;
11. Dynamometer dial gauge – it measures the dynamometer ring's deflection, in order to determine the shearing resistance force;
12. Motor – this part drives the saturation box during the shearing process;
13. Upper shearing box – this part opposes the shearing process, maintaining the top half of the sample immobile;
14. Lower shearing box – this part pushes the lower half of the sample, in order to induce shear;
15. Fixing bar – allows the user to change the 6.00x6.00cm shearing box, which is appropriate for the fine soils, with the 10.00x10.00cm box, in which sands may be sheared;
16. Porous stone – this part has a double role: the first is to allow the water to drain out of the sample during the shearing or consolidation stages; the second role is to ensure the necessary grip to ensure that the two soil halves will slide one from the other;
17. Loading plate – situated on top of the porous stone, it allows the transformation of the punctual force transferred by the ram, into an equally distributed pressure;
18. Soil sample – it is a rectangular sample, having the sides equal to 6.00 or 10.00cm and a thickness of 2cm.

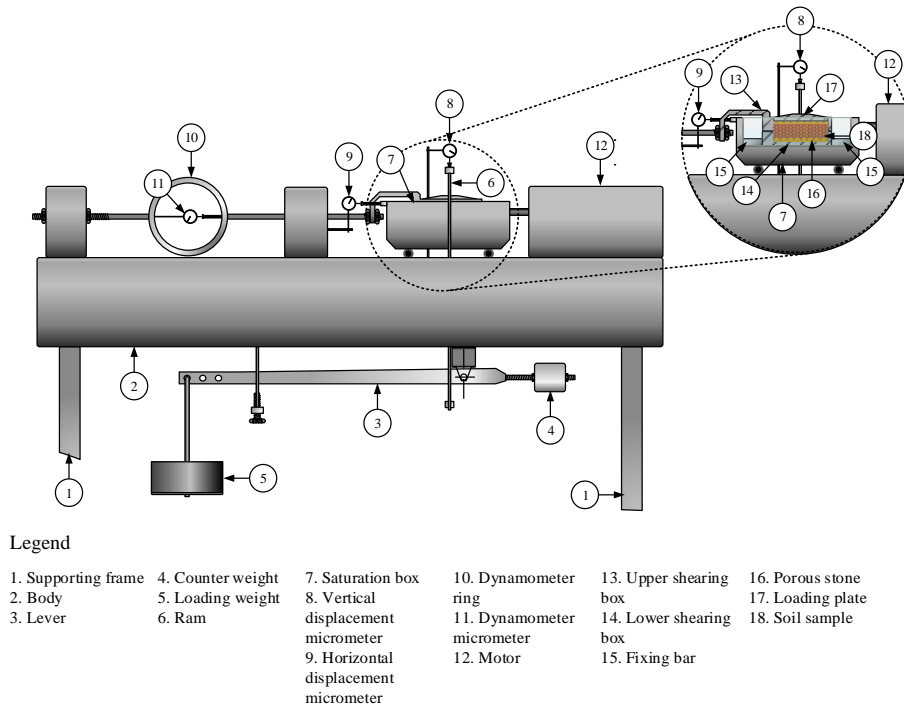


Fig. 10.28: The direct shearing apparatus conceptual components

The direct shear test may be one of the three aforementioned cases: UU (unconsolidated undrained, which translates in no consolidation stage and high shearing speed), CU (consolidated undrained – the consolidation stage is followed by the shearing step, which is also conducted at high shearing speed), and CD (consolidated drained – where the consolidation stage is followed by a shearing step having low shearing speed).

Lower speed allows the water inside the soil to be drained, obtaining higher values of the internal friction angle and lower cohesion (typical for drained conditions), while a high shearing speed does not provide sufficient time for the water to exit the sample, resulting in higher cohesion and lower values of the internal friction angle (typical for undrained conditions).

In order to properly conduct the direct shear test, the following steps must be completed (the procedure is standardized in STAS 8942/2 [28]):

- first of all, the soil sample is to be cut under the form of the required mould (Fig. 10.29);

- the obtained cut sample is introduced inside the shear box and into the saturation box, having the two porous stones (plates) on the top and lower faces; also, on top of the upper porous stone the loading plate will be positioned (Fig. 10.30);
- the guiding system that reaches the motor and the dynamometer ring is to be locked, maintaining a firm contact with the shearing box;
- the ram is brought in contact with the loading plate and, following the placement of the loading weights;
- the ram is lowered, and if the case, the consolidation stage will begin; if the case of UU type, the shearing stage is immediately;
- in the case of a consolidation stage (CU and CD type), the process will last up to the moment where the sum of the relative displacements recorded during three consecutives readings located at one hour away from each other is less or equal to 0.01mm;
- during the shearing stage, the readings of the three dial gauges are to be recorded; if manual, in the case of the CD type shearing, the monitoring will be conducted at 1, 2, 3, 4, 6, 8, 10, 15, 20, 25, 30minutes and at every 10minutes up to the test completion; in the case of UU and CU types, the monitoring will be conducted at every 15seconds.



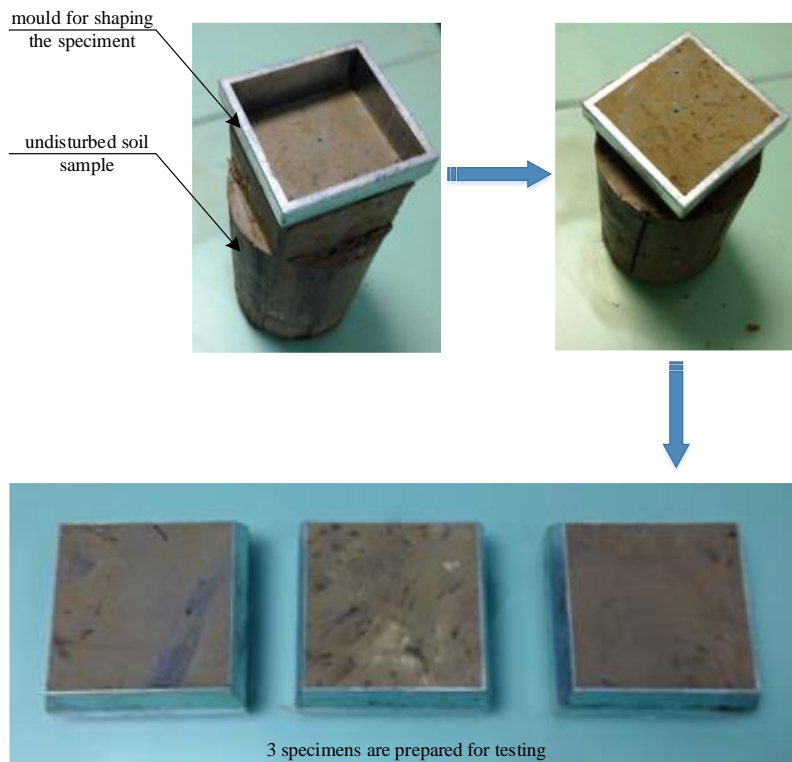


Fig. 10.29: Shaping the specimens for the direct shear test

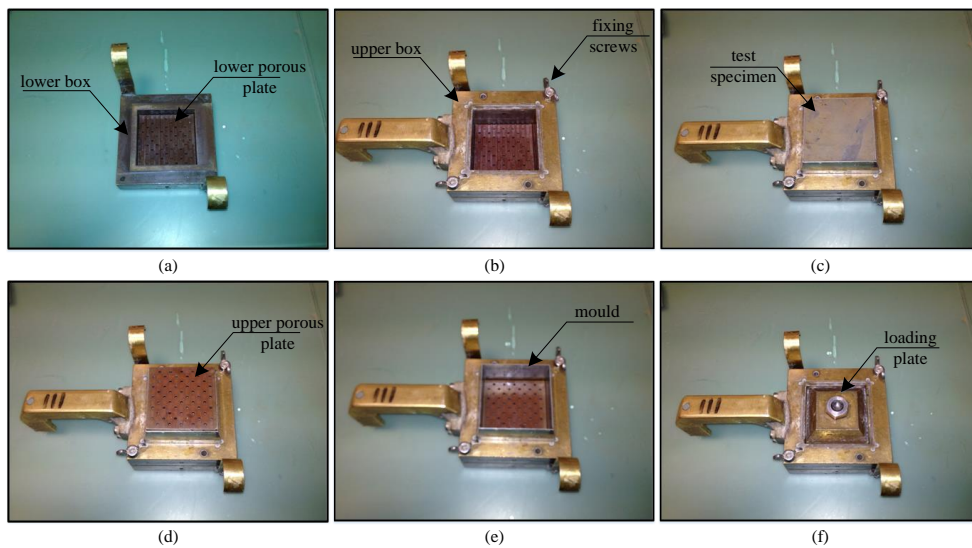


Fig. 10.30: Placing the test specimen inside the shear box

Standardized direct shearing tests are considered to be completed when the sample reaches 20% of the dimension parallel to the advancement direction.

The minimum required number of samples in order to determine a soil's resistance parameters is three. In order to obtain three different points along the normal stress axis, three weight setups will be considered. These setups represent three different vertical loads to which the samples are subjected during the test, and generally are chosen either around the geological stress existing at the depth from which the sample was recovered, either around the stress state that is expected to be reached following the construction of the structure.

### **10.2.2 Triaxial compression test**

A more advanced method to be considered in order to obtain the shear resistance parameters, which allows a more accurate simulation of the stress evolution that a soil will undergo, is the triaxial compression apparatus.

There are two main types of apparatuses:

- imposed deformation-measured stresses, which allows only typical compression tests along the loading stress path;
- imposed stress-measured deformation, which allows all types of tests and have the ability of covering all the possible stress paths situated in the positive deviator area (axial compression).

From the components point of view, the apparatus is made of the following parts:

1. Pressure cell – allows the usage of a certain fluid (air, water, oil) to be used in order to create a hydrostatical stress around the sample;
2. Locking system – locks the cell into the pedestal, so that higher cell pressures may be used;
3. Top port – it represents basically a tap that is used during the setup of the sample and at the end of the test, when the sample is taken out;
4. Loading ram – by using this part, vertical compression stresses are applied to the sample, inducing deviatoric stresses;
5. Vertical load transducer – it is an electronic sensor that determines the axial force applied to the sample; in the case of older apparatuses, it is replaced with a dynamometric ring situated outside the cell;

6. Pedestal – it is the body of the triaxial, containing the drainage and pore water pressure lines embedded in it;
7. O-rings – by using these rubber rings, the membrane is kept in tight contact with the top cap, and pedestal, respectively;
8. Membrane – this membrane has the role of separating the sample's environment from the cell, in order to control and monitor separately the two;
9. Top cap – this part has a double role: to act as a rigid loading plate, transforming the axial force into an axial stress, and, in the same time, to allow the inflow/outflow of water to/from the sample;
10. Porous stone – allows the migration of water to/from the sample, without losing solid material and/or clogging the water lines;
11. Porewater pressure transducer – this sensor measures the water pressure; the assumption is that in the case of a saturated soil, and if the water inside the sample is able to communicate with, the pressure sensed by the sensor will be equal to the one of the water inside the soil's pores;
12. Back pressure and volume controller – this part is in fact a digital pressure pump, that is able to work also as an electronic burette, imposing the desired pressure and monitoring the volume lost; the back-pressure line is used to saturate the sample;
13. Draining water line – this line has two roles: the first is that of a line through which air or water may leave the sample, under the action of the water brought in by means of the back pressure line; the second is to help during the consolidation stage, by linking it to the back pressure line, so that the pressure controller keeps constant the pore water pressure and monitor the outflow of water;
14. Cell pressure and volume controller – this pressure controller imposes the hydrostatical stress around the sample and monitor the volume of the cell fluid.

Regarding the back pressure and cell pressure controllers, in the case of older setups, these are provided by additional equipment such as compressors or Bishop cells.

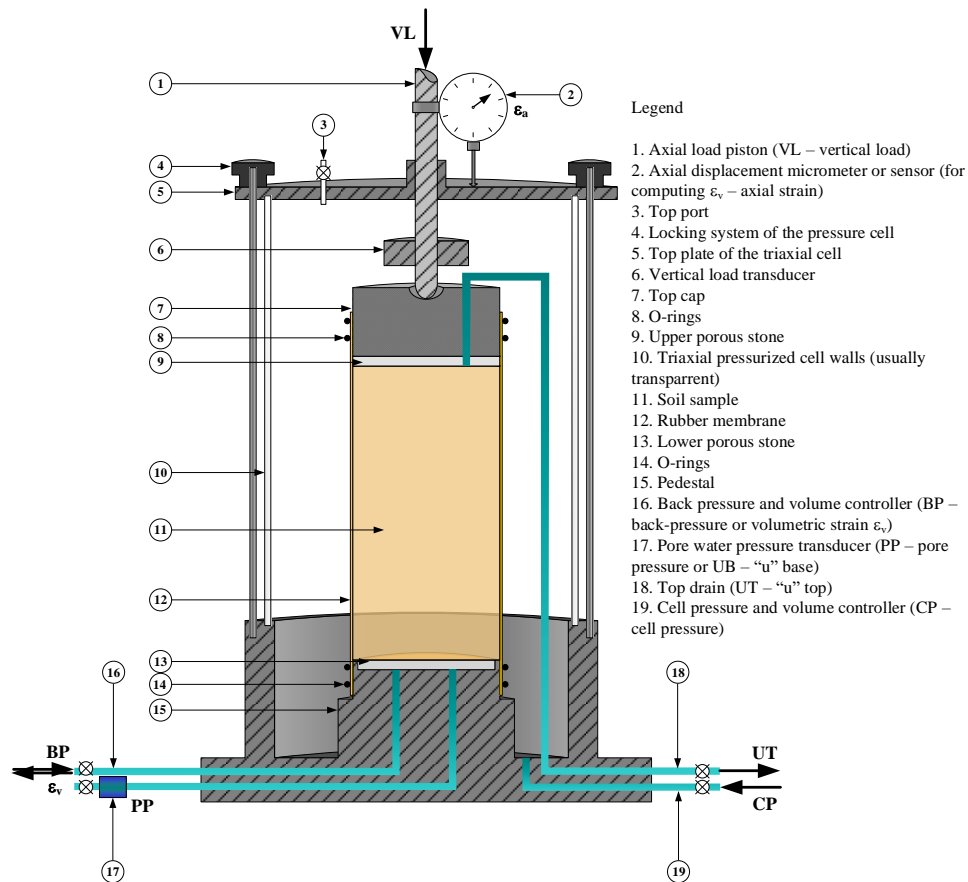


Fig. 10.31: The triaxial compression test apparatus

Regarding the possibilities of conducting a triaxial compression test, a variety of tests may be considered:

- from the point of view of the consolidation stage, there are three types that may be used: unconsolidated, isotropically consolidated and anisotropically consolidated along  $K_0$  line (only for the imposed stress-measured deformation apparatuses);
- from the point of view of the shearing process, there are two ways of to induce the critical state: undrained, drained; in the case of the imposed stress, measured deformation apparatus, the stress paths may be used.

Generally, the following steps are required to be covered:

- cutting the sample as a cylindrical mould having one of the standard dimensions of 38, 50, 75 or 100mm diameter, and height having a value of twice the diameter;
- inserting the sample into the membrane, by using a vacuum pump, and placing at the top and lower part the two porous stones (plates);
- placing the aforementioned setup on the pedestal, and seal the lower part by adding the O-rings; at the superior part, over the porous stone, add the top cap and seal the superior limit of the membrane by means of O-rings; optionally, in order to better ensure the separation of the two environments, one can use also silicone grease;
- place the cell over the setup, lock the system to the pedestal and fill the cell's volume with fluid;
- reset all the sensors to an initially null value;
- saturate the sample, first by flushing the sample, letting the air out of it, as the water flows in the sample;
- following the saturation stage, an optional consolidation stage may be considered, in the case of CU, CD, CK<sub>0</sub>U and CK<sub>0</sub>D types of test (the total and effective stresses procedures are covered by BS 1377-7 [29] and BS 1377-8 [30]);
- in the case of UU shearing tests, the saturation stage is immediately followed by the shearing step (the procedure is standardized by STAS 8942/5 [31]);
- regarding the shearing step, other than UU, this one is next after the consolidation stage.

Regarding the shearing step, for the imposed deformation-measured stress apparatus, only the loading path may be imposed (Fig. 10.32 stress path 2).

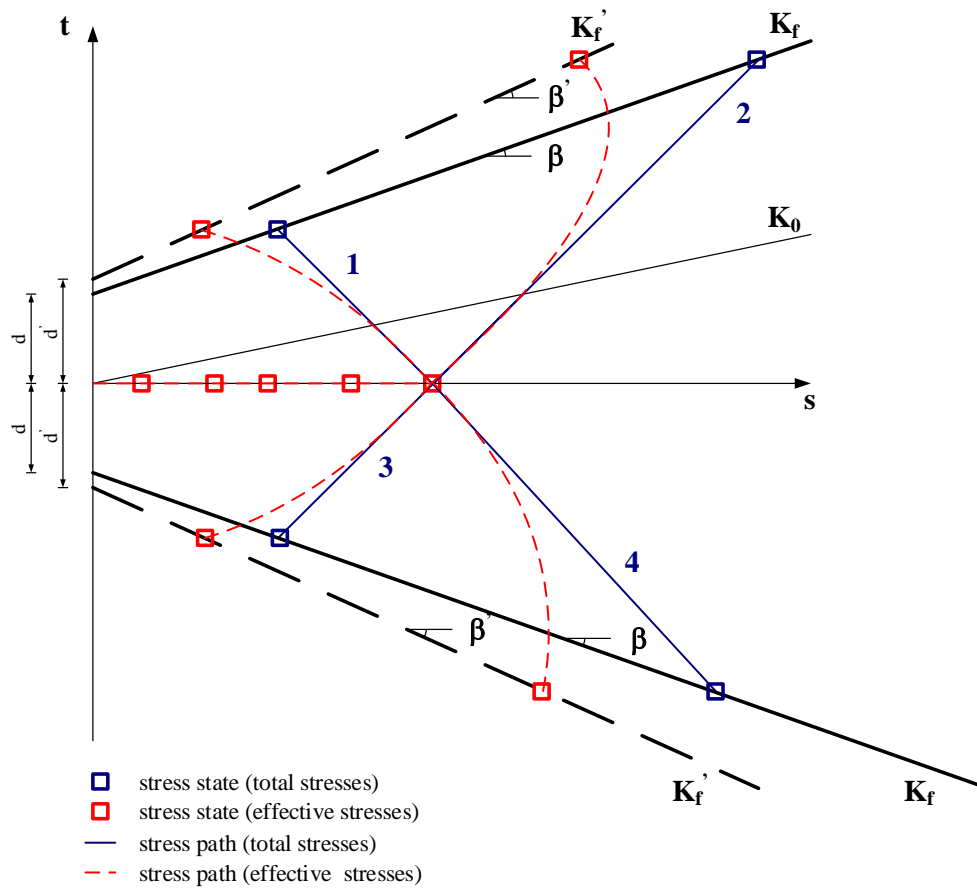


Fig. 10.32: Possible stress paths starting from isotropic consolidation (CU, CD)

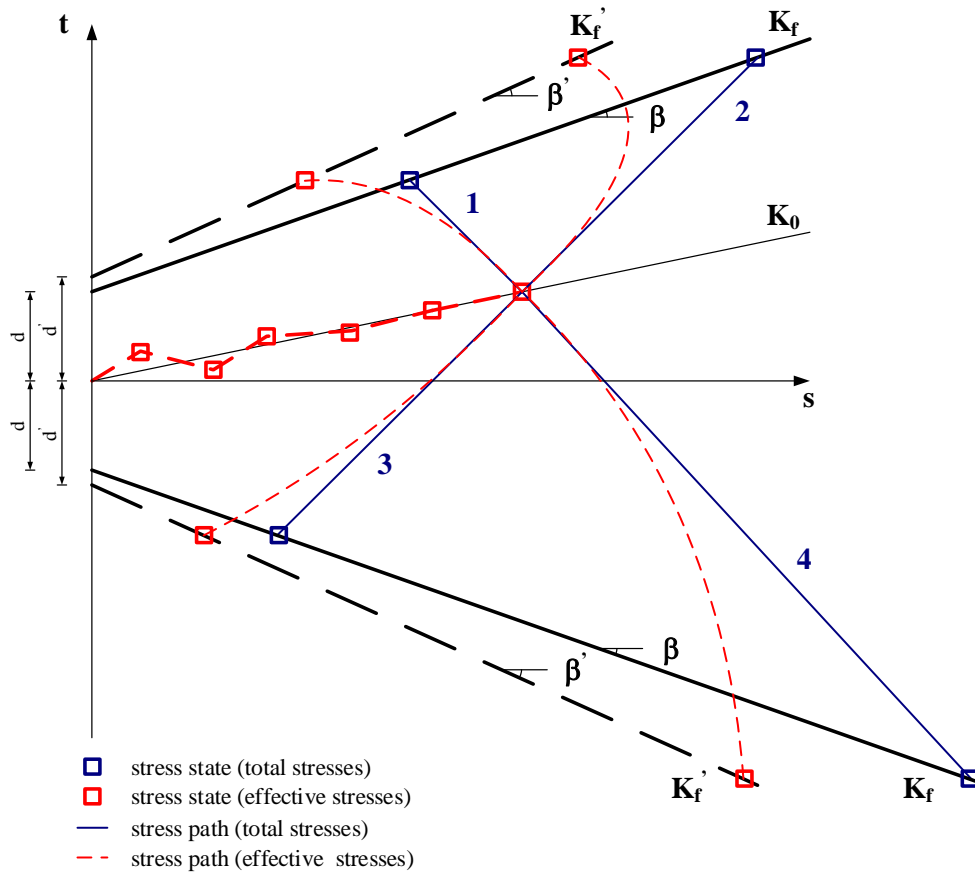


Fig. 10.33: Possible stress paths starting from anisotropic consolidation (CK<sub>0</sub>U, CK<sub>0</sub>D)

### 10.3 Test your understanding

#### Problem 10.1

What are the shear strength parameters of soil?

#### Problem 10.2

What is the difference between the drained and undrained cohesion of soil?

#### Problem 10.3

For what types of soil is the undrained shear strength relevant?

#### Problem 10.4

How is the rate of shear relevant during a direct shear test?

**Problem 10.5**

Why is saturation of the sample important for a CD triaxial compression test?

**Problem 10.6**

How can one obtain the Poisson coefficient for soil in the lab?

**Problem 10.7**

Why is the coefficient of lateral stress at rest only obtained with a triaxial compression test with imposed stress and not with imposed deformation?

**Problem 10.8**

The following results were obtained from direct shear tests on an overconsolidated clay:

Test	Normal force [N]	Shear force at failure [N]	Residual shear force [N]
a	150	157.5	44.2
b	250	199.9	56.6
c	350	257.6	102.9
d	550	363.4	144.5

- Plot the results on a  $\sigma$ - $\tau$  chart
- Estimate the peak shear strength parameters
- Estimate the residual shear strength parameters

**Problem 10.9**

For a direct shear test on a dry sand, the obtained friction angle is  $34^\circ$ . The size of the specimen is 60mm x 60mm x 20mm. Determine the shear force required to produce failure at a normal stress of 250kPa.

**Problem 10.10**

Three specimens were tested from a sand sample using the direct shear. The shear box has the interior dimensions 6x6x2cm. The normal forces applied during the test and the maximum forces measured at shear are given in the table below.

Test	Normal force [daN]	Shear force at failure [daN]
------	--------------------	------------------------------



a	36	21
b	72	42
c	108	65

The following are requested:

- a) Find the normal stresses during the tests
- b) Find the maximum shear stresses acting on the failure surface
- c) Draw the failure line
- d) Find the shear strength parameters

#### Problem 10.11

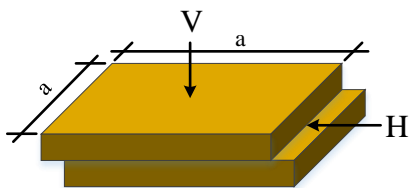
The results in the table below are obtained on four direct shear tests performed on a normally consolidated clay.

Test	Normal force [N]	Shear force at failure [N]
a	200	155
b	300	230
c	400	310
d	500	385

Draw a chart for the shear stress at failure against normal stress and determine the drained angle of friction.

#### Problem 10.12

A rectangular soil sample with the side  $a=6\text{cm}$  and the height  $h=2\text{cm}$  is subjected to a set of two direct shearing tests under vertical loads  $V$ , as depicted in the figure below. The maximum recorded horizontal forces are  $T$  and are given in the table below.



Compute the shearing strength parameters if the maximum recorded horizontal forces,  $H$ , are given in the table below.

Test	V [N]	H [N]
a	360	145
b	540	180

**Problem 10.13**

A dry sand sample is subjected to a direct shear test. The specimen size is 75mm x 75mm x 30mm. The normal applied stress is  $\sigma=214\text{kPa}$  and the recorded shear stress at failure is  $\tau=169\text{kPa}$ . Compute:

- the shear strength parameters;
- the shear force required to produce failure for a normal stress of 156kPa.

**Problem 10.14**

A soil sample is subjected to a set of two CD triaxial compression tests. The diameter of the sample is 50mm. The applied cell pressures during the two tests are  $CP_a=200\text{kPa}$  and  $CP_b=375\text{kPa}$ . The recorded maximum principal stresses at failure are  $\sigma_{1a}=455\text{kPa}$  and  $\sigma_{1b}=742\text{kPa}$ . Compute the effective shearing strength parameters.

**Problem 10.15**

A soil sample is subjected to a set of two CD triaxial compression tests. The diameter of the specimens is 50mm. The applied cell pressures in the two tests are CP and the recorded vertical loads on the specimens at failure are VL, as shown in the table below.

Test	CP [kPa]	VL [N]
a	100	250
b	150	360

The following are required:

- Compute the shear strength parameters;
- Specify the porewater pressure at failure during the tests;
- Compute the shearing strength parameters corresponding to the MIT system of reference,  $\beta$  and  $d$ .

**Problem 10.16**

The  $k_f$  line parameters in  $s$ - $t$  stress coordinates for a soil are  $\beta=9^\circ$  and  $d=46\text{kPa}$ . Compute the internal friction angle and cohesion.

**Problem 10.17**

Which laboratory test can be performed to find Poisson's ratio?

**Problem 10.18**

Is it possible to perform a  $K_0$  anisotropic consolidation stage using a triaxial compression device?

**Problem 10.19**

Is it possible to perform a  $K_0$  anisotropic consolidation stage using a direct shear device?

**Problem 10.20**

An overconsolidated soil is sheared using the direct shear test to a horizontal displacement equal to 20%. The process is then repeated 5 times. How will the value of the maximum shear stress be in the final cycle compared to the first cycle?

**Problem 10.21**

An overconsolidated soil is sheared using the direct shear test to a horizontal displacement equal to 20%. The process is then repeated 5 times. How will the value of the maximum shear stress be in the final cycle compared to a similar material, which is normally consolidated and only sheared once?

**Problem 10.22**

A soil sample has the linear deformation modulus  $E=12\text{MPa}$  and the horizontal thrust coefficient at rest,  $K_0=0.63$ . The sample is loaded into a triaxial compression device and confined with 200kPa cell pressure and 50kPa additional piston pressure. Compute the axial and radial deformation.

**Problem 10.23**

The triaxial compression test results for a soil sample are  $\phi=20^\circ$  and  $c=45\text{kPa}$  in total stresses and  $\phi'=24^\circ$  and  $c'=25\text{kPa}$ . Compute the porewater pressure at failure for a sample subjected to 200kPa cell pressure.

**Problem 10.24**

Is it possible that a set of 3 triaxial compression tests will produce the middle Mohr circle of stress outside larger than the tangent common to the other two circles? Is this possible according to Coulomb failure model?

**Problem 10.25**

How is it possible to obtain the linear deformation modulus from a triaxial compression test?

**Problem 10.26**

Is it possible for the dilatancy / contractancy angle to be larger than the internal friction angle?



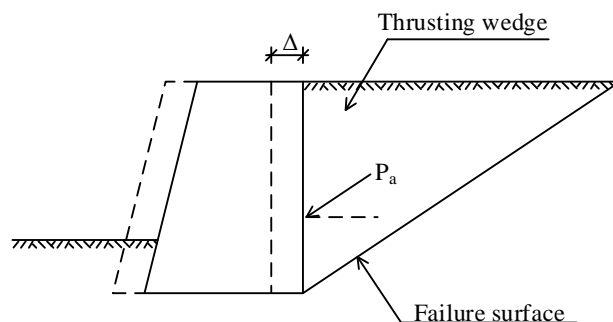
## 11 THE EFFECTS OF SOIL UPON STRUCTURES

### 11.1 General notions

Both for buried structures and for the foundations interacting with the soil we have common reactive forces as follows:

- when the soil pushes upon the structure the forces it exerts is called active force or active thrust;
- when the soil is pushed by the structure it opposes the movement by a force called passive resistance.

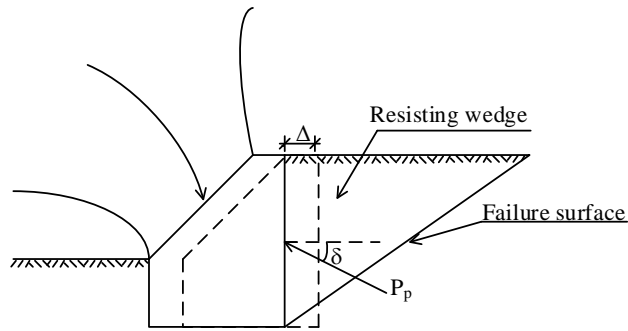
Examples:



$P_a$ - active thrust

$\Delta$ -displacement of the structure

Fig. 11.1 Active thrust (retaining wall)



$P_p$ - passive thrust  
 $\Delta$ -displacement of the structure

Fig. 11.2: Passive resistance (arch bridge)

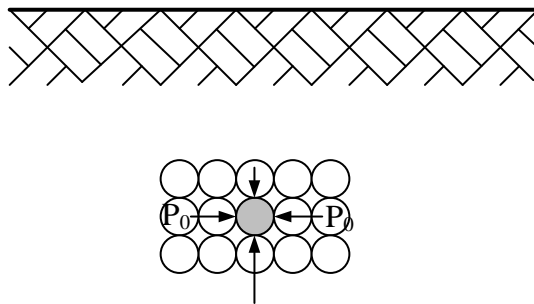


Fig. 11.3 State of rest

The active thrust and the passive resistance are based on the assumption that a soil wedge will be displaced from the rest of the soil mass and it will exert the thrust or the reaction. The horizontal force acting in a point due to the state of rest is a special kind of thrust which is mobilized in the case of elastic state (Fig. 11.3) (no plastic zones occur). The plastic zones in active thrust or passive resistance are around the failure surfaces.

From a magnitude standpoint:

$$P_a < P_0 (P_{k0}) < P_p$$

For the soil to engage in either passive resistance or active thrust, a displacement  $\Delta$  must occur.

In order to reach its full value, a displacement  $\Delta_a$  is necessary for the active thrust, while a much larger displacement (about ten times larger)  $\Delta_p$  is required for the passive resistance (Fig. 11.4).

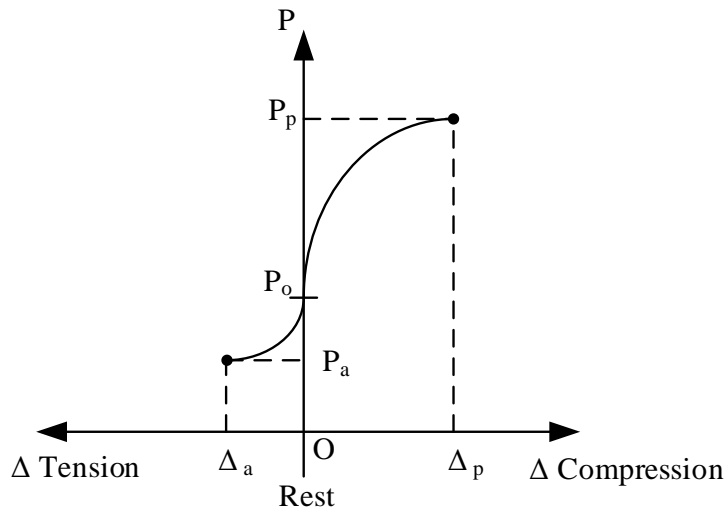
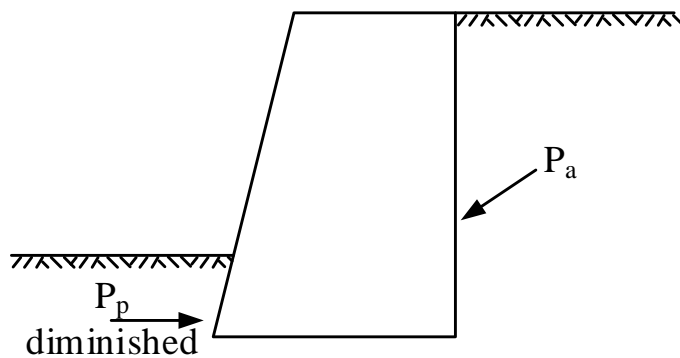


Fig. 11.4 Mobilization curve

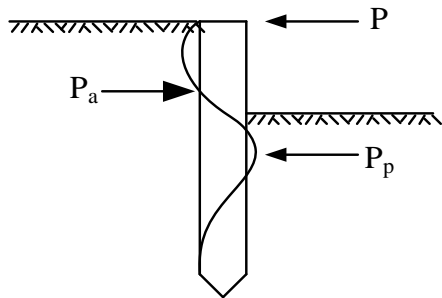
For this reason, the passive strength is generally disregarded or diminished if it acts simultaneously with the active thrust (Fig. 11.5 and Fig. 11.5).



$P_a$ - active thrust  
 $P_p$ -passive thrust

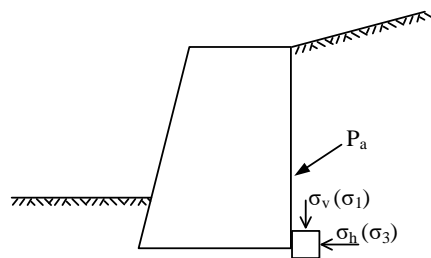
Fig. 11.5 Retaining wall





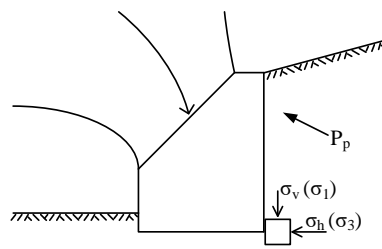
$P_a$ - active thrust  
 $P_p$ -passive thrust  
 $P$ -applied horizontal load

Fig. 11.6 Horizontally loaded pile



$P_a$ - active thrust  
 $\sigma_v$ -vertical stress  
 $\sigma_h$ -horizontal stress  
 $\begin{cases} \sigma_1\text{-constant} \\ \sigma_3 \nearrow \end{cases} \Rightarrow \begin{cases} s \searrow \\ t \nearrow \end{cases}$

Fig. 11.7 Active thrust



$P_p$ -passive resistance  
 $\sigma_v$ -vertical stress  
 $\sigma_h$ -horizontal stress  
 $\begin{cases} \sigma_1\text{-constant} \\ \sigma_3 \searrow \end{cases} \Rightarrow \begin{cases} s \nearrow \\ t \searrow \end{cases}$

Fig. 11.8 Passive resistance

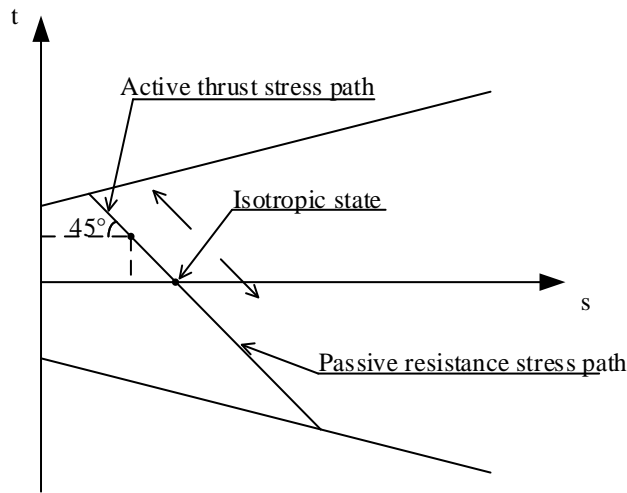


Fig. 11.9 Stress paths for active thrust and passive resistance

## 11.2 Vertical stresses

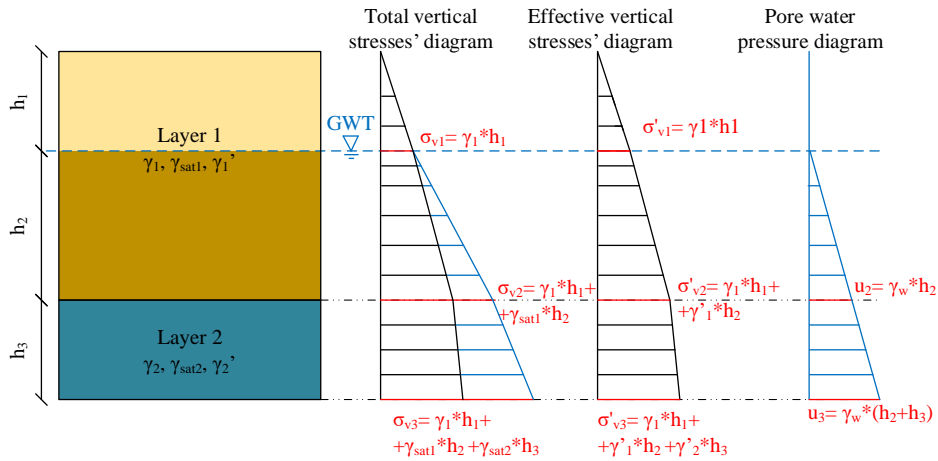


Fig. 11.10: Total and effective vertical stresses and the pore water pressure in a soil mass

In Fig. 11.10 a column of soil is presented, containing two layers of soil. Layer 1 is saturated at depth  $h_1$  (at the level of the ground water table (GWT)) and layer 2 is totally saturated. Seepage of water is not considered in any direction.

The total stress diagram is computed at depth  $h_1$  considering the bulk unit weight of layer 1,  $\gamma_1$ :  $\sigma_{v1} = \gamma_1 h_1$ . After this depth, the saturated unit weight of layer 1 is used to compute the vertical stress. At depth  $h_1 + h_2$ , the total vertical stress is computed by adding the vertical stress at depth  $h_1$  with the vertical stress produced by the saturated part of layer 1:  $\sigma_{v2} = \sigma_{v1} + \gamma_{sat1} h_2 = \gamma_1 h_1 + \gamma_{sat1} h_2$ . The saturated unit weight of the soil is used for computing the total vertical stress induced by the soil having the thickness  $h_2$  because the soil is beneath the ground water table and is considered saturated. The total vertical stress at depth  $h_1 + h_2 + h_3$  is computed adding the total vertical stress induced by layer 1,  $\sigma_{v2}$  together with the stress induced by layer 2 on  $h_3$  thickness. Because layer 2 is beneath the ground water table, layer 2 is considered to be saturated:

$$\sigma_{v3} = \sigma_{v2} + \gamma_{sat2} h_3 = \gamma_1 h_1 + \gamma_{sat1} h_2 + \gamma_{sat2} h_3 \quad (11.1)$$

As shown in chapter 8.4, eq. (8.39), the total stress is equal with the effective stress plus the pore water pressure:  $\sigma = \sigma' + u$ .

Also, the saturated unit weight equals the submerged unit weight plus the unit weight of the water.

$$\gamma_{\text{sat}} = \gamma' + \gamma_w \quad (11.2)$$

At depth  $h_1$ , the effective vertical stress equals the total vertical stress at that depth because the ground water table is beneath, and the pore water pressure is considered to be zero:

$$\sigma_{v1} = \sigma'_{v1} \leftrightarrow \sigma'_{v1} = \gamma_1 h_1 \quad (11.3)$$

At depth  $h_1+h_2$ , the effective vertical stress equals the effective vertical stress at depth  $h_1$  plus the effective vertical stress induced by the  $h_2$  thickness of the saturated soil layer. The unit weight of the soil in the case of effective stresses is considered the submerged unit weight:

$$\sigma'_{v2} = \sigma'_{v1} + \gamma'_1 h_2 = \gamma_1 h_1 + \gamma'_1 h_2 \quad (11.4)$$

The porewater pressure at depth  $h_1+h_2$  is computed as the hydrostatic pressure given by an  $h_2$  water column:  $u_2 = \gamma_w h_2$ .

The total vertical stress at depth  $h_1+h_2$  is:

$$\sigma_{v2} = \sigma'_{v2} + u_2 = \gamma_1 h_1 + \gamma'_1 h_2 + \gamma_w h_2 = \gamma_1 h_1 + h_2 (\gamma'_1 + \gamma_w) = \gamma_1 h_1 + \gamma_{\text{sat}1} h_2 \quad (11.5)$$

At depth  $h_1+h_2+h_3$ , the effective vertical stress equals the effective vertical stress at depth  $h_1+h_2$  plus the effective vertical stress induced by the layer 2 with thickness  $h_3$ :

$$\sigma'_{v3} = \sigma'_{v2} + \gamma'_2 h_3 = \gamma_1 h_1 + \gamma'_1 h_2 + \gamma'_2 h_3 \quad (11.6)$$

The pore water pressure at depth  $h_1+h_2+h_3$  is computed as the hydrostatic pressure given by an  $h_2+h_3$  water column:  $u_3 = \gamma_w (h_2+h_3)$ .

The total vertical stress at depth  $h_1+h_2+h_3$  is:

$$\sigma_{v3} = \sigma'_{v3} + u_3 = \gamma_1 h_1 + \gamma'_1 h_2 + \gamma'_2 h_3 + \gamma_w (h_2+h_3) = \quad (11.7)$$

$$\gamma_1 h_1 + h_2(\gamma'_1 + \gamma_w) + h_3(\gamma'_2 + \gamma_w) = \gamma_1 h_1 + \gamma_{sat1} h_2 + \gamma_{sat2} h_3$$

### 11.3 State of rest

The state of rest is attained when no lateral displacements are possible in a point due to the fact that the horizontal stresses are constant in all the neighbouring points at a certain depth, thus obtaining equilibrium. In the state of rest, the effective horizontal stresses are proportional with the effective vertical stress with a proportionality of  $K_0$ :  $K_0 = \frac{\sigma'_h}{\sigma'_v}$ .  $K_0$  was defined in chapter 8.5 and is particular for each layer of soil.

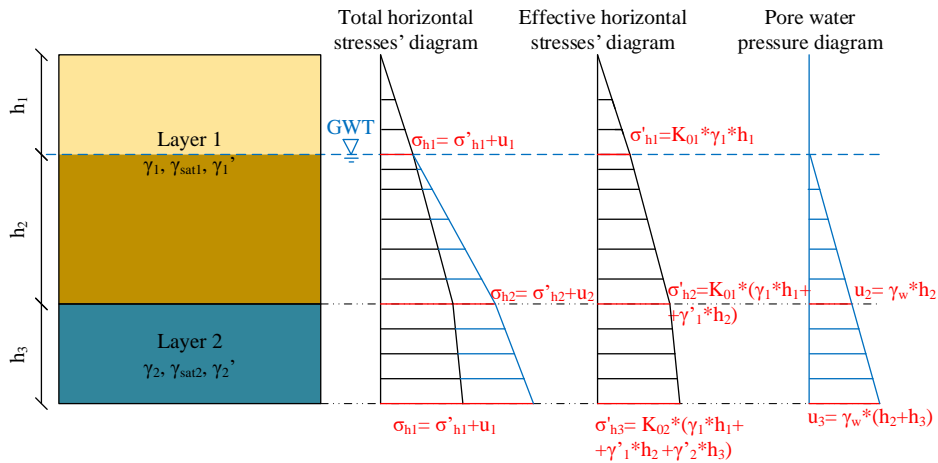


Fig. 11.11: Total and effective horizontal stresses and the pore water pressure in a soil mass

In Fig. 11.11, the same soil column from Fig. 11.10 is presented together with the horizontal stresses (total and effective stresses) and the pore water pressure presented. The horizontal stresses are produced by the vertical stresses presented in Fig. 11.10.

For layer 1, the coefficient of soil thrust at rest is  $K_{01}$  and for layer 2 the coefficient of soil thrust at rest is  $K_{02}$ . The effective horizontal stress in one point is computed by multiplying the coefficient of soil thrust at rest for the layer found at that depth and the effective vertical stress at that point. The pore water pressure is computed as a hydrostatic pressure, so the pressure is the same on all directions. The total horizontal stress is computed as the sum

of the effective horizontal stress and the pore water pressure at that specific point.

At depth  $h_1$ , the effective horizontal stress is computed as the effective vertical stress multiplied with the coefficient  $K_0$  for layer 1,  $K_{01}$ :

$$\sigma'_{h1} = K_{01} \sigma'_{v1} = K_{01} \gamma_1 h_1 \quad (11.8)$$

The porewater pressure is zero at this point because the ground water table is below this depth. The total horizontal stress at this depth equals the effective horizontal stress, because the porewater pressure is zero:

$$\sigma_{h1} = \sigma'_{h1} = K_{01} \sigma'_{v1} \quad (11.9)$$

At depth  $h_1+h_2$ , the effective horizontal stress is computed as the product of the effective vertical stress and the coefficient of soil thrust at rest for layer 1,  $K_{01}$ :

$$\sigma'_{h2} = K_{01} \sigma'_{v2} = K_{01} (\gamma_1 h_1 + \gamma'_1 h_2) \quad (11.10)$$

The porewater pressure at depth  $h_1+h_2$  is computed as the hydrostatic pressure at depth  $h_2$ :  $u_2 = \gamma_w h_2$ . The total horizontal stress is the sum of the effective horizontal stress and the pore water pressure at that depth:

$$\sigma_{h2} = \sigma'_{h2} + u_2 = K_{01} (\gamma_1 h_1 + \gamma'_1 h_2) + \gamma_w h_2 \quad (11.11)$$

At depth  $h_1+h_2+h_3$ , the effective horizontal stress is computed by multiplying the effective vertical stress and the coefficient of soil thrust at rest for layer 2,  $K_{02}$ :

$$\sigma'_{h3} = K_{02} \sigma'_{v3} = K_{02} (\gamma_1 h_1 + \gamma'_1 h_2 + \gamma'_2 h_3) \quad (11.12)$$

The pore water pressure at depth  $h_1+h_2+h_3$  is computed as the hydrostatic pressure at depth  $h_2+h_3$ :  $u_3 = \gamma_w (h_2+h_3)$ . The total horizontal stress is the sum of the effective horizontal stress and the pore water pressure at that depth:

$$\sigma_{h3} = \sigma'_{h3} + u_3 = K_{02} (\gamma_1 h_1 + \gamma'_1 h_2 + \gamma'_2 h_3) + \gamma_w (h_2+h_3) \quad (11.13)$$

### 11.4 Coulomb's model for active thrust

Coulomb proposed a condition that limit equilibrium exists in the soil mass where slips along a plane inclined with an angle  $\alpha$  with respect to the horizontal.

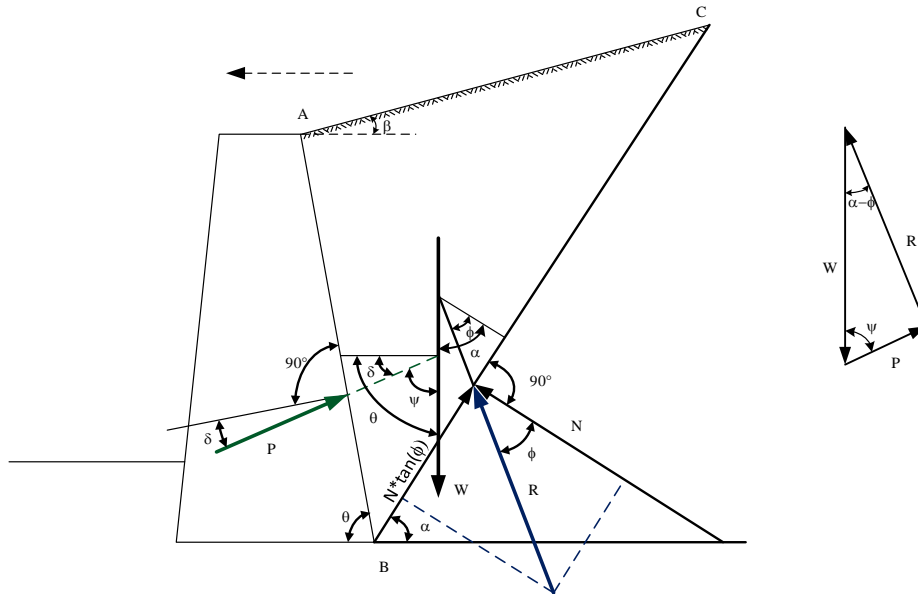


Fig. 11.12 Coulomb's model for active thrust

For this model it is considered a retaining wall punched by the thrust induced by a cohesionless soil. There are taken into account the following forces:

- $G$  – the own weight of the wedge punching the wall;
- $P$  – the interaction force between the retaining wall and the soil wedge;
- $R$  – the soil mass reaction.

Due to the forward motion of the wall by decompression on the whole back face and along the failure surface, a relative displacement will occur inducing reactive friction forces. The angle of friction between concrete and soil is  $\delta$ , while the internal friction angle is  $\phi$ . Since no other forces appear in the system, the polygon formed by  $G$ ,  $P$  and  $R$  has to be closed. The failure surface angle is denoted by  $\alpha$ , while the back-surface inclination of the retaining wall is denoted by  $\theta$ .

$$\frac{P}{\sin(\alpha-\phi)} = \frac{G}{\sin(180^\circ-(\alpha-\phi)-\psi)} = \frac{R}{\sin\psi} \quad (11.14)$$

$$P = \frac{G \cdot \sin(\alpha-\phi)}{\sin(\alpha-\phi+\psi)} \quad (11.15)$$

From this relationship it may be noticed that the only unknown is actually the failure surface angle  $\alpha$ , in other words,  $G=G(\alpha)$ .

In order to solve this problem, there are several solutions. We can differentiate  $P$  with respect to  $\alpha$  and search for the value of  $\alpha$  for which the derivative cancels:

$$\frac{\partial P}{\partial \alpha} = 0 \quad (11.16)$$

A second solution is Culmann graphical method and the third approach is the use of Rankine's hypothesis for simplifying the system.

### 11.5 Culmann's graphical method

This method considers all Coulomb hypotheses built in a step-by-step graphical manner. Looking for the position of the failure surface it is known that it lays only between the wall's back face and the stable slope surface inclined with the angle  $\phi$  and called support line (BD). With respect to the support line is drawn a line inclined with the angle  $\psi$ , called orientation line.

There are proposed several failure surfaces  $BC_1, BC_2, \dots, BC_i, \dots, BC_n$ , which correspond to the prisms  $ABC_1, ABC_2, \dots, ABC_i, \dots, ABC_n$ , such that the areas of the triangles are equal ( $A_{ABC1} = A_{ABC2} = \dots = A_{ABCi} = \dots = A_{ABCn}$ ).

For every assumed failure surface "i" it is computed the own weight,  $W_i$ , and its slope  $\alpha_i$ . On the support line it is drawn at a certain scale the wedge weight  $W_i$  and from its end it is drawn a parallel line to the orientation line until the assumed failure surface is reached, intersecting it in the point  $P_i$ , being the active thrust  $P_i$  of the  $ABC_i$  prism. The tips of all  $P_i$  vectors are connected through a curved line and then it is drawn a line parallel to the support line and tangent to the curve. The tangency point  $P$  represents the maximum value

of the active thrust  $P_{\max}=P_a$ . The failure surface is obtained by connecting B with P.

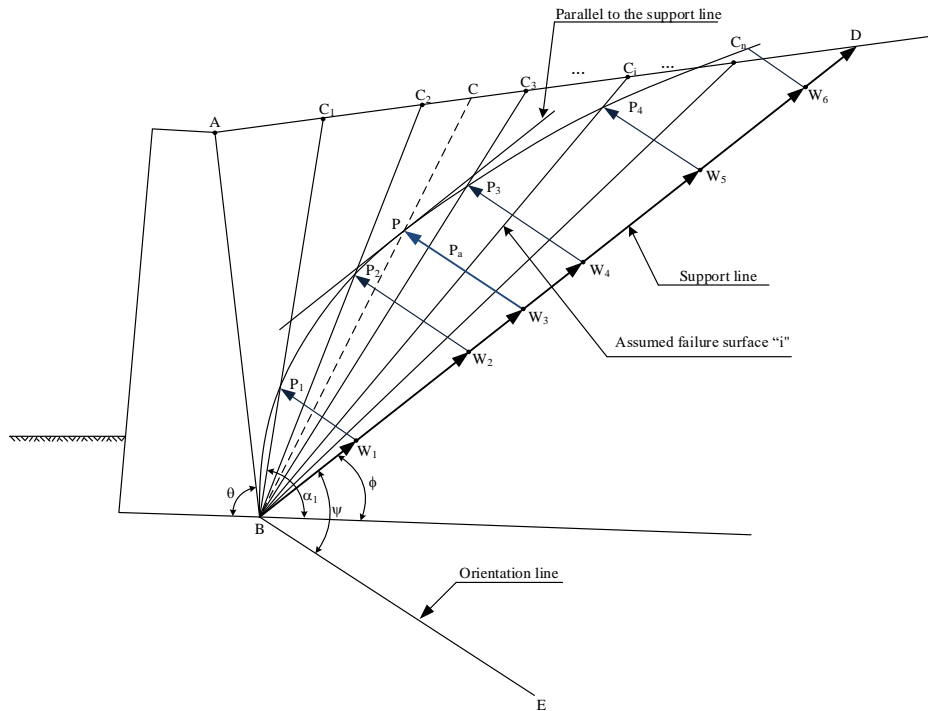


Fig. 11.13 Culmann's graphical method



### 11.6 Rankine model in active and passive case

In the state of rest, the horizontal and vertical directions are principal ones. So, in the active or passive state if we preserve these directions, we can always find for the base point of the walls back face the circle's pole. This is achieved by removing all the effects that induce tangential stresses on the vertical and horizontal directions.

The hypotheses stated by Rankine are the following:

- the wall back face has to be vertical ( $\theta=90^\circ$ );
- the soil surface is horizontal ( $\beta=0^\circ$ );
- the friction between soil and concrete is neglected ( $\delta=0$ );
- only uniformly distributed loads are allowed on the wedge.

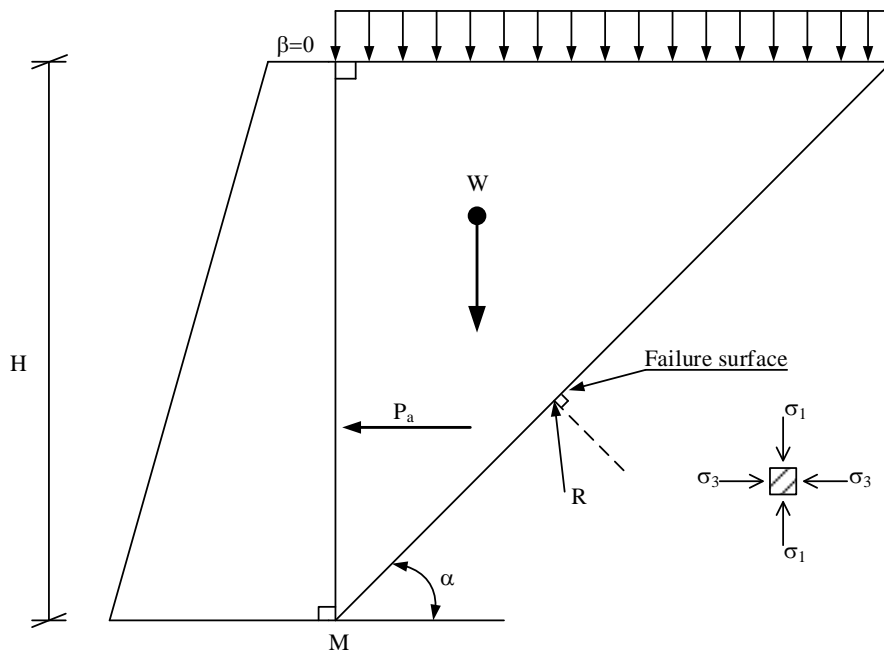


Fig. 11.14 Rankine Model

Due to these hypotheses we know that the point  $M$  simultaneously belongs to the wall back face (thus having vertical and horizontal principal directions) and to the failure surface (meaning that the Mohr's circle is tangent to the failure criterion).

Assuming that we are dealing with a cohesionless soil, the situation is presented below, in Fig. 11.15.

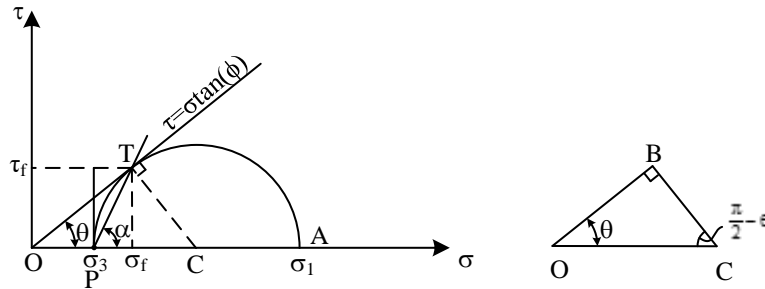


Fig. 11.15 Reaching the failure criterion by attaining the active pressure (unloading stress path)

In Mohr's circle corresponding to the point M it is built the pole which lays coincident with  $\sigma_3$ . The pair of stresses for which the failure occurs is  $\sigma_f - \tau_f$ .

The direction of the failure surface (the value of the angle  $\alpha$ ) may be found by joining the pole with the combination of stresses of failure.

B is a tangency point of the failure surface to the state of stress, meaning that BC is normal to OB. So, in the OBC triangle the angle  $\angle BCO$  is  $\frac{\pi}{2} - \phi$ . Its complement, the angle  $\angle BCA$  is  $\frac{\pi}{2} + \phi$ , meaning that the arch  $\widehat{AB}$  measured in the centre is  $\frac{\pi}{2} + \phi$ .

The same arch is determined from the circle by the angle  $\alpha = \angle BPA = \frac{\angle BCA}{2} = \frac{\pi}{4} + \frac{\phi}{2} = 45^\circ - \frac{\phi}{2}$ .

Knowing that:

$$\left. \begin{array}{l} \psi = \pi \\ \alpha = \frac{\pi}{4} + \frac{\phi}{2} \\ P = \frac{G \cdot \sin(\alpha - \phi)}{\sin(\psi + \alpha - \phi)} \end{array} \right\} \Rightarrow P = G \cdot \tan^2 \left( \frac{\pi}{4} - \frac{\phi}{2} \right) \quad (11.17)$$

Considering that P and G are unitary forces acting on an infinitesimal area, we obtain:

$$\sigma_h = \sigma_v \cdot k_a \tag{11.18}$$

where

$$k_a = \tan^2\left(45^\circ - \frac{\phi}{2}\right) \tag{11.19}$$

$k_a$  is known as the coefficient of active pressure. Generalising for cohesive soils:

$$\sigma_h = \sigma_v \cdot k_a - 2 \cdot c \cdot \sqrt{k_a} \tag{11.20}$$

It results that the effect of the cohesion is constant distributed leading to a distribution like the one in Fig. 11.16.

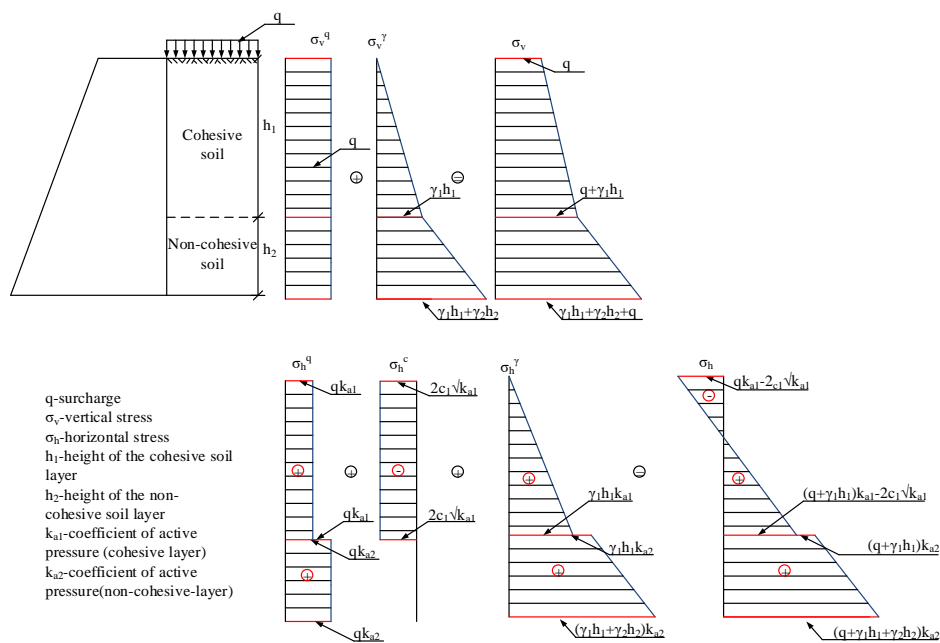


Fig. 11.16: Example of active stress distribution

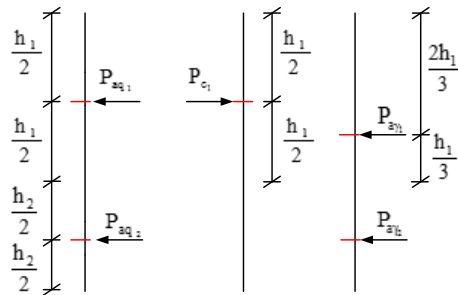


Fig. 11.17: Example for computing the active pressure point of application

The application point of the whole active force is found using the principle of effects' superposition, being computed as a weighted average. The distances are all computed with respect to a datum, usually considered the base point of the back face.

The distribution is applied only to the solid skeleton, so in the case of ground water table the pore water distribution is isotropic and  $\gamma'$  is used.

In the case of the passive resistance we have similarly:

$$\sigma_h = \sigma_v \cdot k_p + 2 \cdot c \cdot \sqrt{k_p} \quad (11.21)$$

where

$$k_p = \tan^2\left(45^\circ + \frac{\phi}{2}\right) \quad (11.22)$$

Remark: The effect of shear in strength parameters has to be always beneficial.

$$k_p > 1 \quad (11.23)$$

$$k_0 \approx 0.6 \quad (11.24)$$

$$k_a \approx 0.4 \quad (11.25)$$

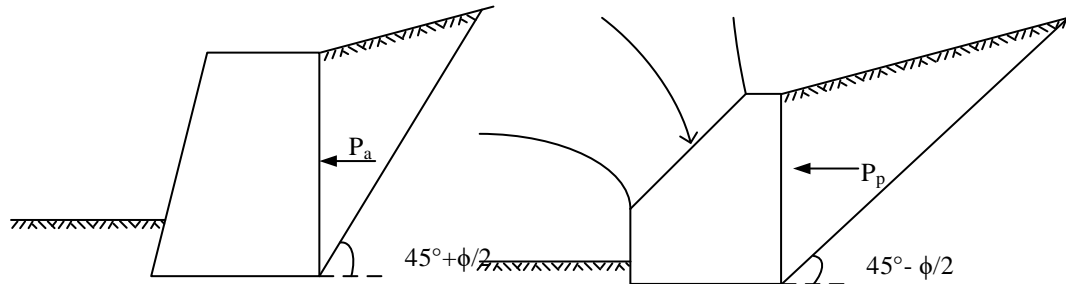


Fig. 11.18

Fig. 11.19

### 11.1 Test your understanding

#### Problem 11.1

What is the minimum horizontal stress created by soil?

#### Problem 11.2

What is the maximum horizontal stress created by soil?

#### Problem 11.3

How does groundwater affect the soil thrust upon a structure?

#### Problem 11.4

How does the shear strength parameters influence the soil active thrust?

#### Problem 11.5

How does the shear strength parameters influence the soil thrust?

#### Problem 11.6

A soil mass has the following properties:

- $\gamma = 18.5\text{kN/m}^3$ ;
- $\gamma_{\text{sat}} = 20.2\text{kN/m}^3$ ;
- $\phi' = 27^\circ$ ;
- $c' = 5\text{kPa}$ .

Draw the vertical stress diagram for 10m depth, considering the groundwater table to be found at 5m depth.

#### Problem 11.7

A soil mass has the following properties:

- $\gamma = 17.5\text{kN/m}^3$ ;

- $\gamma_{\text{sat}} = 19.8\text{kN/m}^3$ ;
- $\phi' = 32^\circ$ ;
- $c' = 0\text{kPa}$ .

Draw the horizontal stress diagram for 10m depth, considering the groundwater table to be found at 5m depth.

**Problem 11.8**

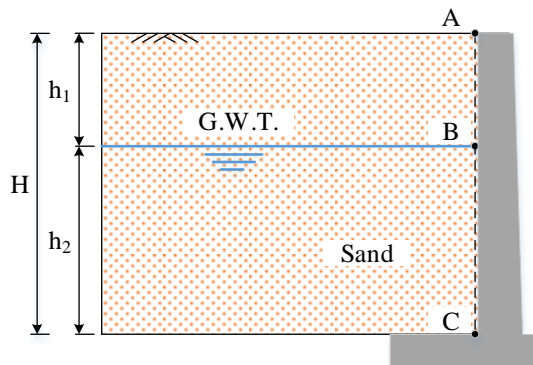
A soil mass has the following properties:

- $\gamma = 19.0\text{kN/m}^3$ ;
- $\gamma_{\text{sat}} = 20.5\text{kN/m}^3$ ;
- $\phi' = 19^\circ$ ;
- $c' = 50\text{kPa}$ .

Draw the horizontal stress diagram for 10m depth, considering there is no groundwater.

**Problem 11.9**

A retaining wall having the thickness  $H=10.5\text{m}$  is backfilled with sand with the bulk unit weight  $19\text{kN/m}^3$  and the saturated unit weight  $20\text{kN/m}^3$ . The shearing strength parameters of the soil are  $\phi'=32^\circ$  and  $c'=0\text{kPa}$ . The groundwater table is located at a depth  $h_1=4.2\text{m}$ . Compute the vertical stresses in the soil along a vertical cross-section and display the vertical stress diagrams. Considering the retaining wall as shown in the picture below, compute the total horizontal stresses acting on the retaining wall (in active conditions) and display the total horizontal stress distribution diagrams.





## 12 SITE INVESTIGATION

The first prerequisite for soil investigation on the site is putting together a preliminary documentation which establishes the future civil engineering work parameters such as the structure's depth and plane extent, approximate loads and special requirements. Using this information, the building's **active zone**, namely **the underground region influenced by the loads from the structure** may be assessed. Furthermore, the documentation regarding the geological background of the site is essential for the preparing of the site in order to set what kind of equipment is necessary to be used for in-situ tests and sampling.

In-situ tests have the advantage that are carried-out on a larger scale (usually acting directly on the soil mass over a large area) and removing the disturbance induced by removing the soil pieces from their place (sampling), transport to the laboratory and extrusion into testing samples. On the other hand, in-situ test may not be as accurate as the laboratory ones since the testing parameters are hard to be measured, the environment itself may have strong influence on the final results which are generally obtained by empirical correlations processing.

The most used in-situ mechanical tests are:

- penetration tests: standard penetration test (SPT), static cone penetration test (CPT), light, heavy or super-heavy dynamic probing test (DPL, DPH, DPSH);
- plate load tests (PLT): to the ground surface or in the borehole;
- Menard pressure-meter test;
- Marchetti dilatometer test (DMT);
- vane test.

The geophysical tests implement different principles of physics for investigating the soil subsurface. The most commonly used methods are:

- electrical resistivity methods: vertical electrical sounding (VES), electrical resistivity tomography (ERT);



- magnetic methods: magnetometric survey;
- electro-magnetic methods: ground penetrating radar (GPR);
- mechanical waves propagation method: spectral analysis of surface waves (SASW), multi-channel analysis of surface waves (MASW), shooting down-hole test, shooting cross hole test.

Sometimes hybrid methods are used for in-situ investigation, for example: seismic Marchetti dilatometer test (SDMT) and seismic cone penetration test (SCPT).

In order to determine soil parameters in laboratory conditions, material samples need to be taken from the site at various depths. Depending on the disturbance induced to the sample, they may be disturbed, case in which the moisture content and texture are preserved, but the structure is remoulded and undisturbed, when the soil retains as much as possible its structure, too.

The means of obtaining soil samples are:

- trenches - open and unsupported excavation reaching a maximum depth of 3m. In case the depth is greater than 1.5 m the stable slope of the trench's walls shall be computed;
- pits - open and supported (using timbering or sheet piles) excavation which reach 10-12m depth (this solution is costly and seldom used);
- boreholes (the most used method of investigation), which may reach depths of tens up to (rarely) hundreds of meters as required.

Depending on the depth of the borehole, the type of soil or rock that will be encountered, and the time available for the drilling works, various drilling machines and methods are used, as described in the following chapters.

### **12.1 Planning the site investigation**

A site investigation program for a future structure can be divided in four phases:

1. Gathering information regarding the structure, such as: base shape and area, future use, column spans, induced loads, requirements of local building codes, etc.

2. Collecting existing information regarding the site from: ortho-photo, morphological, geological, hydro-geological, climate, hazard maps etc.
3. Site visit where the geotechnical engineer visually inspects the site in order to observe area related particularities not depicted in the documents used during the previous stage. Site vegetation may provide information regarding the subsoil type and conditions, cracks of the soil surface or of the neighbouring structures may indicate the existence of soft clays, existing water wells indicate an approximate ground water table depth. Another important information to be gathered during the visit is site accessibility.
4. Detailed site investigation consisting of programmed geotechnical survey works, such as: geotechnical boreholes, in-situ and laboratory tests.

As a rule of thumb to the necessary investigation depth, from consideration of the active zone of the structure (stress distribution of loads in the soil mass), the following depths may be used:

- For direct foundations the investigated depth should be greater than the depth at which the vertical total stress induced by the foundation is equal to 10% of the stress applied by the foundation base.
- For retaining walls, the investigation depth has to be at least two times greater than the probable length of the retaining structure
- For roads the investigated depth ranges from two to six meters keeping in mind the roads importance class.
- For landslides the investigated depth has to be two times greater than the depth at which the failure surface is located.



Fig. 12.1 Manually dug trench.



Fig. 12.2 Mechanically excavated trench.

## 12.2 Manual drilling

Manual drilling is used for depths up to 10-15m (exceptionally up to 30m) in fine to medium coarse soils (not suitable for gravels). It's the most cost-efficient method for shallow investigation depth, that usually provides (depending on the drilling personnel and the quality of the samplers) the best soil and water samples. It can be performed on sites with rough terrain (steep slopes) and limited access (basements, sites with bad access roads for large vehicles), with minimum mobilization costs. Limitations: manual drilling is considerably slower than mechanical drilling, being totally inefficient for great depths. Also, below the ground water table drilling is very slow and the quality of the soil sample decreases. The auger is driven into the soil as a result of the torque moment produced by the two operators of the rig. When the auger reaches a depth equal to its length and becomes filled with drill debris, its advancing is hindered so it is extracted together with the drilling rods in order to be emptied. For every 2 meters depth or for every change in lithology, after the extraction procedure a gravitational sampler is introduced into the borehole to retrieve an undisturbed soil sample. The soil sample is best retrieved in thin-walled (1-2 mm) steel tubes with inner diameters greater than 75 mm called Shelby Tubes. An alternative option, which sometimes yields better samples, is the use of plastic liners confined in a specially designed metal tube.

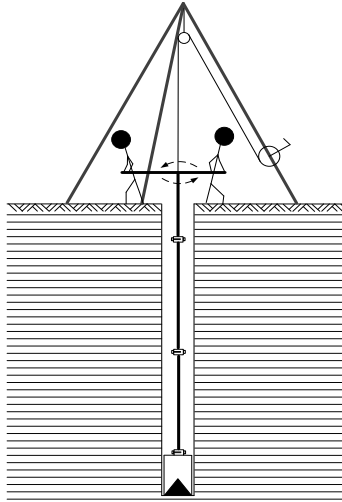


Fig. 12.3 Principle of manual drilling.



Fig. 12.4 Manual drilling.

- Mechanical drilling works mainly by the same principles as the manual drilling but it has multiple advantages:
  - it is much faster since the drilling tool (corer) is longer (1÷3m) and spins with a higher RPM and also the drilling line more easily retrieved
  - it can drill in coarse soils and cemented rocks
  - it may reach greater depths, even up to 12 m depth (in the field of geotechnical engineering the investigated depths reach a usual maximum value of 50 m)

There are various types of mechanical drilling methods, only a few of them being used for geotechnical engineering purposes.

### 12.3 Direct circulation drilling

The drilling rods are hollow and provide a channel for the circulation of the drilling fluid to the bottom of the borehole through the tip of the core barrel. The drilling fluid plays multiple roles: it lubricates, cools and cleans the drilling bits (the tip part of the core barrel made of sharp hard metal alloys), provides hydrostatic pressure which stabilizes the borehole walls and removes the drill cuttings (“detritus” = soil and rock fragments dislocated by the drilling bits during drilling) from the bottom of the borehole and carries

them towards the surface. This method is the most commonly used in geotechnical engineering investigations. The steps of performing a borehole are very similar to the ones from manual drilling (advancement of the core barrel, extraction of the drilling line and Shelby tubes soil sampling), but this method conveys more information about the ground lithology, since it allows for the extraction of only slightly disturbed samples within the core barrel while drilling in cohesive soils

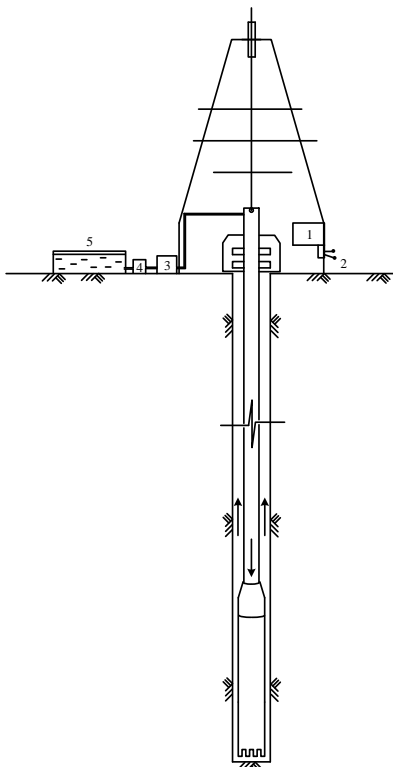


Fig. 12.5: Mechanical drilling principle



Fig. 12.6: Mechanical drilling (wire line)

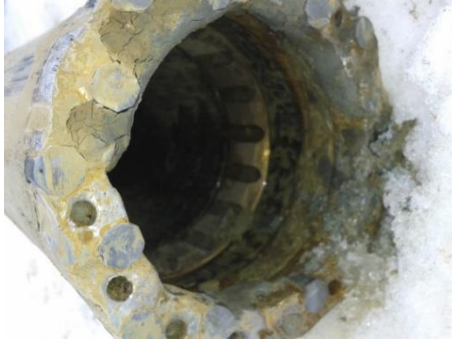


Fig. 12.7: Drilling bit



Fig. 12.8: Core catcher



Fig. 12.9: Retrieving the soil sample in Shelby tube



Fig. 12.10: Core boxes

#### **12.4 Reverse circulation drilling**

Reverse circulation drilling works in the same way as direct circulation drilling, except that the flow direction of the drilling fluid is reversed. The cuttings are pumped upwards to a large collection facility at the surface

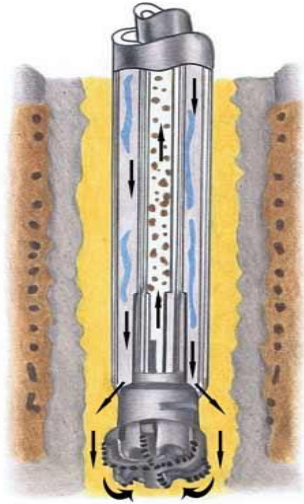


Fig. 12.11: Reverse circulation drilling

In Romania the typical reverse circulation rig was FA-12 which was used mainly for water wells, sometimes for pile boring and was based on two different systems: absorption and airlift. For the airlift system, the fluid was pumped through two small pipes attached to the exterior of the drilling line tube instead the larger outer tube and the absorption system worked with a vacuum pump. The airlift system is also used for pumping wells sand removal.

## 12.5 Sampling methods

Based on the laboratory tests requirements, soil samples can be provided as both disturbed and undisturbed. Disturbed samples maintain only the initial moisture content, while undisturbed ones also maintain the original structure and mechanical properties of the soil from the site.

### 12.5.1 Moulds

The knife is used to prevent sample disturbance while the collar is used to provide a supplementary amount of soil which allows proper trimming of the sample at the mould face. Samples taken by moulds must preserve their original moisture content. Since the soil is trimmed at the mould face, sealants can't be used and the best way to carry them is in small tight bags.



Fig. 12.12: Sampling moulds at the soil's surface

### **12.5.2 Boxes**

Usually made of wooden panels, boxes are used to keep block samples from mechanical damage. The block samples are cut directly from the open excavation (trenches or pits), sealed in plastic bags, wrapped with adhesive tape and then boxed. Although large samples provide better quality, their dimension is limited to 30x30x30cm for the sake of transportation and handling. Blocks do not have to be perfectly rectangular but they must fit well in boxes.





Fig. 12.13: Shaping a block sample

### ***12.5.3 Shelby (Osterberg) tubes***

They are stainless thin-walled (referring to the ratio tube length to diameter and tube thickness to knife cutting part thickness) steel tubes used to sample soil from boreholes. The tube is pressed or driven into the base of the borehole and when it is filled with soil it is pulled to the surface. Immediately after extraction, the tubes must be sealed with paraffin wax for preserving the moisture content of the sample. Additional plastic caps are attached to each end of the tube in order to protect the paraffin sealing. Each Shelby tube must be labeled with the corresponding site, borehole number, sampling depth and date.



Fig. 12.14: Waxing the Shelby tubes



Fig. 12.15: Sealed Shelby tube

## **12.6 Standard penetration test (SPT)**

The standard penetration test (SPT) was developed in the early 20<sup>th</sup> century by Harry Mohr, an engineer working for Gow Construction Co., a construction company in Boston. The procedure was initially standardized around the '20s by Mohr, but became more popular after Karl Terzaghi sponsored its adoption through ASCE's Committee on Sampling and Testing of the Soil Mechanics and Foundations Division of ASCE. Some of the first studies were performed at Harvard by Juul Hvorslev and by late '40s, Terzaghi and Mohr developed correlations between allowable bearing pressure and SPT blowcounts in sand.

SPT is used mainly in cohesionless soils, where undisturbed sampling is very difficult. The test is performed inside the borehole and consists in counting the number of blows (from a slide hammer with a weight of 63.5kg falling through a distance of 760mm) required for the advance of a thick-walled sample tube (outer diameter of 50mm and an inside diameter of 35mm) over a distance of 45cm. The penetration depth is divided into three intervals of 15

cm. The number of blows for the first interval is recorded, but is not taken into account in the final processing (the first 15 cm are considered the fixing distance). The last two sets of readings (for the final 30cm) are reported and usually denoted by  $N_{30}$  or  $N_{SPT}$ .

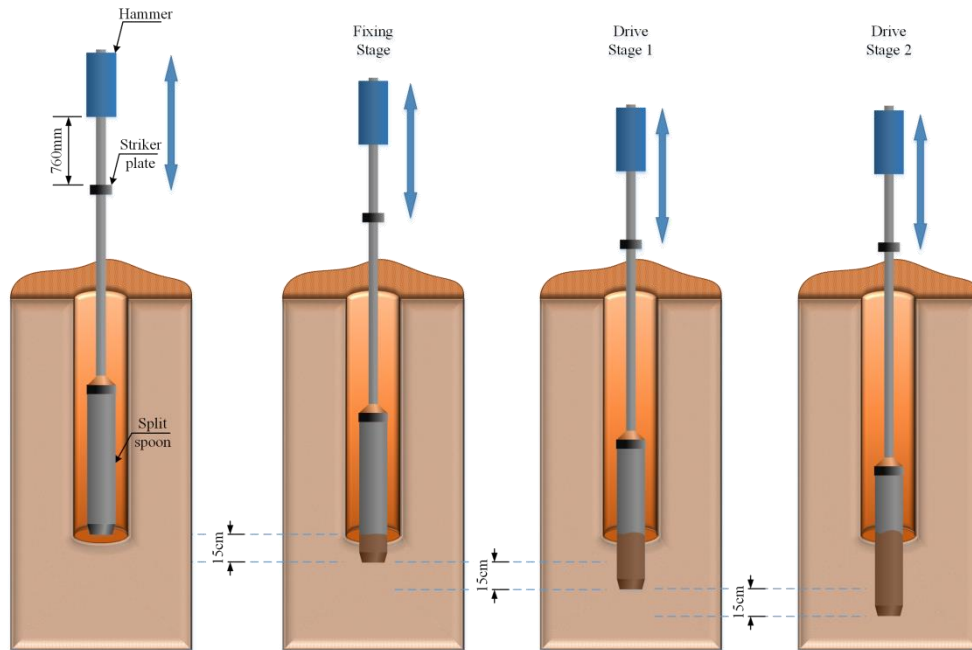


Fig. 12.16 The Standard Penetration Test



Fig. 12.17 Modern split spoon sampler

The value used for geotechnical parameters assessment is usually based on  $N_{60}$ , which is a corrected value of  $N_{SPT}$  to a 60% energy ratio. Following the determination of  $N_{60}$ , there may be a need for overburden pressure correction also, but only for cohesionless soils, resulting  $(N_1)_{60}$ . Furthermore, for fine sand or silt under groundwater table with  $N_{SPT} > 15$ , a dilatancy correction is also to be made, resulting  $(N_1)_{60(CORR)}$ .

Obtaining  $N_{60}$  is based on corrections due to various factors, as described in the formula below:

$$N_{60} = N_{SPT} \frac{C_H C_B C_S C_R}{0.6} \quad (12.1)$$

where

$C_H$  – hammer correction, found in Tab. 12.1;

$C_B$  – borehole diameter correction, found in Tab. 12.2;

$C_S$  – split sampler correction, equal to 1.0 for standard sampler (other samplers have 1.2 factors but are not recommended);

$C_R$  – rod length correction, found in Tab. 12.3.

Tab. 12.1: Hammer correction values

Hammer type	Hammer release mechanism	Correction factor, C <sub>H</sub>
Automatic	Trip	0.70
Donut	Hand dropped	0.60
	Cathead + 2 turns	0.50
Safety	Cathead + 2 turns	0.58
Drop / Pin	Hand dropped	0.45

Tab. 12.2: Borehole diameter correction values

Borehole diameter	Correction factor, C <sub>B</sub>
65 ÷ 115 mm	1.00
150 mm	1.05
200 mm	1.15

Tab. 12.3: Rod length correction values

Rod length	Correction factor, C <sub>R</sub>
< 4 m	0.75
4 ÷ 6 m	0.85
6 ÷ 10 m	0.95
> 10 m	1.00

As previously stated, the overburden pressure influences the penetration resistance in cohesionless soils. After a certain depth, the penetration resistance will be higher due to the overburden pressure. This was only introduced in 1957 by Gibbs & Holtz [32] and several attempts have been made to introduce a correction (using 280kPa and 138kPa reference pressures). It was only after 1974 that the geotechnical community has agreed to use 100kPa reference pressure, using Peck's proposal [33] corresponding to an average overburden pressure at 5m depth. Since then, all SPT values in cohesionless soils are corrected as follows:

$$(N_1)_{60} = C_N N_{60} \quad (12.2)$$

where C<sub>N</sub> is the overburden pressure correction factor, which can be computed using one of the following relations:

$$C_N = 0.77 \lg \left( \frac{2000}{\sigma'_0} \right), [33] \quad (12.3)$$

$$C_N = \sqrt{\frac{100}{\sigma'_0}}, [34] \quad (12.4)$$

where  $\sigma'_0$  is the effective pressure at the corresponding depth.

Finally, below the groundwater table, the SPT value needs to be corrected, which is usually done using the relation proposed by Terzaghi and Peck [35]:

$$(N_1)_{60(\text{CORR})} = 7.5 + 0.5(N_1)_{60} \quad (12.5)$$

### 12.6.1 Density index

The density index of soil can be assessed by means of SPT results using various correlations proposed by different authors. Eurocode 7 [36] proposes the following relation for sand, which is introduced by Meyerhof [37]:

$$I_D = \sqrt{\frac{N_{60}}{a + b \sigma'_0}} \quad (12.6)$$

The values of parameters a and b were studied and proposed by Skempton [38], which also noticed a constant ratio between  $(N_1)_{60}$  and  $I_D^2$ , hence:

$$I_D = \sqrt{\frac{(N_1)_{60}}{c}} \quad (12.7)$$

Tab. 12.4: Values of parameters for density index, reported by Skempton

Soil type	a	b	c
Fine sand (Ogishima Island)	17	17	34
30-50 years infill (Kawagishi-cho)	18	26	44
Relatively recent alluvial sand (Niigata)	27	28	55
Medium alluvial sand (Niigata, river site)	46	26	72
Dense coarse sand	45	20	65
Fine uncemented sand (Norwich Crag)	38	50	88

For normally consolidated natural sand deposits, the best average correlation between blow count and relative density is described in the table below, as

reported by Skempton from Terzaghi and Peck (also recommended by Eurocode 7):

Tab. 12.5: Density index classification [35]

$I_D=0$	15	35	50	65	85	100%
very loose	loose		medium		dense	very dense
$(N_1)_{60=0}$	3	8	15	25	42	58

Generally, it is noted that for non-loose sands ( $I_D > 0.35$ ), the c coefficient is approximately 60, hence:

$$I_D \cong \sqrt{\frac{(N_1)_{60}}{60}}, \text{ for } I_D > 0.35 \quad (12.8)$$

A similar classification is given by Gibs-Holtz (Tab. 12.6) and AASHTO (Tab. 12.14).

Tab. 12.6: Density index classification [32]

$I_D=0$	15	35	65	85	100%
very loose	loose		medium	dense	very dense
$(N_1)_{60=0}$	4	10	25	50	

Tab. 12.7: Density index classification [39]

$I_D=0$	20	40	70	85	100%
very loose	loose		medium	dense	very dense
$(N_1)_{60=0}$	4	10	25	50	

The need for an analytical relation for finding the density index has lead Meyerhof [37] – equation (12.9) – and Cubrinovski and Ishihara [40] – equation (12.10) – to the relations shown below.

$$I_D = \sqrt{\frac{N_{60}}{17 + 24 \frac{\sigma'_0}{p_a}}} \quad (12.9)$$

where

$\sigma'_0$  – effective overburden stress at test depth;

$p_a$  – atmospheric pressure.

$$I_D = \sqrt{\frac{N_{60} \left(0.23 + \frac{0.06}{d_{50}}\right)^{1.7}}{9} \frac{98}{\sigma'_0}} \quad (12.10)$$

where  $d_{50}$  is the diameter for which 50% of the particles by mass are smaller, in mm.

Finally, a more recent research proposed by Mayne [41] recommends a relation that takes into account the grain size, the age of the deposit and the overconsolidation ratio:

$$I_D = \sqrt{\frac{(N_1)_{60}}{[60 + 25 \lg(d_{50})] \cdot \left[1.2 + 0.05 \lg\left(\frac{t}{100}\right)\right] \cdot \text{OCR}^{0.18}}} \quad (12.11)$$

where

- t – estimated age of the deposit [years];
- OCR – overconsolidation ratio

### 12.6.2 Consistency index

Similar to the estimation of density index, various authors have established correlations between the SPT blowcount and the consistency index, when performing the test in cohesive materials. Peck et al. [33] proposed a classification, as shown in Tab. 12.8, while AASHTO [39] recommends the classification described in Tab. 12.9.

Tab. 12.8: Consistency index classification [33]

$I_c=0 \dots 0.25$	0.50	0.75	0.85	1
very soft	soft	firm	stiff	very stiff
$N_{60}=0 \dots 2$	4	8	16	32

Tab. 12.9: Consistency index classification [39]

$I_c=0 \dots 0.25$	0.50	0.75	0.85	1
very soft	soft	firm	stiff	very stiff
$N_{60}=0 \dots 1$	4	8	15	30



### 12.6.3 Unit weight

The unit weight estimation can be made based on recommendations given by Peck et al. [33] and Bowles [42]. Tab. 12.10 shows bulk unit weight values are for cohesionless soils and saturated unit weight estimations for cohesive materials. Furthermore, submerged unit weight estimates are found in Tab. 12.11.

Tab. 12.10: Bulk and saturated unit weight estimated values

$N_{60}$	$\gamma$ [kN/m <sup>3</sup> ] cohesionless soil	$N_{60}$	$\gamma_{sat}$ [kN/m <sup>3</sup> ] cohesive soil
0...4	<15.7	0...2	<15.7
		2...4	15.7...18.8
4...10	14.9...19.6	4...8	17.3...19.6
10...30	17.3...20.4	8...16	18.1...20.4
30...50	17.3...22.0	16...32	18.8...22.0
>50	>20.4	>32	>20.4

Tab. 12.11: Submerged unit weight estimated values

$N_{60}$	$\gamma'$ [kN/m <sup>3</sup> ] cohesionless soil
0...4	<9.4
4...10	8.6...10.2
10...30	9.4...11.0
30...50	10.5...13.4
>50	>11.8

Based on the tables shown above, the following relations were obtained to estimated various unit weights analytically:

$$\gamma_{sat} = 16.8 + 0.15 N_{60} \text{ [kN/m}^3\text{]}, \text{ for cohesive soils} \quad (12.12)$$

$$\gamma = 16.0 + 0.1 N_{60} \text{ [kN/m}^3\text{]}, \text{ for cohesionless soils} \quad (12.13)$$

$$\gamma' = 8.8 + 0.01 N_{60} \text{ [kN/m}^3\text{]}, \text{ for cohesive soils} \quad (12.14)$$

#### **12.6.4 Internal friction angle**

Estimation of the internal friction angle can be made using various studies, the relations, scope and authors being shown below. For sandy soil, Peck et al. [43] proposed the following relation:

$$\phi' = 27 + 0.3 N_{60} \quad (12.15)$$

Research conducted by Dunham (1954) on various soils have yielded the following equations:

$$\phi' = 25 + \sqrt{12 N_{60}}, \text{ for angular and well-graded soil} \quad (12.16)$$

$$\phi' = 20 + \sqrt{12 N_{60}}, \text{ for round and well-graded soil or angular and uniform-graded} \quad (12.17)$$

$$\phi' = 15 + \sqrt{12 N_{60}}, \text{ for round and uniform-graded soil} \quad (12.18)$$

Osaki et al. (1959) found the following relation for sandy soils:

$$\phi' = 15 + \sqrt{20 N_{60}}, \text{ for angular and well-graded soil} \quad (12.19)$$

Peck et al. [33] recommends the following for granular soils in general:

$$\phi' = 27.1 + 0.3 N_{60} + 0.00054 N_{60}^2 \quad (12.20)$$

More recent research, like Kuhawy and Mayne (1990), supporting the findings of Shmertmann (1975) are recommending for cohesionless soil:

$$\phi' = \tan^{-1} \left[ \frac{N_{60}}{12.2 + 20.3 \frac{\sigma'_0}{p_a}} \right]^{0.34} \quad (12.21)$$

where

$\sigma'_0$  – the effective pressure at the corresponding depth;  
 $p_a$  – the atmospheric pressure.

### 12.6.5 Undrained cohesion

A large amount of research was conducted on the topic of undrained cohesion correlation with SPT blowcount. Tab. 12.12 shows a selection of equations found in literature, together with the scope of application.

Tab. 12.12: Various correlations for undrained cohesion

$c_u$ [kPa]	Soil type	Source
$12.5 \cdot N_{60}$	Clay	[44]
$10 \cdot N_{60}$	Silty clay	
$6.25 \cdot N_{60}$	Fine soils	[45]
$29 \cdot N_{60}^{0.72}$	Fine soils	[46]
$12.5 \cdot N_{60}$	High plasticity soils	[47]
$7.5 \cdot N_{60}$	Medium plasticity soils	
$3.75 \cdot N_{60}$	Low plasticity soils	
$12 \cdot N_{60}$	Clay	[48]
$4.85 \cdot N_{60}$	High plasticity soils	[49]
$6.82 \cdot N_{60}$		
$3.35 \cdot N_{60}$	Low plasticity soils	
$4.93 \cdot N_{60}$		
$4.32 \cdot N_{60}$	Fine soils	
$6.18 \cdot N_{60}$		
$6 \div 7 \cdot N_{60}$	$I_p < 20$	[50]
$4 \div 5 \cdot N_{60}$	$20 < I_p < 30$	
$4.2 \cdot N_{60}$	$30 < I_p$	
$12.5 \cdot N_{60}$	Clay	[51]
$15 \cdot N_{60}$		
$13.9 \cdot N_{60} + 74.2$	Fine soils	[52]
$4.1 \cdot N_{60}$	Fine soils	[53]
$3.33 \cdot N_{60} - 0.75 \cdot w + 0.20 \cdot w_L + 1.67 \cdot I_p$		[54]
$3.24 \cdot N_{60} - 0.53 \cdot w - 0.43 \cdot w_L + 2.14 \cdot I_p$		

### **12.6.6 Linear deformation modulus**

Estimating the linear deformation modulus based on SPT test results can be a discouraging process since there are many relations available, each obtained from very specific tests, and they yield very different results. For practicality reasons, we will only mention the relation we consider to be the most suitable in assessing the linear deformation modulus, since it is fairly conservative. It is described by Bowles [55] as follows:

$$E_s = \beta_0 \sqrt{\text{OCR}} + \beta_1 N_{60} \quad (12.22)$$

where

- OCR – the overconsolidation ratio;
- $\beta_0, \beta_1$  – factors given in the table below.

Tab. 12.13: Factors to be used with equation (12.22)

Soil type	$\beta_0$ [kPa]	$\beta_1$ [kPa]
Clean sands (no fines)	5000	1200
Silty sands and clayey sands	2500	600

The overconsolidation ratio should generally be taken as 1, unless there are strong arguments and clear evidence of overconsolidation.

### **12.7 Cone penetration test (CPT)**

The CPT also known as the Dutch Penetration Test consists in pushing an instrumented cone at constant rate of 2 cm/s (procedure called static penetration), and continuous recording starting from the ground surface of the tip resistance on the cone tip and the sleeve friction on a cylindrical surface with the height between 130 to 170mm immediately after the cone. Because a large reaction force is needed, the test requires a heavy truck (CPT truck) working as an operation platform, too. The cone is usually equipped with a porewater pressure sensor and sometimes with a seismic sensor.

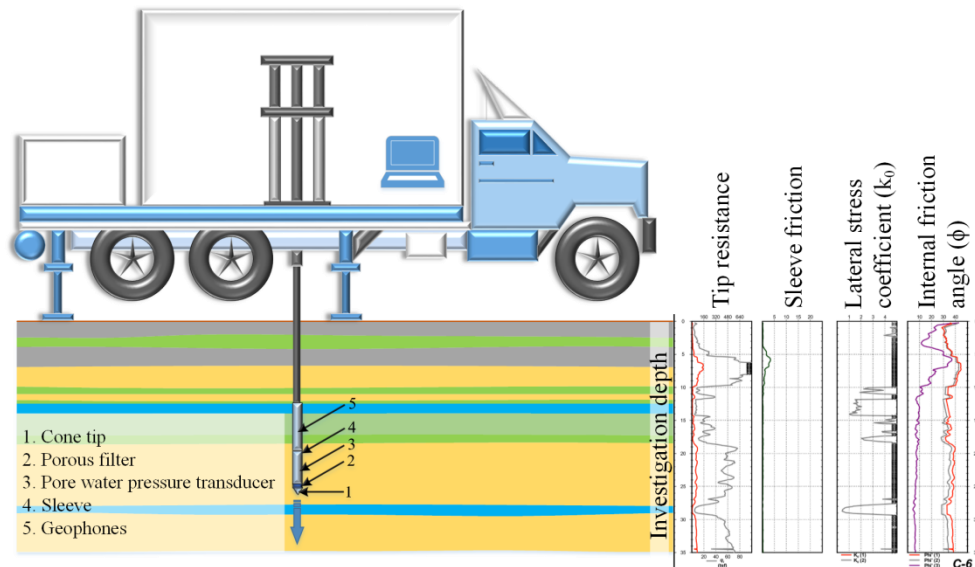


Fig. 12.18: The Cone Penetration Test

### 12.7.1 Tip (cone) resistance

The main parameter obtained from a CPT is the tip (or cone) resistance,  $q_c$ . It is determined as the ratio between the force recorded by the machine and the surface area of the cone.

$$q_c = \frac{Q_c}{A_c} \quad (12.23)$$

If the porewater pressure is also recorded, the corrected tip resistance may be computed according to Lune et al. [56]:

$$q_t = q_c + (1 + a_n)u_2 \quad (12.24)$$

where

$q_t$  – corrected tip resistance;

$q_c$  – tip resistance, computed according to (12.23);

$a_n$  – dimensionless parameter, found in the lab or supplied by the manufacturer;

$u_2$  – the recorded value of the porewater pressure.

A correction with overburden stress is used for the tip resistance, as follows:

$$Q_{tn} = \left( \frac{q_t - \sigma_{v0}}{p_a} \right) \left( \frac{p_a}{\sigma'_{v0}} \right)^n \quad (12.25)$$

where

$q_t$  – tip resistance corrected with porewater pressure;

$\sigma_{v0}$  – geologic stress;

$(q_t - \sigma_{v0})$  – net tip resistance;

$p_a$  – atmospheric pressure (typically 100kPa);

$n$  – parameter computed based on  $I_c$ , the SBT (soil behaviour type)

index – see chapter 12.7.4.

$Q_{tn}$  and  $n$  are computed together, iteratively, until the variation of  $n$  between two consecutive computations is less than 0.01. Typical values for  $n$  are:

- $n=0.5$  for clean sand, with  $I_c < 1.64$ ;
- $n=1.0$  for clays, with  $I_c > 3.30$ ;
- $n=(I_c-1.64)0.3+0.5$ , with  $1.64 < I_c < 3.30$ .

### **12.7.2 Sleeve friction**

The sleeve friction,  $f_s$ , is found as the ration between the recorded force on the lateral surface of the cylinder and its area:

$$f_s = \frac{F_s}{A_s} \quad (12.26)$$

Also, this value can be corrected with the porewater pressure:

$$f_t = f_s - b_n u_2 \quad (12.27)$$

where

$f_t$  – corrected sleeve friction;

$f_s$  – sleeve friction, computed according to (12.26);

$b_n$  – dimensionless parameter, found in the lab or supplied by the manufacturer;

$u_2$  – the recorded value of the porewater pressure.

### **12.7.3 Friction ratio**

There is frequently employed an indicator called friction ratio, which is the ratio between the sleeve friction and the tip resistance, in percentage:

$$FR = \frac{f_s}{q_c} 100 \text{ [%]} \quad (12.28)$$

with its normalized form taking into account the porewater pressure:

$$R_f = \frac{f_s}{q_t} 100 \text{ [%]} \quad (12.29)$$

and the normalized form taking into account the overburden stress:

$$F_r = \frac{f_s}{q_t - \sigma_{v0}} 100 \text{ [%]} \quad (12.30)$$

The friction ratio is usually used to classify the soil by its behaviour or reaction to the cone being forced through it. High ratios generally indicate clayey materials, which yield relatively low tip resistances, while lower ratios are typical for granular material or dry clays. Typical friction ratios are around 1% to 10%.

#### ***12.7.4 Soil Behaviour Type (SBT) index***

Since the CPT does not retrieve soil samples and sometimes the site investigation is not accompanied by sufficient lithological profiling, there was the need of classifying the soil by means of its behaviour during the CPT – hence the soil behaviour type (SBT) index, denoted by  $I_c$ .

One of the first attempts, which quickly grew popular, was proposed by Robertson et al. [57] showing correlations between the cone resistance and the friction ratio (Fig. 12.19). The areas denoted from 1 to 9, describe the following possible soil types:

1. Sensitive, fine grained
2. Organic soils – clay
3. Clay – silty clay to clay
4. Silt mixtures – clayey silt to silty clay
5. Sand mixtures – silty sand to sandy silt

6. Sands – clean sand to silty sand
7. Gravelly sand to dense sand
8. Very stiff sand to clayey sand\*
9. Very stiff fine grained\*  
\* heavily overconsolidated or cemented

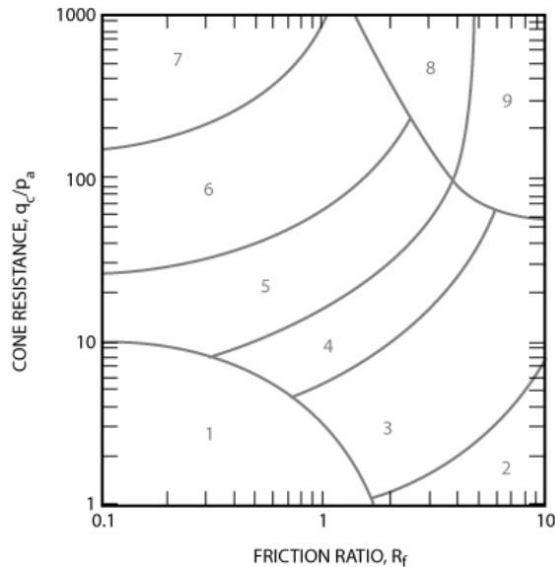


Fig. 12.19: Non-normalized SBT chart [57]

Since both tip resistance and sleeve friction increase with depth due to the increase in effective overburden stress, there was a need of normalizing the classification chart. The normalized approach was introduced by Robertson in 4 years later and is shown in Fig. 12.20. Various zones were introduced, based on test results obtained on different sites. It was observed that most young, un-cemented, insensitive, normally consolidated soils will plot results in a given area. The chart also identifies certain trends in other factors also, such as soil density, OCR, age and cementation and soil sensitivity.



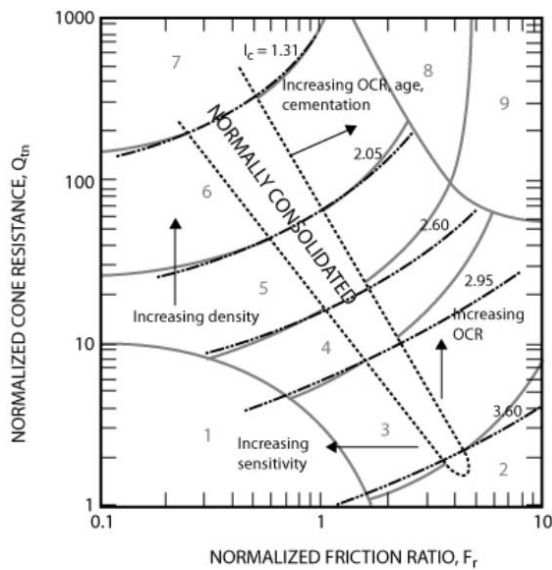


Fig. 12.20: Normalized  $SBT_n$  chart [58]

To simplify the application of the charts presented above, the normalized CPT results ( $Q_t$  and  $F_r$ ) can be combined into one SBT index, denoted by  $I_c$ . The SBT index,  $I_c$ , can be computed using:

$$I_c = \sqrt{(3.47 - \log Q_{t1})^2 + (\log F_r + 1.22)^2} \quad (12.31)$$

where

- $Q_{t1}$  – the normalized tip resistance, using equation (12.25) with  $n=1$ ;
- $F_r$  – normalized friction ratio, using equation (12.30).

### 12.7.5 Equivalent SPT value

Since the Standard Penetration Test is one of the most used in-situ tests, various research has been conducted to find correlations between CPT and SPT. Generally, engineers are more accustomed with SPT results, so they prefer to work with equivalent SPT values from CPT tests. A number of studies have been presented and Robertson and Campanella reviewed them in a set of 2 papers [59] and [60].

Jefferies and Davies [61] found unsatisfactory results using previously published data and suggested improvement for existing relations, by also employing the behaviour type index,  $I_c$ :

$$N_{60} = \frac{\frac{q_t}{p_a}}{8.5 \left(1 - \frac{I_c}{4.6}\right)} \quad (12.32)$$

The above relation was later improved by Robertson [62] to provide better results for insensitive clays:

$$N_{60} = \frac{\frac{q_t}{p_a}}{10^{(1.1268 - 0.2817I_c)}} \quad (12.33)$$

### **12.7.6 Density index**

Based on research published by Baldi et al. [63], one can estimate the density index using the following equation:

$$I_D = \frac{1}{C_2} \ln \frac{Q_{tn}}{C_0} \quad (12.34)$$

where

$C_0$  and  $C_2$  – soil constants, which for normally consolidated, unaged, uncemented, predominantly quartz sand are  $C_0=15.7$  and  $C_2=2.41$ ;

$Q_{tn}$  – normalized CPT resistance, corrected for overburden pressure, computed using the following:

$$Q_{tn} = \left(\frac{q_t}{p_a}\right) \left(\frac{p_a}{\sigma'_{v0}}\right)^{0.5} \quad (12.35)$$

where

$q_t$  – tip resistance corrected with porewater pressure;

$\sigma'_{v0}$  – effective vertical stress;

$p_a$  – atmospheric pressure (typically 100kPa).

For most young, uncemented, silica-based sands, a relation proposed by Kulhawy and Mayne [64] to assess the density index can be simplified to:

$$I_D = \sqrt{\frac{Q_{tn}}{350}} \quad (12.36)$$

### **12.7.7 Unit weight**

A relation proposed by Robertson [65], describing a dimensionless form of the unit weight of soil, normalized to the unit weight of water:

$$\frac{\gamma}{\gamma_w} = 0.27 \log R_f + 0.36 \log \frac{q_t}{p_a} + 1.236 \quad (12.37)$$

where

- $R_f$  – the friction ratio with pore pressure correction – see eq. (12.29);
- $\gamma_m$  – unit weight of water;
- $p_a$  – atmospheric pressure.

### **12.7.8 Internal friction angle**

Robertson and Campanella [59] suggested a correlation to estimate the internal friction angle,  $\phi'$ , for uncemented, unaged, moderately compressible, predominately quartz sands based on controlled CPT results. For sands of higher compressibility, (i.e. carbonated sands or with high mica content), the method predicted low friction angles using the following relation:

$$\tan \phi' = 0.11 + 0.37 \log \frac{q_c}{\sigma'_{v0}} \quad (12.38)$$

For clean, rounded, uncemented quartz sands, Kulhawy and Mayne [64] proposed the following equation, derived from high quality field data:

$$\phi' = 17.6 + 11 \log Q_{tn} \quad (12.39)$$

### **12.7.9 Undrained cohesion**

Theoretical findings indicate the relation between the undrained cohesion and the CPT results has the following form:

$$c_u = \frac{q_t - \sigma_v}{N_{kt}} \quad (12.40)$$

where  $N_{kt}$  is a cone factor value typically ranging from 10 to 18, with an average of 14.  $N_{kt}$  tends to increase with plasticity. When testing sites with limited experience on, estimation of  $c_u$  should be made using the corrected cone factor values from 14 to 16. Upper values will produce more conservative results.

### **12.7.10 Linear deformation modulus**

Correlations between CPT data and linear deformation moduli are sensitive to stress and strain history, aging and mineralogy. However, several attempts have been made in this direction, which for young, uncemented, predominantly silica sands, suggest the following relation:

$$E = 0.015 \cdot 10^{(1.68 + 0.55I_c)} \cdot (q_t - \sigma_{v0}) \quad (12.41)$$

where  $I_c$  is the SBT index, as defined by eq. (12.31).

## **12.8 Dynamic probing (DP)**

The dynamic probing tests consist of driving a scaled rod provided with a non-instrumented cone tip into the soil, continuously, from the ground surface. Depending on the cone shape and the mechanical work applied to the rod, given by the falling weight and the dropping height, the dynamic cone penetration may be light (10kg rammer falling from 0.5m), medium (30kg from 0.5m), heavy (50kg from 0.5m) or super-heavy (63.3kg from 0.75m). The type of dynamic penetration is chosen with respect to the aimed investigation depth and the strength of the soil layers to be passed through. Test results are the number of blows required to drive the rod into the ground over a certain depth, usually over 10cm and denoted by  $N_{10}$ .



Fig. 12.21: Dynamic probing heavy (DPH) equipment

### **12.8.1 Dynamic point resistance**

The first parameter that can be computed from the dynamic probing test is the dynamic point resistance, which can be denoted by  $R_d$ . Computation can be made employing the Dutch formula [66] but using it requires measuring the speed of impact by means of accelerometers, which are usually not available for regular equipment [67]. This was overcome by a simplification made by Butcher et al. [68] which assume a constant acceleration so the formula to compute  $R_d$  becomes:

$$R_d = \frac{m_1^2 \cdot g \cdot h}{A \cdot e \cdot (m_1 + m_2)} \quad (12.42)$$

where

- $R_d$  – the dynamic point resistance [MPa];
- $m_1$  – mass of the hammer [kg];
- $m_2$  – total mass of anvil, guiding system, cone and rods;
- $g$  – gravitational acceleration [ $m/s^2$ ];
- $h$  – fall height of the hammer [m];
- $A$  – the area of the base of the cone [ $m^2$ ];
- $e$  – the average penetration per blow ( $0.1 / N_{10}$ ) [m].

The mass of the hammer and height of fall are standard, depending on the type of test, while the rest of the characteristics may slightly vary depending on the type of equipment. Generally, the values in the table below describe the most common situations.

Tab. 12.14: Common characteristics of dynamic probing equipment

	DPL	DPH
Mass of hammer, $m_1$ [kg]	10	50
Mass of anvil, $m_{\text{anvil}}$ [kg]	2	5
Mass of guiding rods, $m_g$ [kg]	0.5	0.5
Mass of cone, $m_{\text{cone}}$ [kg]	0.5	1
Mass of a rod, $m_{\text{rod}}$ [kg]	3.0	5.5
Surface of the cone, $A$ [ $m^2$ ]	0.001	0.0015
Falling height of the hammer, $h$ [m]	0.5	0.5

### **12.8.2 Density index**

Another geotechnical parameter that can be found is the density index,  $I_D$ , which is a characteristic of granular soils (see chapter 4.4). According to Eurocode 7 [36] there are a few available relations that can be used to assess the density index based on dynamic probing tests, all valid when  $3 \leq N_{10} \leq 50$ .

Above the groundwater table, the following formulas can be employed:

- For uniform sands ( $C_U \leq 3$ ):

$$\begin{aligned} I_D &= 0.15 + 0.260 \lg(N_{10L}) \text{ for DPL} \\ I_D &= 0.10 + 0.435 \lg(N_{10H}) \text{ for DPH} \end{aligned} \quad (12.43)$$

- For non-uniform sands or gravels ( $C_U \geq 6$ )

$$I_D = -0.14 + 0.550 \lg(N_{10H}) \text{ for DPH} \quad (12.44)$$

Below the groundwater table, the Eurocode only refers to formulas valid for uniform sands ( $C_U \leq 3$ ):

$$\begin{aligned} I_D &= 0.21 + 0.230 \lg(N_{10L}) \text{ for DPL} \\ I_D &= 0.23 + 0.380 \lg(N_{10H}) \text{ for DPH} \end{aligned} \quad (12.45)$$

Whenever the methods proposed by Eurocode 7 lose their validity, one can employ the relation shown in C 159 technical guide [69]:

$$I_D \% = 0.98 + 0.554 \lg(N_{10L}) \text{ for DPL} \quad (12.46)$$

Furthermore, various research has been published regarding the processing of dynamic probing results. One notable publication [70] tries to correlate the dynamic probing in dry soils with the density index based on soil grading proposing the following relation:

$$I_D = \left( 104.3312 \cdot e^{\frac{-P_{\text{index}} \sqrt{d_{50}}}{18.1307}} - 1.4769 \right) R_D R_{FC} \text{ for DPH} \quad (12.47)$$

where

$P_{\text{index}}$  – the average penetration per blow ( $100 / N_{10H}$ ) [mm/blow];  
 $d_{50}$  – diameter for which 50% of the particles by mass are smaller

[mm];

$R_D$  – correction factor with depth, found according to (12.48);

$R_{FC}$  – correction factor with fines content, found according to (12.49).

$$R_D = \left( \frac{0.8}{z} \right)^{0.03} \quad (12.48)$$

where  $z$  is the depth, measured in meters.

$$R_{FC} = 1 + 0.003 \cdot F_C \quad (12.49)$$

where  $F_C$  is the percentage of fines by mass.

### **12.8.3 Static cone resistance**

The static cone resistance  $q_c$  can be estimated for various types of granular soils according to C 159 [69]. The equations (12.50) ÷ (12.52) are considered to be valid up to depths of maximum 4.0m.

$$q_c = 0.203 N_{10L} \text{ for fine and medium sands} \quad (12.50)$$

$$q_c = 0.28 N_{20H} \text{ for fine sands} \quad (12.51)$$

$$q_c = 0.66 N_{20H} \text{ for medium and coarse sands} \quad (12.52)$$

### **12.8.4 Oedometric modulus**

According to Eurocode 7 [36], the oedometric modulus can be found based on test results above the groundwater table for uniform sands ( $C_U \leq 3$ ) and low plasticity soils ( $I_P \leq 10$  and  $w_L \leq 35$ ) with at least 0.75 consistency index using the following relation:

$$E_{\text{oed}} = w_1 \cdot p_a \cdot \left( \frac{\sigma'_v + 0.5 \Delta \sigma'_v}{p_a} \right)^{w_2} \quad (12.53)$$

where

$\sigma'_v$  – effective geological stress at the computed depth;

$\Delta \sigma'_v$  – effective vertical stress produced by the foundation at the computed depth;



$p_a$  – atmospheric pressure;  
 $w_2$  – stiffness exponent equal to 0.5 for uniform sands and 0.6 for low plasticity stiff clays;  
 $w_1$  – stiffness coefficient, computed using equation (12.54) for uniform sands or (12.55) for low plasticity stiff clays.

$$\begin{aligned} w_1 &= 71 + 214 \lg(N_{10L}) \text{ for DPL when } 4 \leq N_{10L} \leq 50 \\ w_1 &= 161 + 249 \lg(N_{10H}) \text{ for DPH when } 3 \leq N_{10H} \leq 10 \end{aligned} \quad (12.54)$$

$$\begin{aligned} w_1 &= 30 + 4N_{10L} \text{ for DPL when } 6 \leq N_{10L} \leq 19 \\ w_1 &= 50 + 6N_{10H} \text{ for DPH when } 3 \leq N_{10H} \leq 13 \end{aligned} \quad (12.55)$$

### **12.9 Plate load test**

The plate load test provides a direct measure of the compressibility of soils which are not easily sampled and also of cemented soils and weak (cracked) rocks. The test consists in loading a thick steel plate (square or round shaped) with an area larger than 2500 cm<sup>2</sup> (up to 10000 cm<sup>2</sup>) and recording the deformation of the soil by means of the plate's displacement. The plate is bedded on to the soil to be tested, using sand or cement (to ensure a uniform pressure distribution) and the load is applied in equal increments of about one fifth of the design loading. The test is usually performed at the ground surface and in shallow trenches, but it can be also applied in large diameter cased boreholes.

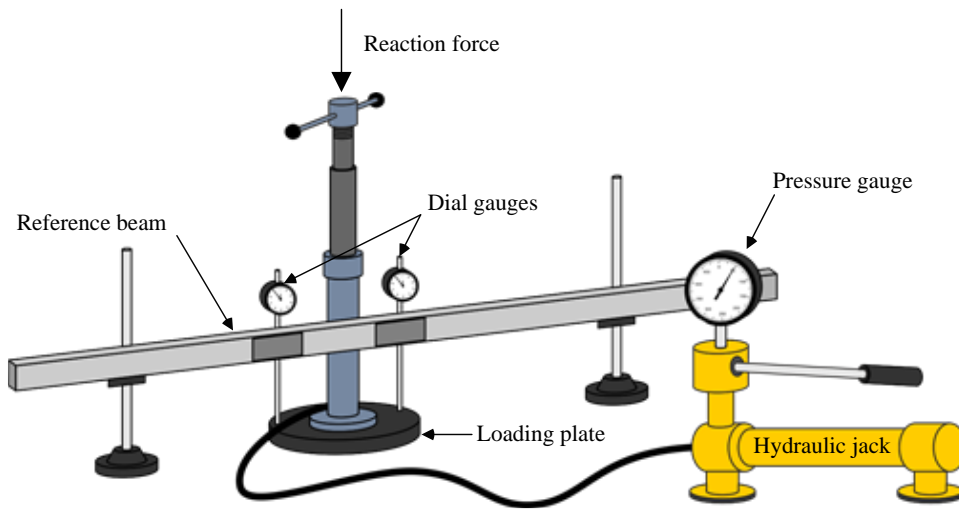


Fig. 12.22: Plate load test equipment



a)



b)



c)



d)



e)



f)

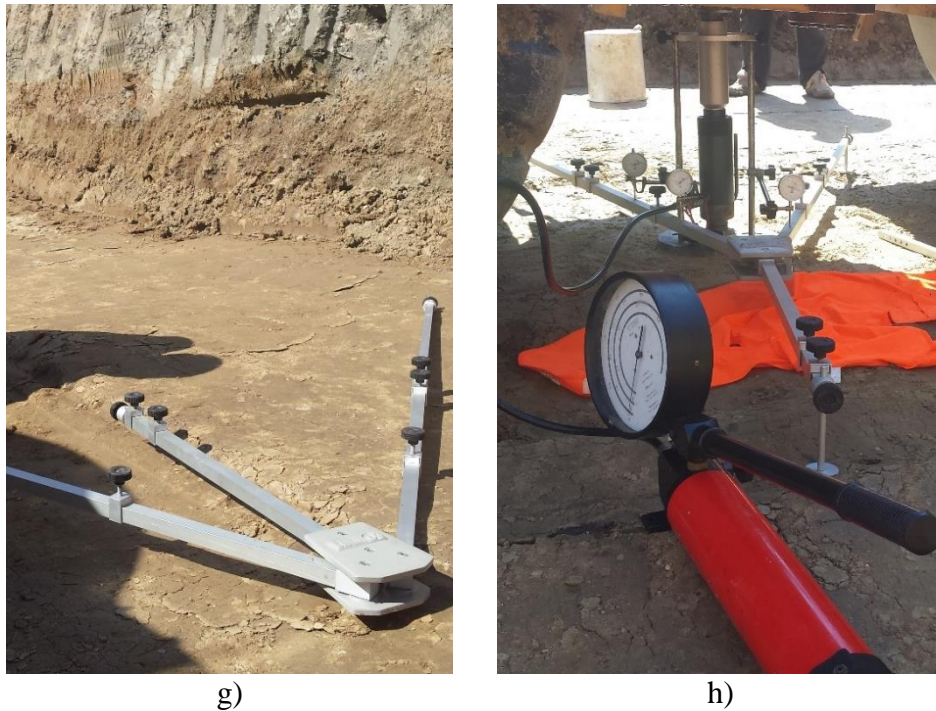


Fig. 12.23: Preparation steps prior to the plate load test

There are two common types of plate load tests, depending on the loading procedure, but they both require the same initial steps in preparation for the test, as described in Fig. 12.23. Preparation for the test is essential since it ensures both the conformity and safety of the test. Step-by-step, the stages described in Fig. 12.23 are as follows:

- a) Sand is poured on the surface where the test is to be conducted;
- b) The sand is spread so that it only forms a thin layer, to ensure a good contact on the base of the plate;
- c) The plate is added and it is carefully levelled to a horizontal position;
- d) A reaction force is provided, usually in the form of a truck or other heavy machinery available on site;
- e) The hydraulic jack and other adjacent elements are added to ensure the contact between the plate and the reaction truck;
- f) The hydraulic pump is connected to the jack;
- g) A reference frame is set-up, to serve as support for the dial gauges;
- h) The dial gauges and the reference frame are added to the plate.

After the installing procedure, the test is performed. Depending on the purpose of the test, there are two common ways to perform it. One testing procedure requires each pressure increment to be applied until the settlement rate is reduced to less than 0.1mm/h. This requires a relatively long testing procedure and is not as commonly performed.

Most commonly, the test is used to assess the quality of compaction works, which is done by the so-called “German” method, by determining the strain modulus,  $E_v$ . The test is performed according to the standard DIN 18134. According to the standard, to determine the strain modulus,  $E_v$ , the load shall be applied in at least 6 stages, with approximately equal increments, until the required maximum stress is reached. Each load increment shall be achieved within 60s and another 120s will pass until reading of the settlement is done and the next load is applied. The load will remain constant during the 120s waiting period.

After reaching the maximum desired load, unloading will be performed in 3 stages: 50%, 25% and approximately 2% of the maximum load. Following unloading, a second loading cycle will be carried out, in which the load is to be increased only to the last but one stage of the first cycle.

For road construction purposes, a 300mm loading plate is usually employed and the maximum applied load is 500kPa. If a settlement of 5mm is reached first, the normal stress measured at this stage is taken as the maximum stress.

When using 600mm plates, the maximum pressure is 250kPa and the maximum settlement is 8mm, while for 762mm plates the maximum values are 200kPa and 13mm respectively.

Processing the results requires charting the load-settlement curve and determining the strain moduli for both loading stages. Calculation of the strain modulus for each load cycle is based on load-settlement fitting curves. These are calculated by means of second-degree polynomial according to the following equation:

$$s = a_0 + a_1 \cdot \sigma_0 + a_2 \cdot \sigma_0^2 \quad (12.56)$$

where

$\sigma_0$  – the average normal stress below the plate [MPa];

- s – the settlement of the plate [mm];
- a<sub>0</sub> – free term of the second-degree polynomial [mm];
- a<sub>1</sub> – first term of the second-degree polynomial [mm/MPa];
- a<sub>2</sub> – second term of the second-degree polynomial [mm/MPa<sup>2</sup>].

For simplicity, the first load (the one with settlement equal to zero) is neglected in computations when fitting the first load-settlement polynomial. However, the first load of the second loading cycle is taken into account when fitting the second load-settlement polynomial.

Finding the parameters of the fitting polynomial is usually done with the aid of computer software, but the standard also formulates a procedure for achieving this by hand. The first strain modulus  $E_{V1}$ , will be evaluated as the secant modulus according to elastic isotropic half-space theory. The secant is determined by the points on the quadratic parabola corresponding to  $0.3\sigma_{0 \max}$  and  $0.7\sigma_{0 \max}$ . The modulus can be computed using the following relation:

$$E_{V1} = \frac{1.5 \cdot r}{a_1 + a_2 \cdot \sigma_{0 \max}} \quad (12.57)$$

where

- r – the radius of the plate [mm];
- a<sub>1,2</sub> – first and second terms of the first loading cycle polynomial [mm/MPa and mm/MPa<sup>2</sup>];
- $\sigma_{0 \max}$  – maximum applied load [MPa].

For the second strain modulus, the following equation will be used:

$$E_{V2} = \frac{1.5 \cdot r}{a_1 + a_2 \cdot \sigma_{0 \max}} \quad (12.58)$$

where

- r – the radius of the plate [mm];
- a<sub>1,2</sub> – first and second terms of the second loading cycle polynomial [mm/MPa and mm/MPa<sup>2</sup>];
- $\sigma_{0 \max}$  – maximum applied load (same as for the first cycle) [MPa].

Usually, for quality control purposes, the scope of works for various projects impose minimum values for  $E_{V2}$  (around 60÷100 MPa, depending on soil

type) and a maximum value for the ratio  $E_{V2} / E_{V1}$  (generally around  $2.2 \div 2.5$ ). A large value of the ratio between the two moduli would imply that the soil was compacted during the test itself and not sufficiently compacted prior to testing.

An example for a plate load test results processing is shown below (the example data is taken from the specific standard). The plate used has a 300 mm diameter and the maximum applied load is 500MPa. Each load-settlement pair is shown in Tab. 12.15.

Tab. 12.15: Typical plate load test results

Cycle	Average pressure $\sigma$ [MPa]	Plate settlements [mm]
contact load	0.010	0.00
load cycle 1	0.080	1.15
	0.160	2.09
	0.250	2.87
	0.330	3.25
	0.420	3.80
	0.500	4.21
unload	0.250	3.96
	0.125	3.71
	0.010	2.59
load cycle 2	0.080	3.23
	0.160	3.53
	0.250	3.79
	0.330	3.99
	0.420	4.13

The data is processed using computer software and the parameters for the two fitting polynomials are found as shown in Tab. 12.16. The results are shown graphically in Fig. 12.24. The relevant data to characterize the tested soil is:  $E_{V2} = 77.74$  MPa and  $E_{V2} / E_{V1} = 2.68$ . These values would usually require more compaction work to be conducted.

Tab. 12.16: Numerical results of the plate load test

Parameter	Load cycle 1	Load cycle 2
-----------	--------------	--------------

$a_0$	0.285	2.595
$a_1$	12.270	7.120
$a_2$	-9.034	-8.451
$E_V$	29.02	77.74
$E_{V2}/E_{V1}$	2.68	

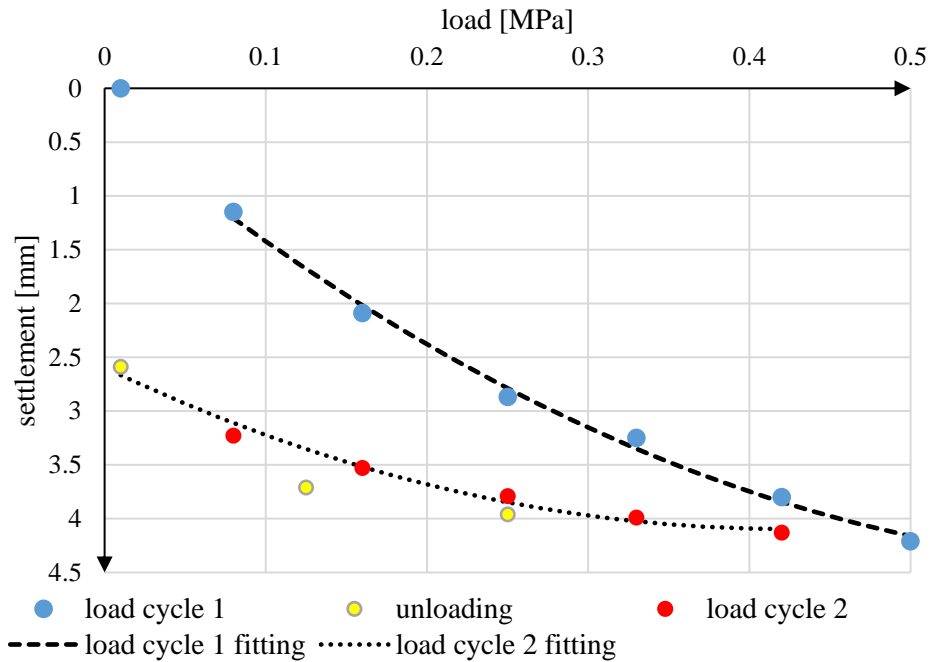


Fig. 12.24: Load-settlement chart for the plate load test

### 12.10 Menard pressuremeter

The pressuremeter is made of a main membrane for which the pressure and volumetric change are recorded. There are three main types of pressuremeter probes: the first, which are used in pre-drilled boreholes, consist only of the inflatable membrane. The second is a self-boring probe, equipped at the bottom with a destructive set of cutting blades. The third type is a displacement probe, which is pushed/driven into the ground. The pressuremeter tests may be conducted under one of the two following possibilities:

- the first is imposing the pressure of the fluid inside the membrane and measuring the lateral deflection of the borehole wall;



- the second method is a step-by-step approach in imposing the borehole wall deflection (volume variation) and recording the pressure variation.

Following the test, a loading, and optional unloading-reloading curves are obtained. These acquired data points are analysed and the final result consist of the lateral earth pressure at-rest

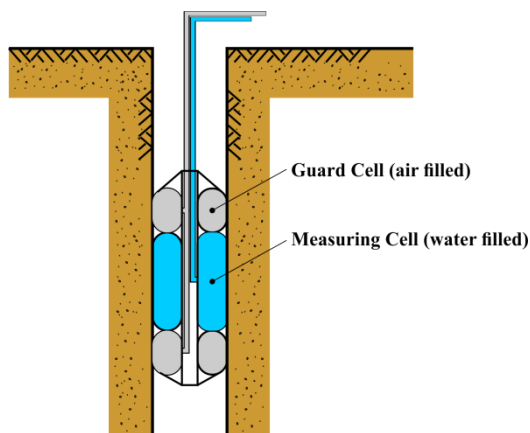


Fig. 12.25: Menard pressuremeter sketch

### **12.11 Marchetti dilatometer test (DMT)**

The flat dilatometer test (DTM) is used for determining the strength and deformability properties of soils through pressure readings from an inserted steel blade equipped with a circular steel membrane that can expand (having a diameter of 60 mm). The test consists in measuring the pressures produced by soil when the steel membrane is at the same level as the blade and when the membrane has deformed 1.1 mm in the direction of the soil. The measurements can be performed in a semi-continuous manner every 20 cm (the blade is pushed into the ground by a CPT truck at a rate of 2 cm/s) or at selected depths (inside the borehole). The test is recommended to be used for clays, silts and sands (the particles must be small in comparison to the membrane diameter). The parameters obtained: material index, horizontal stress index and dilatometer modulus; can characterise the soil lithology, in-situ state of stress and the deformability and shear resistance properties.

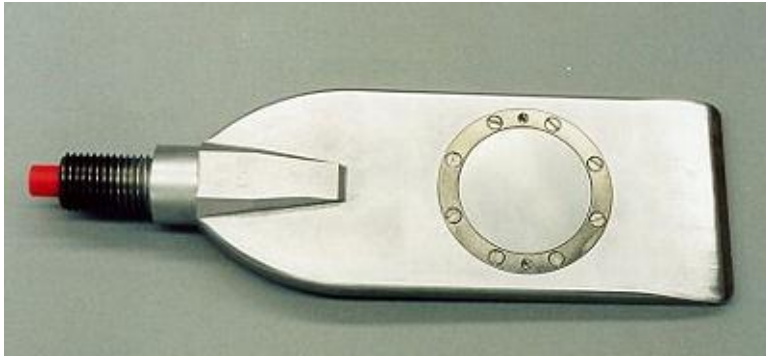


Fig. 12.26 DMT blade.

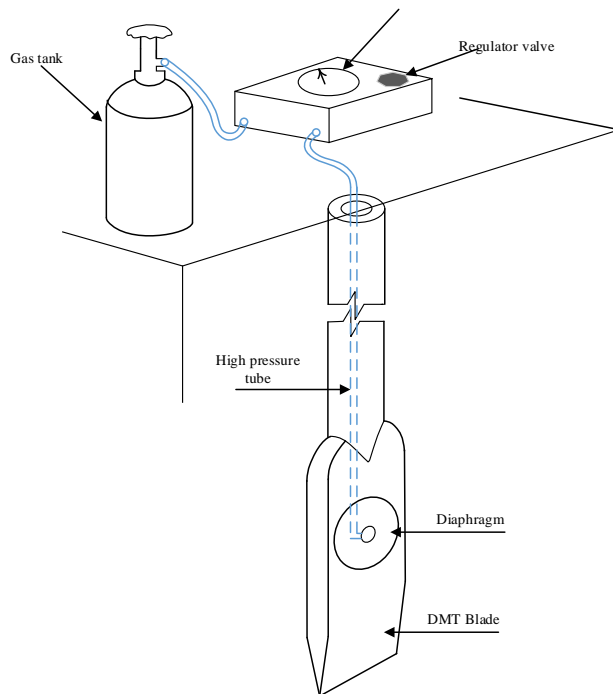


Fig. 12.27: The DMT equipment

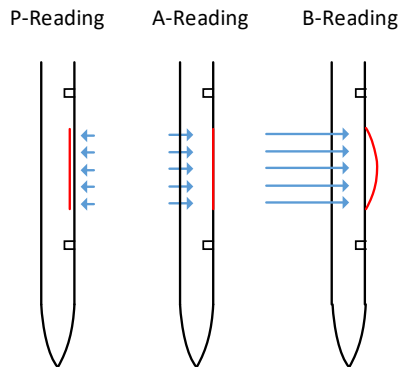


Fig. 12.28: Test steps

### 12.12 Vane test

The Vane test is performed in soft clays and silts (where soil sampling and handling is difficult), for obtaining the undrained shear resistance. The test is performed using four thin, equal sized steel plates welded to a steel rod, creating a 90 angle between each two plates. There are many possible geometric layouts used, but the most common has rectangular plates and a height/diameter ratio of 2 (diameter is usually 20cm). An imposed rotation is applied to the rod (usually 6 /min) and the opposing torque is recorded. Through this rotational movement of the steel plates connected to the rod, a cylindrical failure surface is produced. The recorded torque is divided by the area of the generated failure cylinder, obtaining shear strength of the soil. Under the assumption that the friction angle is 0 , the shear strength is equal to the undrained cohesion of the soil. This assumption generates an overestimation of the cohesion with up to 50%. The test can be performed from the surface, in pre-drilled boreholes. The Vane test can be performed also in laboratory conditions on undisturbed samples (Shelby tubes or boxes) using a small-scale testing equipment (diameter is usually 2cm).

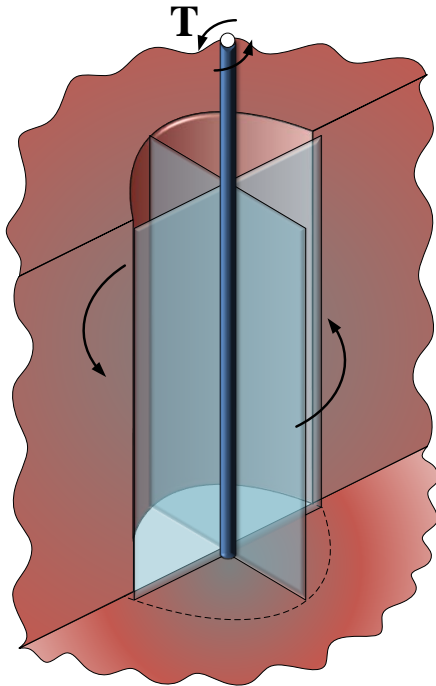


Fig. 12.29: The Vane Test

### 12.13 Test your understanding

#### Problem 12.1

Propose a geotechnical investigation plan for a house with 2 stories in Bucharest on a site with no adjacent buildings. The plan will contain: type, number and depth of investigations. Additionally, propose methods for assessing soil parameters through laboratory or in-situ tests.

#### Problem 12.2

Specify at least two in-situ methods for assessing the shear strength of soil.

#### Problem 12.3

A geotechnical investigation was planned based on 4 boreholes 10m deep, with undisturbed sampling. However, the site conditions showed that only sand and gravel is found below 1.5m depth. Propose some methods to establish the mechanical characteristics of the soil.

#### Problem 12.4

Your client is planning to build a new hotel with 15 stories and 3 basements for parking spaces in an urban area. Propose a set of laboratory tests suitable for the geotechnical investigation.

**Problem 12.5**

The geotechnical investigation performed for a project has shown that the groundwater is found at 4.0m depth, but the construction will require a 6.0m deep excavation, so a dewatering system needs to be designed. What further investigations are required for this purpose?

**Problem 12.6**

A plate load test was performed with a plate having diameter 300mm. The obtained results are shown in the table below. Estimate the two moduli  $E_{v1}$  and  $E_{v2}$  and the ratio between them.

pressure [MPa]	settlement [mm]
0.0100	0.00
0.0500	0.59
0.0900	1.15
0.1300	1.42
0.1700	1.46
0.2100	1.49
0.2500	1.51
0.1250	1.49
0.0625	1.48
0.0125	1.17
0.0500	1.29
0.0900	1.48
0.1300	1.61
0.1700	1.63
0.2100	1.64
0.0125	1.34

**Problem 12.7**

A heavy dynamic probing (DPH) test was performed on a site and the results are shown in the table below. Considering the soil is a non-uniform sand with gravel, with a uniformity coefficient  $C_U = 8.5$ , compute the dynamic

resistance,  $R_d$ , along the investigated depth, considering the characteristics of the equipment are identical to the generic ones.

depth [m]	Number of hits, $N_{10}$ [-]
0.0 - 0.1	8
0.1 - 0.2	31
0.2 - 0.3	31
0.3 - 0.4	19
0.4 - 0.5	15
0.5 - 0.6	13
0.6 - 0.7	20
0.7 - 0.8	12
0.8 - 0.9	12
0.9 - 1.0	11
1.0 - 1.1	8
1.1 - 1.2	8
1.2 - 1.3	7
1.3 - 1.4	7
1.4 - 1.5	5
1.5 - 1.6	5
1.6 - 1.7	3
1.7 - 1.8	4
1.8 - 1.9	4
1.9 - 2.0	6
2.0 - 2.1	6
2.1 - 2.2	7
2.2 - 2.3	8
2.3 - 2.4	7
2.4 - 2.5	9
2.5 - 2.6	8
2.6 - 2.7	8
2.7 - 2.8	7
2.8 - 2.9	7
2.9 - 3.0	7

**Problem 12.8**

A heavy dynamic probing (DPH) test was performed on a site and the results are shown in the table below. Considering the soil is a non-uniform sand with gravel, with a uniformity coefficient  $C_U = 11.2$ , compute the density index,  $I_D$ , along the investigated depth.

depth [m]	Number of hits, $N_{10}$ [-]
0.0 - 0.1	2
0.1 - 0.2	7
0.2 - 0.3	19
0.3 - 0.4	26
0.4 - 0.5	17
0.5 - 0.6	12
0.6 - 0.7	10
0.7 - 0.8	11
0.8 - 0.9	13
0.9 - 1.0	12
1.0 - 1.1	12
1.1 - 1.2	10
1.2 - 1.3	9
1.3 - 1.4	11
1.4 - 1.5	11
1.5 - 1.6	11
1.6 - 1.7	11
1.7 - 1.8	16
1.8 - 1.9	16
1.9 - 2.0	13
2.0 - 2.1	10
2.1 - 2.2	14
2.2 - 2.3	14
2.3 - 2.4	14
2.4 - 2.5	14
2.5 - 2.6	15
2.6 - 2.7	14
2.7 - 2.8	9
2.8 - 2.9	5
2.9 - 3.0	3

**Problem 12.9**

A lightweight dynamic probing (DPL) test was performed on a site and the results are shown in the table below. Considering the soil is a uniform sand with a uniformity coefficient  $C_U = 2.7$ , compute the porosity,  $n$ , along the investigated depth.

depth [m]	Number of hits, $N_{10}$ [-]
0.0 - 0.1	6
0.1 - 0.2	13
0.2 - 0.3	13
0.3 - 0.4	11
0.4 - 0.5	11
0.5 - 0.6	12
0.6 - 0.7	6
0.7 - 0.8	12
0.8 - 0.9	18
0.9 - 1.0	19
1.0 - 1.1	18
1.1 - 1.2	23
1.2 - 1.3	29
1.3 - 1.4	23
1.4 - 1.5	28
1.5 - 1.6	22
1.6 - 1.7	26
1.7 - 1.8	22
1.8 - 1.9	29
1.9 - 2.0	30
2.0 - 2.1	40
2.1 - 2.2	21
2.2 - 2.3	11
2.3 - 2.4	10
2.4 - 2.5	8
2.5 - 2.6	11
2.6 - 2.7	10
2.7 - 2.8	10
2.8 - 2.9	20
2.9 - 3.0	21





## **BIBLIOGRAPHY**

- [1] S. J. Broggs, Principles of sedimentology and stratigraphy, Pearson Education Ltd, 2014.
- [2] SR EN ISO 14688-1, *Partea 1: Identificare și descriere*, Asociația de Standardizare din România, 2004.
- [3] SR EN ISO 14688-2, *Partea 2: Principii pentru o clasificare*, Asociația de Standardizare din România, 2005.
- [4] STAS 1913/5, *Determinarea granulozității*, Asociația de Standardizare din România, 1985.
- [5] SR ISO 3310-1, *Partea 1: Site pentru cernere din țesături metalice*, Asociația de Standardizare din România, 2000.
- [6] ISO 3310-2, *Partea 2: Site pentru cernere din table metalice perforate*, International Standard Organization, 2013.
- [7] SR ISO 3310-3, *Partea 3: Site pentru cernere din folii electroperforate*, Asociația de Standardizare din România, 1998.
- [8] STAS 1913/2, *Determinarea densității scheletului pământului*, Asociația de Standardizare din România, 1976.
- [9] "Fraunhofer," [Online]. Available: [http://www.hoki.ibp.fhg.de/wufi/grundl\\_poros\\_e.html](http://www.hoki.ibp.fhg.de/wufi/grundl_poros_e.html).
- [10] STAS 1913/1-82 *Teren de fundare. Determinarea umidității*, 1982.
- [11] BS 1377-2:1980 *Methods of test for soils for civil engineering purposes - Part 2: Classification tests*, 1990.
- [12] ASTM D 2216-98 *Standard test method for laboratory determination of water (moisture) content of soil and rock by mass*, 1998.
- [13] "Maths Calculations," Kym Presde, [Online]. Available: <http://maths2010.org.uk/wp-content/uploads/2011/07/math-problem1.jpg>. [Accessed 2013].

- [14] STAS 1913/1, *Determinarea umiditatii*, Asociația de Standardizare din România, 1982.
- [15] "VOS instrumenten," [Online]. Available: [http://www.vosinstrumenten.nl/\\_clientfiles/producten/Duran/1\\_24781.jpg](http://www.vosinstrumenten.nl/_clientfiles/producten/Duran/1_24781.jpg). [Accessed 2013].
- [16] *ASTM D 854-10 Standard test method for specific gravity of soil solids by water pycnometer*, 2010.
- [17] STAS 1913/3, *Determinarea densității pământurilor*, Asociația de Standardizare din România, 1976.
- [18] STAS 13006, *Determinarea densității maxime corespunzătoare stării uscate a pământurilor necoezive*, Asociația de Standardizare din România, 1991.
- [19] J. K. Mitchell and K. Soga, *Fundamentals of soil behavior*, New Jersey: John Wiley & Sons, 2005.
- [20] STAS 1913/4, *Determinarea limitelor de plasticitate*, Asociația de Standardizare din România, 1986.
- [21] STAS 1913/6, *Determinarea permeabilității în laborator*, Asociația de Standardizare din România, 1976.
- [22] STAS 8942/1, *Determinarea compresibilității pământurilor prin încercarea în edometru*, Asociația de Standardizare din România, 1989.
- [23] STAS 1913/12, *Determinarea caracteristicilor fizice și mecanice ale pământurilor cu umflări și contracții mari*, Asociația de Standardizare din România, 1988.
- [24] A. W. Skempton, "The pore-pressure coefficients A and B," *Géotechnique*, pp. 143-147, 1954.
- [25] R. Makhnenko and J. Labuz, "Saturation of porous rock and measurement of the B coefficient," in *47th US Rock Mechanics / Geomechanics Symposium*, San Francisco, 2013.
- [26] "Direct Shear Apparatus," Controls Group, [Online]. Available: [http://www.controls-group.com/backend/prodotti/img\\_upload/img\\_big/1202091458100\\_1\\_autoshear\\_27\\_wf2160.....jpg](http://www.controls-group.com/backend/prodotti/img_upload/img_big/1202091458100_1_autoshear_27_wf2160.....jpg). [Accessed 2013].
- [27] "Shear Box in-Place," Controls Group, [Online]. Available: [http://www.controls-group.com/backend/prodotti/img\\_upload/img\\_big/1202091458110\\_2](http://www.controls-group.com/backend/prodotti/img_upload/img_big/1202091458110_2)

- \_detail\_of\_shear\_box\_housing\_resistance techno\_polimeric\_materia  
l.jpg. [Accessed 2013].
- [28] STAS 8942/2, *Determinarea rezistenței pământurilor la forfecare prin încercarea de forfecare directă*, Asociația de Standardizare din România, 1982.
- [29] BS 1377-7, *Part 7: Shear strenght tests (total stress)*, British Standard, 1990.
- [30] BS 1377-8, *Part 8: Shear strenght tests (effective stress)*, British Standard, 1990.
- [31] STAS 8942/5, *Determinarea rezistenței la forfecare prin compresiune triaxială pe probe neconsolidate-nedrenate (UU) pe pământuri coezive*, Asociația de Standardizare din România, 1975.
- [32] H. J. Gibbs and W. G. Holtz, "Research on determining the density of sands by spoon penetration testing," in *Proceedings of the 4th International Conference on Soil Mechanics and Foundation Engineering*, 1957.
- [33] R. B. Peck, W. E. Hanson and T. H. Thornburn, *Foundation engineering*, 2nd ed., New York, 1974.
- [34] S. S. C. Liao and R. V. Whitman, "Overburden correction factors for SPT in sand," *ASCE Journal of Geotechnical Engineering*, pp. 373-377, 1986.
- [35] K. Terzaghi and R. B. Peck, *Soil mechanics in engineering practice*, New York: Wiley, 1948.
- [36] SR EN 1997-2, *Geotechnical design - Part 2: Ground investigation and testing*, ASRO, 2007.
- [37] G. G. Meyerhof, "Discussion on research on determining the density of sands by spoon penetration testing," in *Proceedings of the 4th International Conference in Soil Mechanics and Foundation Engineering*, London, 1957.
- [38] A. W. Skempton, "Standard penetration test procedures and the effects in sands of overburden pressure, relative density, particle size, ageing and overconsolidation," *Géotechnique*, pp. 425-447, 1986.
- [39] AASHTO American Association of State Highway and Transportation Officials, *Manual on subsurface investigations*, 1988.

- [40] M. Cubrinovski and K. Ishihara, "Empirical correlation between SPT N-value and relative density for sandy soils," *Soils and Foundations*, vol. 39, no. 5, pp. 61-92, 1999.
- [41] P. W. Mayne, "Stress-strain-strength-flow parameters from enhanced in-situ tests," in *Proceedings of International Conference on In-Situ Measurement of Soil Properties and Case Histories*, 2001.
- [42] J. E. Bowles, *Foundation analysis and design*, McGraw-Hill, 1977.
- [43] R. B. Peck, W. E. Hanson and T. H. Thornburn, *Foundation Engineering*, New York: John Wiley & Sons, 1953.
- [44] G. Sanglerat, *The Penetration and Soil Exploration; Interpretation of Penetration Diagrams - Theory and Practice*, Amsterdam: Elsevier Publishing Co, 1972, p. 464.
- [45] K. Terzaghi and R. Peck, *Soil Mechanics in Engineering Practice*, New York: John Wiley, 1967, p. 729.
- [46] A. Hara, T. Ohta, M. Niwa, S. Tanaka and T. Banno, "Shear modulus and shear strength of cohesive soils," *Soils and Foundation*, vol. 14, no. 3, pp. 1-12, 1974.
- [47] G. F. Sowers, *Introductory Soil Mechanics and Foundations*, 4th ed., New York: Macmillan, 1979, p. 621.
- [48] I. Nixon, "Standard penetration test: state of the art report," in *Proceedings of the 2nd European Symposium on Penetration Testing*, Amsterdam, 1982.
- [49] O. Sivrikaya and E. Toğrol, "Relations between SPT-N and  $q_u$ ," in *5th International Congress on Advances Civil engineering*, Istanbul, 2002.
- [50] M. A. Stroud, "The standard penetration test in insensitive clays and soft rock," in *1st European Symposium on Penetration Testing*, Stockholm, 1974.
- [51] L. Décourt, "The Standard Penetration Test," Oslo, 1990.
- [52] L. Ajayi and L. Balogun, *Penetration testing in tropical lateritic and residual soils – Nigerian experience*, Rotterdam, 1988.
- [53] H. Hettiarachchi and T. Brown, "Use of SPT Blow Counts to Estimate Shear Strength Properties of Soils: Energy Balance Approach," *Journal of Geotechnical and Geoenvironmental Engineering*, vol. 135, no. 6, 2009.

- [54] O. Sirvikaya, "Comparison of Artificial Neural Networks Models with Correlative Works on Undrained Shear Strength," *Eurasian Soil Science*, vol. 42, no. 13, p. 1487–1496, 2009.
- [55] J. E. Bowles, *Foundation analysis and design*, New York: McGraw-Hill, 1982.
- [56] T. Lunne, P. Robertson and J. Powell, *Cone Penetration Testing in Geotechnical Practice*, London: EF Spon/Blackie Academic, Routledge Publishers, 1997, p. 312.
- [57] P. K. Robertson, R. G. Campanella, D. Gillespie and J. Greig, "Use of piezometer cone data," in *In-situ '86 use of in-situ testing in Geotechnical Engineering*, Reston, 1986.
- [58] P. K. Robertson, "Soil classification using the cone penetration test," *Canadian Geotechnical Journal*, vol. 27, no. 1, pp. 151-158, 1990.
- [59] P. K. Robertson and R. G. Campanella, "Interpretation of cone penetration tests - Part I (sand)," *Canadian Geotechnical Journal*, vol. 20, no. 4, pp. 718-733, 1983.
- [60] P. K. Robertson and C. R. G, "Interpretation of cone penetration tests - Part II (clay)," *Canadian Geotechnical Journal*, vol. 20, no. 4, pp. 718-733, 1983.
- [61] M. G. Jefferies and M. P. Davies, "Use of CPTU to estimate equivalent SPT N60," *Geotechnical Testing Journal*, vol. 16, no. 4, pp. 458-468, 1993.
- [62] P. K. Robertson, "Interpretation of in-situ tests - some insights," in *Proceedings of ISC'4*, Recife, 2012.
- [63] G. Baldi, R. Bellotti, V. N. Ghionna, M. Jamiolkowski and D. F. C. Lo Presti, "Modulus of sands from CPTs and DMTs," in *Proceedings of the 12th International Conference on Soil Mechanics and Foundation Engineering*, Rio de Janeiro, 1989.
- [64] F. H. Kulhawy and P. H. Mayne, *Manual on estimating soil properties for foundation design*, Electric Power Research Institute, 1990.
- [65] P. K. Robertson, "Soil behaviour type from the CPT: an update," in *2nd International Symposium on Cone Penetration Testing*, Hunington Beach, 2010.
- [66] M. Cassn, "Les essais in situ en mécanique des sols," *Réalisation et Interprétation*, vol. 1, pp. 146-151, 1988.

- [67] D. D. Langton, The panda light-weight penetrometer for soil investigation and monitoring material compaction, 2000.
- [68] A. P. Butcher, K. McElmeel and P. J. J. M, "Dynamic probing and its use in clay soils," in *Proceedings of the International Conference on Advances in Site Investigation Practice*, 1996.
- [69] Institutul central de cercetare, proiectare și directivare în construcții (ICCPDC), *Instrucțiuni tehnice pentru cercetarea terenului de fundare prin metoda penetrării cu con, penetrare statică, penetrare dinamică, vibropenetrare*, 1989.
- [70] M. J. Alam, M. S. Hossain and A. K. Azad, "Development of correlation between dynamic cone resistance and relative density of sand," *Journal of Civil Engineering, Institute of Engineers, Bangladesh*, vol. 42, no. 1, pp. 63-76, 2014.
- [71] K. Head, *Manual of soil laboratory testing*, 3rd ed., vol. I: Soil classification and compaction tests, Dunbeath, Caithness: Whittles Publishing, 2006, p. 416.